Instabilities and Propagation Properties in Two-Component Reaction-Diffusion Systems

Samir Shams Eldeen, MSc

Thesis submitted to The University of Nottingham

for the degree of Doctor of Philosophy

November 2011

Abstract

This thesis deals with a detailed linear analysis for a two-component reaction-diffusion system with constant diffusion coefficients. A comprehensive linear stability analysis results in three types of instabilities: (1) stationary periodic instability, (2) oscillatory uniform and (3) stationary uniform. The first instability involves pattern formation and the other two do not. Precise parameter regimes are identified for each.

Travelling wave analysis is performed for the system and a detailed and comprehensive analysis is undertaken of a linear mechanism governing the development and propagation of nonlinear patterns. This analysis focuses on a linear selection mechanism that gives some insights into the selected speed of invasion of an unstable state by a stable one, as described both by a fixed form of travelling wave and by a modulated travelling wave.

Acknowledgements

I would like to thank my supervisors, Prof. J.R. King and Dr. Stephen Cox , for their endless support and help. Great thanks for their patience and for encouraging me throughout my study.

Also, I really want to thank Dr. R. Tew for his support in my first year. Thanks are also due to all my friends and colleagues in the school of Mathematical Sciences, The University of Nottingham.

Great thanks are also due to the Egyptian government for offering me this chance to study abroad and for its financial and social support during all my study.

Finally yet most importantly, I would like thank my wife, without her love, help, patience and support, it would be difficult to finish this work. She stopped his work and give all of here time and effort to our children and me with all sincere and love. My love is to my lovely daughter Nada, and my two sons, Mohamed and Yusuf.

Great thanks are due to my mother, my father, my brothers and my sisters for their prayers and to all of my friends and colleagues back home.

Contents

Chapter 1

Introduction

1.1 Reaction-Diffusion Equations

Reaction-diffusion equations are a very important class of partial differential equations. This class of equations is used whenever the spatial spread of a population or chemical species is of importance. For spatial spread, reaction-diffusion models have successfully been used in epidemic problems, pattern formation in different biological and ecological systems and in signal transport. Good overviews are given in Murray [55] and Britton [13]. The evolution equations for reaction-diffusion are readily obtained from the law of conservation of mass [54]. For several interacting species or chemicals, for example m species, the system of equations can appear in the matrix form

$$\frac{\partial \bar{\mathbf{u}}}{\partial t} = \mathbf{D}\nabla^2 \bar{\mathbf{u}} + \bar{\mathbf{f}}, \tag{1.1}$$

where ∇^2 is the Laplacian operator and the vector function $\bar{\mathbf{u}} = (u_1, u_2, ..., u_m)$ represents the concentrations or densities of the species that each diffuses with its own positive constant diffusion coefficient D_i, $i = 1, ..., m$. These coefficients are the diagonal elements of the diagonal matrix $\mathbf{D}$, the matrix of diffusivities, assuming that there is no cross-diffusion.

The species or chemicals interact according to the vector source term $\bar{\mathbf{f}}$, the reaction kinetics. Numerous studies concerned with reaction-diffusion processes mainly use the above equation in modelling systems in many disciplines including biology, chemistry, ecology, epidemiology and so on.

Nonlinear reaction-diffusion equation models have been widely used to account for pattern forming phenomena. From a theoretical point of view, one may distinguish two types of reaction-diffusion structures: (i) global structures resulting from intrinsic symmetry-breaking instabilities, e.g., Turing structures [71], and (ii) localized structures associated with fronts, i.e., steep spatial changes of concentration or densities which correspond to transitions between two states with fast kinetics, e.g., travelling waves [13].

1.2 Travelling Waves

A travelling wave is a wave which travels at constant speed without change in shape. If $u(\mathbf{x},t)$ represents a travelling wave, the shape of u will be the same for all time and the speed of propagation of this shape is a constant. If we look at this wave in a travelling frame moving at the same speed it will appear stationary [55]. One of the most important properties of nonlinear parabolic systems is their ability to support travelling wave solutions. Unlike the linear wave equation, for example, which is hyperbolic and propagates any wave profile with a specific speed, reaction-diffusion equations may allow various wave profiles to propagate, each one with its own characteristic speed [33].

Travelling wave solution can be written in the form $u(\mathbf{x},t) = V(\mathbf{z}) = V(\mathbf{x} - \mathbf{c}t)$ for some velocity $\mathbf{c}$. Plane wave is a class of travelling waves with $V(\mathbf{z}) = U(\mathbf{z} \cdot \mathbf{s})$ for some vector $\mathbf{s}$) (i.e., $u = U(\mathbf{z} \cdot \mathbf{s} - ct)$), c a scalar). This class of waves, plane waves, is categorized in one dimension as [26] :

- Wave trains (U periodic)

- Wave fronts ($U(-\infty)$ and $U(\infty)$ exist and are unequal)

- Pulses ($U(\pm\infty)$ exist and are equal; U not constant)

and there are other forms in two dimension ($\mathbf{x} = (x,y)$, $x = r\cos\theta$, $y = r\sin\theta$):

- Target patterns ($u(\mathbf{x},t) = U(r,t)$, U periodic in t)

- Rotating Spiral patterns ($u(\mathbf{x},t) = U(r, \theta - ct)$, U periodic in second argument)

In many natural phenomena we encounter propagating fronts separating different phases. Propagating fronts play an important role in the spread of epidemics, in population dynamics, or the propagation of flames and chemical reactions. Therefore, reaction-diffusion equations have become a prototype for describing propagating front behaviour, from chemical waves to biological population. The construction and study of wave solutions for nonlinear reaction-diffusion systems is an area of great interest, not only in the applications of the waves themselves, but also in their use in gaining a better understanding of phenomena in large domains [33].

The propagation of a front into an unstable state is a problem that emerges in many branches of the natural sciences. These fronts may be classified as: (1) *Uniformly translating fronts*, which are in the form $u(z) = u(x - ct)$, where c is the front speed. In this class of fronts invasion could be either monotonic or oscillatory (see figure 1.1 (a) and (b)). (2) *Pattern forming fronts*, a front that generates a nontrivial pattern behind the wavefront. The front has a finite speed while the pattern is often stationary (see figure 1.1 (c)). Thus these pattern fronts are typically not in the form $u(x - ct)$, and instead they are spatially and temporally periodic: they are of the type $u(z,t) = u(x - ct,t)$, with $u(z,t)$ periodic in t with period T, $u(z,t) = u(z,t+T)$.
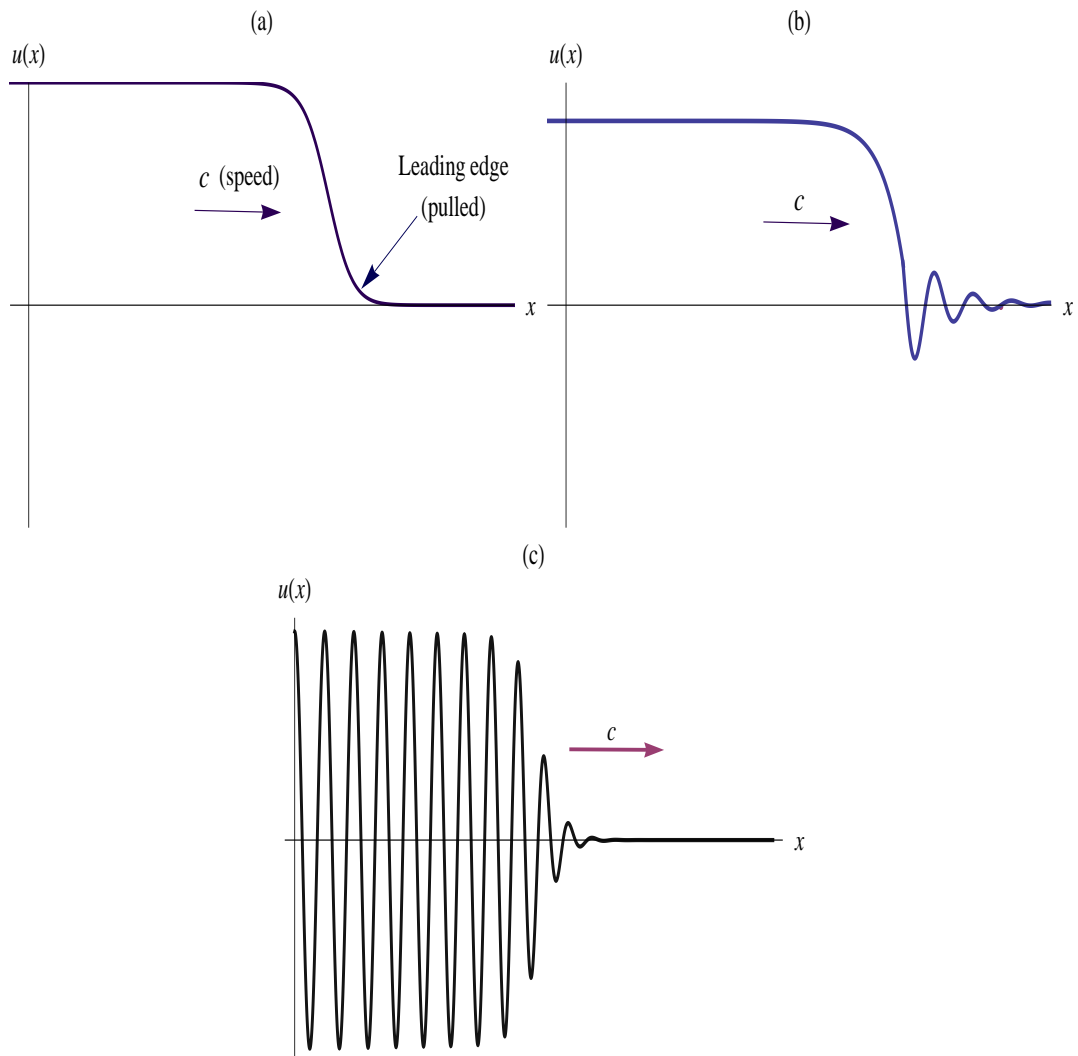
Figure 1.1: Schematic representation of some front types, all moving to the right with speed c. (a) Monotonic uniform translating front. (b) Front invading the unstable state in oscillatory manner. (c) Pattern forming front, a front moving to the right leaving a pattern behind. There are possible states behind the front, such as limit cycles, stationary patterns, and oscillatory patterns.

1.3 Front Selection

The prototypical model for reaction-diffusion systems is the Fisher-type nonlinear diffusion equation (scalar monostable), which we use here to illustrate some general principles:

$$\frac{\partial u}{\partial t} = \frac{\partial^2 u}{\partial x^2} + F(u),$$
(1.2)

where $u > 0$ may be interpreted as a population density, $F(0) = F(1) = 0$. This equation was introduced in 1937 by R.A. Fisher [28], with $F(u) = u(1-u)$. At the same time by A.N. Kolmogorov, together with I.G. Petrovskii and N.S. Piskunov [42] (hereafter (1.2) referred to as FKPP). In their work of 1937, Kolmogorov et al. proved the existence of front solutions $u = U(x - ct)$, characterized by their velocity, c, such that

$$c \geq c_0 = 2\sqrt{F'(0)},$$
(1.3)

and this result is obtained by a linearisation about $u = 0$. Moreover, under some assumption on F, they proved that the FKPP-equation, equation (1.2), with a sufficiently decaying initial data has solutions with speed c_0. For more general monostable equations, it was shown rigorously by Aronson and Weinberger [3], for a sufficiently localized initial condition the solutions of (1.2) evolve into fronts with a minimal allowed speed c_{min}, such that

$$2\sqrt{F'(0)} \leq c_{min} \leq 2\sup_u \sqrt{F(u)/u},$$
(1.4)

thus the propagating speed is either equal to or larger than c_0. Also, they showed that a monotonic travelling wave exists for all speeds $c \geq c_{min}$, and none for $c < c_{min}$. Therefore, from these results two selection mechanisms appeared: a *linear* and *nonlinear* selection of the propagation speed. In a linear selection mechanism the front dynamics can be understood by linear analysis since it is essentially determined by linearisation near the unstable

5

steady state ($u = 0$ in case of FKPP equation), so the front is pulled by its leading edge (see figure 1.1(a)), and in this case the selected front is called *pulled* front. However, for the selected fronts with speeds larger than the linear front speed, the details of the nonlinearity of the reaction term, $F(u)$, are important. In this case, the front dynamics are referred to as *pushed*, meaning that the front is pushed by its (nonlinear) interior, and a nonlinear analysis is required to determined the front speed. A nonlinear selection principle has been proposed to that aim (see [74]). Fisher's equation has been studied extensively, considering the travelling wave existence problem and the speed of propagation. There is now a great deal of literature on this subject, see for example [38, 44, 45, 47, 68, 69].

A few scenarios have been proposed regarding the selection mechanism on some non-linear reaction-diffusion equations, many for scalar equations. Some of the famous methods used are the marginal stability hypothesis (linear selection) [5, 18, 23, 72] (for a review see [73]) , structural stability hypothesis [58], construction of exact solutions [22], variational methods [6, 7], and asymptotic methods [8, 35, 40, 46]. Also, investigation of the front speed dependence on the system parameters has been discussed numerically (see [76]).

1.4   Fisher's Equation

In this section we demonstrate the propagation properties of a front solution to the FKPP equation. We obtain the eigenvalues that depend on the wave speed, then we can specify the front linear speed, which is the minimal wave speed. We can also indicate which front type the equation supports. Consider the equation (FKPP)

$$\frac{\partial u}{\partial t} = D\frac{\partial^2 u}{\partial x^2} + au(1-u),\tag{1.5}$$

where D and a are positive parameters. Now rescaling by inserting

$$x^* = \sqrt{\frac{a}{D}}x, \qquad t^* = at, \tag{1.6}$$

and then omitting asterisks, for simplicity, results in

$$\frac{\partial u}{\partial t} = \frac{\partial^2 u}{\partial x^2} + u(1-u). \tag{1.7}$$

There are two steady states: $u = 1$ which is a stable steady state, while $u = 0$ is unstable, the two states are spatially homogeneous. This indicates that for suitable initial conditions, the wavefront solution is where u at one end (say the stable state) as $x \to -\infty$, and approaches the other state as $x \to \infty$. Hence, this suggests we should look for a travelling wavefront solution of (1.5). If such a solution exists, it can be written as

$$u(x,t) = \phi(z), \qquad z = x - ct, \tag{1.8}$$

where c is the front speed, which may negative or positive, because (1.7) is invariant for the $x \to -x$ change of variable. In our analysis we assume $c \geq 0$. When we substitute from (1.8) into (1.7), we obtain an ordinary differential equation

$$\frac{d^2\phi}{dz^2} + c\frac{d\phi}{dz} + \phi(1-\phi) = 0, \tag{1.9}$$

where the wavefront solution $\phi(z)$ satisfies

$$\lim_{z \to \infty} \phi(z) = 0, \qquad \lim_{z \to -\infty} \phi(z) = 1. \tag{1.10}$$

Now, from (1.9), the character of the front solution ϕ depends on the speed c, thus we have an eigenvalue problem. We aim to determine the value(s) of c for which a solution

$\phi(z)$ exists and satisfies (1.10). In this problem, the uniform stable state $\phi = 1$ invades the unstable $\phi = 0$, and we aim to give insights on the manner of invasion and its dependence on the speed c. Therefore, we need to investigate the behaviour of the wave profile $\phi(z)$ near the steady states thus we need the linearization (to know the response to small perturbations). When we linearize (1.9) in the far field, we obtain the perturbation equation

$$\frac{d^2\varphi}{dz^2} + c\frac{d\varphi}{dz} + (1 - 2\phi_0)\,\varphi = 0, \tag{1.11}$$

where $\varphi = \varphi(z)$ is the perturbation around the the steady state ϕ_0, i.e. $\phi(z) = \phi_0 + \varphi(z)$, and ϕ_0 equals 0 or 1, the unstable and stable state, respectively. Equation (1.11) is linear, thus its solution can be put in the form

$$\varphi(z) \propto e^{\mu z}, \tag{1.12}$$

where μ is the eigenvalue. When we substitute into (1.11), we obtain the characteristic equation

$$\mu^2 + c\mu + 1 - 2\phi_0 = 0, \tag{1.13}$$

which is quadratic in μ and then the two eigenvalues are

$$\mu_{1,2} = -\frac{c}{2} \pm \left[\frac{c^2}{4} - 1 + 2\phi_0\right]^{1/2}. \tag{1.14}$$

In the vicinity of the stable state $\phi_0 = 1$, the eigenvalues are $-c/2 \pm (c^2/4 + 1)^{1/2}$, which are real and of opposite sign at any speed c, so excluding exponential growth corresponds to imposing one boundary condition. For the unstable state $\phi_0 = 0$, the two eigenvalues are $-c/2 \pm (c^2/4 - 1)^{1/2}$. If $c \geq 2$ the two eigenvalues are real and negative (the case when $c = 2$ gives a double eigenvalue, $\mu = -1$). Hence ϕ reaches 0 monotonically and the front profile is like the front shown in figure 1.1 (a). However, if $c < 2$, the eigenvalues

are complex conjugates with a negative real part. In this case ϕ reaches 0 in an oscillatory manner (similar to the front in figure 1.1 (b)). The fastest decay of the slowest decaying exponential occurs in the repeated root case, at $c = 2$.

If we look for a travelling wavefront solution to (1.7) for which $0 \leq u \leq 1$, oscillatory invasion is not accepted, the allowable wave profile must satisfy the monotonicity of the solution. Therefore, the minimum wave speed is $c_{min} = 2$, which is the wave speed at which the eigenvalues associated with the leading edge of the front switch from real to complex. Also, we can say that this wave speed occurs when a double root exists, and can be obtained by solving (1.13) with the double root equation $2\mu + c = 0$ (differentiate (1.13) with respect to μ). An equivalent method, a phase plane method, can be used to prove that a wavefront solution exists with rang of wave speeds satisfies $c \geq c_{min} = 2$. In the original dimensional equation (1.5) (using (1.6)), the range satisfies

$$c \geq c_{min} = 2\sqrt{Da}. \tag{1.15}$$

1.5   Linear (pulled) Front Speed

From the previous section we noticed that a minimum wave speed can be obtained from a double eigenvalue condition. In this section we aim to demonstrate how we can use this double root criterion to determine the linear (pulled) regime. In the first place, we introduce the travelling wave coordinates $(z,t) = (x - ct, t)$ into dynamical equations, then we linearize the obtained equations around the unstable rest state. This results in a perturbation equation. After that we substitute the ansatz (corresponding for $v \neq 0$ to modulated travelling wave solution with a time period $T = 2\pi/v$)

$$u = e^{ivt}e^{\mu z}, \tag{1.16}$$

9

into the perturbation equation to obtain a characteristic equation

$$Q(\mu;c,\nu) = 0, \tag{1.17}$$

where Q is a polynomial in the eigenvalue μ (its degree equals the order of the differential equation). The travelling front parameters are ν (modulating frequency) and c (wave speed), which are both real. From (1.16), when the modulating frequency ν is zero, the front may be a uniformly translating one, $u(x - ct)$, or a modulated one, but in the latter T (the time period) cannot be determined by the linearisation. However if the modulating frequency ν takes a nonzero value the wave is necessarily of modulated type with $e^{i\nu T} = 1$, so that $T = 2\pi/\nu$ or some integer multiple of that value. If a steady state periodic pattern is left behind the wavefront it will typically have a spatial wave length $2\pi c/\nu = cT$.

A linear front speed is the speed at which a double eigenvalue occurs. Thus we need to determine the wave speed that satisfies the characteristic equation (1.17) and the double root equation

$$\frac{\partial}{\partial \mu} Q(\mu;c,\nu) = 0. \tag{1.18}$$

Now let us apply the above conditions (double root conditions), equations (1.17) and (1.18), on the FKKP-equation (1.7). In the travelling wave coordinates $(z,t) = (x - ct,t)$, we have

$$\frac{\partial^2}{\partial x^2} = \frac{\partial^2}{\partial z^2}, \qquad \frac{\partial}{\partial t} = \frac{\partial}{\partial t} - c\frac{\partial}{\partial z}, \tag{1.19}$$

and then equation (1.7) will be

$$\frac{\partial^2 u}{\partial z^2} + c\frac{\partial u}{\partial z} - \frac{\partial u}{\partial t} + u(1 - u) = 0. \tag{1.20}$$

Linearizing around the the unstable state $u = 0$, and then substituting the perturbation

10

displayed in (1.16), results in the characteristic equation (1.17) where

$$Q(\mu; c, \nu) = \mu^2 + c\mu + 1 - i\nu, \tag{1.21}$$

and a minimal front speed $c = c_0$ is the speed that satisfies (1.17) and (1.18). Therefore, c_0 is given by

$$\mu^2 + c_0\mu + 1 - i\nu = 0, \qquad 2\mu + c_0 = 0, \tag{1.22}$$

and when we solve, we find that $c_0 = 2$, $\mu = -1$ and $\nu = 0$. This suggests that for all wave speeds $c \geq c_0 = 2$, a monotonic front solution exists (the stable state $u = 1$ invades $u = 0$ in monotonic manner) and a patterned front solution ($\nu \neq 0$) does not occur.
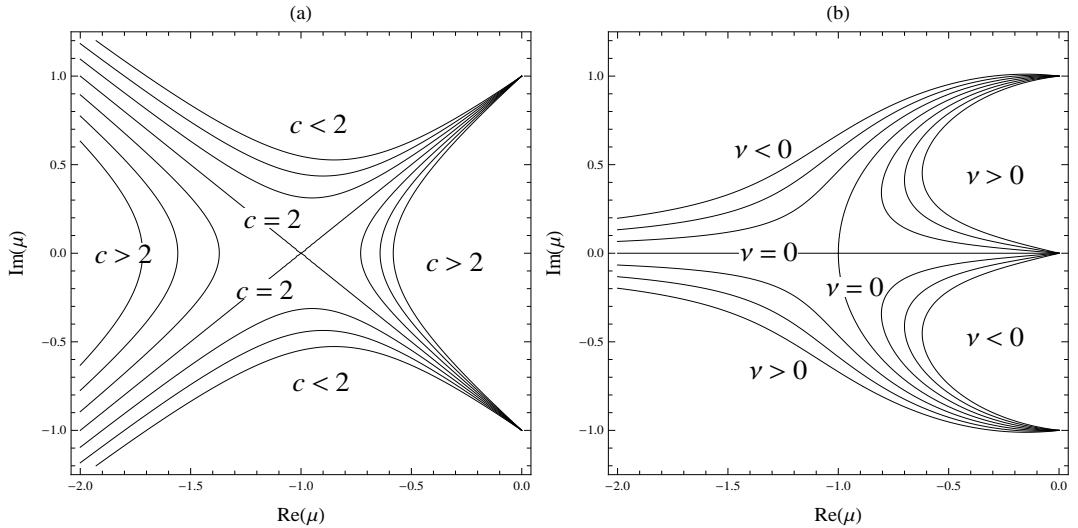
Figure 1.2: $Re\mu$, $Im\mu$ space, (a) Constant speed contours, saddle point occurs at $c = c_0 = 2$. (b) Constant ν contours, a saddle exists when $\nu = 0$.

Figure 1.2 shows constant c and ν contours in $Re(\mu)$, $Im(\mu)$ space. Equations which represent the contours are obtained as follows. Substitute $\mu = X + iY$ into the characteristic equation $\mu^2 + c\mu + 1 - i\nu = 0$. This results in a complex equation, which gives the two real equations $X^2 - Y^2 + cX + 1 = 0$, $2XY + cY - \nu = 0$. The first equation represents the contours for c, shown in figure 1.2(a). When we eliminate c, we obtain

11

$Y(1 - X^2 - Y^2) + vX = 0$ which represents the v contours (shown in figure 1.2(b)). From figure 1.2, a saddle point appears when a double root exists, and this happened when $c = 2$ and $v = 0$. These results coincide with the well known results in the previous section.

In this chapter we demonstrated the propagation properties in the FKPP-equation, and the task was easy as the the eigenvalues are known explicitly. This in general cannot happen in higher order equations, thus we need more computations. Therefore, in chapter 2, we study two higher order differential equations, to demonstrate how we can deal with equations of degree greater than two when we apply the double root condition that gives us some insights on the minimal front speed. Our main goal is to extend this linear analysis to cover a two-component reaction-diffusion system. In chapter 3, we give a comprehensive instability analysis of the system, and different kinds of bifurcations are recognised. A travelling wave analysis is performed to determine a linear front speed of propagation using the double root mechanism, and this analysis in details is presented in chapters 4, 5 and 6.

Chapter 2

Higher order Scalar Reaction-Diffusion Equation

In this chapter we aim to investigate the instability and the propagation properties of reaction-diffusion equations of fourth order. We study two equations, the extended Fisher Kolmogorov equation (EFK), and the Swift-Hohenberg equation (SH). Both have been studied before by related methods (see, [7, 60, 64, 73]) but the analysis here will be instructive for what follows. These two equations support patterned front solutions, and in this chapter the double eigenvalue mechanism is used to provide evidence for that and to determine a minimal front speed. In our discussion for each equation, we start with linear stability analysis, then we perform a travelling wave analysis to uncover the propagation properties of the front solution. A minimal front speed is determined, also indicating the type of the front (patterned front ($v \neq 0$) or not ($v = 0$) if we adopt the simplest assumptions about the form of the front that are consistent with the linearised analysis).

2.1 The Extended Fisher-Kolmogorov Equation

The extended Fisher Kolmogorov equation (EFK) is given by

$$\frac{\partial u}{\partial t} = \frac{\partial^2 u}{\partial x^2} - \gamma \frac{\partial^4 u}{\partial x^4} + u - u^3. \qquad (\gamma > 0) \qquad (2.1)$$

In the following we discuss the instability of (2.1). Assume that $u = u_s$ is the rest state, which can be either 0 or ± 1. Linearizing (2.1) about the steady state gives the perturbation equation

$$\frac{\partial \widehat{u}}{\partial t} = \frac{\partial^2 \widehat{u}}{\partial x^2} - \gamma \frac{\partial^4 \widehat{u}}{\partial x^4} + (1 - 3u_s^2)\widehat{u}, \qquad (\gamma > 0) \qquad (2.2)$$

where $\widehat{u}$ is the perturbation. We study the evolution modes of a given wave number k, where the perturbation $\widehat{u} = \widehat{u}_0 e^{ikx} e^{\sigma t}$, and σ is the temporal growth rate. Substituting into (2.2) results in the dispersion relation

$$\sigma = -k^2 - \gamma k^4 + (1 - 3u_s^2). \qquad (2.3)$$

The temporal growth rate σ is plotted versus the wave number k, shown in figure 2.1. Thus we can say that the steady states $u_s = \pm 1$ are stable and $u_s = 0$ is unstable for the band $0 \le k < k_+$, where $k_+^2 = (-1 + (1 + 4\gamma)^{1/2})/2\gamma$. For this type of instability, while a non-trivial pattern can arise when the unstable state is perturbed, it is the uniform perturbation that grows most rapidly.

Now we aim to discuss the front solution properties of the EFK equation. We suppose that there are two rest states 0 and 1, where $u(\infty) = 0$ and $u(-\infty) = 1$. A front solution connecting these two states can exist, and in the following we aim to determine the minimal front speed. Linearising (2.1) around the unstable steady state $u = 0$, and in the

14
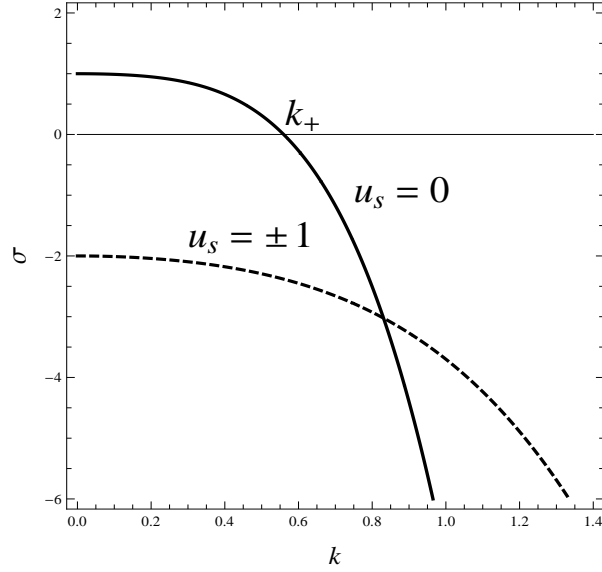
Figure 2.1: Dispersion relation of (2.1), equation (2.3). The solid line represent the growth rate when the steady state $u = 0$, and the dashed when $u = \pm 1$.

travelling wave coordinates $(z, t) = (x - ct, t)$, one can deduce the linearized equation

$$\frac{\partial u}{\partial t} - c\frac{\partial u}{\partial z} = \frac{\partial^2 u}{\partial z^2} - \gamma\frac{\partial^4 u}{\partial z^4} + u, \tag{2.4}$$

and substituting the ansatz $u = e^{i\nu t} e^{\mu z}$ gives the characteristic equation

$$Q = \gamma\mu^4 - \mu^2 - c\mu - 1 + i\nu = 0, \tag{2.5}$$

where ν and c are real and μ is complex. The minimal allowable wave speed $c = c_0$ occurs when there is a double root for $Q = 0$. To determine this speed we evaluate the double root condition $Q = \partial Q/\partial \mu = 0$, i. e.

$$\gamma\mu^4 - \mu^2 - c\mu - 1 + i\nu = 0 \quad \text{and} \quad 4\gamma\mu^3 - 2\mu - c = 0, \tag{2.6}$$

which is a necessary condition for the minimal front speed to exist. To find c and ν, we

15

eliminate the eigenvalue μ using the conditions (2.6). We use Sylvester's Dialytic Method of Elimination (see appendix A) to obtain

$$R(c, v; \gamma) = 0, \tag{2.7}$$

where $R(\cdot)$ is the determinant of Sylvester's matrix, which appears as

$$R(c, v; \gamma) = \begin{vmatrix} \gamma & 0 & -1 & -c & -1+iv & 0 & 0 \\ 0 & \gamma & 0 & -1 & -c & -1+iv & 0 \\ 0 & 0 & \gamma & 0 & -1 & -c & -1+iv \\ 4\gamma & 0 & -2 & -c & 0 & 0 & 0 \\ 0 & 4\gamma & 0 & -2 & -c & 0 & 0 \\ 0 & 0 & 4\gamma & 0 & -2 & -c & 0 \\ 0 & 0 & 0 & 4\gamma & 0 & -2 & -c \end{vmatrix}. \tag{2.8}$$

Some of the determinant elements are complex. Therefore, equation (2.7) gives two real equations. These two equations are

$$v\left(9\gamma c^2 + 16\gamma^2\left(v^2 - 3\right) - 16\gamma - 1\right) = 0, \tag{2.9}$$

$$-27\gamma c^4 + 4(36\gamma + 1)c^2 + 128\gamma(6\gamma + 1)v^2 - 16(4\gamma + 1)^2 = 0. \tag{2.10}$$

Now we solve (2.9) and (2.10) for c and v. When $v = 0$, equation (2.9) is already satisfied. Then from (2.10) (with $v = 0$), fortunately we obtain two solutions explicitly

16

for the wave speed. These two wave speeds are

$$c_1 = 2\left[\frac{1+36\gamma-(1-12\gamma)^{3/2}}{54\gamma}\right]^{1/2}, \qquad v_1 = 0 \qquad (2.11)$$

$$c_2 = 2\left[\frac{1+36\gamma+(1-12\gamma)^{3/2}}{54\gamma}\right]^{1/2}, \qquad v_2 = 0, \qquad (2.12)$$

provided that $\gamma < 1/12$. Now there are two solutions for the double root conditions (2.9) and (2.10), the two speeds c_1 and c_2 with $v = 0$. These two speeds are plotted versus the parameter γ and shown in figure 2.2 (a), as solid lines (they meet at $\gamma = 1/12$). A third possible solution of (2.9) and (2.10) for $v \neq 0$ exists, and can be determined explicitly as

$$c_3 = 2\left[\frac{-17-72\gamma+(7+24\gamma)^{3/2}}{54\gamma}\right]^{1/2} \qquad (2.13)$$

$$v_3 = \left[\frac{37+192\gamma+144\gamma^2-2(7+24\gamma)^{3/2}}{48\gamma^2}\right]^{1/2}, \qquad (2.14)$$

provided that $\gamma \geq 1/12$. The variation of c_3 and v_3 with γ is shown in figure 2.2 (a) and (b), as dashed lines.

Now we have all possible solutions of (2.9) and (2.10), which represent the wave speed and the modulating frequency that meet the double eigenvalue condition. We aim to give insights on the character of double eigenvalue and the other two roots of the characteristic equation (2.5). When $v = 0$, the coefficient sequence of the characteristic polynomial is $\gamma, 0, -1, -c, -1$. Hence, there is only one sign change in the coefficients signs, and according to Descartes' Rule of signs (see appendix B.1), there will be at most one real positive root. Also, one can apply Routh-Hurwitz (RH) criterion (appendix B.2). We find that the RH conditions are not satisfied (some of the characteristic polynomial coefficients are negative), hence there is at least one root with positive real part. From this result, Descartes' and RH criteria, we can say that for $v = 0$, there always a positive root of the

17
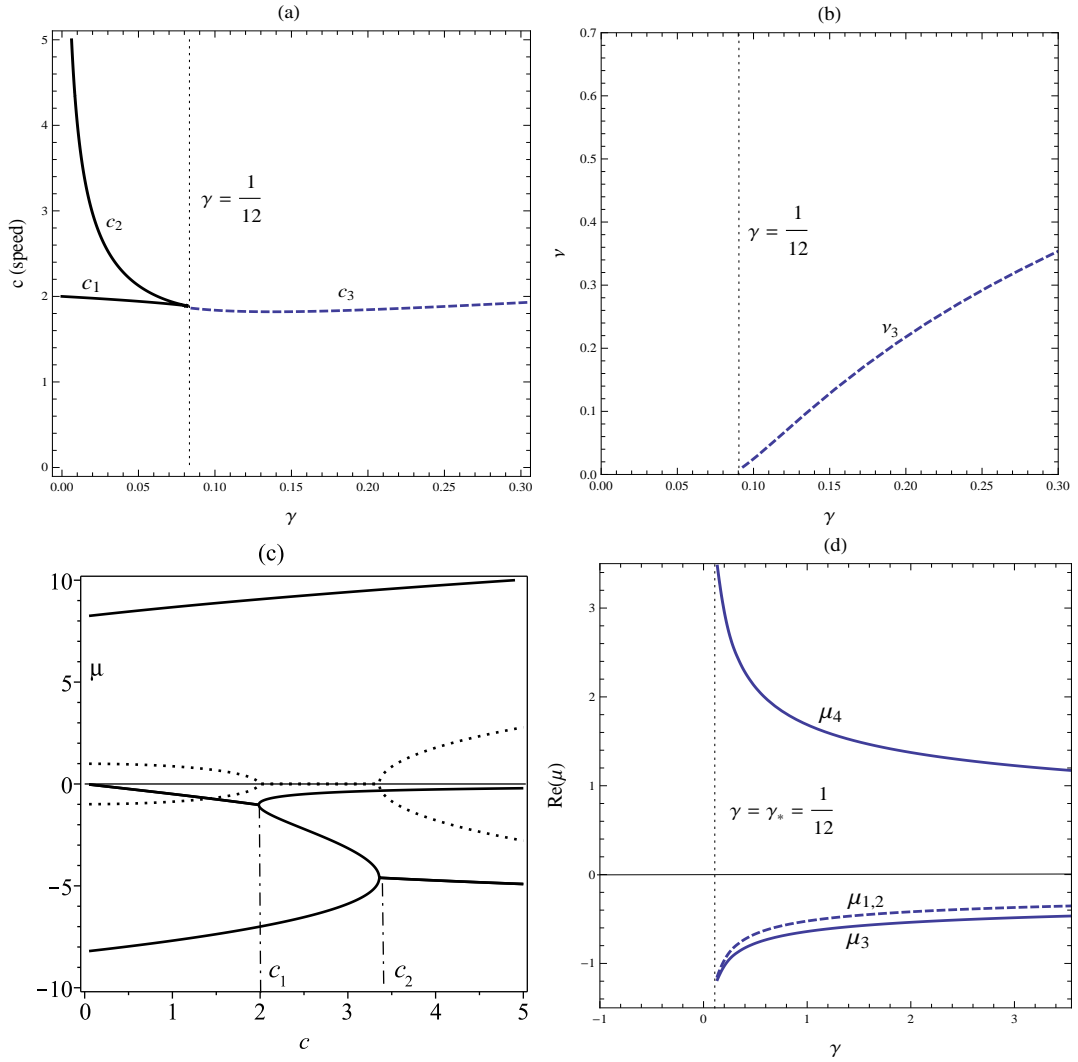
Figure 2.2: (a) and (b) Double root locus for the extended Fisher-Kolmogorov equation, from equations (2.11)-(2.14), a transition from $v = 0$ to $v \neq 0$ occurs at $\gamma = 1/12$ where a negative triple root exists. (c) Variation of the four roots of (2.5), when $\gamma = 0.02 < 1/12$ and $v = 0$, solid lines represent $Re\mu$, and dashed for $Im\mu$, c_1 and c_2 are the double root speeds. (d) Character of the real part of a double root (dashed line) and the real part of he other two roots (solid lines) with γ ($\gamma \geq 1/12$) at $c = c_3$ and $v = v_3$.

characteristic equation. The other three roots are: one negative and two which are either negative or complex with negative real part. Figure 2.2 (c) shows the four eigenvalues when $v = 0$ and $\gamma = 0.02 < 1/12$ versus wave speed c. Two negative double roots exist, one at speed $c = c_1$ and the other at c_2, $(c_1 < c_2)$. A positive real root always exists, and the other three roots are negative, that occurs when $c_1 \leq c \leq c_2$, and otherwise they are one negative and the other two are complex with negative real part. At c_1 the double root is negative and the other negative root is decaying faster. Hence for $c = c_1$ only one exponential must be excluded as $z \rightarrow \infty$ for the repeated root to dominate there and this is the speed selected in practice for the EFK equation. However, at c_2 both the other exponentials must be excluded as the double root is negative and the other two are one negative which is decaying slower than the double eigenvalue and one is positive.

It is obvious from figure 2.2 (a) that when $\gamma = \gamma_* = 1/12$ the three wave speeds c_1, c_2 and c_3 coincide and at this point $v = 0$. It is obvious from figure 2.2 (b) that a transition from zero to nonzero modulating frequency v takes place when $\gamma = 1/12$. Also, we can see from figure 2.2 (c), as $\gamma \rightarrow 1/12$ the two speeds c_1 and c_2 are very close, and when $\gamma = 1/12$ a negative real triple root arises. Therefore we can say that a transition occurs when the characteristic equation (2.5) has a real triple root at $v = 0$. We can determine the transition point by solving the triple root conditions

$$Q = \partial Q / \partial \mu = \partial^2 Q / \partial \mu^2 = 0, \qquad (v = 0) \qquad (2.15)$$

where Q is the characteristic equation which displayed in (2.5). Hence these conditions appear as

$$\gamma \mu^4 - \mu^2 - c\mu - 1 = 0, \quad 4\gamma \mu^3 - 2\mu - c = 0, \quad 6\gamma \mu^2 - 1 = 0, \qquad (2.16)$$

and when we solve these equations, we find $\gamma = 1/12, c = 4\sqrt{2}/3$ and $\mu = -\sqrt{2}$. We use

19
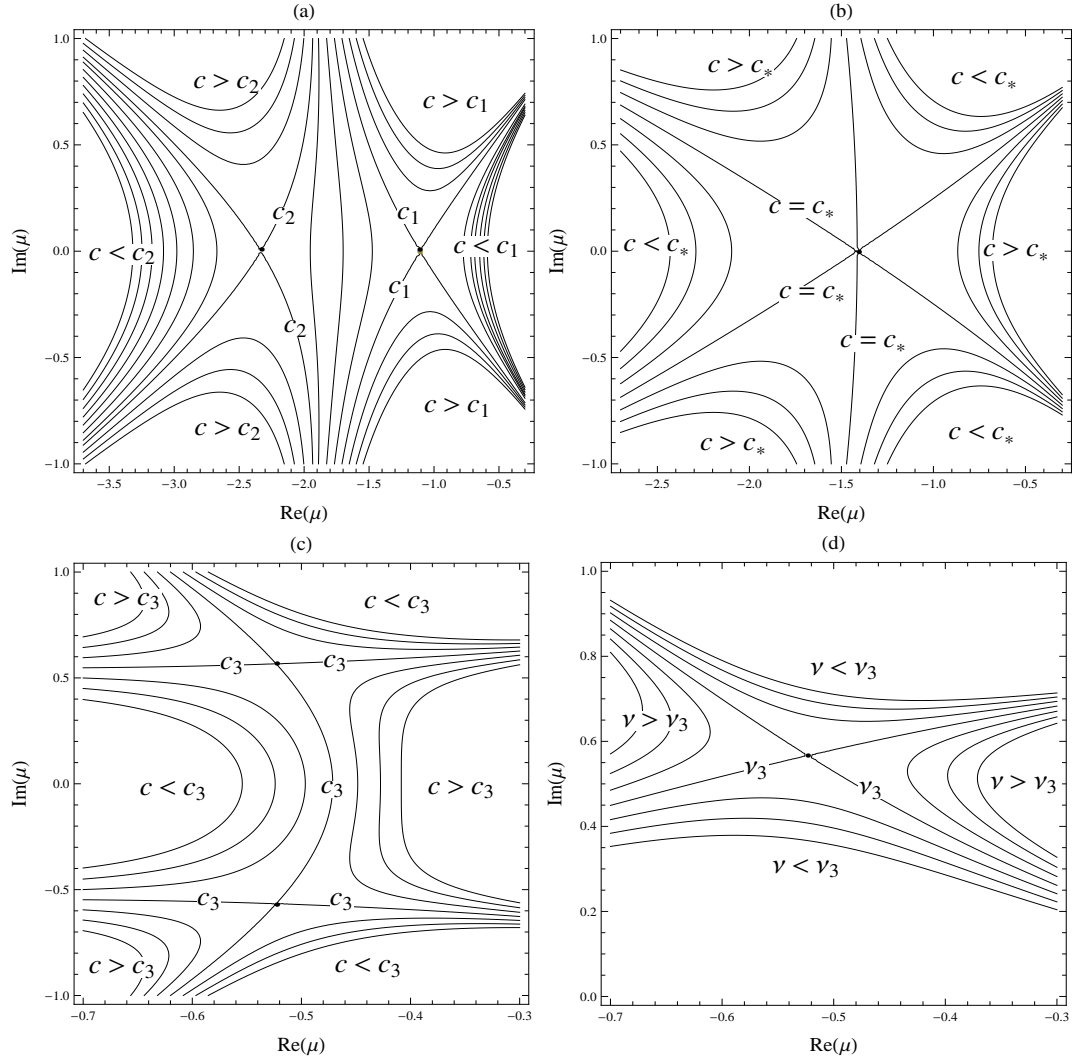
Figure 2.3: $Re\mu$, $Im\mu$ space plot. Constant speed contours, equation (2.17): (a) $\gamma = 0.05$, two real double roots exist at $\nu = 0$ and speeds $c_1 \simeq 1.94$ and $c_2 \simeq 2.13$, (b) $\gamma = 1/12$, triple root exits at $\nu = 0$ and $c = c_* \simeq 1.89$ and (c) $\gamma = 1$, a complex double root exits at speed $c_3 \simeq 2.49$ and $\nu_3 \simeq 0.76$. (d) $Re\mu$, $Im\mu$ versus ν, equation (2.18), at $\gamma = 1$, a double root exists at the saddle point (when $\nu \simeq 0.76$).

20

a triple root condition in our analysis in later chapters when we discuss reaction-diffusion systems.

When $\gamma > 1/12$, the double root speed and the corresponding modulating frequency ν are displayed in (2.13) and (2.14), which are shown in figure 2.2 (a) and (b) in dashed lines. At $c = c_3$ the characteristic equation (2.5) has a complex double root with negative real part, and the other two roots are complex, one with negative real part (decaying faster that the double root) and the other with positive real part, see figure 2.2 (d).

Figure 2.3 shows the character of a double root discussed above. The plots in this figure are constant speed c and frequency ν contours in $Re\mu$, $Im\mu$ space. A saddle point indicates that a double root exists. Equations which represent these contours can be obtained by substituting $\mu = X + iY$ into the characteristic equation (2.5) and then simplifying to obtain

$$\gamma(X^4 - 6X^2Y^2 + Y^4) - X^2 + Y^2 - cX - 1 \;=\; 0, \tag{2.17}$$

$$Y(\gamma[-3X^4 - 2X^2Y^2 + Y^4] + X^2 + Y^2 - 1) - \nu X \;=\; 0. \tag{2.18}$$
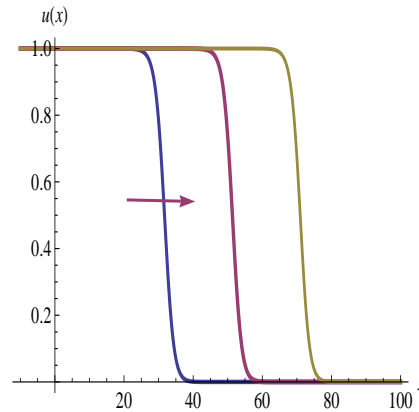
Figure 2.4: Solution of the EFK equation (2.1) when $\gamma = 0.02$, and $t = 20, 30, 40$ (left to right). The initial condition is $u(x,0) = 0.03e^{-x^2}$. The uniform state $u = 1$ invades $u = 0$ monotonically. These solutions are constructed using Mathematica 8 Package (NDSolve).
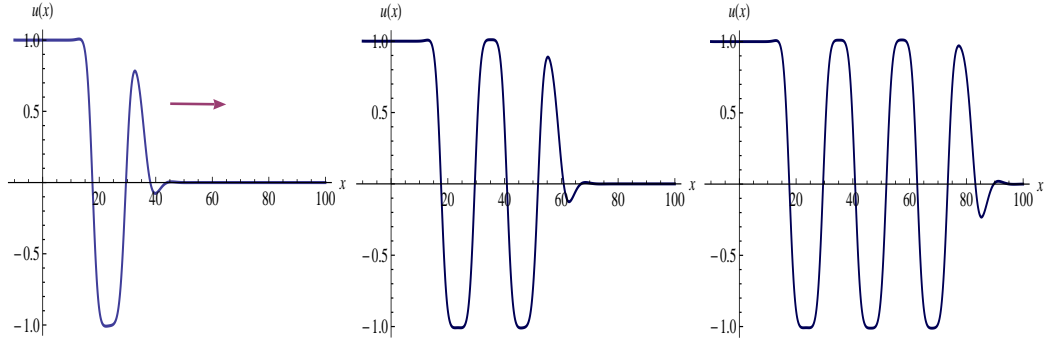
Figure 2.5: Solution of the EFK equation (2.1) when $\gamma = 1.0$, and $t = 20, 30, 40$ (left to right), the initial condition is a Gaussian of height 0.03 ($u(x,0) = 0.03e^{-x^2}$). A pattern invades the steady state $u = 0$.

Figure 2.4 shows solutions of the EFK equation (2.1) when $\gamma = 0.02 < 1/12$, at $t = 20, 30$ and 40, and a uniform translating front travels to the right with a minimal speed $c = c_1$ displayed in (2.11). Solutions when $\gamma = 1.0 > 1/12$ at $t = 20, 30$ and 40, are shown in figure 2.5. There is a pattern left behind the front invading the unstable state $u = 0$ with a minimal linear speed $c = c_3$ shown in (2.13). These solutions are constructed using Mathematica 8 Package (NDSolve).

2.2 Swift-Hohenberg Equation

In this section we give insights into propagating properties in the Swift-Hohenberg (SH) equation. By using the double root mechanism we show that the SH equation

$$\frac{\partial u}{\partial t} = (\varepsilon - 1)u - 2\frac{\partial^2 u}{\partial x^2} - \frac{\partial^4 u}{\partial x^4} - u^3, \qquad 0 < \varepsilon < 1, \tag{2.19}$$

supports pattern formed front solutions. First let us discuss the instability of the equation. There is one steady state $u = u_s = 0$, and in the following we discuss its instability type. At $u = 0$, the dispersion relation of (2.19) (assuming that the perturbation is in the form

22

$e^{ikx}e^{\sigma t}$) is

$$\sigma = 2k^2 - k^4 + (\varepsilon - 1), \tag{2.20}$$

Thus for $0 < \varepsilon < 1$, there is a band of wave numbers $k_- < k < k_+$, for which $u = 0$ is unstable (the fastest growing mode $k = 1$), see figure 2.6 . Therefore, we can say that a pattern can arise as a result of disturbing the zero state.
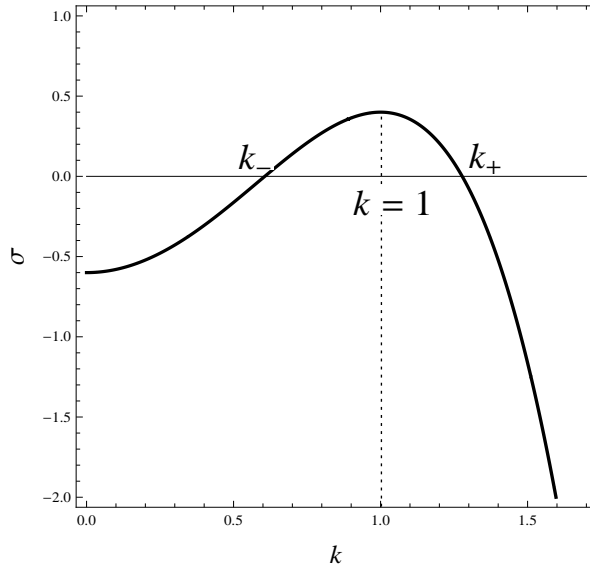
Figure 2.6: Dispersion relation of (2.19), equation (2.20). The fastest growing mode $k = 1$, the unstable wave numbers $k_- < k < k_+$.

In the following we aim to discuss the propagation properties of the SH equation solution. We linearise equation (2.19) around $u = 0$ (unstable steady state) and then in the travelling wave coordinates $(z, t) = (x - ct, t)$ the perturbation equation is

$$\frac{\partial u}{\partial t} - c\frac{\partial u}{\partial z} = -2\frac{\partial^2 u}{\partial z^2} - \frac{\partial^4 u}{\partial z^4} + (\varepsilon - 1)u, \tag{2.21}$$

where $u = u(z, t) = u(x - ct, t)$, assuming that u is the perturbation, and c is the wave

speed. Then we substitute $u = u_0 e^{i\nu t} e^{\mu z}$ to obtain the following characteristic equation

$$\mu^4 + 2\mu^2 - c\mu - (\varepsilon - 1) + i\nu = 0, \qquad (2.22)$$

where the eigenvalue μ is complex, while c and ν are real.

Now we find the double root condition. As in the previous section, the quartic equation $Q = \mu^4 + 2\mu^2 - c\mu - (\varepsilon - 1) + i\nu = 0$ results in two real equations, which can be put in the form

$$27c^4 + 32c^2(9\varepsilon - 8) + 256\left(\nu^2 + \varepsilon^3 - \varepsilon^2 - 3\nu^2\varepsilon\right) = 0 \qquad (2.23)$$

$$\nu\left(8\left(\nu^2 - 3\varepsilon^2 + 2\varepsilon\right) - 9c^2\right) = 0, \qquad (2.24)$$

and when we solve for c and ν, we find two possible solutions. The first is given by

$$c_1 = \frac{4}{3\sqrt{3}}\left[8 - 9\varepsilon + (4 - 3\varepsilon)^{3/2}\right]^{1/2}, \qquad \nu_1 = 0, \qquad (2.25)$$

which corresponds to a positive double eigenvalue for (2.22) (we will see later when we discuss the roots' character), while the other solution is

$$c_2 = \frac{4}{3\sqrt{3}}\left[-1 + 18\varepsilon + (1 + 6\varepsilon)^{3/2}\right]^{1/2}, \qquad (2.26)$$

$$\nu_2 = \frac{4}{\sqrt{3}}\left[-2 + 30\varepsilon + 9\varepsilon^2 + 2(1 + 6\varepsilon)^{3/2}\right]^{1/2}, \qquad (2.27)$$

where a double complex root with negative real part exists. Figure 2.7 (a) and (b) show these two solutions versus the parameter ε $(0 < \varepsilon < 1)$.

In the following we discuss the eigenvalues' character. Let us start with the case $\nu = 0$. From (2.22), and when $0 < \varepsilon < 1$, the coefficients' signs always support two sign changes. According to Descartes' rule, there will be at most two positive real roots

24
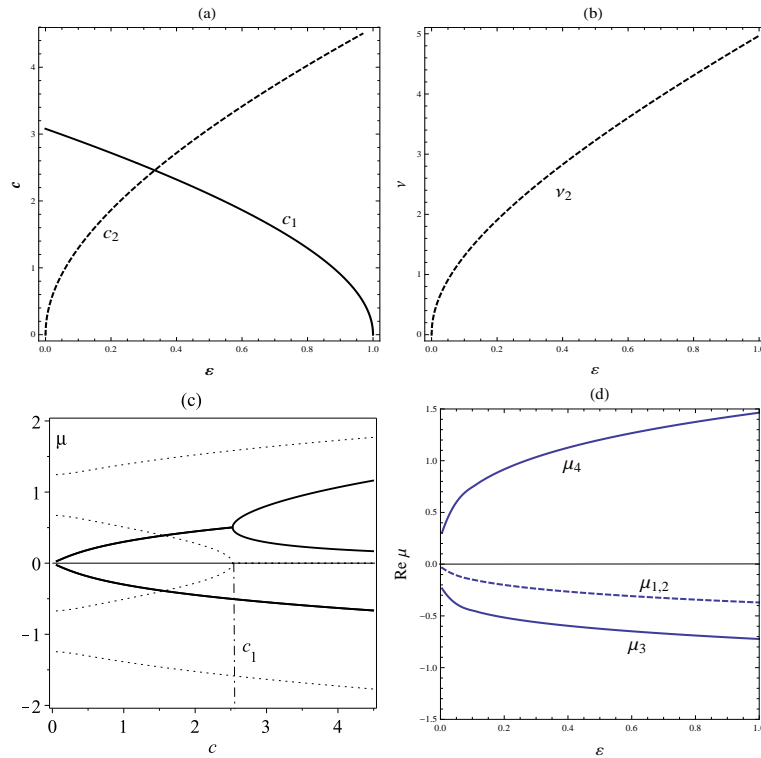
Figure 2.7: (a) and (b) Double root locus for the SH equation, (a) Speed versus ε , (b) modulating frequency versus ε, solid lines represent (2.25) where a positive double root, and on the dashed lines a double complex root with negative real part, from (2.26)-(2.27). (c) The four roots versus the wave speed, solid lies represent the real part and dotted lines for imaginary parts, a positive double root exits at $c = c_1$ and the other two roots are complex with negative real parts (the roots of (2.22) when $v = 0$ and $\varepsilon = 0.3$). (d) The real parts of a double root (dashed line) and the corresponding other two roots (solid lines, one positive and the other is negative and less than the double root) versus ε, the roots computed at $c = c_2$ and $v = v_2$ shown in (2.26) and (2.27).

or none. Since not all the polynomial coefficients are negative, the RH criterion is not satisfied. Therefore, there will be at least one complex root with positive real part. From this result, we can say that the characteristic equation must have two roots, which are either positive or complex with positive real parts (a positive double root exists at $c = c_1$), and the other two roots are complex with negative real part. The four eigenvalues versus the speed c are shown in figure 2.7 (c), the roots of (2.22) when $v = 0$ and $\varepsilon = 0.3$. For a nonzero value for v, equation (2.22) always has a complex double root with negative real part, and the other two roots are complex, one with negative and one with positive real part, the double root is the dominant, see figure 2.7 (d).
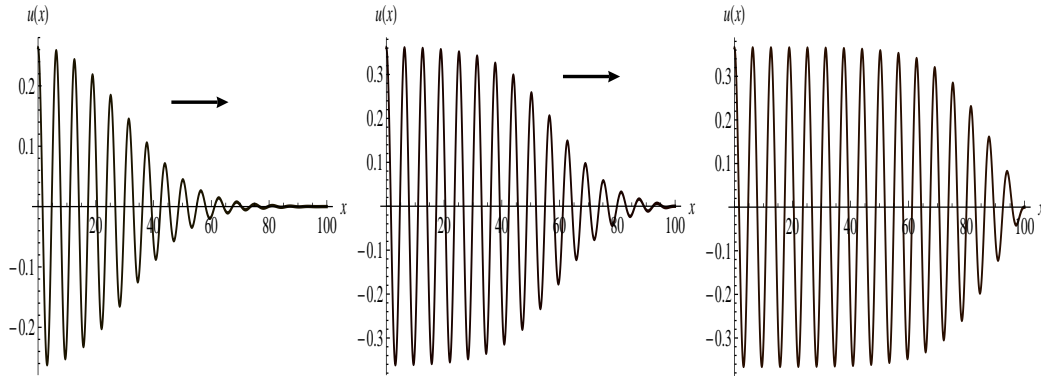
Figure 2.8: Solution of the SH equation when $\varepsilon = 0.1$, and at $t = 70, 90, 110$ (left to right). The initial condition is a Gaussian of height 0.01. A pattern invades the unstable state $u = 0$, the front moving to the right. These solution are obtained using Mathematica 8 Package NDSolve.

From the above investigation of the eigenvalues, we can deduce the following. At $c = c_1$ a real positive double root exists, while at $c = c_2$ there is a complex double root with negative real part. Hence, in practice, $c = c_2$ is the speed selected in practice for the SH equation. Thus we can say that a front invades the unstable state $u = 0$ with a minimal speed $c = c_2$, and leaves a pattern behind. Figure 2.8 shows solutions of the SH equation when $\varepsilon = 0.1$ at successive times. Therefore, equation (2.19) supports patterned front solutions.

2.3 Summary

We have discussed the propagation properties in two examples of higher order reaction-diffusion equations, the EFK and the SH equation. We have demonstrated how to recognise two types of front solutions, uniform translating and patterned fronts for these two equations. A linear front speed is determined using the double root condition, similar results obtained by the marginal stability mechanism (see, [7, 64, 73]). The double root speed and the associated angular frequency are computed from the resultant of the characteristic equation using the Sylvester's Dialytic Method of Elimination. To ensure the existence of a front, we need to give insight on the character of the double roots and the other two roots (with the help of RH criterion and Descartes' rule of signs, appendix A, as it is hard to obtain the four roots explicitly). The double root has to be slowest decaying one present for the selection mechanism to make sense.

Now in this chapter we have given a brief outline on the properties of a front solution of two examples of reaction-diffusion equation of fourth order. We consider the above analysis as a motivation and a guide in to analyse reaction-diffusion systems. The next chapters are devoted for discussing a two-component reaction-diffusion system. We mainly investigate the instabilities that arise and find a minimal front speed (linear pulled regime). Instabilities in a two-component reaction-diffusion system are discussed in chapter 3, which indicates the kinds of instabilities of rest states. Then we continue with a travelling wave analysis in chapters 4-6.

Chapter 3

Instabilities in Two-Component Reaction-Diffusion Systems

3.1 Introduction

3.1.1 Two-component reaction-diffusion systems

Reaction-diffusion systems can give rise to a number of interesting phenomena, like e.g., threshold behaviour, multiple steady states and hysteresis, spatial patterns, moving fronts or pulses and oscillations. The study of these phenomena needs a variety of different methods from many areas of mathematics, for example numerical methods, bifurcation and stability theory, singular perturbation theory and many others. Linear analysis is a generally used method for evaluating the behaviour of perturbations in a nonlinear system in the vicinity of a stationary state. In linear analysis one takes into account only the terms that are linear in perturbations to the steady state so it cannot predict the post-bifurcation behaviour of the system. However, within its limitations the method is typically quite effective in predicting the existence of an instability and its characteristic wave number [30].

In this chapter we aim to discuss the possible bifurcations that may arise in a two-component reaction-diffusion system. In the case of two-species models (say $U(\mathbf{x},t)$ and $V(\mathbf{x},t)$), the system (1.1) is then in the form

$$
\begin{aligned}
\frac{\partial U}{\partial t} &= D_U \nabla^2 U + F(U,V), \\
\frac{\partial V}{\partial t} &= D_V \nabla^2 V + G(U,V),
\end{aligned}
\tag{3.1}
$$

where F and G are the kinetics, which are the only nonlinear terms that appear in the system. The form of the kinetics F and G in (3.1) determines the behaviour of the system. These terms can be derived from the formulae describing the reaction by using the law of mass action [54] or devised based on phenomenological considerations. There are numerous possibilities for the exact form of the reaction kinetics depending on the chemical reaction being modeled, including the Gray-Scott model [31, 32], the Gierer-Meinhardt model [29], the Schnackenberg model [20, 21], the Brusselator model [12, 48, 81], and the Lengyel-Epstein model [50].

3.1.2 Pattern Forming Phenomena

Pattern formation in mathematics refers to the process that, by changing a bifurcation parameter, a spatially homogeneous steady state loses stability to spatially inhomogeneous perturbations, and stable inhomogeneous solutions may arise. Alan Turing showed in 1952 that a particular mathematical system could produce spatial patterns from an arbitrary initial state [71]. He demonstrated that such a reaction-diffusion system in a closed spatially extended domain could, under appropriate parameter constraints, evolve into a spatially heterogeneous pattern, due to small fluctuations in chemical concentrations initiated by thermal noise alone. This phenomenon was termed diffusion-driven instability [57]. Since Turing's paper, pattern formation in nonlinear complex systems has become

29

one of the central problems of the natural, social, and technological sciences. The study of biological pattern formation has gained popularity since the 1970s: Segel and Jackson [65] were the first to apply Turing's ideas to a problem in population dynamics. At the same time, Gierer and Meinhardt [29] gave a biologically justified formulation of a Turing model and studied its properties by employing numerical simulation. In the literature, many reaction-diffusion models have been proposed and analysed, both mathematically and via numerical simulation (for reviews see, for example [13, 27, 33, 55]). The vast majority of models studied involve only two components since this is the simplest such system that exhibits the fundamental property of diffusion-driven instability.

Nowadays, pattern formation has become a broad interest and stimulates many detailed studies. There are numerous works in the literature concerned with pattern formation studying the types of diffusion instability for two and more species systems. Researchers have been investigating many kinds of spatial, temporal, and spatiotemporal patterns in biology [41, 49, 53], chemistry [50, 57, 75, 80], physics [2, 17, 36], ecology [4, 56, 59] and in epidemiology [51].

3.1.3   Bifurcation

With some control parameters continuously changing, a nonlinear reaction-diffusion system initially in a homogeneous steady state may undergo a bifurcation to form patterns. Studies of reaction-diffusion systems have led to the characterization of three basic types of symmetry-breaking bifurcations (Hopf, Turing, and wave bifurcation), responsible for the emergence of these patterns. The classification of these bifurcations is based on linear stability analysis of a homogeneous state [17, 79].

In the following we analyse different types of bifurcation that may arise in reaction-diffusion systems. Assume that the solution, the perturbation of the linearized version of (3.1), is proportional to $e^{\sigma t + i\vec{k} \cdot \vec{x}}$. The space-independent **Hopf bifurcation** breaks the

temporal symmetry of the system and gives rise to oscillations that are uniform in space and periodic in time and in this case

$$Re(\sigma) = 0, \qquad Im(\sigma) \neq 0 \quad \text{at} \ k = 0, \tag{3.2}$$

If instead this instability is stationary in time, the bifurcation type is called stationary uniform and essentially it does not involve pattern formation (we call this type monotonic in this chapter).

The (stationary) **Turing bifurcation** breaks the spatial symmetry, leading to the formation of patterns that are stationary in time and periodic in space. In this type

$$Re(\sigma) = 0, \qquad Im(\sigma) = 0 \quad \text{at} \ k = k_T \neq 0. \tag{3.3}$$

The **wave bifurcation** (oscillatory Turing or finite-wavelength Hopf) breaks both spatial and temporal symmetries, generating patterns that are periodic in both space and time and in this type

$$Re(\sigma) = 0, \qquad Im(\sigma) \neq 0 \quad \text{at} \ k = k_w \neq 0. \tag{3.4}$$

In reaction-diffusion systems, most studies have been devoted to patterns which emerge in excitable systems near a Hopf bifurcation [24, 37, 70] and to Turing structures arising from Turing instability[14, 37, 55]. More recently, attention has turned towards patterns arising from the wave instability [19, 34, 78, 82]. The wave instability plays an important role in pattern formation in many systems, such as binary fluid convection [16], heterogeneous chemical reactions [15, 62], and electrochemical systems [62].

The individual bifurcations and patterns emerging from them are well characterized. However, there have been fewer studies of the characteristics when the symmetry-breaking instabilities interact. Pattern formation arising from interaction between Hopf and Turing

modes have been analyzed in detail for specific models [25, 52, 61, 81]. Pattern formation arising near the Hopf and wave bifurcations was studied and a large variety of simple and complex patterns were observed [19, 82]. Also, there are systems that possess a range of parameters where Turing and wave instabilities interact and as a result patterns due to this interaction were investigated [75, 79].

In section 2, we give different canonical forms for the linearized system of (3.1). Also, we derive the characteristic equations and the conditions for stability. In section 3.2, we give a discussion when the diffusion ratio $\lambda = D_V/D_U$ is unity, which is a special case as we will see later (this case gives useful information about necessary conditions for pattern formation), and we continue the discussion for both $0 \leq \lambda < 1$ and $\lambda > 1$ in section 4 and 5, respectively. At the end of this chapter, in section 6, we give a summary of the obtained results in the form of tables.

3.2 Linear Stability Analysis

The first stage of pattern formation can usually be investigated by linear stability analysis. In the following subsections, we present some basics of the linear stability analysis that will lead to the dispersion relation, which helps us in constructing the stability diagram (bifurcation diagram).

3.2.1 Linearised system

Assume that system (3.1) has a spatially uniform steady state

$$U(\mathbf{x},t) = U_0, \qquad V(\mathbf{x},t) = V_0, \tag{3.5}$$

where

$$F(U_0, V_0) = 0, \qquad G(U_0, V_0) = 0. \tag{3.6}$$

The above uniform steady state solution can be either stable or unstable in respect to disturbances. In order to examine under what conditions the spatially homogeneous state becomes unstable with respect to small spatially inhomogeneous fluctuations, we perturb the steady state (U_0, V_0) with small perturbations $(\hat{U}(\mathbf{x}, t), \hat{V}(\mathbf{x}, t))$ so that

$$U(\mathbf{x}, t) = U_0 + \hat{U}(\mathbf{x}, t), \tag{3.7}$$

$$V(\mathbf{x}, t) = V_0 + \hat{V}(\mathbf{x}, t). \tag{3.8}$$

We consider the problem in one spatial dimension $\hat{x}$ and to facilitate later rescalings set $t = \hat{t}$. We substitute from (3.7) and (3.8) into (3.1) to obtain

$$\frac{\partial(U_0 + \hat{U})}{\partial \hat{t}} = D_u \frac{\partial^2(U_0 + \hat{U})}{\partial \hat{x}^2} + F(U_0 + \hat{U}, V_0 + \hat{V}), \tag{3.9}$$

$$\frac{\partial(V_0 + \hat{V})}{\partial \hat{t}} = D_v \frac{\partial^2(V_0 + \hat{V})}{\partial \hat{x}^2} + G(U_0 + \hat{U}, V_0 + \hat{V}). \tag{3.10}$$

Now, using the fact that (U_0, V_0) is a uniform steady state solution and linearizing the kinetics, F and G, around the steady state, gives

$$\frac{\partial \hat{U}}{\partial \hat{t}} = D_u \frac{\partial^2 \hat{U}}{\partial \hat{x}^2} + a\hat{U} + b\hat{V}, \tag{3.11}$$

$$\frac{\partial \hat{V}}{\partial \hat{t}} = D_v \frac{\partial^2 \hat{V}}{\partial \hat{x}^2} + c\hat{U} + d\hat{V}, \tag{3.12}$$

where D_u, D_v, a, b, c, and d are all real numbers (the first two are non-negative; the other

four can take either sign) and

$$\begin{pmatrix} a & b \\ c & d \end{pmatrix} = \begin{pmatrix} \frac{\partial F}{\partial U} & \frac{\partial F}{\partial V} \\ \frac{\partial G}{\partial U} & \frac{\partial G}{\partial V} \end{pmatrix}_{(U_0, V_0)}. \tag{3.13}$$

The above linearized system, (3.11)-(3.12), provides the linear stability equations determining the behaviour of small perturbations $(\hat{U}, \hat{V})$ to the steady state solution (U_0, V_0). Now we aim to reduce the number of parameters appearing in these equations to express them in a canonical form. To eliminate the parameter a, we put the solution in the form

$$\hat{U} = e^{a\hat{t}}\hat{u}, \quad \hat{V} = e^{a\hat{t}}\hat{v}. \tag{3.14}$$

Then we substitute into the system (3.11)-(3.12) to obtain

$$\frac{\partial \hat{u}}{\partial \hat{t}} = D_u \frac{\partial^2 \hat{u}}{\partial \hat{x}^2} + b\hat{v}, \tag{3.15}$$

$$\frac{\partial \hat{v}}{\partial \hat{t}} = D_v \frac{\partial^2 \hat{v}}{\partial \hat{x}^2} + c\hat{u} + (d-a)\hat{v}. \tag{3.16}$$

Now, we substitute the following new variables

$$u = \frac{\hat{u}}{b}, \quad v = \frac{\hat{v}}{|d-a|}, \quad x = \sqrt{\frac{|d-a|}{D_u}}\,\hat{x}, \quad t = |d-a|\hat{t}, \tag{3.17}$$

so that (3.15) and (3.16) become

$$\frac{\partial u}{\partial t} = \frac{\partial^2 u}{\partial x^2} + v, \tag{3.18}$$

$$\frac{\partial v}{\partial t} = \lambda \frac{\partial^2 v}{\partial x^2} + \alpha u \pm v, \tag{3.19}$$

34

where

$$\lambda = \frac{D_v}{D_u}, \quad \alpha = \frac{bc}{(d-a)^2},$$
(3.20)

provided that $a \neq d$ and $b \neq 0$, noting that $b \neq 0$ is necessary for the two equations to be coupled fully. The positive sign in (3.19) corresponds to the case when $(d - a) > 0$, and the negative is for $(d - a) < 0$. From the above system, displayed in (3.18) and (3.19), which contains only two parameters, $\lambda \geq 0$ and α, without loss of generality $0 \leq \lambda \leq 1$ holds, but it may sometimes also be convenient to consider $\lambda > 1$.

We assumed above that $a \neq d$ for the validity of (3.17); however, for a comprehensive study we must also take into account the case when $a = d$. In this case, when $a = d$, the system displayed in (3.15) and (3.16) becomes

$$\frac{\partial \hat{u}}{\partial \hat{t}} = D_u \frac{\partial^2 \hat{u}}{\partial \hat{x}^2} + b\hat{v},$$
(3.21)

$$\frac{\partial \hat{v}}{\partial \hat{t}} = D_v \frac{\partial^2 \hat{v}}{\partial \hat{x}^2} + c\hat{u},$$
(3.22)

and for further elimination of parameters, we substitute the following

$$u = \frac{\hat{u}}{\sqrt{|bc|}}, \quad v = \frac{\hat{v}}{c}, \quad x = \sqrt{\frac{\sqrt{|bc|}}{D_u}}\,\hat{x}, \quad t = \sqrt{|bc|}\hat{t},$$
(3.23)

into (3.21) and (3.22) to obtain

$$\frac{\partial u}{\partial t} = \frac{\partial^2 u}{\partial x^2} \pm v,$$
(3.24)

$$\frac{\partial v}{\partial t} = \lambda \frac{\partial^2 v}{\partial x^2} + u.$$
(3.25)

Now, we aim to obtain the eigenvalues of the two systems displayed in (3.18) and (3.19), and also the two systems displayed in (3.24) and (3.25), the four systems are dis-

played in table 3.1. So, in the next two sections we give the derivation of the characteristic equation and also the stability condition corresponding to each system.

Table 3.1: The four different canonical forms of a linearised RD system

System	Equations	Conditions
I	$\dfrac{\partial u}{\partial t} = \dfrac{\partial^2 u}{\partial x^2} + v$ $\dfrac{\partial v}{\partial t} = \lambda \dfrac{\partial^2 v}{\partial x^2} + \alpha u + v$	$G_V - F_U > 0$
II	$\dfrac{\partial u}{\partial t} = \dfrac{\partial^2 u}{\partial x^2} + v$ $\dfrac{\partial v}{\partial t} = \lambda \dfrac{\partial^2 v}{\partial x^2} + \alpha u - v$	$G_V - F_U < 0$
III	$\dfrac{\partial u}{\partial t} = \dfrac{\partial^2 u}{\partial x^2} + v$ $\dfrac{\partial v}{\partial t} = \lambda \dfrac{\partial^2 v}{\partial x^2} + u$	$G_V - F_U = 0, F_V G_U > 0$
IV	$\dfrac{\partial u}{\partial t} = \dfrac{\partial^2 u}{\partial x^2} - v$ $\dfrac{\partial v}{\partial t} = \lambda \dfrac{\partial^2 v}{\partial x^2} + u$	$G_V - F_U = 0, F_V G_U < 0$

3.2.2   The characteristic equation

As the coefficients involved with the systems displayed in equations (3.18)-(3.19) and also (3.24)-(3.25) are constants, we assume the solution of these systems in the Fourier form

$$\begin{pmatrix} u \\ v \end{pmatrix} = \begin{pmatrix} c_1 \\ c_2 \end{pmatrix} e^{\sigma t + ikx}, \tag{3.26}$$

36

where σ is the rate of growth or decay of perturbations, k is the perturbation wave number, and c_1, c_2 are constants. We substitute (3.26) into (3.18) and (3.19) to obtain

$$\left[\sigma \mathbf{I} + k^2 \mathbf{D} - \mathbf{R_1} \right] \mathbf{E} = \mathbf{0}, \tag{3.27}$$

and into (3.24) and (3.25) to obtain

$$\left[\sigma \mathbf{I} + k^2 \mathbf{D} - \mathbf{R_2} \right] \mathbf{E} = \mathbf{0}, \tag{3.28}$$

where $\mathbf{I}$ and $\mathbf{0}$ are the identity and the zero matrix respectively. The matrices $\mathbf{D}$, $\mathbf{R_1}$, $\mathbf{R_2}$, and the vector $\mathbf{E}$ are defined as

$$\mathbf{D} = \begin{pmatrix} 1 & 0 \\ 0 & \lambda \end{pmatrix}, \quad \mathbf{R_1} = \begin{pmatrix} 0 & 1 \\ \alpha & \pm 1 \end{pmatrix}, \quad \mathbf{R_2} = \begin{pmatrix} 0 & \pm 1 \\ 1 & 0 \end{pmatrix}, \quad \mathbf{E} = \begin{pmatrix} c_1 \\ c_2 \end{pmatrix}. \tag{3.29}$$

From the linear algebraic systems displayed in (3.27) and (3.28), the determinant of the coefficient matrix must be zero for nontrivial solutions, and as a result, we obtain a quadratic equation for the eigenvalue σ. In the case of the system displayed in (3.18) and (3.19), $a \neq d$, the characteristic equation is

$$\det \left[\sigma \mathbf{I} + k^2 \mathbf{D} - \mathbf{R_1} \right] = 0, \tag{3.30}$$

and for the system displayed in (3.24) and (3.25), when $a = d$, the characteristic equation is given by

$$\det \left[\sigma \mathbf{I} + k^2 \mathbf{D} - \mathbf{R_2} \right] = 0. \tag{3.31}$$

In each case, the eigenvalues are the two solutions of the relevant characteristic equation (dispersion relation). The eigenvalue σ is thus given as a function of the wave mode

k. In the analysis below, we focus most on the larger of the two roots, since this is the growth rate of the most dangerous perturbation.

3.2.3 Condition for stability

In this section we give expressions for the net growth rate for each case, these help us to find the stability condition(s) and then we can construct the stability diagram. Now let the perturbations $(\hat{U}, \hat{V})$ be such that

$$
\begin{pmatrix} \hat{U} \\ \hat{V} \end{pmatrix} \propto e^{\bar{\sigma}t + i\bar{k}x}, \tag{3.32}
$$

then in the case of $a \neq d$, we refer to (3.14), (3.17), and (3.26), and undo the substitutions (omitting hats) to obtain

$$
\bar{\sigma} = \sigma_{R_1} = a + |d - a|\sigma, \qquad \bar{k} = \sqrt{\frac{|d - a|}{D_u}} k, \tag{3.33}
$$

where σ is the solution of the characteristic equation (3.30). Hence the growth rate, $Re(\sigma_{R_1}^+)$, can be written as

$$
Re(\sigma_{R_1}^+) = a + |d - a| Re(\sigma^+), \tag{3.34}
$$

where σ^+ the larger root of the characteristic equation (3.30), then for a solution to be stable, the maximum of the growth rate, $Re(\sigma_{R_1}^+)_m$, must be negative, i.e. $a + |d - a| Re(\sigma^+)_m < 0$, or equivalently

$$
\delta_1 + Re(\sigma^+)_m \quad < \quad 0 \qquad \text{if} \qquad a \neq d, \tag{3.35}
$$

where $\delta_1 = \frac{a}{|d-a|}$, and σ_m^+ is the maximum of the larger root of the characteristic equation (3.30).

Now we aim to find a stability condition similar to (3.35) in the case $a = d$. When we refer to equations (3.14), (3.23), and (3.26), we find that

$$\overline{\sigma} = \sigma_{R_2} = a + \sqrt{|bc|}\sigma, \qquad \overline{k} = \sqrt{\frac{\sqrt{|bc|}}{D_u}}k, \tag{3.36}$$

where σ is the solution of the characteristic equation (3.31). Hence for stability, $a + \sqrt{|bc|}Re(\sigma^+)_m < 0$, or

$$\delta_2 + Re(\sigma^+)_m \quad < \quad 0 \qquad \text{if} \qquad a = d, \tag{3.37}$$

where $\delta_2 = \frac{a}{\sqrt{|bc|}}$ (provided that $b \neq 0$ and $c \neq 0$), and $Re(\sigma^+)_m$ is the maximum of the larger root of the characteristic equation (3.31).

Making use of the above stability conditions (3.35) and (3.37), we can construct the stability diagram in each case. The stability diagram is a parameter space plot that indicates the stable and unstable regions. We construct these plots at the most unstable wave number k, at which the maximum of $Re(\sigma_{R_1}^+)$ and $Re(\sigma_{R_2}^+)$ occurs, in the two cases $a \neq d$ and $a = d$. Thus we give insights into the change of the eigenvalues σ of the canonical forms of linearised systems (displayed in Table 3.1), due to a change in the wave number k, focusing on the fastest growing mode or the slowest decreasing mode. We study in three separate sections each of the four systems (I, II, III, and IV), see table 3.1, considering equal diffusivity $\lambda = 1$, then $0 \leq \lambda < 1$ and finally $\lambda > 1$. We end each section by a summary table. The tables include k_* which is the wave number corresponding to the fastest growing or the slowest decaying perturbation mode, and σ_* is the corresponding eigenvalue and the corresponding parameter regimes. From these tables we give a comprehensive investigation of the instabilities in a two-component reaction diffusion

systems.

3.3   A : Analysis for $\lambda = 1$

In this section we give a detailed analysis for each case of the four cases shown in table 3.1, considering the diffusion ratio to be unity, i.e. $\lambda = 1$. The results from this case indicate that unequal diffusion coefficients is a necessary condition for stationary periodic and oscillatory periodic instabilities to arise. We study the dispersion relation and its dependence on the system parameters and construct the stability diagram.

3.3.1   Case I

Here we discuss the system of the form

$$\frac{\partial u}{\partial t} \;=\; \frac{\partial^2 u}{\partial x^2} + v, \tag{3.38}$$

$$\frac{\partial v}{\partial t} \;=\; \frac{\partial^2 v}{\partial x^2} + \alpha u + v. \tag{3.39}$$

In this case the characteristic equation is given by (3.30), and referring to (3.29) we find that

$$\mathbf{D} = \begin{pmatrix} 1 & 0 \\ 0 & 1 \end{pmatrix}, \quad \mathbf{R_1} = \begin{pmatrix} 0 & 1 \\ \alpha & 1 \end{pmatrix}, \tag{3.40}$$

then substitute into (3.30) to obtain the quadratic equation

$$\sigma_{A1}^2 + \left[2k^2 - 1\right]\sigma_{A1} + k^4 - k^2 - \alpha = 0, \tag{3.41}$$

where σ_{A1} is the eigenvalue of the system (3.38)-(3.39), and is given by

$$\sigma_{A1} = \frac{1}{2}\left[1 - 2k^2 \pm \sqrt{1 + 4\alpha}\right]. \tag{3.42}$$

From the above form for σ_{A1}, the roots are complex if $\alpha < -1/4$ and real for $\alpha \geq -1/4$. Also, the real part of the larger root, $Re(\sigma_{A1}^{+})$, (the growth rate) can be put in the form

$$Re(\sigma_{A1}^{+}) = \begin{cases} \frac{1}{2}(1 - 2k^2 + \sqrt{1+4\alpha}) & \text{if} \quad \alpha \geq -1/4 \\ \frac{1}{2}(1 - 2k^2) & \text{if} \quad \alpha < -1/4 \end{cases} \tag{3.43}$$

which is a monotonic decreasing function in k. Hence the maximum $Re(\sigma_{A1}^{+})_m$ always occurs at $k = 0$ and appears in the form

$$Re(\sigma_{A1}^{+})_m = \begin{cases} \frac{1}{2}(1 + \sqrt{1+4\alpha}) & \alpha \geq -1/4, & Im(\sigma_{A1}) = 0 \\ \frac{1}{2} & \alpha < -1/4, & Im(\sigma_{A1}) = \frac{1}{2}\sqrt{|1+4\alpha|}. \end{cases} \tag{3.44}$$
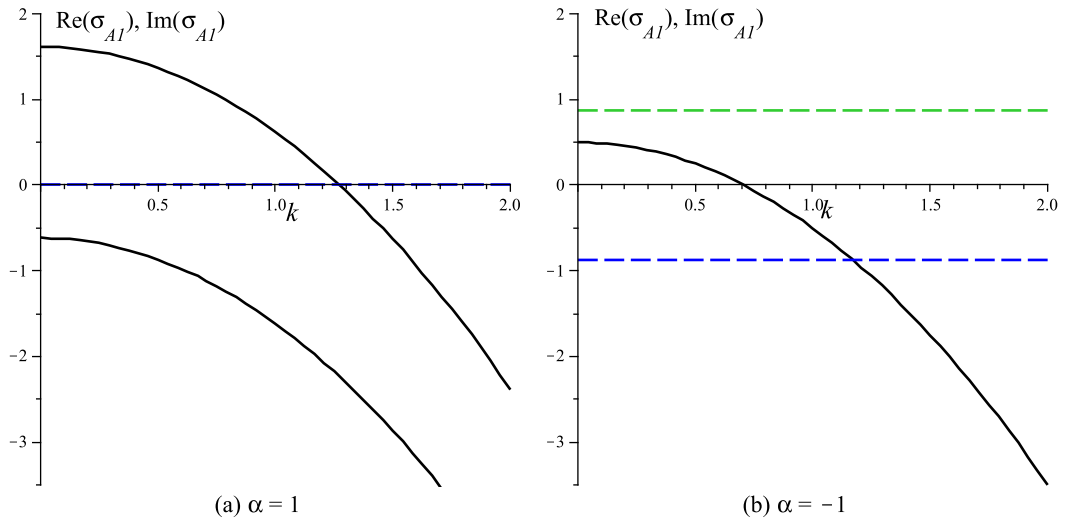
Figure 3.1: The eigenvalues at different values of α, from equation (3.42). (a) $\alpha = 1$, (b) $\alpha = -1$. The solid line represents the real part and the dashed line represents the imaginary.

Figure 3.1 shows the dispersion relation at different values of α and figure 3.2 shows the stability diagram; the boundary curve between the the stable and unstable regions is given by (form (3.35), condition for stability)

$$Re(\sigma_{A1}^{+})_m + \delta_1 = 0 \tag{3.45}$$

41

where $Re(\sigma_{A1}^+)_m$ is given by (3.44). It is obvious that for $\alpha < -1/4$, there is a Hopf bifurcation as the stability is crossed; for $\alpha \geq -1/4$, by contrast, there is a monotonic bifurcation at zero wave number.
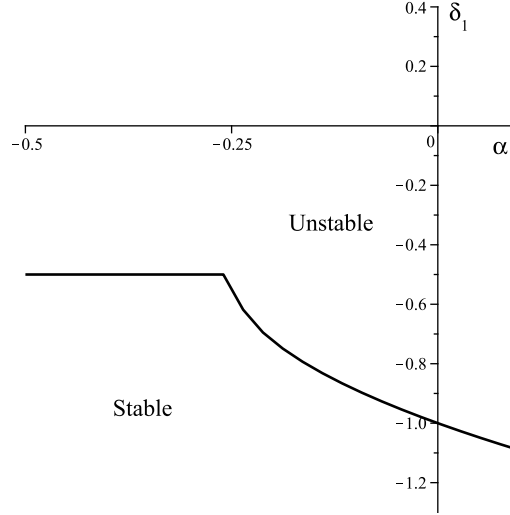
Figure 3.2: The stability diagram for the system shown in (3.38) and (3.39). The boundary between the two regions represents equation (3.45).

3.3.2 Case II

In this subsection we discuss the system

$$\frac{\partial u}{\partial t} = \frac{\partial^2 u}{\partial x^2} + v, \tag{3.46}$$

$$\frac{\partial v}{\partial t} = \frac{\partial^2 v}{\partial x^2} + \alpha u - v. \tag{3.47}$$

The characteristic equation is given by (3.30). From (3.29) and for $\lambda = 1$, we find that

$$\mathbf{D} = \begin{pmatrix} 1 & 0 \\ 0 & 1 \end{pmatrix}, \quad \mathbf{R_1} = \begin{pmatrix} 0 & 1 \\ \alpha & -1 \end{pmatrix}, \tag{3.48}$$

42

then substitute into (3.30) to obtain

$$\sigma_{A2}^2 + \left[2k^2 + 1\right]\sigma_{A2} + k^4 + k^2 - \alpha = 0, \tag{3.49}$$

where σ_{A2} is the eigenvalue of the system (3.46)-(3.47) and hence takes the form

$$\sigma_{A2} = \frac{1}{2}\left[-1 - 2k^2 \pm \sqrt{1 + 4\alpha}\right]. \tag{3.50}$$
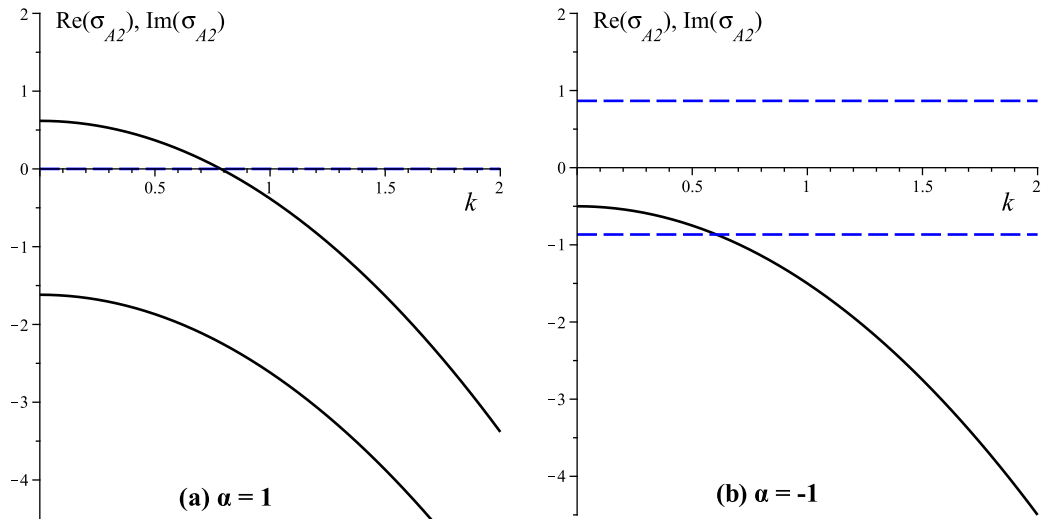
Figure 3.3: The eigenvalues at different values of α, from equation (3.50). (a) $\alpha = 1$, (b) $\alpha = -1$. The solid line represents the real part and the dashed line represents the imaginary part.

Therefore, we can say that the roots are complex if $\alpha < -1/4$ and purely real for $\alpha \geq -1/4$. Also, for the larger eigenvalue, σ_{A2}^+, the real part can be put in the form

$$Re(\sigma_{A2}^+) = \begin{cases} \frac{1}{2}(-1 - 2k^2 + \sqrt{1 + 4\alpha}) & \text{if} \quad \alpha \geq -1/4 \\ \frac{1}{2}(-1 - 2k^2) & \text{if} \quad \alpha < -1/4, \end{cases} \tag{3.51}$$

which is a monotonic decreasing function in k. Hence, the maximum, $Re(\sigma_{A2}^+)_m$ always

43

occurs at $k = 0$ and takes the form

$$Re(\sigma_{A2}^+)_m = \begin{cases} \frac{1}{2}(-1 + \sqrt{1 + 4\alpha}) & \alpha \geq -1/4, \qquad Im(\sigma_{A2}^+) = 0 \\ -\frac{1}{2} & \alpha < -1/4, \quad Im(\sigma_{A2}^+) = \frac{1}{2}\sqrt{|1 + 4\alpha|}. \end{cases} \qquad (3.52)$$
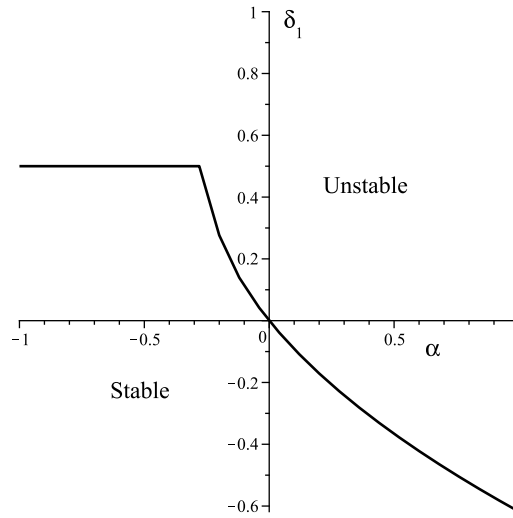
Figure 3.4: The stability diagram for the system displayed in (3.46) and (3.47). The boundary between the two regions represents equation (3.53).

The dispersion relation is shown in figure 3.3 at two different values of α. Figure 3.4 shows the stability diagram, where the curve that separates the two regions is given by (from (3.35), condition for stability)

$$Re(\sigma_{A2}^+)_m + \delta_1 = 0, \qquad (3.53)$$

where $Re(\sigma_{A2}^+)_m$ is given by (3.52). Also, in this case when $\alpha < -1/4$, Hopf instability can arise; when $\alpha \geq -1/4$, monotonic instability at zero wave number may arise.

3.3.3 Case III

In this subsection we discuss the system

$$\frac{\partial u}{\partial t} = \frac{\partial^2 u}{\partial x^2} + v, \qquad (3.54)$$

$$\frac{\partial v}{\partial t} = \frac{\partial^2 v}{\partial x^2} + u, \qquad (3.55)$$

and from (3.29) we substitute

$$\mathbf{D} = \begin{pmatrix} 1 & 0 \\ 0 & 1 \end{pmatrix}, \quad \mathbf{R_2} = \begin{pmatrix} 0 & 1 \\ 1 & 0 \end{pmatrix} \qquad (3.56)$$

into (3.31) to obtain

$$\sigma_{A3}^2 + 2k^2 \sigma_{A3} + k^4 - 1 = 0, \qquad (3.57)$$

where σ_{A3} is the eigenvalue of the system (3.54)-(3.55) and hence is given by

$$\sigma_{A3} = -k^2 \pm 1. \qquad (3.58)$$

The two eigenvlaues are purely real for any value of k and are each a monotonic decreasing function of k. Hence the maximum value of the larger root, $(\sigma_{A3})_m = 1$, always occurs at $k = 0$. Then the maximum growth rate in this case equals $\delta_2 + 1$, and from (3.37), the system is stable if $\delta_2 < -1$ and unstable if $\delta_2 > -1$. We can add that in this case, only a monotonic instability occurs at $k = 0$ (neither Hopf nor Turing bifurcations can arise).

3.3.4 Case IV

In this case the system appears in the form

$$\frac{\partial u}{\partial t} = \frac{\partial^2 u}{\partial x^2} - v, \tag{3.59}$$

$$\frac{\partial v}{\partial t} = \frac{\partial^2 v}{\partial x^2} + u, \tag{3.60}$$

and from (3.29), we substitute

$$\mathbf{D} = \begin{pmatrix} 1 & 0 \\ 0 & 1 \end{pmatrix}, \quad \mathbf{R_2} = \begin{pmatrix} 0 & -1 \\ 1 & 0 \end{pmatrix} \tag{3.61}$$

into (3.31) to obtain the quadratic equation

$$\sigma_{A4}^2 + 2k^2\sigma_{A4} + k^4 + 1 = 0, \tag{3.62}$$

where σ_{A4} is the eigenvalue of the system (3.59)-(3.60), which is thus given by

$$\sigma_{A4} = -k^2 \pm i. \tag{3.63}$$

The two roots are complex conjugates for any value of k. The real part is a monotonic decreasing function of k. Hence the maximum, $Re(\sigma_{A4})_m = 0$, always occurs at $k = 0$. Thus, the maximum growth rate in this case equals δ_2, so the system is stable if $\delta_2 < 0$ and unstable if $\delta_2 > 0$, and we can say that only Hopf bifurcations can occur.

To end this section, we give a summary of the above obtained results in table 3.2, where k_* is the wave number corresponding to the fastest growing or the slowest decaying perturbation mode, and σ_* is the corresponding eigenvalue. We conclude that for $\lambda = 1$ the maximum growth rate always occurs at $k = 0$ and the growth rate is a monotonic

decreasing function of the wave number k. It follows that a Turing instability never arises

for $\lambda = 1$ (i.e. $D_U = D_V$); this is consistent with the established result that a Turing

bifurcation requires the diffusion coefficients to be different [55]. However, there can be

oscillatory (Hopf) and/or monotonic instability at $k = 0$.

Table 3.2: Instabilities for the four systems when $\lambda = 1$

System	k_*^2	$Re(\sigma_*)$	$Im(\sigma_*)$	Conditions	Kind of Bifn.
I	0	$\frac{1}{2}(1+\sqrt{1+4\alpha})$	0	$\alpha \geq -1/4$	Monotonic
	0	$\frac{1}{2}$	$\frac{1}{2}(\sqrt{\|1+4\alpha\|})$	$\alpha < -1/4$	Hopf
II	0	$\frac{1}{2}(-1+\sqrt{1+4\alpha})$	0	$\alpha \geq -1/4$	Monotonic
	0	$-\frac{1}{2}$	$\frac{1}{2}(\sqrt{\|1+4\alpha\|})$	$\alpha < -1/4$	Hopf
III	0	1	0	$--$	Monotonic
IV	0	0	1	$--$	Hopf

3.4 B : Analysis for $0 \leq \lambda < 1$

In the previous section we studied how the eigenvalues behave for the four different cases

assuming that $\lambda = 1$. In this section we study the previous stated four systems I, II, III,

and IV, but when $0 \leq \lambda < 1$.

3.4.1 Case I

Here we discuss the system

$$\frac{\partial u}{\partial t} = \frac{\partial^2 u}{\partial x^2} + v, \tag{3.64}$$

$$\frac{\partial v}{\partial t} = \lambda \frac{\partial^2 v}{\partial x^2} + \alpha u + v. \tag{3.65}$$

In this case the characteristic equation is given by (3.30), and referring to (3.29), we find that

$$\mathbf{D} = \begin{pmatrix} 1 & 0 \\ 0 & \lambda \end{pmatrix}, \quad \mathbf{R_1} = \begin{pmatrix} 0 & 1 \\ \alpha & 1 \end{pmatrix}, \tag{3.66}$$

then we substitute into (3.30) to obtain

$$\sigma_{B1}^2 + \left[(1+\lambda)k^2 - 1\right]\sigma_{B1} + \lambda k^4 - k^2 - \alpha = 0, \tag{3.67}$$

where σ_{B1} is the eigenvalue of the system (3.64)-(3.65), and given by

$$\sigma_{B1} = \frac{1}{2}\left[1 - (1+\lambda)k^2 \pm \sqrt{[1 + (1-\lambda)k^2]^2 + 4\alpha}\right]. \tag{3.68}$$
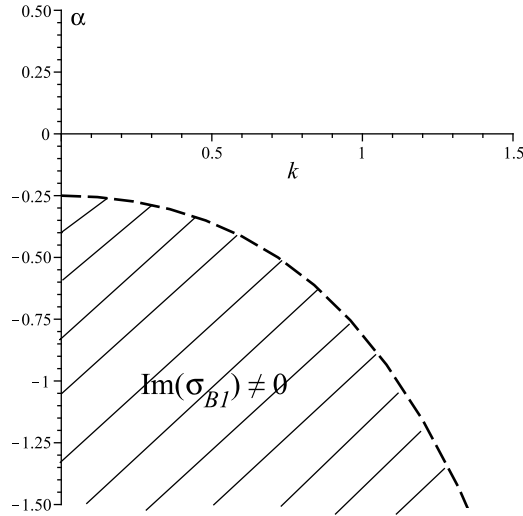
Figure 3.5: Typical domain for complex eigenvalues, σ_{B1}, $0 < \lambda < 1$. The dashed curve shows, for $\lambda = 0.5$, the condition for a repeated root (switch between purely real and complex eigenvalues), given by $[1 + k^2/2]^2 + 4\alpha = 0$.

Figure 3.5 shows the domain for complex eigenvalues when $\lambda = 0.5$. For $\alpha \geq -1/4$, the two eigenvalues are purely real, for whatever values of k and λ. For $\alpha < -1/4$, the eigenvalues are complex when $0 \leq k < k_r$, then the roots change to purely real when

$k \geq k_r$, where

$$k_r = \left(\frac{(-4\alpha)^{1/2} - 1}{1 - \lambda} \right)^{1/2}, \tag{3.69}$$

which is the wave number at which a repeated root exists. Also, we see from (3.68) that for large values of k the two roots are pure real and distinct and take the approximate values $-\lambda k^2$ and $-k^2$, respectively, consistent with the dominance of the diffusion terms in (3.64)-(3.65) in that limit. When λ is close to 1 the dashed curve opens to be the horizontal line $\alpha = -1/4$, consistent with the earlier results of section 3.3.1.

In our analysis, we need to examine the extreme values for the real part of the larger root (growth rate), which is useful in the linear stability analysis, where we focus most on the most positive eigenvalue. Since the eigenvalues may change from complex to real as k increases (when $\alpha < -1/4$), in order to determine the maximum growth rate over all k, we need to consider both types of eigenvalues, then determine the global maximum.

Let us discuss first the case when the eigenvalues are complex. This case may arise only when $\alpha < -1/4$, and for small k (i.e. $0 \leq k < k_r$). From (3.68), when the eigenvalues are complex, the real part is

$$Re(\sigma_{B1}) = \frac{1}{2} \left[1 - (1 + \lambda)k^2 \right], \tag{3.70}$$

which is a monotonic decreasing function of k; the maximum value is $1/2$, occuring at $k = 0$. Therefore, we can say that

$$Re(\sigma_{B1}) \leq \frac{1}{2} \quad \text{and} \quad Im(\sigma_{B1}) \neq 0 \quad \text{when} \quad \alpha < -1/4 \quad \text{and} \quad 0 \leq k < k_r. \tag{3.71}$$

When the roots are purely real, we aim to examine any maxima of σ_{B1}. Let σ_{B1} have a maximum at $k = k_*$, differentiate both sides of (3.68), focusing on the larger root, then

49

from the condition

$$\left(\frac{d\sigma_{B1}}{dk}\right)_{k=k_*} = 0, \tag{3.72}$$

we obtain

$$k_*^2 \left[\lambda \left((1-\lambda)k_*^2 + 1\right)^2 + (1+\lambda)^2\alpha\right] = 0. \tag{3.73}$$

We try to find the possible solutions for (3.73), the non-negative real values of k_*, and the corresponding values of σ_{B1}. The first possible solution is

$$k_* = k_{B11} = 0, \tag{3.74}$$

then we substitute into the dispersion relation (3.68), for the bigger root, to obtain the first maximum, σ_{B11} that given by

$$\sigma_{B11} = \frac{1}{2}\left(1 + \sqrt{1+4\alpha}\right), \qquad \alpha \geq -1/4, \tag{3.75}$$

Thus the first possibility for a maximum value, σ_{B11} (purely real), exists at $k = 0$ and when $\alpha \geq -1/4$.

The second possible nonnegative root of (3.73) is $k_* = k_{B12}$ that satisfies

$$\lambda \left((1-\lambda)k_{B12}^2 + 1\right)^2 + (1+\lambda)^2\alpha = 0, \tag{3.76}$$

which gives

$$k_{B12}^2 = \frac{1}{1-\lambda}\left[-1 + \sqrt{\frac{-\alpha(1+\lambda)^2}{\lambda}}\right], \qquad 0 < \lambda < 1, \tag{3.77}$$

provided that

$$\lambda + \alpha(1+\lambda)^2 \leq 0, \tag{3.78}$$

and hence α must be non-positive for the existence of a maximum at $k_* = k_{B12}$ and from (3.69)

$$
\begin{aligned}
k_{B12}^2 - k_r^2 &= \frac{1}{1-\lambda}\left[-1 + \sqrt{\frac{-\alpha(1+\lambda)^2}{\lambda}}\right] - \left(\frac{(-4\alpha)^{1/2} - 1}{1-\lambda}\right) \\
&= \frac{(-\alpha)^{1/2}(1-\lambda^{1/2})^2}{\lambda^{1/2}(1-\lambda)} > 0,
\end{aligned}
$$

hence k_{B12} is always greater than k_r as we will see in plotting the eigenvalues versus the wave number $(k_{B12} > k_r)$. The value of the maximum σ_{B12} can be obtained by direct substitution of k_{B12} into (3.68) or differentiating (3.67) with respect to k, to give

$$
2\sigma_{B1}\frac{d\sigma_{B1}}{dk} + \left((1+\lambda)k^2 - 1\right)\frac{d\sigma_{B1}}{dk} + 2(1+\lambda)k\sigma_{B1} + 4\lambda k^3 - 2k = 0,
$$

then the condition shown in (3.72), after substituting $k = k_{B12}$ and $\sigma_{B1} = \sigma_{B12}$, gives

$$
\sigma_{B12} = \frac{1 - 2\lambda k_{B12}^2}{1+\lambda}, \tag{3.79}
$$

provided that the condition (3.78) is satisfied.

We construct a graph in α, λ space (figure 3.6) in which we show the regions where the maximum occurs and the corresponding nature of the eigenvalue. From the above analysis, we conclude that there is always a maximum at $k = 0$. If $\alpha \geq -\frac{1}{4}$ (regions I and II in figure 3.6), the roots are pure real and there is a maximum, σ_{B11}, given by (3.75), and if $\alpha < -\frac{1}{4}$ (regions III and IV), the roots are complex, then we consider the real part of the roots, hence we find that the real part has a maximum which is $1/2$ (see (3.71)). Furthermore, there can also be a maximum at a positive k (regions II, III, and IV), the roots are pure real and this maximum, σ_{B12}, is given by (3.79), and occurs at $k = k_{B12}$
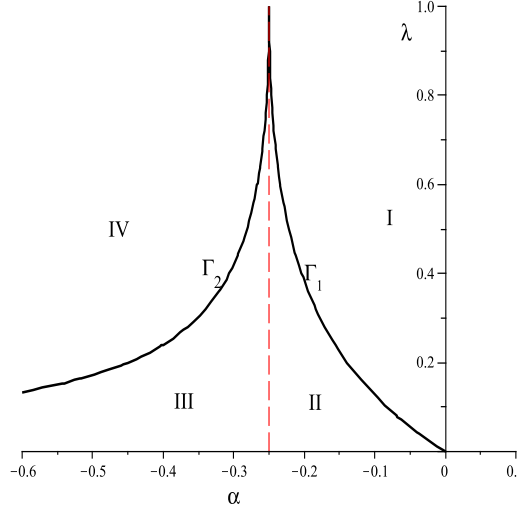
Figure 3.6: The α, λ space, Γ_1 given by $\lambda + \alpha(1+\lambda)^2 = 0$, and Γ_2 given by $(1+\lambda)^2 + 16\lambda\alpha = 0$. Region I (on the right of Γ_1): the maximum of the growth rate occurs at $k = 0$ and $Im(\sigma_{B1}) = 0$. Regions II and III (bounded by Γ_1 and Γ_2): the maximum occurs at $k > 0$ and $Im(\sigma_{B1}) = 0$. Region IV: the maximum equals to $1/2$ and occurs at $k = 0$, $Im(\sigma_{B1}) \neq 0$.

displayed in (3.77); see figure 3.7, which shows constant-k contours inside the regions I, II and III, these curves represent equation (3.76) at different value of k_{B12}.

Next we determine the global maximum of the larger root in the different regions in α, λ space, that gives insights on the most unstable wave number. In region I, figure 3.7, the only existing maximum is σ_{B11}, which occurs at zero wave number, hence the most dangerous wave number is $k = 0$ and as the eigenvalues are pure real, only a monotonic bifurcation may exist. In regions II and III (bounded by the curves Γ_1 and Γ_2) σ_{B12} is the maximum. However in region IV, $1/2$, which is the real part of the complex root is the maximum (see (3.71)). We can prove that as follows. We substitute k_{B12} from (3.77) into (3.79)

$$\sigma_{B12} = \frac{1}{1+\lambda}\left[1 - \frac{2\lambda}{1-\lambda}\left(-1 + \sqrt{\frac{-\alpha(1+\lambda)^2}{\lambda}}\right)\right],$$

52
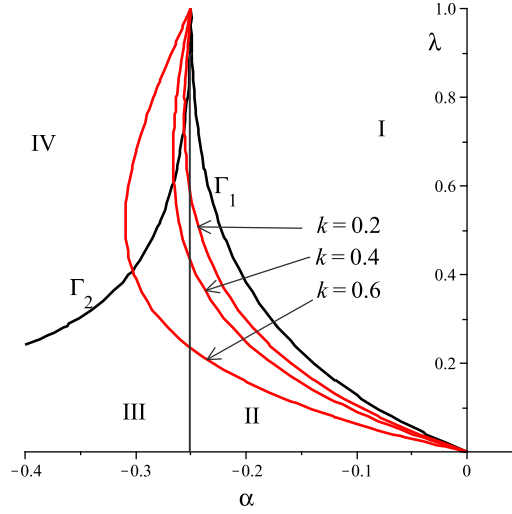
Figure 3.7: The α, λ space, constant k-contours are shown in the region left to Γ_1 in a maximum, σ_{B12} occurs at $k = k_{B12} > 0$ and $Im(\sigma_{B1}) = 0$, (shown are $k = 0.2, 0.4$ and 0.6), represent equation (3.76).

then we simplify to obtain

$$\sigma_{B12} = \frac{1}{1-\lambda}\left[1 - 2(-\alpha\lambda)^{1/2}\right]. \tag{3.80}$$

Now in region II where $-1/4 < \alpha < 0$, σ_{B12} and σ_{B11} are increasing functions of α. Therefore, they take their minimum values at $\alpha = -1/4$, then when we substitute $\alpha = -1/4$ into (3.80) and (3.75), respectively, we can say that $\sigma_{B12} > 1/(1+\lambda^{1/2})$ and $\sigma_{B11} > 1/2$. From this result, we can say that $\sigma_{B12} - \sigma_{B11} > 1/(1+\lambda^{1/2}) - 1/2$, then we simplify to obtain $\sigma_{B12} - \sigma_{B11} > (1-\lambda^{1/2})/2(1+\lambda^{1/2}) > 0$, hence we find that $\sigma_{B12} > \sigma_{B11}$, i.e., σ_{B12} is the maximum in region II and as this maximum occurs at a non-zero value of k, $k = k_{B12}$, that means Turing bifurcation can exist. In regions III and IV, when $\alpha < -1/4$, there are two maximum values, σ_{B12} that occurs at $k = k_{B12}$ and $1/2$ which is the real part of a complex eigenvalue that arise at $k = 0$. From (3.80)

$$\sigma_{B12} - \frac{1}{2} = \frac{1}{1-\lambda}\left[1 - 2(-\alpha\lambda)^{1/2}\right] - 1/2,$$

53

then rearranging terms gives

$$2(1-\lambda)(\sigma_{B12} - \frac{1}{2}) = 1 + \lambda - 4\sqrt{-\alpha\lambda}, \qquad (\alpha < -1/4). \qquad (3.81)$$

Hence for $0 \leq \lambda < 1$, $\sigma_{B12} = \frac{1}{2}$ if $1 + \lambda - 4\sqrt{-\alpha\lambda} = 0$ or equivalently, $(1+\lambda)^2 + 16\alpha\lambda = 0$, which represents the boundary curve between regions III and IV (the curve Γ_2, see figure 3.7). Also, we can say that for $\alpha < -1/4$ and $(1+\lambda)^2 + 16\alpha\lambda > 0$ (region III), $\sigma_{B12} > 1/2$, and as a result, σ_{B12} is the maximum in region III and Turing bifurcations may exist. However, when $(1+\lambda)^2 + 16\alpha\lambda < 0$ (region IV), $\sigma_{B12} < 1/2$, and then the real part of the complex root at $k = 0$ (which is $1/2$) is the maximum, and as a result there can be a Hopf bifurcation. Figure 3.8 shows the variation of the eigenvalues with k at different values of λ ($\lambda = 0.2, 0.5, 0.7$). Figure 3.8(a) shows the transition between regions I and II (occurs at $\lambda = 1/2$), figure 3.8(b) shows the eigenvalues on the border line between the two regions II and III (at $\alpha = -1/4$), and the switching between regions III and IV (transition between Hopf and Turing bifurcations takes place at $\lambda = 0.5$) is shown in figure 3.8(c).

From the above discussion, we can obtain the maximum value of the growth rate, $Re(\sigma_{B1}^+)_m$, which helps us in constructing the stability diagram. This depends on the regions in the α, λ space, as follows:

$$Re(\sigma_{B1}^+)_m = \begin{cases} \sigma_{B11} & \text{region I} \\ \sigma_{B12} & \text{regions II and III} \\ 1/2 & \text{region IV}, \end{cases}$$
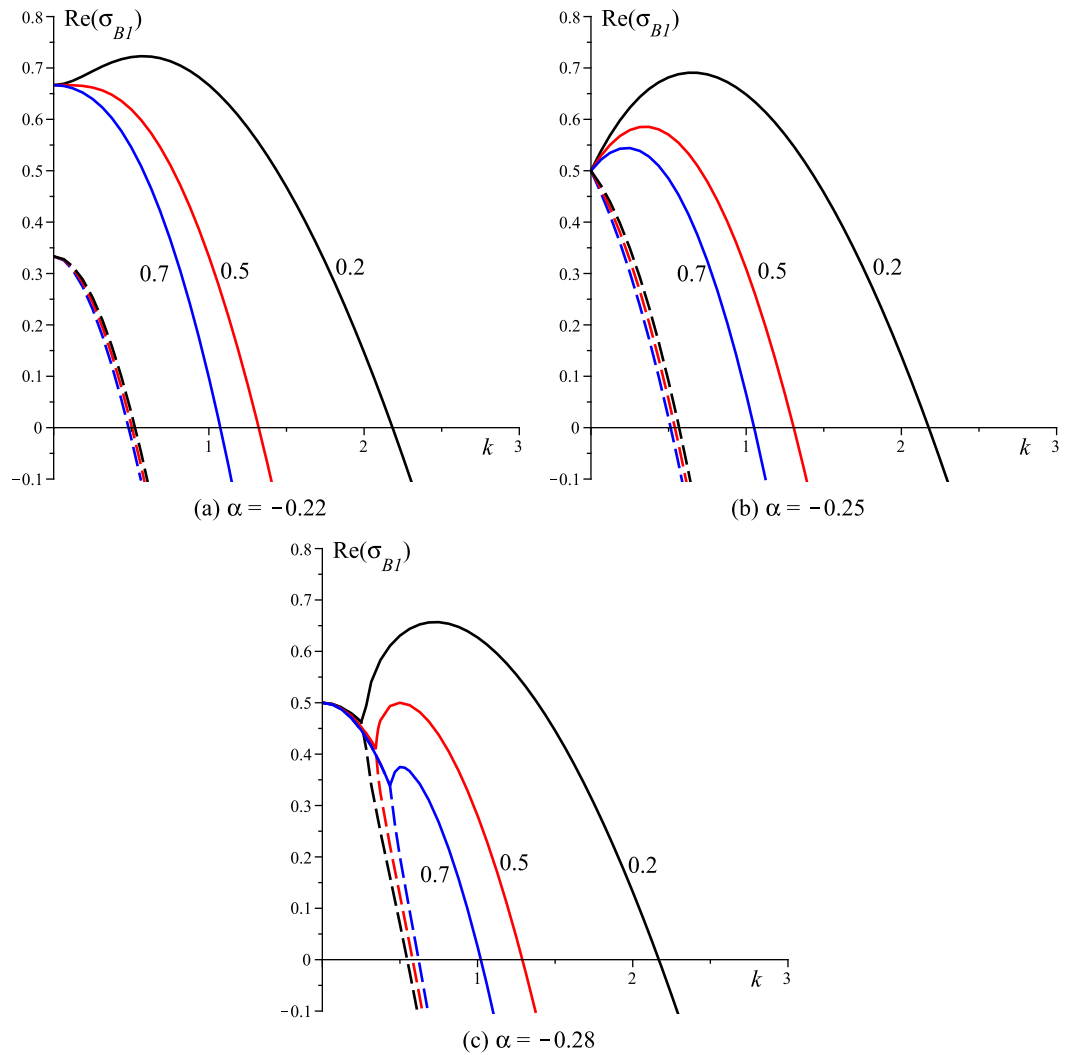
Figure 3.8: Variation of the eigenvalues with k at different values of λ, ($\lambda = 0.2, 0.5, 0.7$) (a) $\alpha = -0.22$, the transition between the two regions I and II, (b) $\alpha = -0.25$, the boundary between II and III, (d) $\alpha = -0.28$, transition between III and IV (In (c) $\lambda = 0.2$ seems to give Turing and $\lambda = 0.7$ seems to give Hopf, $\lambda = 0.5$ is a critical value).

or can be written as

$$Re(\sigma^+_{B1})_m = \begin{cases} \frac{1}{2}(1+\sqrt{1+4\alpha}) & \alpha \geq \frac{-\lambda}{(1+\lambda)^2}, & Im(\sigma_{B1}) = 0 \\ \frac{1-2\lambda k^2_{B12}}{1+\lambda} & \frac{-(1+\lambda)^2}{16\lambda} \leq \alpha < \frac{-\lambda}{(1+\lambda)^2}, & Im(\sigma_{B1}) = 0 \\ 1/2 & \alpha < \frac{-(1+\lambda)^2}{16\lambda}, & Im(\sigma_{B1}) = \sqrt{|\alpha+1/4|}, \end{cases}$$

(3.82)

where k_{B12} is given by (3.77), and from this relation and referring to (3.34) and (3.35), we can construct the stability diagram. Figure 3.9 shows this diagram at different values of λ.
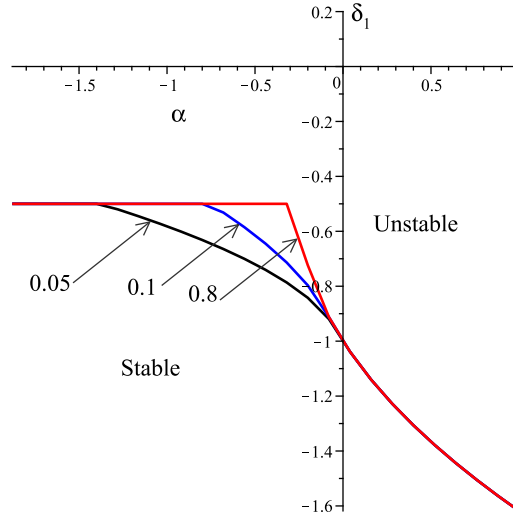
Figure 3.9: The stability diagram for different values of λ, $\lambda = 0.05, 0.1$ and 0.8. The equation of the boundary curve is given by $Re(\sigma^+_{B1})_m + \delta_1 = 0$.

Finally, we conclude that in this case, a monotonic bifurcation can exist at $k = 0$ in region I and Turing in regions II and III (see figure 3.8). Also, on the boundary curve Γ_2, $\alpha = \frac{-(1+\lambda)^2}{16\lambda}$, between regions III and IV, the switch between Turing and Hopf bifurcations takes place. A Hopf bifurcation exists in region IV, while Turing arises in region III (see figure 3.8(c)). Furthermore, when $\lambda = 0$ a Turing bifurcation arises only when $\alpha < 0$, and Hopf does not exist.

3.4.2 Case II

Here we discuss the system

$$\frac{\partial u}{\partial t} = \frac{\partial^2 u}{\partial x^2} + v, \tag{3.83}$$

$$\frac{\partial v}{\partial t} = \lambda \frac{\partial^2 v}{\partial x^2} + \alpha u - v. \tag{3.84}$$

The characteristic equation is given by (3.30), and from (3.29)

$$\mathbf{D} = \begin{pmatrix} 1 & 0 \\ 0 & \lambda \end{pmatrix}, \quad \mathbf{R_1} = \begin{pmatrix} 0 & 1 \\ \alpha & -1 \end{pmatrix}, \tag{3.85}$$

then we substitute into (3.30) to obtain

$$\sigma_{B2}^2 + \left[(1+\lambda)k^2 + 1 \right] \sigma_{B2} + \lambda k^4 + k^2 - \alpha = 0, \tag{3.86}$$

and hence the two eigenvalues are

$$\sigma_{B2} = \frac{1}{2} \left[-1 - (1+\lambda)k^2 \pm \sqrt{\left[(1-\lambda)k^2 - 1 \right]^2 + 4\alpha} \right]. \tag{3.87}$$

Figure 3.10 shows the domain for the complex eigenvalue (computed at $\lambda = 0.5$). When λ is close to unity, the curve opens to be the line $\alpha = -1/4$. Also, the eigenvalues are complex when $-1/4 < \alpha < 0$ and $k_1 < k < k_2$, and also when $\alpha < -1/4$ and $0 \le k < k_2$, where k_1 and k_2 (wave numbers where a repeated root exists) are given by

$$k_1 = \sqrt{\frac{1}{1-\lambda}(1 - 2\sqrt{-\alpha})}, \qquad -1/4 < \alpha < 0, \tag{3.88}$$

$$k_2 = \sqrt{\frac{1}{1-\lambda}(1 + 2\sqrt{-\alpha})}, \qquad \alpha < 0. \tag{3.89}$$
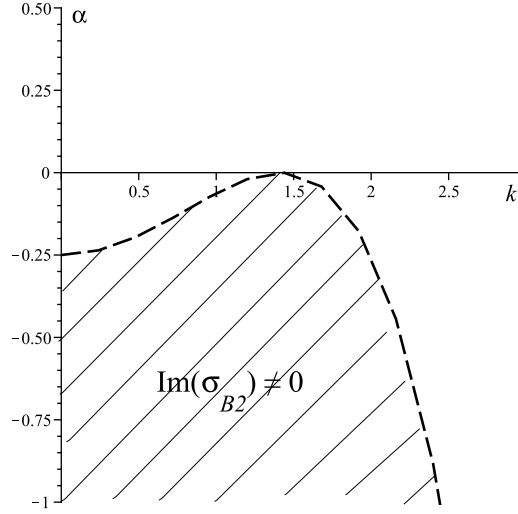
Figure 3.10: Typical domain for a complex root displayed in (3.87), $\lambda < 1$. The graph for $\lambda = 0.5$ and the dashed curve represents $(k^2/2 - 1)^2 + 4\alpha = 0$.

We follow a similar method to the previous case to examine the extreme values of the bigger root in this case. In this case, σ_{B2} has always a maximum at $k = 0$ (say σ_{B21}). When $\alpha \geq -1/4$, σ_{B2} is real (purely real root, see figure 3.10), and σ_{B21} is given by

$$\sigma_{B21} = \frac{1}{2}\left(-1 + \sqrt{1 + 4\alpha}\right) \geq -1/2, \qquad \alpha \geq -\frac{1}{4}, \qquad (3.90)$$

and when $\alpha < -1/4$, $-1/2$ is the maximum value of the real part of σ_{B2} and $Im(\sigma_{B2}) = \frac{1}{2}\sqrt{1 + 4\alpha} \neq 0$. Furthermore, there can also be a maximum at a non-zero value of k (at which the root is pure real), this positive value of the wave number can be obtained as follows. Suppose that σ_{B2} has a maximum at $k = k_*$, we differentiate both sides of (3.87) with respect to k, focusing on the larger root, then we substitute the condition of the maxima to obtain

$$k_*^2\left[\lambda\left((1-\lambda)k_*^2 - 1\right)^2 + (1+\lambda)^2\alpha\right] = 0, \qquad (3.91)$$

58

then we solve for a possible positive root of (3.91), $k_* = k_{B21}$, which has the form

$$k_{B22}^2 = \frac{1}{1-\lambda}\left[1 + \sqrt{\frac{-\alpha(1+\lambda)^2}{\lambda}}\right], \qquad 0 < \lambda < 1, \quad \alpha \leq 0, \qquad (3.92)$$

and from (3.89)

$$
\begin{aligned}
k_{B22}^2 - k_2^2 &= \frac{1}{1-\lambda}\left[1 + \sqrt{\frac{-\alpha(1+\lambda)^2}{\lambda}}\right] - \frac{1}{1-\lambda}(1 - 2\sqrt{-\alpha}) \\
&= \frac{\sqrt{-\alpha}(1 - \sqrt{\lambda})^2}{\sqrt{\lambda}(1-\lambda)} > 0,
\end{aligned}
$$

hence we can say $k_{B22} > k_2$ (see figure 3.11 (b) and (c)).

The value of σ_{B22} can be obtained by differentiating (3.86) with respect to k then substituting the condition for a maximum and inserting $k = k_{B22}$ into the result to obtain

$$\sigma_{B22} = -\frac{1 + 2\lambda k_{B22}^2}{1+\lambda}, \qquad \alpha \leq 0. \qquad (3.93)$$

Now we aim to check the global maximum, which corresponds to the most unstable wave number. First, for $\alpha \geq 0$ (see figure 3.11(a)), there is only one maximum, which occurs at zero wave number, σ_{B21}, given by (3.90) and as the roots are pure real, there is a monotonic bifurcation at $k = 0$. Second, for $-1/4 \leq \alpha < 0$ (see figure 3.11(b), eigenvalues at $\alpha = -0.15$), there are two maximum values where the roots are pure real, σ_{B21} and σ_{B22}, and in the following we aim to examine which one is the global maximum. From (3.93)

$$
\begin{aligned}
\sigma_{B22} + \frac{1}{2} &= -\frac{1 + 2\lambda k_{B22}^2}{1+\lambda} + \frac{1}{2} \\
&= -\frac{1-\lambda}{2(1+\lambda)} - \frac{2\lambda k_{B22}^2}{(1+\lambda)} < 0, \qquad (3.94)
\end{aligned}
$$

hence $\sigma_{B22} < -1/2$, and as $-1/2 \leq \sigma_{B21} < 0$ when $-1/4 \leq \alpha < 0$ (see (3.90)), then

59
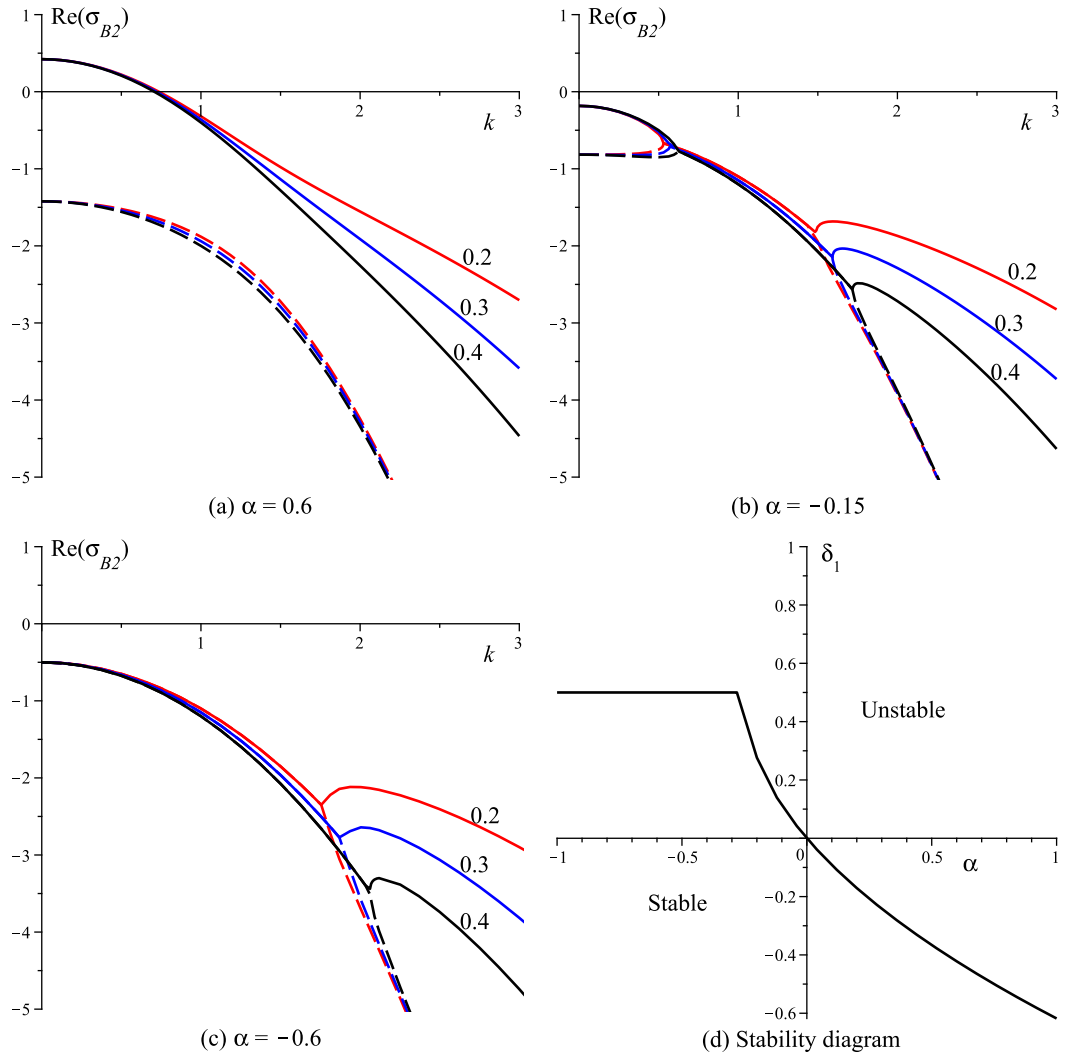
Figure 3.11: The real part of the eigenvalues (equation (3.87)) at $\lambda = 0.2, 0.3$ and 0.4, (a) $\alpha = 0.6$, (b) $\alpha = -0.15$, and (c) $\alpha = -0.6$ (Hopf bifurcation). (d) The stability diagram; the equation of the boundary curve is given by $Re(\sigma_{B2}^+)_m + \delta_1 = 0$

σ_{B21} is the maximum, and since the roots are pure real it follows that there is a monotonic bifurcation at $k = 0$. Third and finally, for $\alpha < -1/4$ (see figure 3.11(c), the eigenvalues at $\alpha = -0.6$), there two maximum values: the first is $-1/2$, which occurs at $k = 0$ where the eigenvalues are complex, and the second is σ_{B22}, which occurs at a positive wave number $k = k_{B22}$ where the eigenvalues are pure real. From (3.94), as $\sigma_{B22} < -1/2$ then the global maximum is the first (the real part of a complex root that occurs at $k = 0$), and hence a Hopf bifurcation can arise.

From the above discussion we can say that the maximum of the real part of the larger root $Re(\sigma_{B2}^+)_m$ can be written as

$$Re(\sigma_{B2}^+)_m = \begin{cases} \frac{1}{2}(-1 + \sqrt{1 + 4\alpha}) & \alpha \geq -1/4, \qquad Im(\sigma_{B2}) = 0 \\ -\frac{1}{2} & \alpha < -1/4, \quad Im(\sigma_{B2}) = \frac{1}{2}\sqrt{|1 + 4\alpha|} \end{cases} \qquad (3.95)$$

In figure 3.11, we show in (a), (b), and (c) the dispersion relation at different values of α and λ, and the stability diagram in (d). In this case, we conclude that the most unstable wave number is $k = 0$ and the associated eigenvalue is given by (3.95). Therefore, there is no Turing instability; however, a monotonic bifurcation can exist at $k = 0$ when $\alpha \geq -1/4$, and a Hopf bifurcation can exist when $\alpha < -1/4$.

3.4.3 Case III

In this subsection we consider the system

$$\frac{\partial u}{\partial t} = \frac{\partial^2 u}{\partial x^2} + v, \qquad (3.96)$$

$$\frac{\partial v}{\partial t} = \lambda \frac{\partial^2 v}{\partial x^2} + u. \qquad (3.97)$$

From (3.29) we substitute

$$\mathbf{D} = \begin{pmatrix} 1 & 0 \\ 0 & \lambda \end{pmatrix}, \quad \mathbf{R_2} = \begin{pmatrix} 0 & 1 \\ 1 & 0 \end{pmatrix}, \tag{3.98}$$

into (3.31) to obtain

$$\sigma_{B3}^2 + (1+\lambda)k^2\sigma_{B3} + \lambda k^4 - 1 = 0, \tag{3.99}$$

and hence the two eigenvalues of the system (3.96)-(3.97) are given by

$$\sigma_{B3} = \frac{1}{2}\left[-(1+\lambda)k^2 \pm \sqrt{(1-\lambda)^2 k^4 + 4}\right]. \tag{3.100}$$

For all values of λ and wave number k, the eigenvalues are pure real. Also, the maximum value of the larger root, $(\sigma_{B3}^+)_m = 1$ and occurs at $k = 0$. To show this, we assume that the larger root, σ_{B3}^+, has its maximum at $k = k_*$, then

$$\left(\frac{d}{dk}\sigma_{B3}^+\right)_{k=k_*} = 0,$$

or

$$k_*(\lambda(1-\lambda)^2 k_*^4 + (1+\lambda)^2) = 0, \tag{3.101}$$

which has only one possible solution $k_* = 0$. Figure 3.12 shows the two eigenvalues when $\lambda = 0.5$.

In this case, the roots are pure real for any value of k and λ. The roots are monotonic decreasing functions in k and the maximum value of the larger root, $(\sigma_{B3})_m = 1$, which occurs at $k = 0$ for any λ. Hence, the system is stable if $\delta_2 < -1$ and unstable if $\delta_2 > -1$ and neither Hopf nor Turing bifurcation can exist, only monotonic bifurcation can arise. Also, we can say that, as the most unstable wave number and the growth rate are independent of λ, the above analysis also applies when we discuss the system (3.96)-
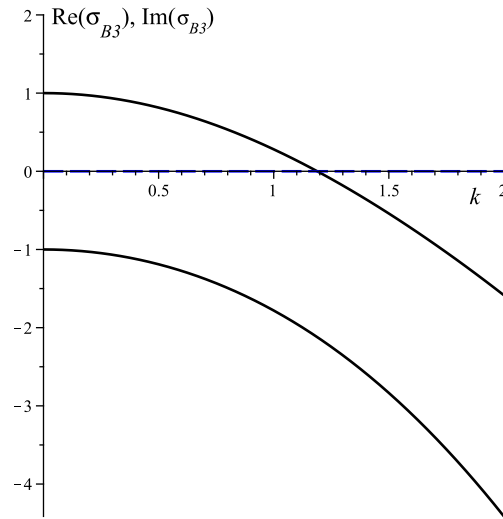
Figure 3.12: The eigenvalues of the system (3.96)-(3.97), given by equation (3.100), at $\lambda = 0.5$. The eigenvalues are pure real roots and we see that the maximum of each occurs at $k = 0$.

(3.97) in the next section in case C3 when $\lambda > 1$.

3.4.4 Case IV

In this subsection we are concerned with the system

$$\frac{\partial u}{\partial t} = \frac{\partial^2 u}{\partial x^2} - v, \tag{3.102}$$

$$\frac{\partial v}{\partial t} = \lambda \frac{\partial^2 v}{\partial x^2} + u, \tag{3.103}$$

and from (3.29) we substitute

$$\mathbf{D} = \begin{pmatrix} 1 & 0 \\ 0 & \lambda \end{pmatrix}, \quad \mathbf{R_2} = \begin{pmatrix} 0 & -1 \\ 1 & 0 \end{pmatrix} \tag{3.104}$$

into (3.31) to obtain

$$\sigma_{B4}^2 + (1+\lambda)k^2\sigma_{B4} + \lambda k^4 + 1 = 0, \tag{3.105}$$

63

and hence the two roots are given by

$$\sigma_{B4} = \frac{1}{2}\left[-(1+\lambda)k^2 \pm \sqrt{(1-\lambda)^2 k^4 - 4}\right]. \tag{3.106}$$
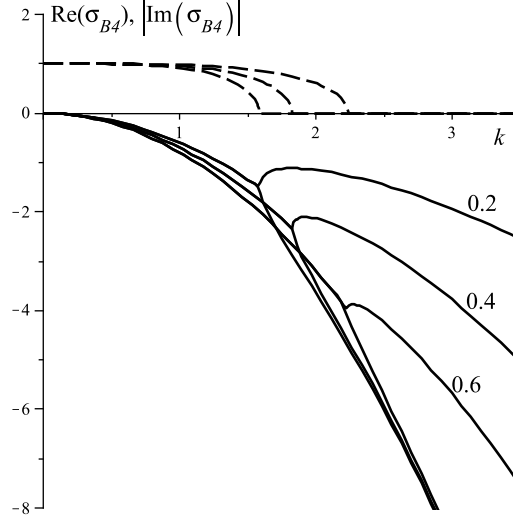
Figure 3.13: The eigenvalues σ_{B4} of the system (3.102)-(3.103), given by equation (3.106), at $\lambda = 0.2, 0.4$ and 0.6. The maximum occurs at $k = 0$, where the roots are pure complex (Hopf bifurcation).

The two roots are complex for $0 \leq k < \sqrt{2/|1-\lambda|}$ and pure real for $k \geq \sqrt{2/|1-\lambda|}$ at any value of $\lambda \neq 1$ (for $\lambda = 1$ the roots are complex, studied in subsection 3.3.4). Figure 3.13 shows the roots, displayed in (3.106), at different values of λ. When the roots are complex, the maximum value of the real part is zero and this occurs at $k = 0$ and for any λ. When the roots are real, the larger root has a maximum that is always negative for any λ and k. To show this, suppose that σ_{B4} has a maximum at $k = k_*$, differentiate both sides of (3.105) and substitute the condition for an extreme value, then simplify to obtain the maximum value $(\sigma_{B4})_m = -2\lambda k_*^2/(1+\lambda)$, which is negative for any k and λ. We conclude that the most unstable wave mode is $k = 0$, where correspondingly, $Re(\sigma_{B4}) = 0$ and $Im(\sigma_{B4}) = 1$; hence there is always a Hopf bifurcation. The growth rate equals δ_2. Hence, the system is stable if $\delta_2 < 0$ and unstable if $\delta_2 > 0$. Also, since the results above

64

are valid for any value of λ, there is no need for additional discussion of the case $\lambda > 1$ and the above results are sufficient.

In table 3.3, we give a summary of our results for the above analysis, for the four cases, focusing on the fastest growing mode k_*, and the corresponding eigenvalue (real and imaginary parts); indicating the corresponding condition(s) on system parameters and the kind of bifurcations appear. From this table, in case I, when $\lambda = 1$ Turing bifurcation disappears (as k_* goes to infinity), and this table coincides with thee summary table 3.2 in the previous section ($\lambda = 1$) in all cases.

Table 3.3: Instabilities for the four systems when $0 \leq \lambda < 1$

System	k_*^2	$Re(\sigma_*)$	$Im(\sigma_*)$	Conditions	Kind of Bifn.
I	0	$\frac{1}{2}(1+\sqrt{1+4\alpha})$	0	$\alpha \geq \dfrac{-\lambda}{(1+\lambda)^2}$	Monotonic
	$\dfrac{1}{1-\lambda}\left[-1+\sqrt{\sqrt{\dfrac{-\alpha(1+\lambda)^2}{\lambda}}}\,\right]$	$\dfrac{1-2\lambda k_*^2}{1+\lambda}$	0	$\dfrac{-(1+\lambda)^2}{16\lambda} < \alpha < \dfrac{-\lambda}{(1+\lambda)^2}$	Turing
	0	$\dfrac{1}{2}$	$\dfrac{1}{2}(\sqrt{\lvert 1+4\alpha\rvert})$	$\alpha < \dfrac{-(1+\lambda)^2}{16\lambda}$	Hopf
II	0	$\frac{1}{2}(-1+\sqrt{1+4\alpha})$	0	$\alpha \geq -1/4$	Monotonic
	0	$-\dfrac{1}{2}$	$\dfrac{1}{2}(\sqrt{\lvert 1+4\alpha\rvert})$	$\alpha < -1/4$	Hopf
III	0	1	0	$--$	Monotonic
IV	0	0	1	$--$	Hopf

3.5   C : Analysis for $\lambda > 1$

For a comprehensive study of the instabilities of a two-component RD system and for convenience, in this section we study the four systems studied in the previous section (case B), but for $\lambda > 1$. Here we follow the same procedure as in our analysis when $\lambda < 1$. As we study the same systems, we already have the dispersion relations and the equations for the most unstable wave numbers. Therefore, we proceed directly to the analysis using these relations.

3.5.1   Case I

In this subsection we study system I, equations (3.64) and (3.65), for which the eigenvalues (see (3.68)) are

$$\sigma_{C1} = \frac{1}{2}\left[1 - (1+\lambda)k^2 \pm \sqrt{[1 + (1-\lambda)k^2]^2 + 4\alpha}\right]. \tag{3.107}$$

Figure 3.14 shows the domain for a complex eigenvalue (computed at $\lambda = 2$). The eigenvalues are complex when $-1/4 < \alpha < 0$ and $k_3 < k < k_4$, and also when $\alpha < -1/4$ and $0 \le k < k_4$ (a repeated root exists at $k = k_3$ and $k = k_4$, $k_3 < k_4$) where

$$k_3 = \sqrt{\frac{1}{1-\lambda}(-1 + 2\sqrt{-\alpha})}, \qquad -1/4 < \alpha < 0, \tag{3.108}$$

$$k_4 = \sqrt{\frac{1}{1-\lambda}(-1 - 2\sqrt{-\alpha})}, \qquad \alpha < 0. \tag{3.109}$$

For $\alpha \ge 0$ (see figure 3.15(a)), there is only one maximum, which occurs at zero wave number, σ_{C11}, given by

$$\sigma_{C11} = \frac{1}{2}\left(1 + \sqrt{1 + 4\alpha}\right) \ge \frac{1}{2}, \qquad \alpha \ge -1/4, \tag{3.110}$$
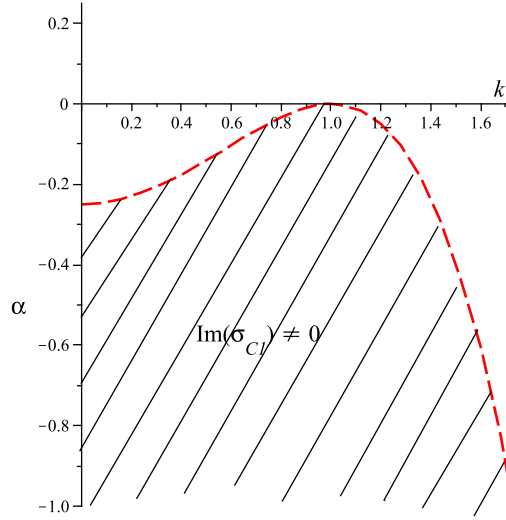
Figure 3.14: Typical domain for a complex root for σ_{C1}. The graph for $\lambda = 2$, the boundary (dashed curve) $[1 - k^2]^2 + 4\alpha = 0$.

hence there is a monotonic bifurcation at $k = 0$ ($\alpha \geq 0$) as the roots are pure real. When $-1/4 < \alpha < 0$ (see figure 3.15(b)), two maximum values appear: σ_{C11} at $k = 0$ and σ_{C12} at $k = k_{C12} > 0$, where σ_{C11} is given by (3.110), and σ_{C12} can be written as (see (3.79))

$$\sigma_{C12} = \frac{1 - 2\lambda k_{C12}^2}{1 + \lambda}, \tag{3.111}$$

where k_{C12} is the possible positive solution of (3.73), which is given by

$$k_{C12}^2 = \frac{1}{1 - \lambda} \left[-1 - \sqrt{\frac{-\alpha(1+\lambda)^2}{\lambda}} \right], \qquad \alpha < 0, \quad \lambda > 1. \tag{3.112}$$

From (3.109)

$$\begin{aligned} k_{C12}^2 - k_4^2 &= \frac{1}{1 - \lambda} \left[-1 - \sqrt{\frac{-\alpha(1+\lambda)^2}{\lambda}} \right] - \frac{1}{1 - \lambda}(-1 - 2\sqrt{-\alpha}) \\ &= \frac{\sqrt{-\alpha}(1 - \sqrt{\lambda})^2}{\sqrt{\lambda}(\lambda - 1)} > 0, \end{aligned} \tag{3.113}$$

hence we can say $k_{C12} > k_4$ (see figure 3.15(b) and (c)).

The two maximum values σ_{C11} and σ_{C12} correspond to a pure real root, and from (3.111), we can say that

$$
\begin{aligned}
\sigma_{C12} - \frac{1}{2} &= \frac{1 - 2\lambda k_{C12}^2}{1 + \lambda} - \frac{1}{2} \\
&= \frac{1 - \lambda}{1 + \lambda} - \frac{2\lambda k_{C12}^2}{1 + \lambda} < 0.
\end{aligned} \tag{3.114}
$$

Hence $\sigma_{C12} < 1/2$, and as $\sigma_{C11} \geq 1/2$ (see (3.110)), σ_{C11} is the overall maximum. As the roots are pure real, there is a monotonic bifurcation at $k = 0$. Finally, when $\alpha < -1/4$ (see figure 3.15(c)), there are two maximum values: the first is $1/2$, which occurs at $k = 0$ where the eigenvalues are complex, and the second is σ_{C12}, which occurs at a positive wave number $k = k_{C12}$ where the eigenvalues are pure real. From above, as $\sigma_{C12} < 1/2$, the global maximum is the first (the real part of the complex root at zero wave number) and hence Hopf bifurcation can exist.

From the above analysis the maximum growth rate in this case, which always occurs at $k = 0$, can be put in the form

$$
Re(\sigma_{C1}^+)_m = \begin{cases} \frac{1}{2}(1 + \sqrt{1 + 4\alpha}) & \alpha \geq -1/4, \quad Im(\sigma_{C1}) = 0 \\ \frac{1}{2} & \alpha < -1/4, \quad Im(\sigma_{C1}) = \frac{1}{2}\sqrt{|1 + 4\alpha|}. \end{cases} \tag{3.115}
$$

Hence we conclude that a Turing instability cannot arise, since the most unstable wave number is $k = 0$, while a monotonic and Hopf bifurcations arise. Making use of (3.115), we construct the stability diagram shown in figure 3.15(d).
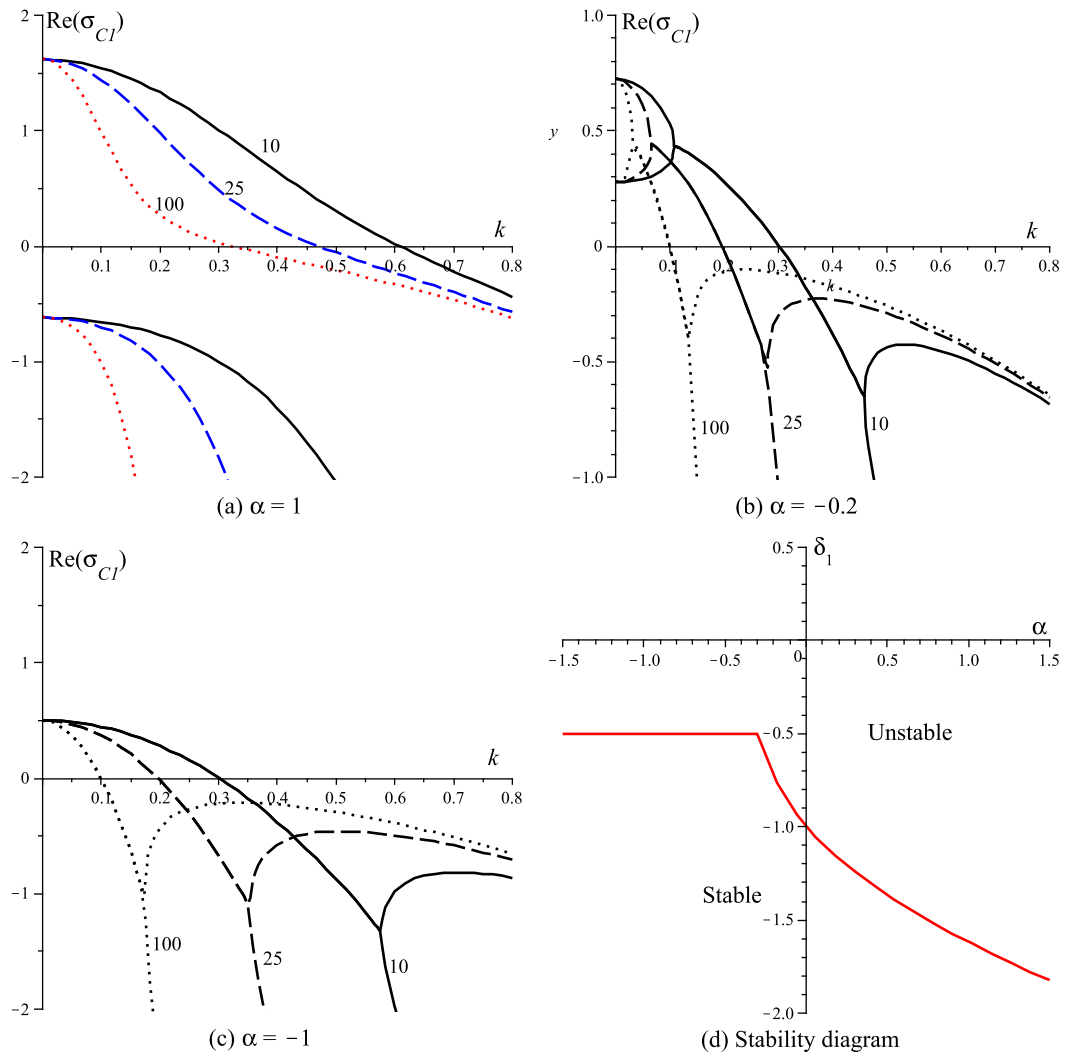
Figure 3.15: The real part of the eigenvalues (equation (3.107)) at $\lambda = 10, 25$ and 100, (a) $\alpha = 1$, (b) $\alpha = -0.2$, and (c) $\alpha = -1$ (Hopf bifurcation). (d) The stability diagram; the equation of the boundary curve is given by $Re(\sigma_{C1}^+)_m + \delta_1 = 0$

3.5.2 Case II

We study the system discussed in case B2, (3.83)-(3.84), but for $\lambda > 1$. Here the eigenvalues are (same as in case B2, see (3.87))

$$\sigma_{C2} = \frac{1}{2}\left[-1 - (1+\lambda)k^2 \pm \sqrt{[(1-\lambda)k^2 - 1]^2 + 4\alpha} \right]. \qquad (3.116)$$

However in this case the domain of complex roots is different, as shown in figure 3.16 (compared to case B2, figure 3.10). We notice that complex roots appear only when $\alpha < -1/4$ and $0 \leq k < k_0$, where

$$k_0 = \left(\frac{1 - (-4\alpha)^{1/2}}{(1-\lambda)} \right)^{1/2}, \qquad \alpha < -1/4, \qquad (3.117)$$

which is the wave number at which there is a repeated root.
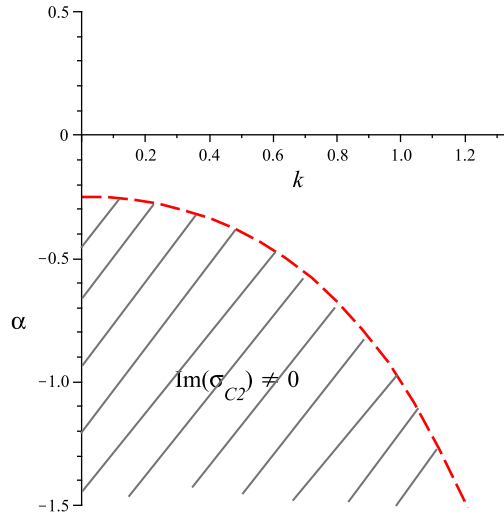
Figure 3.16: Typical domain for complex eigenvalues from (3.116) with $\lambda > 1$. The dashed curve shows the boundary (existence of a repeated root) at $\lambda = 2$.

Here we can also say that (as in our discussion of case B1), there is always a maximum at wave number $k = 0$, and if $\alpha \geq -1/4$ (regions I and II in α, λ space, see figure

3.17(a)), the eigenvalues are pure real (see figure 3.17(b), larger root at $\alpha = -0.15$) and the maximum value, σ_{C21}, is given by

$$\sigma_{C21} = \frac{1}{2}\left(-1 + \sqrt{1+4\alpha}\right) \geq -1/2, \qquad \alpha \geq -\frac{1}{4}. \qquad (3.118)$$

When $\alpha < -1/4$ (regions III and IV in α, λ space, see figure 3.17(a)), and at $k = 0$ the eigenvalues are complex and $-1/2$ is the maximum of the real part (see figure 3.17(c)). Furthermore, there can also be a maximum, $\sigma_C = \sigma_{C22}$ at a positive $k = k_{C22}$. This maximum appears in regions II, III and IV in α, λ space, where $\lambda + \alpha(1+\lambda)^2 \leq 0$. The wave number $k = k_{C22}$ (the possible positive solution of (3.91)) is given by

$$k_{C22}^2 = \frac{1}{1-\lambda}\left[1 - \sqrt{\frac{-\alpha(1+\lambda)^2}{\lambda}}\right], \qquad \lambda > 1, \quad \alpha \leq \frac{-\lambda}{(1+\lambda)^2}, \qquad (3.119)$$

and for $\alpha < -1/4$ and from (3.117)

$$\begin{aligned} k_{C22}^2 - k_0^2 &= \frac{1}{1-\lambda}\left[1 - \sqrt{\frac{-\alpha(1+\lambda)^2}{\lambda}}\right] - \frac{1-(-4\alpha)^{1/2}}{(1-\lambda)} \\ &= \frac{\sqrt{-\alpha}(1-\sqrt{\lambda})^2}{\sqrt{\lambda}(\lambda-1)} > 0, \end{aligned} \qquad (3.120)$$

hence we can say $k_{C22} > k_0$ (see figure 3.17(c), the eigenvalues at $\alpha = -0.4$). The value of σ_{C22} in terms of k_{C22} can be written as (refer to (3.93))

$$\sigma_{C22} = -\frac{1+2\lambda k_{C22}^2}{1+\lambda}, \qquad \lambda > 1, \quad \alpha \leq \frac{-\lambda}{(1+\lambda)^2}. \qquad (3.121)$$

Now as we give insights on maxima of σ_{C2}, we aim to investigate the global maximum appear in the different regions in α, λ space. From the above, σ_{C21} is the only maximum that appears in region I (on the right of the curve Γ_1, where $\lambda + \alpha(1+\lambda)^2 = 0$), and as the roots are pure real, there is a monotonic bifurcation at $k = 0$. In region II (bounded

(a) α, λ space

(b) Larger root at $\alpha = -0.15$

(c) Roots at $\alpha = -0.4$
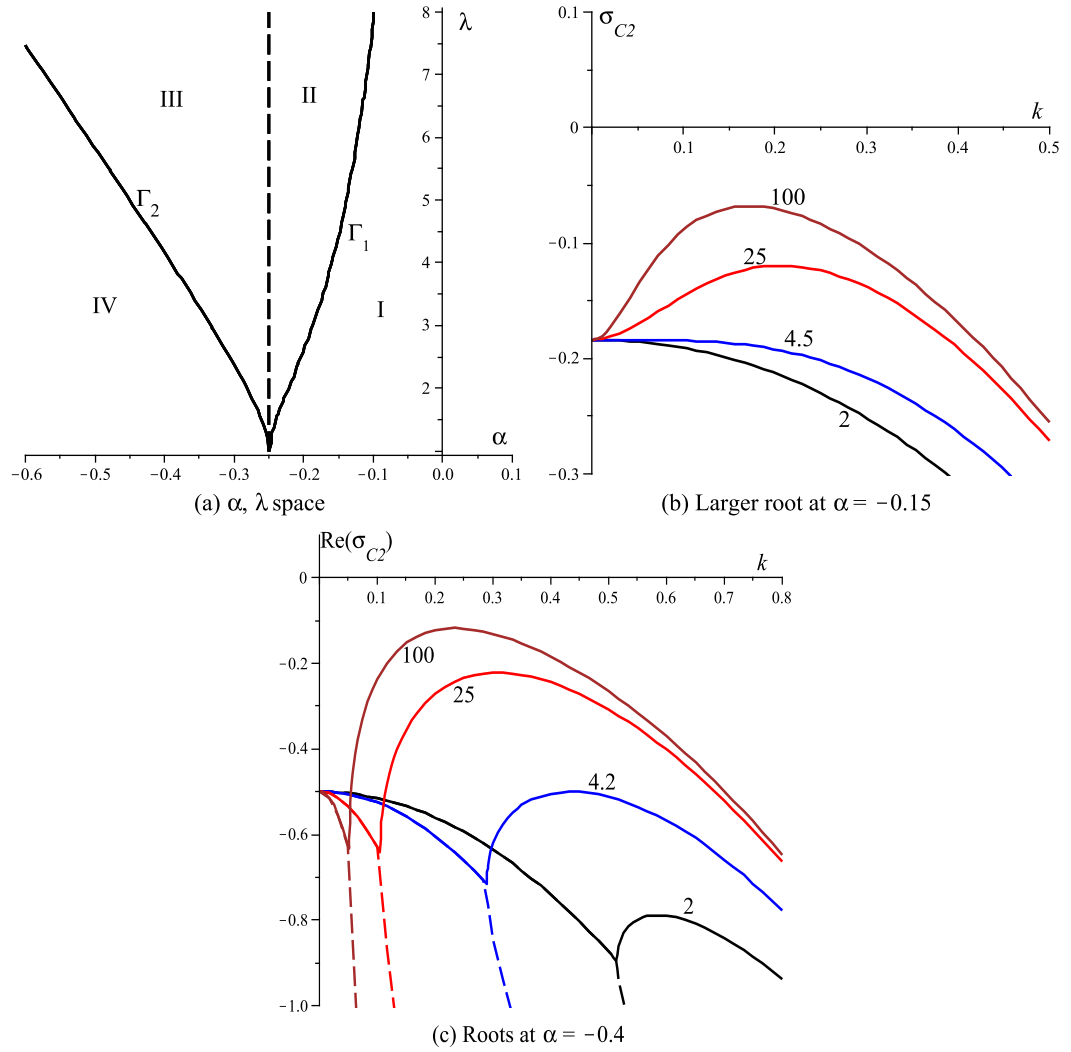
Figure 3.17: (a) α, λ space. Γ_1 is given by $\lambda + \alpha(1+\lambda)^2 = 0$ and Γ_2 by $(1+\lambda)^2 + 16\lambda\alpha = 0$ (boundary between Hopf and Turing bifurcations). In region I (on the right of Γ_1) the maximum of the growth rate occurs at $k = 0$ and $Im(\sigma_{C2}) = 0$. In region II and region III (Turing), the maximum occurs at $k > 0$ and $Im(\sigma_{C2}) = 0$. In region IV (Hopf) the maximum equals $-1/2$ and occurs at $k = 0$, $Im(\sigma_{C2}) \neq 0$. (b) The bigger root at $\alpha = -0.15$. (c) The real part of the eigenvalues at $\alpha = -0.4$.

by Γ_1 and the line $\alpha = -1/4$), there are two maximum, σ_{C21} and σ_{C22}, and σ_{C22} is the global maximum; and we demonstrate that as follows. From (3.119), we substitute k_{C22} into (3.121) to obtain

$$
\begin{aligned}
\sigma_{C22} &= -\frac{1}{1+\lambda}\left(1+\frac{2\lambda}{1-\lambda}\left[1-\sqrt{\frac{-\alpha(1+\lambda)^2}{\lambda}}\right]\frac{1+2\lambda k_{C22}^2}{1+\lambda}\right) \\
&= \frac{1}{\lambda-1}\left(1-2\sqrt{-\alpha\lambda}\right).
\end{aligned} \tag{3.122}
$$

Now when $-1/4 < \alpha < 0$ and as σ_{C22} and σ_{C21} are increasing functions of α, we can say that (substitute $\alpha = -1/4$ into (3.118) and (3.122), respectively) $\sigma_{C22} > -1/(1+\lambda^{1/2})$ and $\sigma_{C21} > -1/2$. Then $\sigma_{C22} - \sigma_{C21} > (-1+\lambda^{1/2})/2(1+\lambda^{1/2}) > 0$. Therefore, in region II, $\sigma_{C22} > \sigma_{C21}$, i.e., σ_{C22} is the maximum; since this maximum occurs at a non-zero value of k, $k = k_{B12}$, Turing bifurcations can exist. Figure 3.17(b) shows the larger root at $\alpha = -0.15$ and different values for λ and the transition between the two regions I and II takes place at $\lambda = 4.5$ (on the boundary curve Γ_1, see figure 3.17(a)). Finally, when $\alpha < -1/4$ there are two maximum values: σ_{C22} (the maximum in region III), which occurs at $k = k_{C22}$ and $-1/2$ (the maximum in region IV) which is the real part of a complex eigenvalue that arises at $k = 0$ (see figure 3.17(c), the roots when $\alpha = -0.4$ and different values of λ). To prove this, from (3.122)

$$
\begin{aligned}
\sigma_{C22} + 1/2 &= \frac{1}{\lambda-1}\left(1-2\sqrt{-\alpha\lambda}\right)+1/2 \\
&= \frac{1}{2(\lambda-1)}\left(1+\lambda-4\sqrt{-\alpha\lambda}\right), \qquad (\alpha < -1/4) \tag{3.123}
\end{aligned}
$$

and rearranging terms gives

$$
2(\lambda-1)(\sigma_{C22}+1/2) = 1+\lambda-4\sqrt{-\alpha\lambda}, \qquad (\alpha < -1/4, \lambda > 1). \tag{3.124}
$$

Therefore, $\sigma_{C22} = -1/2$ if $1 + \lambda - 4\sqrt{-\alpha\lambda} = 0$, or equivalently, $(1+\lambda)^2 + 16\alpha\lambda = 0$, which represents the boundary curve between regions III and IV (the curve Γ_2, see figure 3.17(a)). Also, when $\alpha < -1/4$ and $(1+\lambda)^2 + 16\alpha\lambda > 0$ (region III), $\sigma_{C22} > -1/2$, and as a result σ_{C22} is the maximum in region III and then Turing bifurcation may exist. However, when $(1+\lambda)^2 + 16\alpha\lambda < 0$ (region IV), $\sigma_{C22} < -1/2$, and then the real part of the complex root at $k = 0$ (which is $-1/2$) is the maximum, and Hopf bifurcations can exist (see figure 3.17(c), the eigenvalues at when $\alpha = -0.6$ and different value of λ, a transition between Turing and Hopf bifurcations occurs at $\lambda = 4.2$).

From the above discussion we can say that the maximum growth rate, $Re(\sigma_{C3}^+)_m$ can be written as

$$
Re(\sigma_{C2}^+)_m = \begin{cases} \sigma_{C21} & \text{region I} \\ \sigma_{C22} & \text{regions II and III} \\ -1/2 & \text{region IV} \end{cases}
$$
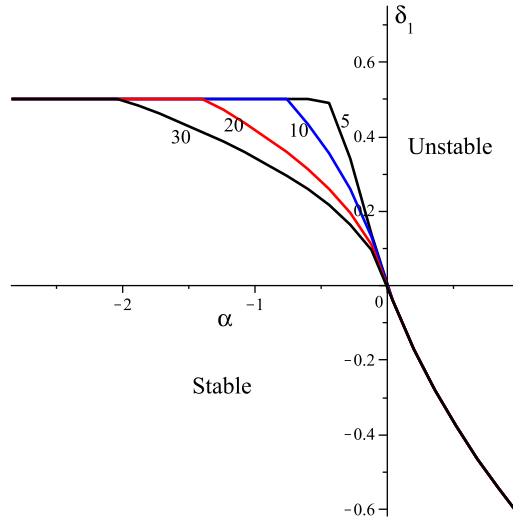
Figure 3.18: The stability diagram for different values of λ, $\lambda = 5, 10, 20$, and 30. The equation of the boundary curve is given by $Re(\sigma_{C2}^+)_m + \delta_1 = 0$.

or

$$Re(\sigma_{C2}^+)_m = \begin{cases} \frac{1}{2}(-1+\sqrt{1+4\alpha}) & \alpha \geq \frac{-\lambda}{(1+\lambda)^2}, \quad Im(\sigma_{C2}) = 0 \\ -\frac{1+2\lambda k_{C22}^2}{1+\lambda} & -\frac{(1+\lambda)^2}{16\lambda} \leq \alpha < \frac{-\lambda}{(1+\lambda)^2}, \quad Im(\sigma_{C2}) = 0 \\ -1/2 & \alpha < -\frac{(1+\lambda)^2}{16\lambda}, \quad Im(\sigma_{C2}) \neq 0 \end{cases} \quad (3.125)$$

where k_{C22} is given by (3.119). We use equation (3.125) to construct the stability diagram shown in figure 3.18 at different values of λ. We conclude that a Turing bifurcation arises in regions II and III (see figure 3.17), while Hopf arises in region IV.

3.5.3 Case III

We consider the system displayed in (3.96) and (3.97) in the case of $\lambda > 1$. From the previous discussion in case B3, the eigenvalues are

$$\sigma_{C3} = \frac{1}{2} \left[-(1+\lambda)k^2 \pm \sqrt{(1-\lambda)^2 k^4 + 4} \right]. \quad (3.126)$$

Referring to the analysis in case B3, we recall that the roots are pure real for any value of k and λ.

The roots are monotonic decreasing functions of k and the maximum value of the larger root, $(\sigma_{C3})_m = 1$, always occurs at $k = 0$. The growth rate equals $\delta_2 + 1$. Hence the system is stable if $\delta_2 < -1$ and unstable if $\delta_2 > -1$. Figure 3.19 shows the two roots displayed in (3.126) at two different values of λ, the roots are pure real and the maximum at $k = 0$, hence only monotonic bifurcation can exist.

3.5.4 Case IV

Here we focus on the system (3.102)-(3.103) when $\lambda > 1$. Referring to the case B4, the eigenvalues are
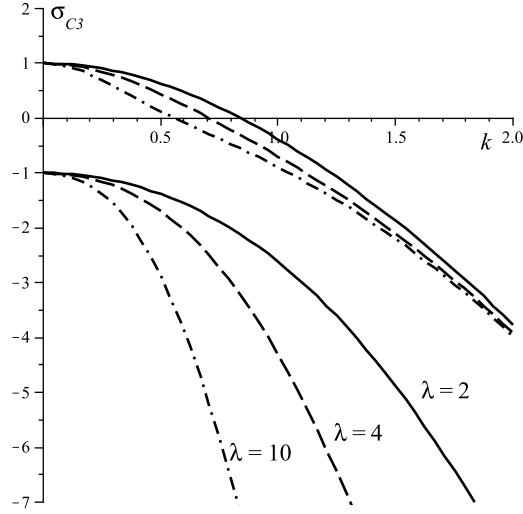
Figure 3.19: The two roots of equation (3.126) at two different values of λ: (a) $\lambda = 2$, (b) $\lambda = 10$. In each case the roots are pure real and the maximum at $k = 0$.

$$\sigma_{C4} = \frac{1}{2}\left[-(1+\lambda)k^2 \pm \sqrt{(1-\lambda)^2 k^4 - 4}\right].\tag{3.127}$$

Figure 3.20 shows σ_{C4} at different values of the diffusion ratio, $\lambda = 2, 4$ and 10. From the previous analysis for the case B4, we conclude that the most unstable wave mode is $k = 0$, at which $Re(\sigma_{C4}) = 0$ and $Im(\sigma_{C4}) = 1$. Also, the maximum growth rate equals δ_2. Hence, the system is stable if $\delta_2 < 0$ and unstable if $\delta_2 > 0$. In this case, only Hopf bifurcation occurs.

In table 3.4, we give a summary of our results for the above analysis in this section, for the four cases, focusing on the fastest growing mode k_*, the corresponding eigenvalue, and the relevant associated condition(s) on the system parameters. From this table, in case II, when $\lambda = 1$ Turing bifurcation disappears (as k_* goes to infinity), and this table coincides with thee summary table 3.2 in the previous section ($\lambda = 1$) in all cases.

77

Table 3.4: Instabilities for the four systems when $\lambda > 1$

System	k_*^2	$Re(\sigma_*)$	$Im(\sigma_*)$	Conditions	Kind of Bifu.
I	0	$\frac{1}{2}(1+\sqrt{1+4\alpha})$	0	$\alpha \geq -1/4$	Monotonic
	0	$\frac{1}{2}$	$\frac{1}{2}\left(\sqrt{\lvert 1+4\alpha\rvert}\right)$	$\alpha < -1/4$	Hopf
II	0	$\frac{1}{2}(-1+\sqrt{1+4\alpha})$	0	$\alpha \geq \dfrac{-\lambda}{(1+\lambda)^2}$	Monotonic
	$\dfrac{1}{1-\lambda}\left[1-\sqrt{\dfrac{-\alpha(1+\lambda)^2}{\lambda}}\right]$	$-\dfrac{1+2\lambda k_*^2}{1+\lambda}$	0	$\dfrac{-(1+\lambda)^2}{16\lambda} < \alpha < \dfrac{-\lambda}{(1+\lambda)^2}$	Turing
	0	$-\dfrac{1}{2}$	$\frac{1}{2}\left(\sqrt{\lvert 1+4\alpha\rvert}\right)$	$\alpha < \dfrac{-(1+\lambda)^2}{16\lambda}$	Hopf
III	0	1	0	$--$	Monotonic
IV	0	0	1	$--$	Hopf
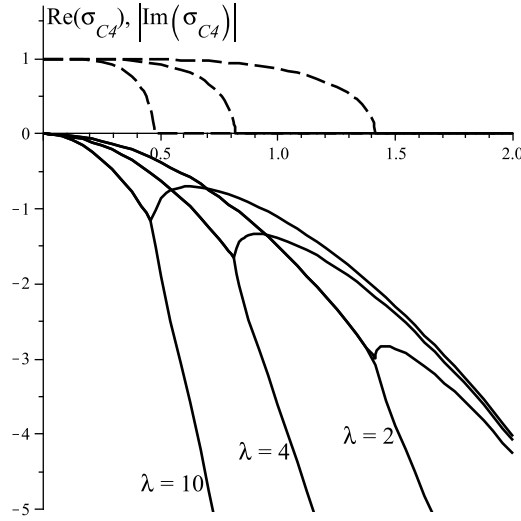
Figure 3.20: Case C4: The eigenvalues of the system (3.102)-(3.103), given by equation (3.106), at $\lambda = 2, 4$ and 10. The maximum is at $k = 0$, where the roots are complex.

3.6 Summary of Results

In this section we end the chapter by giving a summary of the instabilities that arise in two-component reaction-diffusion systems, that we rewrite the results in each section in terms of the parameters in the original system, i.e., the diffusion coefficients D_u, D_v and the reaction parameters f_u, f_v, g_u, g_v. We use the above tables and redo substitutions for the two parameters α and λ (refer to (3.20)), the eigenvalues and wave numbers using (3.33) and (3.36).

Now we can say that for two-component reaction-diffusion equations of the form

$$\begin{aligned}
\frac{\partial u}{\partial t} &= D_u \nabla^2 u + f(u, v), \\
\frac{\partial v}{\partial t} &= D_v \nabla^2 v + g(u, v),
\end{aligned} \tag{3.128}$$

three types of bifurcation types arise; stationary periodic , oscillatory uniform, and stationary uniform. The following tables give a summary of the instabilities in the three cases: $D_u = D_v$ in table 3.5, $D_u > D_v$ in table 3.6 and $D_u < D_v$ in table 3.7. In each case,

we indicate wave number of the fastest growing (or the slowest decreasing) mode, the corresponding eigenvalue, and the conditions connecting the system parameters. When the instability is stationary periodic, the pattern wave number $k = k_T$ is given by

$$k_T = \left[\frac{-|g_v - f_u| + (D_u + D_v)(|f_v g_u|/D_u D_v)^{\frac{1}{2}}}{|D_u - D_v|} \right]^{1/2}. \qquad (3.129)$$

From our results we notice that $D_u \neq D_v$ must be satisfied for stationary periodic instability, and this result is confirmed earlier when we discussed the special case $D_u = D_v$ ($\lambda = 1$) in section 3.3, this is a well known results (refer for example to [13, 55]). From our analysis here, we have given a complete classification of the instabilities that arise in a two-component reaction diffusion system. However most of the work in the literature, regarding the instabilities, focuses on specific types of instability (specially Turing bifurcation, of course when pattern formation is concerned), and for certain models. For example see, in discussing Hopf bifurcation [24, 37, 70], Turing instability [14, 37, 55], and interaction between Hopf and Turing [25, 52, 61, 81]. As our instability study gives comprehensive classification of the bifurcations, it is useful when we study two-component reaction-diffusion systems, specially to pattern formation and front propagation problems.

Table 3.5: Instabilities of (3.128) when $D_v = D_u$.

k_*^2	$Re(\sigma_*)$	$Im(\sigma_*)$	Conditions	Kind of Bifu.
0	$f_u + \frac{1}{2}\left[|g_v - f_u| + \left((g_v - f_u)^2 + 4f_v g_u\right)^{\frac{1}{2}}\right]$	0	$g_v - f_u > 0,$ $(g_v - f_u)^2 + 4f_v g_u \geq 0$	Stationary Uniform
0	$f_u + \frac{1}{2}|g_v - f_u|$	$\frac{1}{2}\left(|(g_v - f_u)^2 + 4f_v g_u|\right)^{\frac{1}{2}}$	$g_v - f_u > 0,$ $(g_v - f_u)^2 + 4f_v g_u < 0$	Oscillatory Uniform
0	$f_u - \frac{1}{2}\left[|g_v - f_u| - \left((g_v - f_u)^2 + 4f_v g_u\right)^{\frac{1}{2}}\right]$	0	$g_v - f_u < 0,$ $(g_v - f_u)^2 + 4f_v g_u \geq 0$	Stationary Uniform
0	$f_u - \frac{1}{2}|g_v - f_u|$	$\frac{1}{2}\left(|(g_v - f_u)^2 + 4f_v g_u|\right)^{\frac{1}{2}}$	$g_v - f_u < 0,$ $(g_v - f_u)^2 + 4f_v g_u < 0$	Oscillatory Uniform
0	$f_u + (f_v g_u)^{\frac{1}{2}}$	0	$g_v - f_u = 0, f_v g_u > 0$	Stationary Uniform
0	f_u	$(|f_v g_u|)^{\frac{1}{2}}$	$g_v - f_u = 0, f_v g_u < 0$	Oscillatory Uniform

Table 3.6: Instabilities of (3.128) when $D_v < D_u$.

k_*^2	$Re(\sigma_*)$	$Im(\sigma_*)$	Conditions	Bifu.
0	$f_u + \frac{1}{2}\left[|g_v - f_u| + \left((g_v - f_u)^2 + 4f_v g_u\right)^{\frac{1}{2}}\right]$	0	$g_v - f_u > 0,$ $D_u D_v(g_v - f_u)^2 + (D_u + D_v)^2 f_v g_u \geq 0$	Stationary Uniform
k_T^2	$f_u + \frac{|g_v - f_u||D_u - 2D_u D_v k_T^2|}{D_u + D_v}$	0	$g_v - f_u > 0,$ $D_u D_v(g_v - f_u)^2 + (D_u + D_v)^2 f_v g_u < 0$ $16 D_u D_v f_v g_u + (D_u + D_v)^2(g_v - f_u)^2 > 0$	Stationary Periodic
0	$f_u + \frac{1}{2}|g_v - f_u|$	$\frac{1}{2}\left(\left|(g_v - f_u)^2 + 4f_v g_u\right|\right)^{\frac{1}{2}}$	$g_v - f_u > 0,$ $16 D_u D_v f_v g_u + (D_u + D_v)^2(g_v - f_u)^2 \leq 0$	Oscillatory Uniform
0	$f_u - \frac{1}{2}\left[|g_v - f_u| - \left((g_v - f_u)^2 + 4f_v g_u\right)^{\frac{1}{2}}\right]$	0	$g_v - f_u < 0,$ $(g_v - f_u)^2 + 4f_v g_u \geq 0$	Stationary Uniform
0	$f_u - \frac{1}{2}|g_v - f_u|$	$\frac{1}{2}\left(\left|(g_v - f_u)^2 + 4f_v g_u\right|\right)^{\frac{1}{2}}$	$g_v - f_u < 0,$ $(g_v - f_u)^2 + 4f_v g_u < 0$	Oscillatory Uniform
0	$f_u + (f_v g_u)^{\frac{1}{2}}$	0	$g_v - f_u = 0, f_v g_u > 0$	Stationary Uniform
0	f_u	$(|f_v g_u|)^{\frac{1}{2}}$	$g_v - f_u = 0, f_v g_u < 0$	Oscillatory Uniform

$$k_T^2 = \frac{-|g_v - f_u| + (D_u + D_v)\left(-f_v g_u / D_u D_v\right)^{\frac{1}{2}}}{D_u - D_v}$$

Table 3.7: Instabilities of (3.128) when $D_v > D_u$.

k_*^2	$Re(\sigma_*)$	$Im(\sigma_*)$	Conditions	Bifu.
0	$f_u + \frac{1}{2}\left[\|g_v - f_u\| + ((g_v - f_u)^2 + 4f_v g_u)^{\frac{1}{2}}\right]$	0	$g_v - f_u > 0,$ $(g_v - f_u)^2 + 4f_v g_u \geq 0$	Stationary Uniform
0	$f_u + \frac{1}{2}\|g_v - f_u\|$	$\frac{1}{2}\left(\|(g_v - f_u)^2 + 4f_v g_u\|\right)^{\frac{1}{2}}$	$g_v - f_u > 0$ $(g_v - f_u)^2 + 4f_v g_u < 0$	Oscillatory Uniform
0	$f_u + \frac{1}{2}\left[\|g_v - f_u\| + ((g_v - f_u)^2 + 4f_v g_u)^{\frac{1}{2}}\right]$	0	$g_v - f_u < 0,$ $D_u D_v(g_v - f_u)^2 + (D_u + D_v)^2 f_v g_u \geq 0$	Stationary Uniform
k_T^2	$f_u - \frac{\|g_v - f_u\|D_u + 2D_u D_v k_T^2}{D_u + D_v}$	0	$g_v - f_u < 0,$ $D_u D_v(g_v - f_u)^2 + (D_u + D_v)^2 f_v g_u < 0,$ $16D_u D_v f_v g_u + (D_u + D_v)^2(g_v - f_u)^2 > 0$	Stationary Periodic
0	$f_u + \frac{1}{2}\|g_v - f_u\|$	$\frac{1}{2}\left(\|(g_v - f_u)^2 + 4f_v g_u\|\right)^{\frac{1}{2}}$	$g_v - f_u < 0,$ $16D_u D_v f_v g_u + (D_u + D_v)^2(g_v - f_u)^2 \leq 0$	Oscillatory Uniform
0	$f_u + (f_v g_u)^{\frac{1}{2}}$	0	$g_v - f_u = 0, f_v g_u > 0$	Stationary Uniform
0	f_u	$(\|f_v g_u\|)^{\frac{1}{2}}$	$g_v - f_u = 0, f_v g_u < 0$	Oscillatory Uniform

$$k_T^2 = \frac{-|g_v - f_u| + (D_u + D_v)(-f_v g_u/D_u D_v)^{\frac{1}{2}}}{D_v - D_u}$$

Chapter 4

Modulated Travelling Wave and the Characteristic Equations

In the first two chapters the FKKP, EFK, and SH equations have been discussed. We performed a traveling wave analysis. We introduced a linear selection mechanism that gives some insights into the selected speed of invasion of an unstable state by a stable one, as described both by a fixed form of travelling wave and by a modulated travelling wave. In the travelling wave coordinates for a linearised system, we deduced a characteristic equation. Then we used the double root mechanism to give some insights on the minimum front speed. The results obtained in the first two chapters motivates us to use this linear mechanism for the two-component reaction-diffusion systems. Therefore, in this chapter, for reaction-diffusion system we deduce the modulated travelling wave equations and then the characteristic equations (different cases are considered to give a comprehensive study). In the next two chapters, we discuss the mechanism considering equal and unequal diffusion coefficients.

4.1 Linearised Reaction-Diffusion Equations

In one space dimension, say x, a standard mathematical form for reaction-diffusion models with two interacting components $U(x,t)$ and $V(x,t)$ is

$$
\begin{aligned}
\frac{\partial U}{\partial t} &= D_U \frac{\partial^2 U}{\partial x^2} + f(U,V), \\
\frac{\partial V}{\partial t} &= D_V \frac{\partial^2 V}{\partial x^2} + g(U,V),
\end{aligned}
\tag{4.1}
$$

where D_U and D_V are the diffusion coefficients, and f and g are the kinetic terms, which are the only nonlinear terms that appear in the system. We assume that the system (4.1) has a spatially uniform steady state (U_0, V_0) (can be translated to the origin $(0,0)$), then the linearised equations of the perturbation (u,v) around the steady state can be written as

$$
\frac{\partial u}{\partial t} = D_U \frac{\partial^2 u}{\partial x^2} + a_1 u + b_1 v,
\tag{4.2}
$$

$$
\frac{\partial v}{\partial t} = D_V \frac{\partial^2 v}{\partial x^2} + a_2 u + b_2 v,
\tag{4.3}
$$

where D_U, D_V, a_1, b_1, a_2, and b_2 are all real numbers, the first two are positive and the other four are the elements of the Jacobian matrix

$$
\begin{pmatrix} a_1 & b_1 \\ a_2 & b_2 \end{pmatrix} = \begin{pmatrix} \frac{\partial f}{\partial U} & \frac{\partial f}{\partial V} \\ \frac{\partial g}{\partial U} & \frac{\partial g}{\partial V} \end{pmatrix}_{(U_0, V_0)},
\tag{4.4}
$$

and take either signs.

We use the transformation (to reduce the number of parameters)

$$
\hat{x} = \sqrt{\frac{|a_1|}{D_U}}\, x, \qquad \hat{t} = |a_1| t, \qquad \hat{u} = \frac{u}{b_1}, \qquad \hat{v} = \frac{v}{|a_1|}
\tag{4.5}
$$

and then dropping hats (for simplicity) gives

$$u_t = u_{xx} \pm u + v, \tag{4.6}$$

$$v_t = \lambda v_{xx} + \gamma u + \eta v, \tag{4.7}$$

where

$$\lambda = \frac{D_V}{D_U}, \quad \gamma = \frac{b_1 a_2}{a_1^2}, \quad \eta = \frac{b_2}{|a_1|}, \quad a_1 \neq 0, \tag{4.8}$$

and the $\pm$ sign leads to two cases, say S1 and S2. The first case S1 ivolves the positive sign that corresponds to the case $a_1 > 0$, while the negative sign in the other case S2 corresponds to $a_1 < 0$. We cannot reduce (4.2) and (4.3) to the system (4.6) and (4.7) when $a_1 = 0$, thus we next consider the case $a_1 = 0$ to give a comprehensive discussion of the system (4.1). If $a_1 = 0$ and when we use the transformations

$$\hat{x} = \sqrt{\frac{|b_2|}{D_U}} x, \qquad \hat{t} = |b_2| t, \qquad \hat{u} = \frac{u}{|b_2|}, \qquad \hat{v} = \frac{v}{a_2}, \tag{4.9}$$

equations (4.2) and (4.3) become

$$u_t = u_{xx} + \rho v, \tag{4.10}$$

$$v_t = \lambda v_{xx} + u \pm v, \tag{4.11}$$

where

$$\rho = \frac{b_1 a_2}{b_2^2} \tag{4.12}$$

and the $\pm$ sign tells us that there are two subcases, namely S3 and S4: the positive sign (when $b_2 > 0$) corresponds to S3 and the negative sign (when $b_2 < 0$) in the case S4. Table 4.1 shows the four canonical forms of the obtained four linearized systems that will be discussed.

Table 4.1: The four different canonical forms for the linearised system of (4.1)

Case	Equations	Conditions
S1	$\dfrac{\partial u}{\partial t} = \dfrac{\partial^2 u}{\partial x^2} + u + v$ $\dfrac{\partial v}{\partial t} = \lambda \dfrac{\partial^2 v}{\partial x^2} + \gamma u + \eta v$	$\dfrac{\partial f}{\partial U} > 0$
S2	$\dfrac{\partial u}{\partial t} = \dfrac{\partial^2 u}{\partial x^2} - u + v$ $\dfrac{\partial v}{\partial t} = \lambda \dfrac{\partial^2 v}{\partial x^2} + \gamma u + \eta v$	$\dfrac{\partial f}{\partial U} < 0$
S3	$\dfrac{\partial u}{\partial t} = \dfrac{\partial^2 u}{\partial x^2} + \rho v$ $\dfrac{\partial v}{\partial t} = \lambda \dfrac{\partial^2 v}{\partial x^2} + u + v$	$\dfrac{\partial f}{\partial U} = 0, \dfrac{\partial g}{\partial V} > 0$
S4	$\dfrac{\partial u}{\partial t} = \dfrac{\partial^2 u}{\partial x^2} + \rho v$ $\dfrac{\partial v}{\partial t} = \lambda \dfrac{\partial^2 v}{\partial x^2} + u - v$	$\dfrac{\partial f}{\partial U} = 0, \dfrac{\partial g}{\partial V} < 0$

4.2 Characteristic Equation

Here the characteristic equations for the four different cases are obtained. In the travelling wave coordinates $(z,t) = (x - ct, t)$, where c is the wave speed and for the two cases S1 and S2, equations (4.6) and (4.7) become

$$u_t - cu_z = u_{zz} \pm u + v, \tag{4.13}$$

$$v_t - cv_z = \lambda v_{zz} + \gamma u + \eta v. \tag{4.14}$$

Let us assume that the system displayed in (4.13) and (4.14) has a solution in the form

$$\begin{pmatrix} u \\ v \end{pmatrix} \propto e^{i\nu t + \mu z}, \tag{4.15}$$

where ν is a real number, and μ (the eigenvalue) is complex. A non-trivial solution of equations (4.13) and (4.14) in the form shown in (4.15) leads to the condition

$$\det \begin{pmatrix} \mu^2 + c\mu - i\nu \pm 1 & 1 \\ \gamma & \lambda \mu^2 + c\mu - i\nu + \eta \end{pmatrix} = 0, \tag{4.16}$$

which gives the characteristic equation

$$(\mu^2 + c\mu \pm 1 - i\nu)(\lambda \mu^2 + c\mu + \eta - i\nu) - \gamma = 0, \tag{4.17}$$

where ν and c are real and μ can be complex. The equation with the positive sign in the first bracket corresponds to case S1 (where $f_U > 0$), and the one with the negative sign is for case $S2$ (where $f_U < 0$).

Similarly for the two cases S3 and S4 the characteristic equations can be deduced as

follows. Referring to the system (4.10) and (4.11), the travelling wave equations are

$$u_t - cu_z \;=\; u_{zz} + \rho v, \tag{4.18}$$

$$v_t - cv_z \;=\; \lambda v_{zz} + u \pm v, \tag{4.19}$$

and a non-trivial solution of equations (4.13) and (4.14) in the form shown in (4.15) leads to the condition

$$\det \begin{pmatrix} \mu^2 + c\mu - i\nu & \rho \\[2mm] 1 & \lambda\mu^2 + c\mu \pm 1 - i\nu \end{pmatrix} = 0, \tag{4.20}$$

which gives the following characteristic equations

$$(\mu^2 + c\mu - i\nu)(\lambda\mu^2 + c\mu \pm 1 - i\nu) - \rho = 0, \tag{4.21}$$

where ν and c are real and μ can be complex. The equation with the positive sign in the second bracket corresponds to case S3, and the one with the negative sign is for case $S4$. For the above four characteristic equations, in the next two chapters, we discuss the eigenvalue character focusing on the double root condition which gives a minimum linear front speed.

4.3   Linear Front Speed

In our analysis, in chapters 5 and 6, we investigate the dependence of the eigenvalues, the roots of the quartic equations (4.17) and (4.21), on the wave speed c. We give insights on the change in the kinds of the roots due to the change in the parameters η, γ, ρ and the diffusion ratio λ. Through our discussion, we determine speeds at which a repeated root exists, and then classify the eigenvalues at these speeds (the double root and the

other two roots). This gives some insights on the minimum wave speed and helps us to understand the speed selection problem for the class of reaction-diffusion equations we study. *A minimal front speed* is the speed at which the double root is the slowest decaying eigenvalue (dominant root), assuming that the state $(u,v) = (0,0)$ at infinity is an unstable one and the front moves to the right. If one of the other two roots is positive or decaying slower than the double root, a boundary condition must be imposed at infinity to discard this root. Thus in our analysis we need to count how many roots are decaying slower than that double root, this gives us some insights on the imposed conditions. The real part of the double root of course needs to be negative to correspond to decay into the trivial state. When there is no double root, as we will see later, the steady state is stable.

In the following chapter, for the four cases shown in table 4.1, we examine the roots of the above characteristic equations separately considering the special case $\lambda = 1$. This case, as we will see later, gives evidence for the double root mechanism in determining a minimum front speed, that is why we put this case in a separate chapter. We determine the double root speed and the associated conditions on the system parameters γ, η, and ρ. Later in chapter 6, we continue discussion with $\lambda \neq 1$.

Chapter 5

Travelling Wave Analysis for Equal Diffusion Coefficients Systems

In this chapter we study system (4.1), when the two components U and V have equal diffusion coefficients, $D_U = D_V = D$, i.e., we aim to perform travelling wave analysis for a system of the form

$$
\begin{aligned}
\frac{\partial U}{\partial t} &= D\frac{\partial^2 U}{\partial x^2} + f(U,V), \\
\frac{\partial V}{\partial t} &= D\frac{\partial^2 V}{\partial x^2} + g(U,V),
\end{aligned}
\tag{5.1}
$$

where D is the diffusion coefficient, which is real. The linearised form of the above system is

$$
\frac{\partial u}{\partial t} = D\frac{\partial^2 u}{\partial x^2} + a_1 u + b_1 v,
\tag{5.2}
$$

$$
\frac{\partial v}{\partial t} = D\frac{\partial^2 v}{\partial x^2} + a_2 u + b_2 v,
\tag{5.3}
$$

where (u,v) is the perturbation around a steady state. The parameters $D, a_1, b_1, a_2,$ and b_2 are all real numbers, the first is positive and the other four are the elements of the Jacobian matrix which is shown in (4.4).

5.1 Decoupled Equations

The linearised equations (5.2) and (5.3) can be decoupled, as we now show. Suppose

$$w(x,t) = u(x,t) + \theta v(x,t), \tag{5.4}$$

where θ is a parameter which depends on the reaction parameters a_1, b_1, a_2, and b_2. Now differentiating both sides of (5.4) with respect to t, and with x twice results in

$$\frac{\partial w}{\partial t} = \frac{\partial u}{\partial t} + \theta \frac{\partial v}{\partial t}, \tag{5.5}$$

$$\frac{\partial^2 w}{\partial x^2} = \frac{\partial^2 u}{\partial x^2} + \theta \frac{\partial^2 v}{\partial x^2}, \tag{5.6}$$

then substitute u_t and v_t, from (5.2) and (5.3) into (5.5) to obtain

$$\frac{\partial w}{\partial t} = D \left(\frac{\partial^2 u}{\partial x^2} + \theta \frac{\partial^2 v}{\partial x^2} \right) + (a_1 + \theta a_2)u + (b_1 + \theta b_2)v, \tag{5.7}$$

which can be put in the form

$$\frac{\partial w}{\partial t} = D \frac{\partial^2 w}{\partial x^2} + Aw, \tag{5.8}$$

where

$$A = a_1 + \theta a_2 \quad \text{and} \quad \theta A = b_1 + \theta b_2. \tag{5.9}$$

Hence θ satisfies the quadratic $a_2 \theta^2 + (a_1 - b_2)\theta - b_1 = 0$; and the two values of θ are

$$\theta_{\pm} = \frac{1}{2a_2} \left(b_2 - a_1 \pm \sqrt{(b_2 - a_1)^2 + 4a_2 b_1} \right), \tag{5.10}$$

and consequently, the parameter A (from (5.9)) takes the two values

$$A_{\pm} = \frac{1}{2} \left(b_2 + a_1 \pm \sqrt{(b_2 - a_1)^2 + 4a_2 b_1} \right). \tag{5.11}$$

From the above results, the linearised equations (5.2) and (5.3) can be decoupled using (5.4) where θ is given by (5.10). The obtained equations are (from (5.8))

$$\frac{\partial w}{\partial t} = D\frac{\partial^2 w}{\partial x^2} + A_{\pm}w, \tag{5.12}$$

where the $A_{\pm}$ are shown in (5.11). Equation (5.12) is of the same type as the scalar equation, we discussed in chapter 1, Fisher's type equation. Thus we can say that a front solution for reaction-diffusion system (5.1) exists, and its characteristic is similar to that of Fisher's equation which we discussed in chapter 1. In the following section, we examine the eigenvalues; the roots of the quartic equations (4.17) and (4.21), deduced in chapter 4, for equal diffusion coefficients. We use the double root mechanism to obtain a minimum front speed, from which we deduce that the front solution is the same as the scalar case (Fisher's type).

5.2 The Characteristic Equations

In this section we aim to examine the character of the eigenvalues of the obtained characteristic equations (4.17) and (4.21) when $\lambda = 1$. Hence for the two cases S1 and S2 the characteristic equations are

$$(\mu^2 + c\mu \pm 1 - i\nu)(\mu^2 + c\mu + \eta - i\nu) - \gamma = 0, \tag{5.13}$$

where c and ν are real, μ is complex, and the parameters η and γ are displayed in (4.8). For the other two cases, S3 and S4, the characteristic equations are given by

$$(\mu^2 + c\mu - i\nu)(\mu^2 + c\mu \pm 1 - i\nu) - \rho = 0, \tag{5.14}$$

93

where c and v are real, μ is complex, and ρ is shown in (4.12). In the following we study each characteristic equation in a separate subsection.

5.2.1 Case S1

In this case the characteristic equation is (5.13) with the positive sign in the first bracket, and appears as

$$\mu^4 + 2c\mu^3 + (c^2 + \eta + 1 - i2v)\mu^2 + c(\eta + 1 - i2v)\mu - iv(\eta + 1) + \eta - \gamma - v^2 = 0. \quad (5.15)$$

Explicit form of the four roots can be obtained. These four eigenvalues are given by

$$-\frac{c}{2} \pm \frac{1}{2}\left(c^2 - 2(\eta + 1) \pm 2\sqrt{(\eta - 1)^2 + 4\gamma + i4v}\right)^{1/2}. \quad (5.16)$$

We examine these roots to find the double root speed. A double root can exist at three wave speeds. The first speed $c = c_1$, which appears as

$$c_1^2 \;=\; 2\left[\eta + 1 + \sqrt{(\eta - 1)^2 + 4\gamma}\right], \qquad v = v_1 = 0, \quad (5.17)$$

provided that $(\eta - 1)^2 + 4\gamma \geq 0$, and if $\eta + 1 < 0$ then $\eta - \gamma < 0$, hence c_1 appears in regions I and II (see figure 5.1, γ, η space plot). Now when we substitute $c = c_1$ and $v = v_1$ from (5.17) into (5.16), the four roots are

$$\mu_{1,2} \;=\; -\frac{1}{\sqrt{2}}\left((\eta + 1) + \sqrt{(\eta - 1)^2 + 4\gamma}\right)^{1/2}, \quad (5.18)$$

$$\mu_3 \;=\; -\frac{1}{\sqrt{2}}\left((\eta + 1) + \sqrt{(\eta - 1)^2 + 4\gamma}\right)^{1/2} - ((\eta - 1)^2 + 4\gamma)^{1/4}, \quad (5.19)$$

$$\mu_4 \;=\; -\frac{1}{\sqrt{2}}\left((\eta + 1) + \sqrt{(\eta - 1)^2 + 4\gamma}\right)^{1/2} + ((\eta - 1)^2 + 4\gamma)^{1/4}, \quad (5.20)$$

94

and they are all real; the double root $\mu_{1,2}$ is negative and $\mu_3 < \mu_{1,2} < 0$, and μ_4 is negative when $\eta - \gamma > 0$ ($\mu_4 > \mu_{1,2}$), and positive when $\eta - \gamma < 0$.
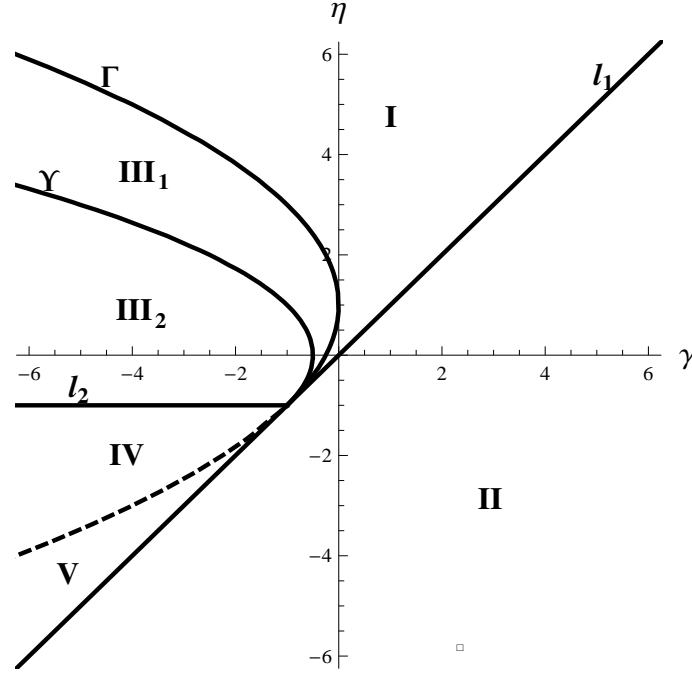
Figure 5.1: γ, η space, showing different regions corresponding to different types roots of (5.15), see table 5.1. Curves Γ, Υ, l_1, and l_2 represent $(\eta - 1)^2 + 4\gamma = 0$, $\eta^2 + 2\gamma + 1 = 0$, $\eta - \gamma = 0$ and $\eta = -1$, respectively. The borderline between regions I and III, the curve Γ (solid), which is the borderline between $\nu = 0$ and $\nu \neq 0$.

The second wave speed $c = c_2$ is given by

$$c_2^2 = 2\left[\eta + 1 - \sqrt{(\eta - 1)^2 + 4\gamma}\right], \qquad \nu_2 = 0, \tag{5.21}$$

provided that $(\eta - 1)^2 + 4\gamma \geq 0$, $\eta + 1 > 0$ and $\eta - \gamma > 0$ (means region I in figure 5.1). When we substitute from (5.21) into (5.16), the four roots are

$$\mu_{1,2} = -\frac{1}{\sqrt{2}}\left((\eta + 1) - \sqrt{(\eta - 1)^2 + 4\gamma}\right)^{1/2}, \tag{5.22}$$

$$\mu_{3,4} = -\frac{1}{\sqrt{2}}\left((\eta + 1) - \sqrt{(\eta - 1)^2 + 4\gamma}\right)^{1/2} \pm i((\eta - 1)^2 + 4\gamma)^{1/4}, \tag{5.23}$$

95

hence the double root is real and negative and the other two roots are complex conjugate with negative real part.

The third wave speed $c = c_3$ where

$$c_3^2 = 2[\eta + 1], \qquad v_3 = \frac{1}{2}\sqrt{-(\eta - 1)^2 - 4\gamma}, \tag{5.24}$$

provided that $\eta + 1 > 0$ and $(\eta - 1)^2 + 4\gamma < 0$ (means region III in figure 5.1). On the boundary curve Γ, where $(\eta - 1)^2 + 4\gamma = 0$ a transition occurs from $v = 0$ and $v \neq 0$. Now the four roots at $c = c_3$ can be put in the form

$$\mu_1 = \mu_2 = -\frac{c_3}{2}, \qquad \mu_3 = -\frac{c_3}{2} - \sqrt{v_3} - i\sqrt{v_3}, \qquad \mu_4 = -\frac{c_3}{2} + \sqrt{v_3} + i\sqrt{v_3}, \tag{5.25}$$

where c_3 and v_3 are given by (5.24). The double root is real and negative and the other two roots are complex, one with negative real part (corresponds to fastest decaying eigenvalue), and the other ($\mu = \mu_4$) with either positive or negative real part (corresponds to slowest decaying eigenvalue). The switching from positive to negative occurs when $Re(\mu_4) = 0$, i. e. $c_3 = 2\sqrt{v_3}$, and when we substitute from (5.24), we obtain $\eta + 1 = \sqrt{-(\eta - 1)^2 - 4\gamma}$ which can be simplified to $\eta^2 + 2\gamma + 1 = 0$. This is the borderline between $Re(\mu_4) > 0$ and $Re(\mu_4) < 0$, which represents the curve Υ, a boundary curve between the two regions III_1 (where $Re(\mu_4) < 0$) and III_2 (where $Re(\mu_4) > 0$), see 5.1.

The eigenvalues in different regions in in γ, η space (see figure 5.1) are summarized in table 5.1. In this table the double root speed and the character of the double root and the other two roots are presented in different parameter regimes. In the roots type column, we use letters to represent the eigenvalue; bold letters represent the double root, where capital for real parts of a complex root, and small for purely real roots, letter p represents a real and positive root while n is used for real and negative eigenvalue. The roots are in

ascending order to count the roots which are slower and faster decaying than the double root, that helps in identifying the imposed conditions to make the double root dominant. For example, the root type $n\mathbf{n}p$ means the double root is real and negative and the other two roots one is positive and one is negative, and the double eigenvalue is the dominant (as the letters are arranged regarding the ascending order of the real part of the roots).

Table 5.1: Types of eigenvalues for (5.15). Bold letters represent the double root, capital for real parts of a complex root, and small for purely real roots. The roots are in ascending order.

Conditions	(Speed)c	Roots Types
$\eta - \gamma \leq 0$	c_1	$n\mathbf{n}p$
$\eta - \gamma > 0, (\eta - 1)^2 + 4\gamma \geq 0, \eta + 1 > 0$	c_1, c_2	$n\mathbf{n}n, NN\mathbf{n}$
$(\eta - 1)^2 + 4\gamma < 0, \eta^2 + 2\gamma + 1 > 0, \eta + 1 > 0$	c_3	$N\mathbf{n}N$
$\eta^2 + 2\gamma + 1 < 0, \eta + 1 > 0$	c_3	$N\mathbf{n}P$
$\eta - \gamma > 0, \eta + 1 < 0$	$-$	$-$

From the above classification of the eigenvalues and the kind of the double root, we notice that the double root is always real and negative. When $\eta - \gamma \leq 0$, a minimum speed is $c = c_1$ (given by (5.17)), and the character of the roots is $n\mathbf{n}p$, i.e. the double root is negative and slowest decay, and there is a positive root. That means a boundary condition must be imposed at infinity to discard this root. For other parameter regimes one can easily knows the double root speed and the character of the roots. Also, from the above table, no double root speed exits when $\eta - \gamma > 0, \eta + 1 < 0$. In the following we interpret that. When we substitute η and γ from (4.8), these conditions are

$$\frac{\partial f}{\partial U}\frac{\partial g}{\partial V} - \frac{\partial f}{\partial V}\frac{\partial g}{\partial U} > 0, \qquad \frac{\partial g}{\partial V} + \frac{\partial f}{\partial U} < 0, \tag{5.26}$$

and when refer to the results of the instability analysis in chapter 3 (from table 3.5), we

find the following. The maximum temporal growth rate σ^* can be put in the form

$$\sigma^* = \frac{1}{2}\left[\frac{\partial g}{\partial V} + \frac{\partial f}{\partial U} + \sqrt{\left(\frac{\partial g}{\partial V} + \frac{\partial f}{\partial U}\right)^2 - 4\left(\frac{\partial f}{\partial U}\frac{\partial g}{\partial V} - \frac{\partial f}{\partial V}\frac{\partial g}{\partial U}\right)}\right], \qquad (5.27)$$

hence from (5.26), the maximum growth rate is always negative, $Re(\sigma^*) < 0$. Therefore, the steady state is always stable. Hence we can conclude that in travelling wave analysis, in some parameter regimes if a characteristic equation has no double root, it proves that the rest state is stable.

5.2.2 Case S2

Here we discuss equation (5.13) with the negative sign in the first bracket. In this case the characteristic equation can be put in the form

$$\mu^4 + 2c\mu^3 + (c^2 + \eta - 1 - i2\nu)\mu^2 + c(\eta - 1 - i2\nu)\mu - i\nu(\eta - 1) - \eta - \gamma - \nu^2 = 0, \quad (5.28)$$

and the four roots are given by

$$-\frac{c}{2} \pm \frac{1}{2}\left(c^2 - 2(\eta - 1) \pm 2\sqrt{(\eta + 1)^2 + 4\gamma} + i4\nu\right)^{1/2}, \qquad (5.29)$$

and we can follow same way as in the previous subsection to discuss the eigenvalues. A summary of eigenvalues types indicated in table 5.2. From (5.29) a double root $\mu = -c/2$ exists at three values of speed c. The first is given by

$$c_1^2 = 2\left[\eta - 1 + \sqrt{(\eta + 1)^2 + 4\gamma}\right], \qquad \nu = \nu_1 = 0, \qquad (5.30)$$

98

provided that $(\eta + 1)^2 + 4\gamma \geq 0$, and if $\eta - 1 < 0$ then $\eta + \gamma > 0$, hence c_1 appears in regions I and II, these regions are shown in figure 5.2. The four roots at $c = c_1$ are

$$\mu_{1,2} = -\frac{1}{\sqrt{2}} \left((\eta - 1) + \sqrt{(\eta + 1)^2 + 4\gamma} \right)^{1/2}, \tag{5.31}$$

$$\mu_3 = -\frac{1}{\sqrt{2}} \left((\eta - 1) + \sqrt{(\eta + 1)^2 + 4\gamma} \right)^{1/2} - ((\eta + 1)^2 + 4\gamma)^{1/4}, \tag{5.32}$$

$$\mu_4 = -\frac{1}{\sqrt{2}} \left((\eta - 1) + \sqrt{(\eta + 1)^2 + 4\gamma} \right)^{1/2} + ((\eta + 1)^2 + 4\gamma)^{1/4}, \tag{5.33}$$

hence they are all real. The double root is negative and the third root is negative such that $\mu_3 < \mu_{1,2} < 0$. The fourth root μ_4 is negative when $\eta + \gamma < 0$ ($\mu_4 > \mu_{1,2}$), and positive when $\eta + \gamma > 0$. The second wave speed $c = c_2$ is given by

$$c_2^2 = 2 \left[\eta - 1 - \sqrt{(\eta + 1)^2 + 4\gamma} \right], \qquad v_2 = 0, \tag{5.34}$$

provided that $(\eta + 1)^2 + 4\gamma \geq 0$, $\eta - 1 > 0$ and $\eta + \gamma < 0$ (region I), and the four roots are

$$\mu_{1,2} = -\frac{1}{\sqrt{2}} \left((\eta - 1) - \sqrt{(\eta + 1)^2 + 4\gamma} \right)^{1/2}, \tag{5.35}$$

$$\mu_{3,4} = -\frac{1}{\sqrt{2}} \left((\eta - 1) - \sqrt{(\eta + 1)^2 + 4\gamma} \right)^{1/2} \pm i((\eta + 1)^2 + 4\gamma)^{1/4}, \tag{5.36}$$

hence the double root is real and negative, while the other two roots are complex with negative real part.

Finally, the third wave speed $c = c_3$, where

$$c_3^2 = 2[\eta - 1], \qquad v_3 = \frac{1}{2}\sqrt{-(\eta + 1)^2 - 4\gamma}, \tag{5.37}$$
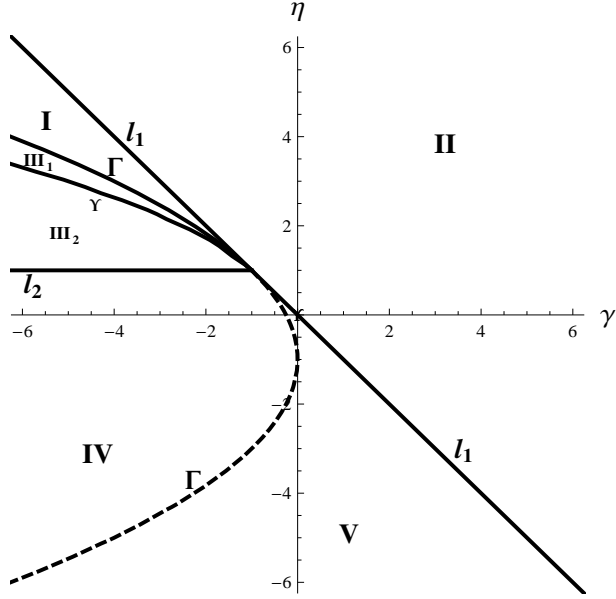
Figure 5.2: γ, η space, showing different regions corresponding to different roots types of (5.28). Curves Γ, Υ, l_1, and l_2 represent $(\eta + 1)^2 + 4\gamma = 0$, $\eta^2 + 2\gamma + 1 = 0$, $\eta + \gamma = 0$ and $\eta = 1$, respectively. The borderline between regions I and III, the curve Γ (solid), which is the borderline between $v = 0$ and $v \neq 0$.

provided that $\eta - 1 > 0$ and $(\eta + 1)^2 + 4\gamma < 0$ (region III), and the four roots are

$$\mu_1 = \mu_2 = -\frac{c_3}{2}, \qquad \mu_3 = -\frac{c_3}{2} - \sqrt{v_3} - i\sqrt{v_3}, \qquad \mu_4 = -\frac{c_3}{2} + \sqrt{v_3} + i\sqrt{v_3}, \quad (5.38)$$

hence the double root is real and negative.The other two roots are complex, one with negative real part, and the other with either positive or negative real part, and as in the previous case we can deduce that the switching occurs when $\eta^2 + 2\gamma + 1 = 0$, the borderline between $Re(\mu_4) > 0$ and $Re(\mu_4) < 0$, which represents the curve Υ, a boundary curve between the two regions III$_1$ (where $Re(\mu_4) < 0$) and III$_2$ (where $Re(\mu_4) > 0$), see 5.1 .

The eigenvalues in different regions in in γ, η space (see figure 5.2) are summarized in table 5.1. In this case a travelling wave solution can exist with a minimum speed c_1, c_2, or c_3 displayed in (5.30), (5.34) and (5.37). Also, when $\eta + \gamma < 0$ and $\eta - 1 < 0$ the rest state is stable.

100

Table 5.2: Types of eigenvalues for (5.28). Bold letters represent the double root, capital for real parts of a complex root, and small for purely real roots. The roots are in ascending order.

Conditions	(Speed)c	Roots Types
$\eta + \gamma \geq 0$	c_1	nnp
$\eta + \gamma < 0, (\eta + 1)^2 + 4\gamma \geq 0, \eta - 1 > 0$	c_1, c_2	nnn, NNn
$(\eta + 1)^2 + 4\gamma < 0, (\eta + 1)^2 + 4\gamma > 0, \eta - 1 > 0$	c_3	NnN
$(\eta + 1)^2 + 4\gamma < 0, (\eta + 1)^2 + 4\gamma > 0, \eta - 1 > 0$	c_3	NnP
$\eta + \gamma < 0, \eta - 1 < 0$	–	–

5.2.3 Case S3

In this case, from (5.14) (with the positive sign in the second bracket), the characteristic equation is

$$\mu^4 + 2c\mu^3 + (c^2 + 1 - i2v)\mu^2 + c(1 - i2v)\mu - iv - \rho - v^2 = 0, \qquad (5.39)$$

which is exactly equation (5.15) when $\eta = 0$ and $\gamma = \rho$. Thus we can say that equation (5.39) has a negative double root $\mu = -c/2$, where c and the parameter v are given by (from equations (5.17), (5.21) and (5.24), with $\eta = 0$ and $\gamma = \rho$)

$$c_1^2 = 2\left[1 + \sqrt{1 + 4\rho}\right], \qquad v_1 = 0, \qquad\qquad \rho > -1/4 \qquad (5.40)$$

$$c_2^2 = 2\left[1 - \sqrt{1 + 4\rho}\right], \qquad v_2 = 0, \qquad\qquad -1/4 < \rho < 0 \qquad (5.41)$$

$$c_3^2 = 2, \qquad\qquad v_3 = \frac{1}{2}(-1 - 4\rho)^{1/2}, \qquad \rho < -1/4. \qquad (5.42)$$

Also, from table 5.1, a summary of the character of the eigenvalues of (5.39) can be obtained. Set $\eta = 0$ and replace γ by ρ to obtain a summarising table 5.3.

Table 5.3: Types of eigenvalues for (5.15). Bold letters represent the double root, capital for real parts of a complex root, and small for purely real roots. The roots are in ascending order.

Conditions	(Speed)c	Roots Types
$\rho > 0$	c_1	nnp
$-1/4 < \rho < 0$	c_1, c_2	nnn, NNn
$-1/2 < \rho < -1/4$	c_3	NnN
$\rho < -1/2$	c_3	NnP

5.2.4 Case S4

We refer to (5.14) (with the negative sign in the second bracket), to obtain the characteristic equation

$$\mu^4 + 2c\mu^3 + (c^2 - 1 - i2\nu)\mu^2 - c(1 + i2\nu)\mu + i\nu - \rho - \nu^2 = 0, \qquad (5.43)$$

and when we compare with (5.28), we find that (5.43) is a special case. If we insert $\eta = 0$ and replace γ by ρ in (5.28), this yields equation (5.43). Thus we can say that from equations (5.30)-(5.37), there is only one speed at which a double root $\mu = -c/2$, which is real and negative, can exist (from equation (5.30)) where

$$c^2 = 2\left[-1 + \sqrt{1 + 4\rho}\right], \qquad \nu = 0, \qquad \rho \geq 0. \qquad (5.44)$$

and the other two roots are real, one negative which is less than the double root and the other is positive. Hence we conclude that for $\rho \geq 0$, equation (5.43) has a negative real double root, however no double roots exist when $\rho < 0$ (the state we linearise around is stable).

5.3 Summary

In this chapter we have discussed a two-component reaction-diffusion system with equal diffusion coefficients, which is displayed in system (5.1). We used a double eigenvalue mechanism to determine a minimum wave speed, and this speed has been determined explicitly. We noticed that if there is a double root, it always negative and real, as can be expected from the relationship of the linearized system with equal diffusion coefficients to the scalar case. This provides evidence for the relevance of the double eigenvalue mechanism we adopt to determine a linear front speed. Also, a borderline between the case $v = 0$ and $v \neq 0$ is determined (here the curve Γ). When a double root exists and one of the other root is complex with a real part which is either positive or negative, a borderline on which the real part switches is deduced (here the curve Υ represents this borderline). From our analysis in this chapter we conclude that solutions of the reaction-diffusion system shown in system (5.1) are similar to that of the scalar case (Fisher's equation).

   In the following chapter we give a detailed discussion for a system of different diffusion coefficients, i. e. $D_u \neq D_v$, specifically when $D_u > D_v$, with no loss of generality. The analysis in this chapter for the special case $\lambda = 1$ was not complicated as we already know the wave speed and the frequency (in explicit form) at which a double root exists, and we even know the four eigenvalues, and the borderlines discussed above, which tells us that equal diffusion coefficients is a limiting case. However, in general it is hard to find a solution of quartic polynomial equation explicitly. Also, the double root conditions may be more complicated than obtained here, and so we must find solutions numerically, and argue the problem graphically as we will see. Also a more complicated formula for curve which is similar to Γ (transition from $v = 0$ to $v \neq 0$) will be deduced in the next chapter, when we discuss the case $0 < \lambda < 1$, and we deduce that Γ is a limiting transition curve when the diffusion ratio tends to one.

Chapter 6

Travelling Wave Analysis for Unequal Diffusion Coefficients Systems

Travelling wave anaysis for equal diffusion coefficients is performed in the previous chapter. In this chapter we continue for reaction-diffusion systems in the case when the diffusion coefficients are different. The four characteristic equations (4.17) and (4.21) are investigated, focusing on a fractional diffusion ratio, i. e. $0 < \lambda < 1$ without loss of generality. This chapter is in four sections, each section being devoted to a separate equation. We classify the eigenvalues when a double root exists, the character of the double root and the other two roots is determined indicating the root dominance (counting the roots that decaying slower than the double root). The wave speed at these conditions can be calculated, which results in a minimal value of the propagating front speed. Also we give a recipe for borderlines between $\nu = 0$ and $\nu \neq 0$, and between the negative real part and positive real part of an eigenvalue when a repeated root exists. These lines are determined explicitly in the case where the diffusion ratio is unity.

6.1 Case S1

In this case $f_u > 0$, and when we refer to (4.17) with the positive sign, the characteristic equation is

$$\lambda\mu^4 + c(1+\lambda)\mu^3 + (\lambda+\eta+c^2-i(\lambda+1)\nu)\mu^2 + c(1+\eta-2i\nu)\mu+\eta-\gamma-\nu^2-i(\eta+1)\nu=0,$$
(6.1)

and the double root equation is

$$4\lambda\mu^3 + 3c(1+\lambda)\mu^2 + 2(\lambda+\eta+c^2-i(\lambda+1)\nu)\mu+c(1+\eta-2i\nu)=0, \qquad (6.2)$$

where ν and c are real and μ can be complex.A summary of a classification of a double root and the corresponding other two roots is shown in tables 6.1 and 6.2, and in the following we discuss these results.

6.1.1 Double root speed

To find the double root speed, we eliminate the eigenvalue μ from equations (6.1) and (6.2) . The eliminant of (6.1) and (6.2), or equivalently the resultant of (6.1), is complex. Thus we obtain from this resultant two real equations, and these two equations are displayed in (A.14) and (A.15). We solve these equations to obtain c and ν, the double eigenvalue speed and frequency, and plots are generated at different regimes of system parameters λ, η and γ. We observe that a double root speed c is zero in two cases. The first is when $\nu^2 = -(1+\gamma)$ for $\eta = -1$ and $\gamma < -1$. The second case when $\nu^2 = 4\lambda\gamma/(1-\lambda)^2$, and $\eta = \lambda, \gamma > 0$. These results can be obtained easily when we substitute $c = 0$ into equations (6.1) and (6.2) and then solve for the modulating frequency ν.

The resultant equations (A.14) and (A.15) reduce to one equation when $\nu = 0$, equation (A.16). From this equation, $c = 0$ when $\eta = \gamma$ or $(\eta-\lambda)^2+4\gamma\lambda = 0$. Also,

we can say that as $\left(4\gamma + (\eta - 1)^2\right) \to 0$, a wave speed c goes to very large values (as $\left(4\gamma + (\eta - 1)^2\right)$ is the coefficient of the largest power, the leading order in (A.16)), hence we may consider $4\gamma + (\eta - 1)^2 = 0$ as an asymptote for the double root wave speed, and this requires $\gamma < 0$. These results help when we plot the speed in different parameter regimes in that we know where the speed goes to zero and also to very large values, as we will see in graphs.

6.1.2   Purely imaginary eigenvalue

Here we discuss the existence of a pure imaginary root for the characteristic equation (6.1). This helps us in the eigenvalue classification. Assume that at $c = C$ equation (6.1) has a pair of pure imaginary roots, say $\mu = \pm i\omega$, where ω is real. We aim to determine the possible non-negative values of C. Now substitute $c = C$ and $\mu = i\omega$ into (6.1) to obtain a complex equation from which we can obtain the two real equations

$$(1 - \omega^2)(\eta - \lambda\omega^2) - (\omega C - v)^2 - \gamma \;=\; 0, \tag{6.3}$$

$$(\omega C - v)(\eta + 1 - (1 + \lambda)\omega^2) \;=\; 0. \tag{6.4}$$

We solve the above two equations to obtain C. The first possible solution is

$$C_1 = \sqrt{\frac{2\lambda v^2}{\lambda + \eta \pm ((\lambda + \eta)^2 - 4\lambda(\eta - \gamma))^{1/2}}}, \tag{6.5}$$

provided that

$$(\lambda + \eta)^2 - 4\lambda(\eta - \gamma) \geq 0, \tag{6.6}$$

In addition, if $\lambda + \eta > 0$, then $\eta - \gamma \geq 0$, and if $\lambda + \eta \leq 0$, then $\eta - \gamma < 0$. The second possible solution is given by

$$C_2 = \sqrt{\frac{1+\lambda}{1+\eta}} \left(v + \sqrt{-\frac{\gamma(1+\lambda)^2 + (\eta-\lambda)^2}{(1+\lambda)^2}} \right), \qquad (6.7)$$

provided that

$$\eta > -1, \quad \gamma(1+\lambda)^2 + (\eta-\lambda)^2 \leq 0, \qquad (6.8)$$

and consequently γ must be negative. It is obvious that when $v = 0$, there is only one speed for a purely imaginary root to exist, which is $C = C_0$ and given by (6.7) when $v = 0$. This speed can be put in the form

$$C_0 = \sqrt{-\frac{\gamma(1+\lambda)^2 + (\eta-\lambda)^2}{(1+\lambda)(1+\eta)}}, \qquad (6.9)$$

provided that the conditions displayed in (6.8) hold.

6.1.3 Triple root condition

Now we discuss the transition curve, where the double root frequency v switches between zero to nonzero value (triple root condition was discussed in chapter 2, the analysis of the EFK equation). The transition occurs when the polynomial equation

$$Q = \lambda\mu^4 + c(1+\lambda)\mu^3 + (\lambda+\eta+c^2)\mu^2 + c(1+\eta)\mu + \eta - \gamma = 0 \qquad (6.10)$$

has a triple root (we discussed this condition in chapter 2). It is clear that a zero triple root exists when $\eta = \gamma = -1$ and $c^2 = 1 - \lambda$. If the triple root is negative, the signs of the polynomial coefficients must be $+++\pm$. However, the sign sequence is $++-+-$ when a positive triple root exists (there must be exactly three sign changes according to

Descartes' rule of signs). Thus in the two sequences, the coefficient of μ, for $c > 0$, must be positive. Hence equation (6.10) has a triple root on the condition $\eta > -1$.

The transition curve can be obtained by solving the three equations (triple root conditions)

$$Q = 0, \qquad \frac{\partial Q}{\partial \mu} = 0, \qquad \frac{\partial^2 Q}{\partial \mu^2} = 0, \qquad (6.11)$$

or

$$\lambda \mu^4 + c(1+\lambda)\mu^3 + (\lambda + \eta + c^2)\mu^2 + c(1+\eta)\mu + \eta - \gamma \;=\; 0, \qquad (6.12)$$

$$4\lambda \mu^3 + 3c(1+\lambda)\mu^2 + 2(\lambda + \eta + c^2)\mu + c(1+\eta) \;=\; 0, \qquad (6.13)$$

$$6\lambda \mu^2 + 3c(1+\lambda)\mu + (\lambda + \eta + c^2) \;=\; 0. \qquad (6.14)$$

From the above conditions we eliminate μ and c (using the elimination method shown in Appendix A) to obtain the triple root condition displayed in (A.17), see Appendix A, which is a closed form in system parameters λ, η and γ.

For different values of λ, the transition curve which is represented by (A.17) is plotted in η, γ space in figure 6.1. The transition curves exists for $\eta \geq -1$, and all satisfy $\gamma = \eta = -1$. We notice that the curves corresponding to $0 < \lambda \leq 1/2$ lie in the region $\gamma \geq -1$, however those for $1/2 < \lambda \leq 1$ exist when $\gamma < 0$. Hence when we classify the eigenvalues, we discuss the character of the double roots considering the above parameter regimes. A summary of the double root and the other two roots classification when $0 < \lambda \leq 1/2$ in table 6.1, and for $1/2 < \lambda \leq 1$ in table 6.2.

In the following we discuss the eigenvalue classification in different parameter regimes. In the eigenvalue classification we use bold letter to represent the double root, capital for real parts of a complex root, and small for purely real roots. The roots are in ascending order to determine the character of the double root and the other two roots as we did in the previous chapter.
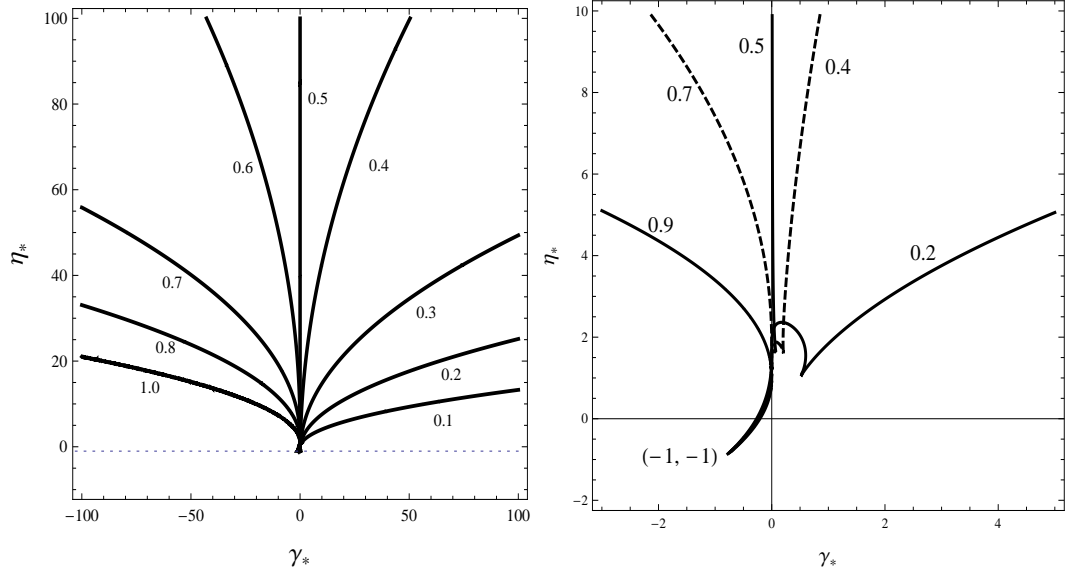
Figure 6.1: (Left) Triple root locus for (6.10) in η, γ space, equation (A.17), for $\lambda = 0.1$ to 1. When $\gamma > 0$ a triple root exists when $0 < \lambda \leq 1/2$, and when $\gamma < 0$, it exists for $1/2 < \lambda \leq 1$. A triple root cannot exist for $\eta < -1$. (Right) A close-up picture for the locus near the origin.

6.1.4 Classification when $\gamma = 0$

When $\gamma = 0$ the four roots of (6.1) are

$$\frac{1}{2}\left(-c \pm \sqrt{c^2 - 4 + i4v}\right), \qquad \frac{1}{2\lambda}\left(-c \pm \sqrt{c^2 - 4\eta\lambda + i4v\lambda}\right), \qquad (6.15)$$

Hence we can say that there is no double root speed when v is nonzero, however there are two speeds $c_1 = 2$ and $c_2 = 2(\eta\lambda)^{1/2}$ when $v = 0$, figure 6.2 shows these two speeds versus the parameter η. In the following we classify the roots at these speeds. When we substitute $c = c_1 = 2$ into (6.15), the four roots are

$$\mu_{1,2} = -1, \quad \mu_3 = \frac{1}{\lambda}\left(-1 - (1-\eta\lambda)^{1/2}\right), \quad \mu_4 = \frac{1}{\lambda}\left(-1 + (1-\eta\lambda)^{1/2}\right), \quad (6.16)$$

109

Hence the double root at c_1 is real and negative and the type of the other two roots (μ_3 and μ_4) depend on the parameters λ and η as follows. When $\eta < 0$, μ_3 is negative real and less than the double root, however μ_4 is positive and real, hence at $c = c_1$ and when $\eta < 0$ the type of the eigenvalues is $n\mathbf{n}p$. When $\eta\lambda > 1$, they are complex conjugate with a negative real part which equals $-1/\lambda$ (this real part is less than the double root), and the type of the roots are $NN\mathbf{n}$. When $\eta\lambda < 1$ and $\eta > 0$, μ_3 and μ_4 are always real and negative; $\mu_3 < -1$ and $\mu_4 \lessgtr -1$ depending on the parameters and we discuss this as follows. Assume that $\mu_4 > -1$, it means

$$\frac{1}{\lambda}\left(-1 + (1 - \eta\lambda)^{1/2}\right) > -1,$$

and when we simplify we obtain the condition $\eta < 2 - \lambda$. Hence we can say that when $0 < \eta < 2 - \lambda$, the eigenvalue $-1 < \mu_4 < 0$ and when $\eta > 2 - \lambda$ and $\eta\lambda < 1$, $\mu_4 < -1$. Thus we can say that at $c = c_1$ and when $0 < \eta < 2 - \lambda$ the roots type is $n\mathbf{n}n$, however when $2 - \lambda < \eta < 1/\lambda$, the type is $nn\mathbf{n}$.

In the following we discuss the double root speed $c = c_2$. When we substitute $c = c_2 = 2(\eta\lambda)^{1/2}$ into (6.15), the four roots are

$$\mu_{1,2} = -\sqrt{\eta/\lambda}, \qquad \mu_3 = -\sqrt{\eta\lambda} - \sqrt{\eta\lambda - 1}, \qquad \mu_4 = -\sqrt{\eta\lambda} + \sqrt{\eta\lambda - 1},$$

$$(6.17)$$

provided that $\eta > 0$. The double root is real and negative, and when $0 < \eta < 1/\lambda$ the other two roots are complex conjugate with a negative real part (greater than the double root), then the type of the eigenvalues is $\mathbf{n}NN$. When $\eta > 1/\lambda$, μ_3 and μ_4 are negative and real, and the double root is always less than these two roots, hence the roots type is $\mathbf{n}nn$. A summary for the above obtained results for $\gamma = 0$ is shown in table 6.1. In figure 6.2a, the double root speeds c_1 and c_2 versus η are plotted, and vertical dotted lines indicate the roots types transition. At $\gamma = 0$ and $\lambda = 0.4$, we plot the four eigenvalues versus speed c
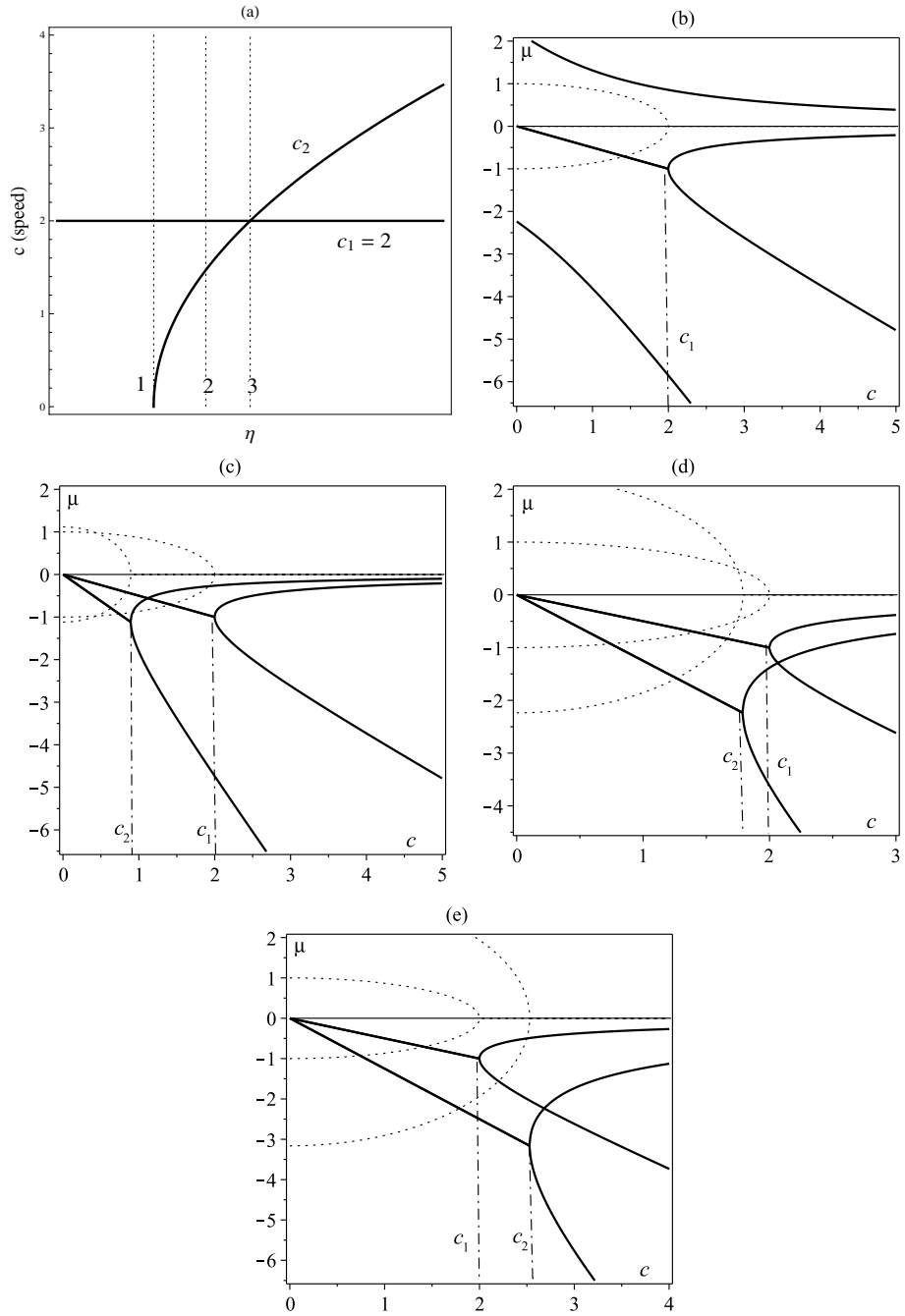
Figure 6.2: (a) Double root locus for equation (6.1), c versus η when $\gamma = 0$, where $c_1 = 2$ and $c_2 = 2(\eta\lambda)^{1/2}$, the vertical dotted lines are: (1) $\eta = 0$, (2) $\eta = 2 - \lambda$ and (3) $\eta = 1/\lambda$. (b)-(e) The four eigenvalues as a function of speed c, when $\lambda = 0.4$, $\gamma = 0$, and (b) $\eta = -2$, (c) $\eta = 0.5$, (d) $\eta = 2$ and (e) $\eta = 4$, solid lines represent the real part and dotted line represent the imaginary part of eigenvalues.

when $\eta = -2, 0.5, 2$ and 4 (shown in figure 6.2(b)-(e)), these figures show the character of the eigenvalues that given in table 6.1 for $\gamma = 0$.

Table 6.1: Classification of a double root and the other two roots of (6.1) when $0 < \lambda \le 1/2$. Bold letters represent the double root, capital for real parts of a complex root, and small for purely real roots. The roots are in ascending order, $d_1 = (\eta - 1)^2 + 4\gamma$, $d_2 = (\eta - \lambda)^2 + 4\gamma\lambda$, and $d_3 = (\eta - \lambda)^2 + \gamma(1 + \lambda)^2$, and a real triple root exists at $\eta = \eta_*$.

	Conditions	(Speed)c	Roots Types	Figures
$\gamma = 0$	$\eta \le 0$	c_1	$n\mathbf{n}p$	
	$0 < \eta \le 2 - \lambda$	c_1, c_2	$n\mathbf{n}n, \mathbf{n}NN$	6.2
	$2 - \lambda < \eta \le 1/\lambda$	c_1, c_2	$nn\mathbf{n}, \mathbf{n}NN$	
	$\eta > 1/\lambda$	c_1, c_2	$NN\mathbf{n}, \mathbf{n}nn$	
$\gamma > 0$	$\eta \le \lambda$	c_4	$n\mathbf{n}p$	
	$\lambda < \eta \le \eta_*$	c_4	$n\mathbf{n}p$	
		c_5	$NPP/\mathbf{N}NP$	6.3 , 6.4
	$\eta_* < \eta \le \gamma$	c_2, c_3, c_4	$\mathbf{n}np, n\mathbf{n}p, nn\mathbf{p}$	
	$\eta > \gamma$	c_1, c_2, c_3, c_4	$NN\mathbf{n}, \mathbf{n}nn, n\mathbf{n}n, nn\mathbf{n}$	
$-1 < \gamma < 0$	$\eta \le \gamma$	c_1	$n\mathbf{n}p$	
	$\eta > \gamma, d_1 \ge 0$	c_1, c_4	$n\mathbf{n}n, \mathbf{n}PP$	
	$d_1 < 0, \eta \le \eta_*$	c_1, c_2, c_4	$n\mathbf{n}n, nn\mathbf{n}, \mathbf{n}PP$	
	$d_1 < 0, \eta > \eta_*$	c_4	$\mathbf{n}NN$	6.5
		c_5	NNN	
	$d_1 > 0$	c_3/c_4	$NN\mathbf{n}, n\mathbf{n}n/\mathbf{n}NN, nn\mathbf{n}$	
		c_5	NNN	
$\gamma < -1$	$\eta \le \gamma$	c_1	$n\mathbf{n}p$	
	$\eta > \gamma, d_1 \ge 0$	$-$	$-$	
	$d_1 < 0, d_2 \ge 0$	c_2	$nn\mathbf{p}$	
	$d_2 < 0, \eta \le -1$	c_4	$\mathbf{n}PP$	
	$\eta > -1, d_3 \le 0$	c_4	$\mathbf{n}PP, \mathbf{n}NN$	
		c_5	NNP/NNN	6.6 , 6.7
	$d_3 > 0, d_1 < 0$	c_4	$\mathbf{n}NN$	
		c_5	NNN	
	$d_1 > 0$	c_3, c_4	$NN\mathbf{n}, n\mathbf{n}n/\mathbf{n}NN, nn\mathbf{n}$	
		c_5	NNN	

Figure 6.3: Double root locus for equation (6.1), c versus η when $0 < \lambda < 1/2$ and $\gamma > 0$, dotted lines are: (1) $\eta = \lambda$, (2) $\eta = \eta_*$, (3) $\eta = \gamma$ and (4) $v = 2\sqrt{\gamma\lambda}/(1 - \lambda)$. The types of the roots at these speeds are shown in table 6.1.

6.1.5 Classification when $0 < \lambda \leq 1/2$

For $\gamma > 0$ and $0 < \lambda \leq 1/2$, double root speeds and modulating frequency versus η are shown in figure 6.3, which represent the solutions for the double root equations (A.14) and (A.15), shown in Appendix A. The solid lines represent the speed when $v = 0$, and the dashed when $v \neq 0$. In the following we examine the eigenvalue type at these speeds. Let us start with the double root speed $c = c_5$, which exists in the interval $\lambda < \eta < \eta_*$, where η_* satisfies the triple root condition (A.17). To determine the character of the double root and the other two roots, we find the double root and the other two roots at specific system parameters. Assume that $\lambda = 0.2$ and $\gamma = 10$, then solving (A.17) to obtain $\eta = \eta_* \simeq 7.1$, Hence we can say that $0 < c_5 < 2.3$ and it exists for $0.2 < \eta < 7.1$, and at $\eta = 5$ the double root speed $c = c_5 \simeq 1.8$ and the frequency $v = v_5 \simeq 0.35$. For $\lambda = 0.2$ and $\gamma = 10$ and $\eta = 5$, we plot constant speed contours in $Re(\mu)$, $Im(\mu)$ space, see figure 6.4(a), the contours represent speeds around the double root speed $c_5 \simeq 1.8$ where a saddle point exists (these contours represent equation (A.18), Appendix A). Also, in $Re(\mu)$, $Im(\mu)$ space, constant frequency contours are plotted, see figure 6.4(b). The contours represent frequencies around the double root frequency $v = v_5 \simeq 0.35$, and these contours from

113

equation (A.19) (Appendix A). From these plots we know the character of the double root, which is complex with negative real part. To uncover the character of the other two roots, we solve the characteristic equation (6.1). In figure 6.4(c) and (d), when $\lambda = 0.2$ and $\gamma = 10$, we plot the real part of the double root and the other two roots versus η and speed c, respectively, where $0.2 < \eta < 7.1$ and $0 < c_5 < 2.3$. The double root (dashed line) is complex with negative real part and the other two roots are complex, one with positive real part and the real part of the can be either positive or negative (switching occurs when $c = C_1$ shown in (6.5)). From our discussion the type of the eigenvalues when $c = c_5$ can be **N**PP or **N**NP, and this is shown in a summary table 6.1. Thus we can say that to make the double root dominant at $c = c_5$, two conditions must be imposed to discard exponentials correspond to the other two roots.

In the following we examine the roots' character for the other double root speeds, $c = c_i$, $i = 1, 2, 3, 4$ (see figure 6.3, the solid lines). These speeds represent the possible solutions of equation (A.16) (see Appendix A), where the modulating frequency is zero, $v = 0$. We mainly fix the system parameters and solve the characteristic equation (when $v = 0$) at different values of c. Then we plot the four eigenvalues versus the wave speed c (see 6.3(e) and (f)), from these plots we can know the character of the roots. Also, we use the Routh-Hurwitz criterion and Descartes' Rule of signs to examine the roots. Now when $v = 0$, and from (6.1), the sequence of the characteristic polynomial coefficients is

$$\lambda, \quad c(1+\lambda), \quad \lambda + \eta + c^2, \quad c(1+\eta), \quad \eta - \gamma. \tag{6.18}$$

Then for $\gamma > 0$ and $\eta > \gamma$, all the coefficients are positive and Routh-Hurwitz criterion is satisfied (see Appendix B, equations (B.9) and (B.10)), all eigenvalues are either negative and real or complex with negative real parts. Figure 6.3(e) shows the four eigenvalues when $\lambda = 0.2$, $\gamma = 10$ and $\eta = 20$. The solid lines represent the real part and dotted

line represent the imaginary part of eigenvalues. From this figure, there are four repeated roots and all are real and negative. These double roots occurs at speeds c_1, c_2, c_3 and c_4, and the character of the double root and the other two roots are $NN\mathbf{n}, \mathbf{n}nn, n\mathbf{n}n$ and $n\mathbf{n}n$, respectively. If $\eta_* < \eta < \gamma$, there are three double root speed (see figure 6.3), c_2, c_3 and c_4. Routh-Hurwitz criterion is not satisfied (as $\eta - \gamma < 0$). Hence at least there is one root which is complex with positive real part. From (6.18), the sign sequence is $+ + + + -$. Thus there is only one sign change, and according to Descarte's Rule of signs, at most there is one positive and real root. From this result a positive real root always exists and the other three roots are negative or one negative and two are complex conjugate with negative real parts. Hence the eigenvalue type at the double root speeds c_2, c_3 and c_4 is $\mathbf{n}np, n\mathbf{n}p$ and $n\mathbf{n}p$, respectively. When $\eta < \eta_*$, see figure 6.3, there is only one double root which occurs at $c = c_4$ and the type of the eigenvalue is $n\mathbf{n}p$. Figure 6.3(f) shows the eigenvalues variation with speed when $\lambda = 0.2$ and $\gamma = 10$ and $\eta = 5 < \eta_*$ (here $\eta_* \simeq 7.1$). The above results are shown in table 6.1.

Figure 6.5(a) and (b) show the double root speed and frequency when $0 < \lambda \leq 1/2$ and $-1 \leq \gamma < 0$ (the possible solutions of equations (A.14) and (A.15), Appendix A). On the dashed line, where $c = c_5$, the double root and the other two roots are complex with negative real parts. Figure 6.5(c) indicates the variation of the real parts of the double root ($\mu_{1,2}$ dashed line) and the other two roots with η, when $\lambda = 0.2$ and $\gamma = -0.5$. For the double root speeds $c = c_i$, $i = 1, 2, 3, 4$, when $d_1 = (\eta - 1)^2 + 4\gamma$ tends to zero a double root goes to very large values, and this happens at c_2 and c_3, and the speed $c_4 = 0$ when $\eta = \gamma$, see 6.5(a). The eigenvalues types at these speeds are are shown in table 6.1, and the roots versus speed are potted in figures 6.5(d)-(f) at certain values of system parameters. These figures helps to determine the character of the roots at double root speeds.

When $0 < \lambda \leq 1/2$ and $\gamma < -1$, the double root speed and frequency are shown in figure 6.6. From this figure, the speed is zero when $\eta = \gamma$ ($c_1 = 0$), $d_2 = (\eta - \lambda)^2 +$
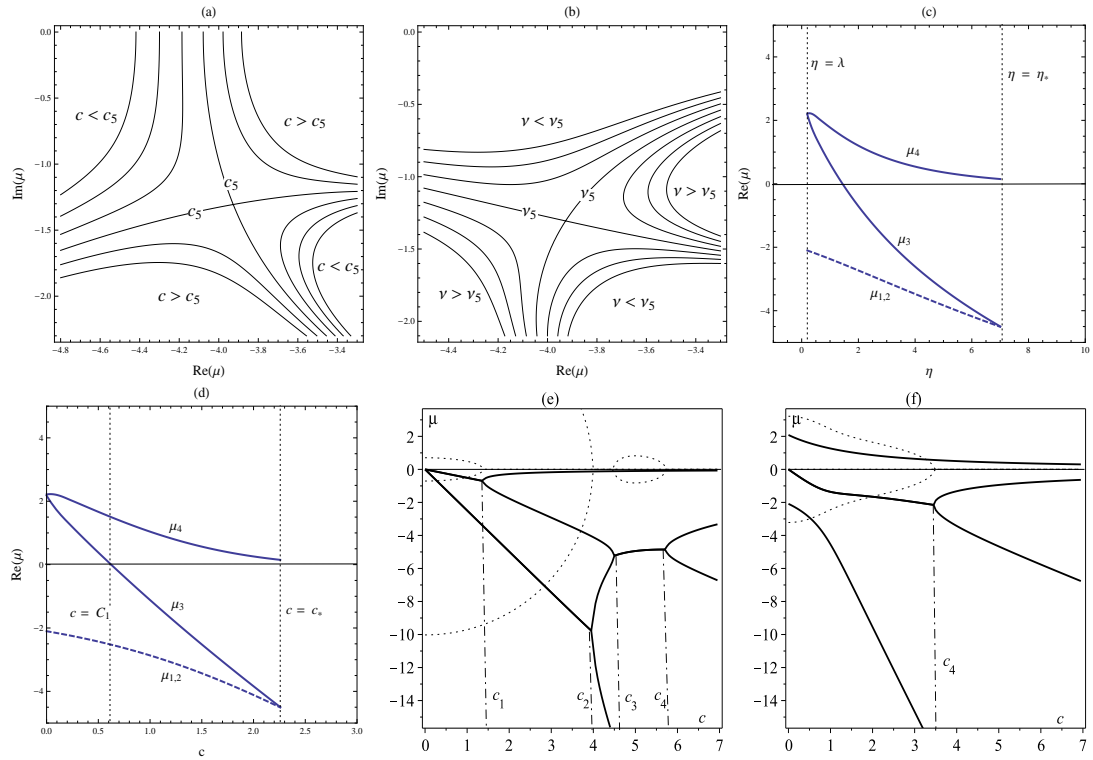
Figure 6.4: The character of the roots at speeds shown in figure 6.3. (a), (b) constant speed and frequency contours in $Re(\mu)$, $Im(\mu)$ space: a saddle point exists at double root speed, at $c = c_5 \simeq 1.8$ in (a), and frequency $\nu = \nu_5 \simeq 0.35$ in (b), the double root is complex with negative real part, $\lambda = 0.2$, $\gamma = 10$ and $\eta = 5$. (c) and (d) The real part of the four eigenvalues versus η and c, dashed line represents the double root. (e) and (f) The four eigenvalues versus the wave speed, solid lines represent the real part and dotted lines for imaginary part, $\lambda = 0.2$, $\gamma = 10$, (e) $\eta = 20$ and (f) $\eta = 5$.
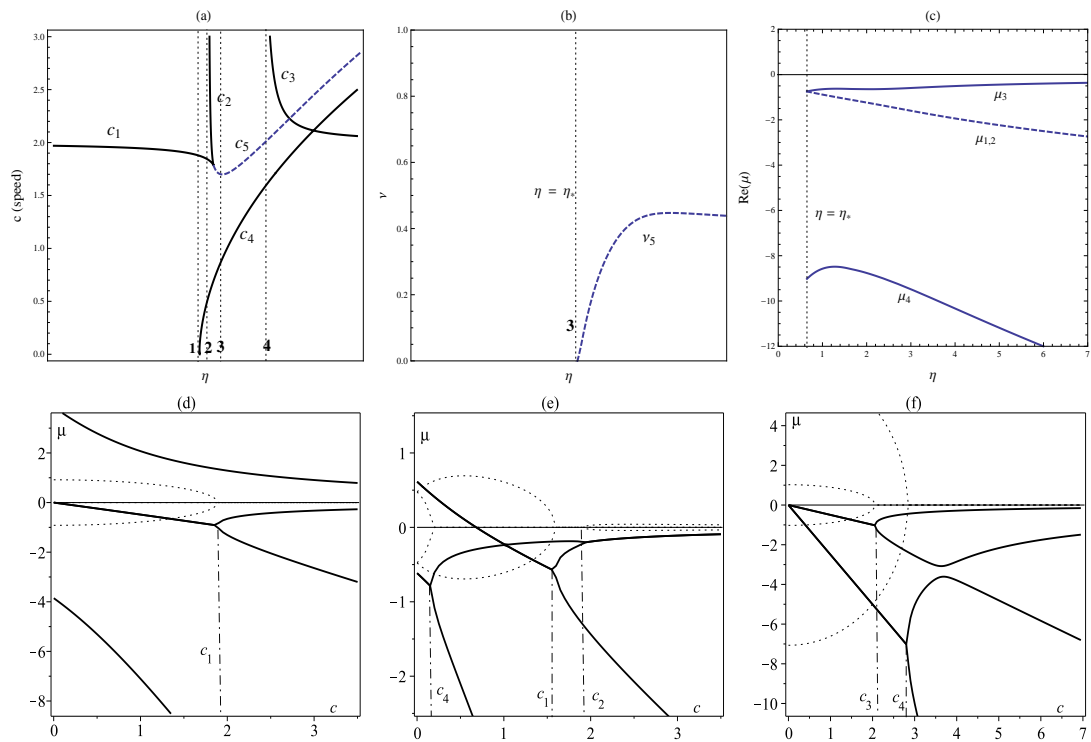
Figure 6.5: (a), (b) Double root locus for equation (6.1) when $0 < \lambda < 1/2$, $-1 \le \gamma < 0$. (1) $\eta = \gamma$, (2) and (4) $(\eta - 1)^2 + 4\gamma = 0$, (3) $\eta = \eta_*$. (c) The real part of the four eigenvalues at $c = c_5$, dashed line represents the double root,$\lambda = 0.2$, $\gamma = -0.5$. (d) - (f) The four eigenvalues as a function of speed c at $\lambda = 0.2$, $\gamma = -0.5$; (d) $\eta = -3$ (e) $\eta = -0.4$, (f) $\eta = 10$, solid lines represent the real part and dotted line represent the imaginary part of eigenvalues.

$4\gamma\lambda = 0$ ($c_2 = c_4 = 0$) and when $\eta = -1$ ($c_5 = 0$, $v_5 = \sqrt{-1-\gamma}$). Also, when when $d_1 = (\eta-1)^2 + 4\gamma$ tends to zero the two speeds c_2 and c_3 tends to be very large. In the following we discuss the type of the roots in these different parameter regimes. When $\eta \leq \gamma$, from (6.18), the coefficient sign sequence is $++\pm--$. Then from Descartes' Rules of Signs, one of the four roots is always positive and real. Thus we can say that when $\eta \leq \gamma$, a negative real double root exists at $c = c_1$ and the other two roots are both real and one is positive and the other is negative. The four eigenvalues are plotted against the speed when $\lambda = 0.3$, $\gamma = -5$ and $\eta = -8$, and shown in figure 6.7(b), and in this case the type of the roots is *n**n**p*. When $\eta > \gamma$ and $d_1 = (\eta-1)^2 + 4\gamma > 0$ (the region between the vertical dotted lines 1 and 2 in figure 6.6(a)), no double root exists and from our results in the previous chapter we can say that in this region the uniform state is stable and no travelling wave can be observed when the state is is perturbed.

If $d_1 = (\eta-1)^2 + 4\gamma < 0$ and $d_2 = (\eta-\lambda)^2 + 4\gamma\lambda > 0$ (the region between the vertical dotted lines 2 and 3 in figure 6.6(a)), a real positive double root exists at $c = c_2$, and the other two roots are real and negative, see figure 6.7(c) which shows the four eigenvalues versus the speed when $\lambda = 0.3$, $\gamma = -5$ and $\eta = -3$. Hence we can say that the roots are of the type *n**n****p***, thus c_2 can not be selected as the double root is positve. When $d_2 = (\eta-\lambda)^2 + 4\gamma\lambda < 0$ and $\eta < -1$ (the region between the vertical dotted lines 3 and 4, see figure 6.6(a)), a real and negative double root exists at $c = c_4$, and the other two roots are complex conjugate with a positive real (roots type **n***PP*).

When $\eta > -1$ and $d_3 = (\eta-\lambda)^2 + \gamma(1+\lambda)^2 < 0$ (the region between the vertical dotted lines 4 and 5 in figure 6.6(a)), a purely imaginary root can exist at $c = C_2$ (from (6.7) and (6.8)). In this region two double roots appear one at $c = c_4$ and the other at $c = c_5$. The double eigenvalue at speed c_4 is real and negative, and the other two roots are complex conjugate with a real part that can be either positve or negative (switching happens at $c = C_2$), hence the roots type are **n***PP* or **n***NN*, see figure 6.7(d). The double

root which arises at $c = c_5$ (and $\eta > -1$) is complex with negative real part, and the other two roots are complex, one with negative real part and the real part of the other can be either positive or negative (transition occurs at $c = C_2$). Figure 6.7(a) shows the real parts of the double root and the other two roots versus speed at $\lambda = 0.3$, $\gamma = -5$, the roots types can be *NN*P or *NN*N. Finally, when $d_1 = (\eta - 1)^2 + 4\gamma > 0$, two real and negative double root exists one at $c = c_3$ and the other at $c = c_4$. The four eigenvalues against speed c shown in figures 6.7(e) and (f) at $\lambda = 0.3$, $\gamma = -5$ and $\eta = 7$ in (e) and $\eta = 10$ in (f). Form these figures one can observe that at $c = c_3$ the roots type can be *NN***n** or *nn***n**, while it can be either **n***NN* or **n***nn* at $c = c_4$. The above results are summarised in table 6.1.
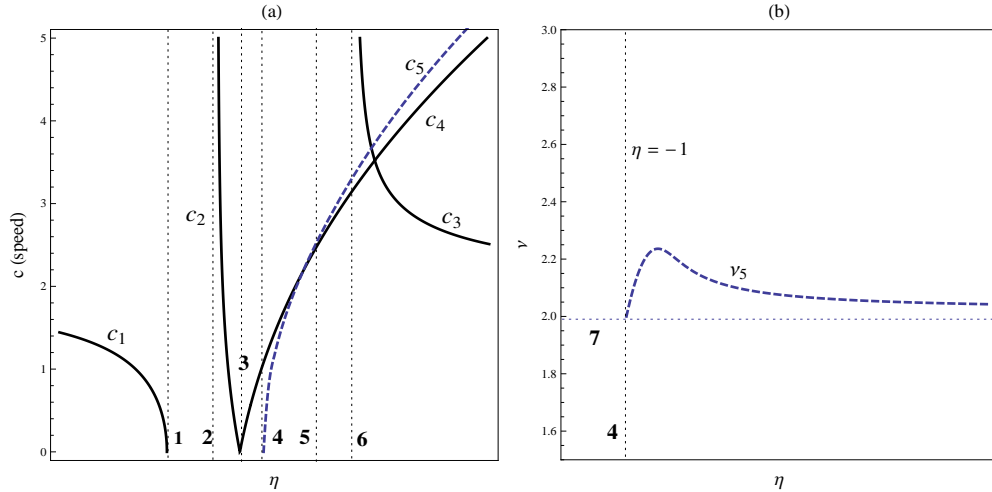
Figure 6.6: Double root locus for (6.1) when $0 < \lambda < 1/2$, $\gamma < -1$. (1) $\eta = \gamma$, (2) and (6) $d1 = (\eta - 1)^2 + 4\gamma = 0$, (3) $d2 = (\eta - \lambda)^2 + 4\gamma\lambda = 0$, (4) $\eta = -1$, (5) $d_3 = (\eta - \lambda)^2 + \gamma(1 + \lambda)^2$ and (7) $v = \sqrt{-1 - \gamma}$.

6.1.6 Classification when $1/2 < \lambda \leq 1$

Table 6.2 gives a summary for the classification of the double root and the other two roots for the characteristic equation (6.1), when $1/2 < \lambda < 1$. The classification is given for different regimes for the parameter γ: $\gamma = 0$, $\gamma > 0$, $-1 < \gamma < 0$ and $\gamma \leq -1$, and in the

119
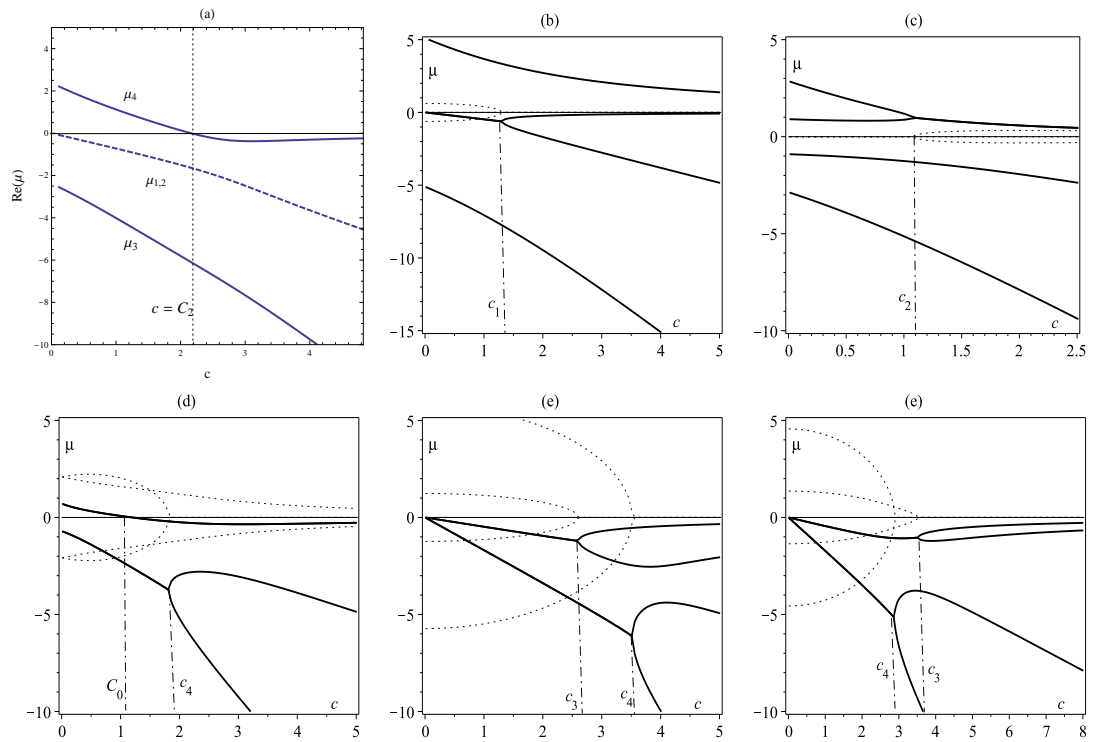
Figure 6.7: The character of double roots in figure 6.6. (a) The variation of the real part of the double root (dashed line, at $c = c_5$) and the other two roots (solid line) with speed c, $\lambda = 0.3$ and $\gamma = -5$. (b)-(f) The four eigenvalues versus speed c when $\lambda = 0.3$, $\gamma = -5$ and at different values of η : (b) -8, (c) -3, (d) 2, (e) 7 and (f) 10.

following we aim to interpret briefly the results shown in this table, following the same way as in the previous case $1/2 < \lambda < 1$.

Table 6.2: Classification of a double root and the other two roots of (6.1) when $1/2 < \lambda \leq 1$. Bold letters represent the double root, capital for real parts of a complex root, and small for purely real roots. The roots are in ascending order, $d_1 = (\eta - 1)^2 + 4\gamma$, $d_2 = (\eta - \lambda)^2 + 4\gamma\lambda$, and $d_3 = (\eta - \lambda)^2 + \gamma(1+\lambda)^2$, and a real triple root exists at $\eta = \eta_*$.

	Conditions	(Speed)c	Roots Types	Figures
$\gamma = 0$		Same classification as in table 6.1		
$\gamma > 0$	$\eta \leq \lambda$	c_1	$n\mathbf{n}p$	
	$\lambda < \eta \leq \gamma$	c_1	$n\mathbf{n}p$	
		c_3	$\mathbf{N}PP/\mathbf{N}NP$	6.8
	$\eta > \gamma$	c_1, c_2	$n\mathbf{n}n, NN\mathbf{n}$	
		c_3	NNP/NNN	
$-1 \leq \gamma < 0$	$\eta \leq \gamma$	c_1	$n\mathbf{n}p$	
	$\eta > \gamma, d_1 \geq 0$	c_1, c_4	$n\mathbf{n}n, \mathbf{n}NN$	
	$d_1 < 0, \eta \leq \eta_{1*}$	c_1, c_2, c_4	$n\mathbf{n}n, nn\mathbf{n}, \mathbf{n}NN$	
	$\eta > \eta_{1*}, d_1 \leq 0,$	c_4	$\mathbf{n}NN$	
		c_7	NNN	
	$d_1 > 0, \eta \leq \eta_{2*}$	c_3/c_4	$NN\mathbf{n}, nn\mathbf{n}/\mathbf{n}NN, \mathbf{n}nn$	6.9, 6.10
		c_7	NNN	
	$\eta \leq \eta_{2*}$	c_3, c_4, c_5, c_6	$NN\mathbf{n}, \mathbf{n}nn, \mathbf{n}nn, \mathbf{n}nn$	
$-1 < \gamma$	$\eta \leq \gamma$	c_1	$n\mathbf{n}p$	
	$\eta > \gamma, d_1 \geq 0$	–	–	
	$d_1 < 0, d_2 \geq 0$	c_2	$nn\mathbf{p}$	
	$d_2 < 0, \eta \leq -1$	c_4	$\mathbf{n}PP$	
	$\eta > -1, d_3 \leq 0$	c_4	$\mathbf{n}PP, \mathbf{n}NN$	
		c_7	NNP/NNN	6.11
	$d_3 > 0, d_1 < 0$	c_4	$\mathbf{n}NN$	
		c_7	NNN	
	$d_1 > 0, \eta \leq \eta_*$	c_3, c_4	$NN\mathbf{n}, nn\mathbf{n}/\mathbf{n}NN, \mathbf{n}nn$	
		c_7	NNN	
	$\eta > \eta_*$	c_3, c_4, c_5, c_6	$NN\mathbf{n}, \mathbf{n}nn, \mathbf{n}nn, \mathbf{n}nn$	

When $\gamma = 0$, the four roots are given by (6.15), and from our previous analysis for $0 < \lambda \leq 1/2$, we can say that the roots types are the same. Therefore, we refer to table 6.1 to classify the roots when $\gamma = 0$. If $\gamma > 0$, a double root speed and frequency versus η shown in figure 6.8(a), which represent the solution of equations (A.14) and (A.15)

(Appendix A). The solid lines represents the two speeds $c = c_1$ and $c = c_2$ (and $v = 0$), where a real negative double root exists, and the other two roots are classified as follows. When $\eta < \gamma$, form (6.18), the coefficient sign sequence is $+ + \pm \pm -$. Hence according to Descartes' Rules of Sign, the real positive roots can be either three or one, and as the double root is real and negative, hence the other two roots are one negative and one positive. Therefore, when $\eta < \gamma$ the double root speed $c = c_1$, and the roots type is nnp (see figure 6.8(d), the four eigenvalues versus speed when $\lambda = 0.7$, $\gamma = 2$ and $\eta = -2$).

If $\eta > \gamma$ and $\gamma > 0$, the coefficient sign sequence is always $+ + + + +$, thus there is no positive real roots. Since the Routh-Hurwitz conditions are satisfied and the double root is negative, then the other two roots are either negative or complex with negative real part. Figure 6.8(e) shows the four eigenvalues $\lambda = 0.7$, $\gamma = 2$ and $\eta = 4$, the roots types are nnn and NNn at speed c_1 and c_2, respectively. The double root speed $c = c_3$ (see 6.8(a), dashed line) exists when $\eta > \lambda$. At this speed the double root is complex with negative real part and the other two roots are complex and their real parts can either be positive or negative. Figure 6.8(c) shows the variation of the real part of the double root (dashed line) and the real part of the other two roots with speed, when $\lambda = 0.7$, $\gamma = 2$. The real part of the other two roots switches from positive to negative at $c = C_1$ (the speed where purely imaginary root exists), which is given by (6.5). The types the roots type at $c = c_3$ can be one of the three types NPP, NNP and NNN.

Figure 6.9(a) and (b) shows a double root speed and frequency versus η when $-1 < \gamma < 0$. The solid line represents speed at which a negative real double root exists, however dashed line is for the speed at which the double root is complex root with negative real part, at $c = c_7$ (and $v = v_7$). From this figure, one can observe that the speed c_7 exists for $\eta_{*1} < \eta < \eta_{*2}$, where a triple root exists at η_{*1} and η_{*2}. This can be understood when when we refer to triple root locus in the γ, η space (see figure 6.1), we find that when $1/2 < \lambda < 1$ and for any value of γ such that $-1 < \gamma < 0$, there are two different
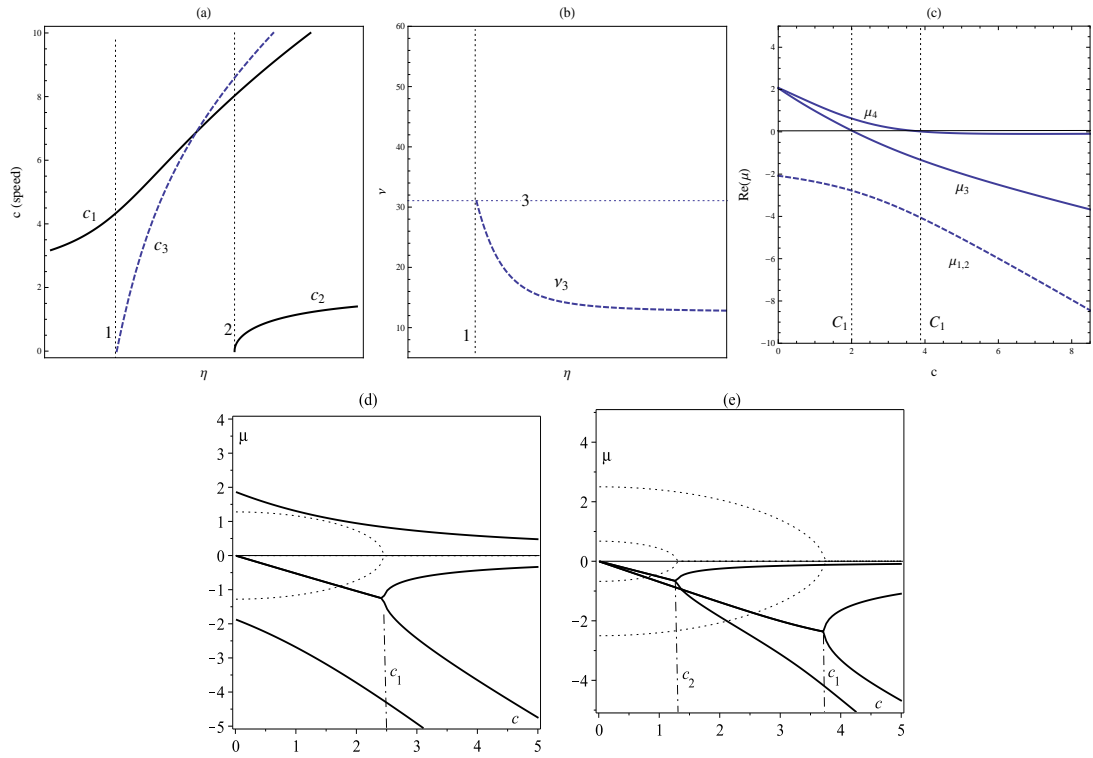
Figure 6.8: (a), (b) Double root locus for equation (6.1) when $1/2 < \lambda < 1$, $\gamma > 0$, dotted lines are: (1) $\eta = \lambda$, (2) $\eta = \gamma$ and (3) $\nu = 2\sqrt{\gamma\lambda}/(1-\lambda)$. (c) The variation of the real part of the double root (dashed line, at $c = c_3$) and the other two roots (solid line) with speed c, $\lambda = 0.7$, $\gamma = 2$. (d) and (e) The four eigenvalues as a function of speed c at $\lambda = 0.7$, $\gamma = 2$ and at different values of η : (d)-2 , (e) 2, solid lines represent the real part and dotted line represent the imaginary part of eigenvalues.
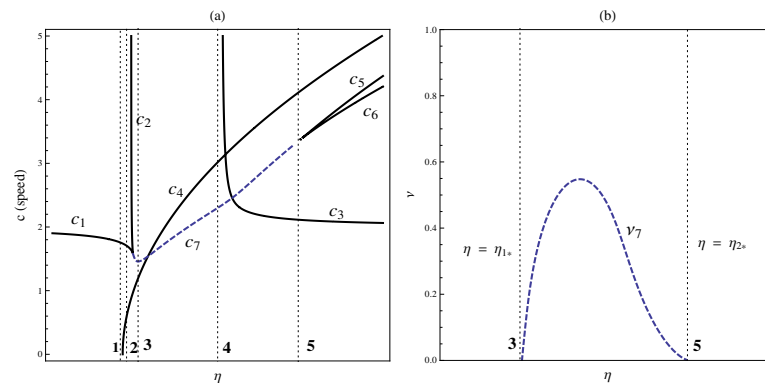
Figure 6.9: (a) and (c) Double root locus for equation (6.1) when $1/2 < \lambda < 1$, $-1 \leq \gamma < 0$. (1) $\eta = \gamma$, (2) and (4) $(\eta - 1)^2 + 4\gamma = 0$, (3) and (5) $\eta = \eta_*$.

123
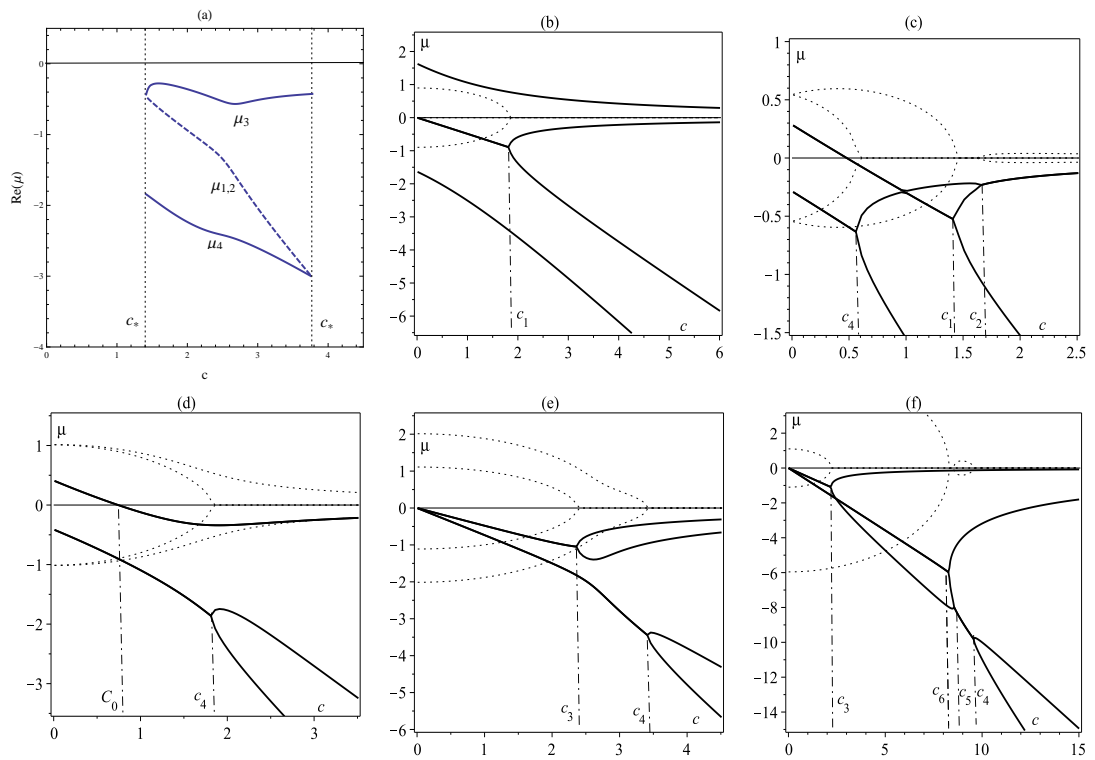
Figure 6.10: The character of the double root and the other tow roots for the double root speeds appear in figure 6.9. (a) The variation of the double root (dashed line, at $c = c_7$) and the other two roots (solid line) with c, $\lambda = 0.7$, $\gamma = -0.5$. (b)-(e) The four eigenvalues versus speed c when $\lambda = 0.7$, $\gamma = -0.5$ and η is: (b) -2, (c) -0.4, (d) 0.5, (e) 2.5 and (f) 3, solid lines represent the real part and dotted line represent the imaginary part of eigenvalues.

124

values of η at which a triple root exists for the characteristic equation. We plot the real parts of the double root and the other two roots, shown in figure 6.10(a), when $\lambda = 0.7$ and $\gamma = -0.5$, and from this figure the roots type is always NNN. For the other double root speeds $c = c_i$, $i = 1, 2, ..., 6$, the character of the double root and the other two roots is known when we plot the four eigenvalues of the characteristic equation versus the speed in different regimes. These plots are depicted in figures 6.10(b)-(f). In case of $1/2 < \lambda < 1$
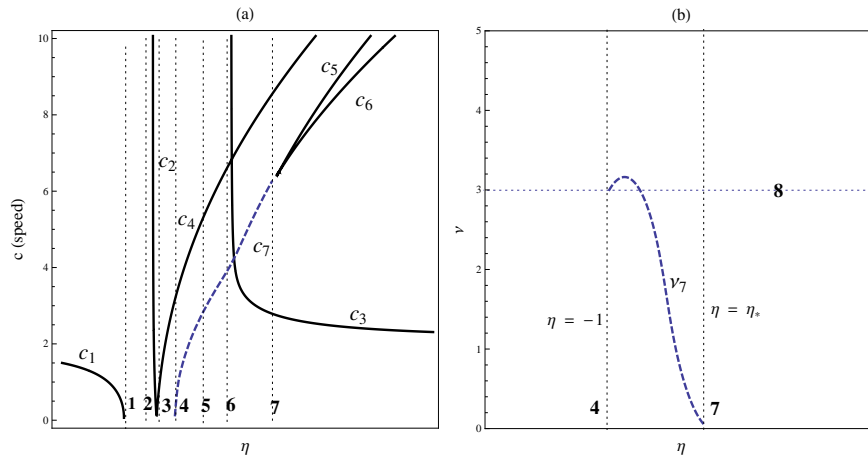
Figure 6.11: (a), (b)Double root locus for equation (6.1) when $1/2 < \lambda < 1$, $\gamma < -1$. (1) $\eta = \gamma$, (2) and (6) $d_1 = (\eta - 1)^2 + 4\gamma = 0$, (3)$d_2 = (\eta - \lambda)^2 + 4\gamma\lambda = 0$, (4) $\eta = -1$, (5) $d_3 = (\eta - \lambda)^2 + \gamma(1 + \lambda)^2 = 0$, (7) $\eta = \eta_*$ and (8) $\nu = \sqrt{-1 - \gamma}$.

and $\gamma < -1$ (see figure 6.11), a positive real double root exists at speed $c = c_2$, a negative real double root exists when $c = c_i$, $i = 1, 3, 4, 5, 6$. There is also a complex double root with negative real part when $c = c_7$ and $\nu = \nu_7$ (the dashed line in figure 6.11), where $-1 < \eta < \eta_*$. Figure 6.12 (a) indicates the real parts of the double root and the other two roots versus the speed when (at $c = c_7$), when $\lambda = 0.7$ and $\gamma = -5$. From this figure we observe that the type of the roots can be either NNP or NNN, and the switching occurs at $c = C_2$ which is given by (6.7). In figures 6.12 (b)-(f), the four eigenvalues are plotted versus speed when $\lambda = 0.7$, $\gamma = -5$ and $\eta = -10, -3.5, 1.0, 5, 20$. These plots indicates the root type at the double root speeds $c = c_i$, $i = 1, 2, ..., 6$, these types are shown in table

6.2.
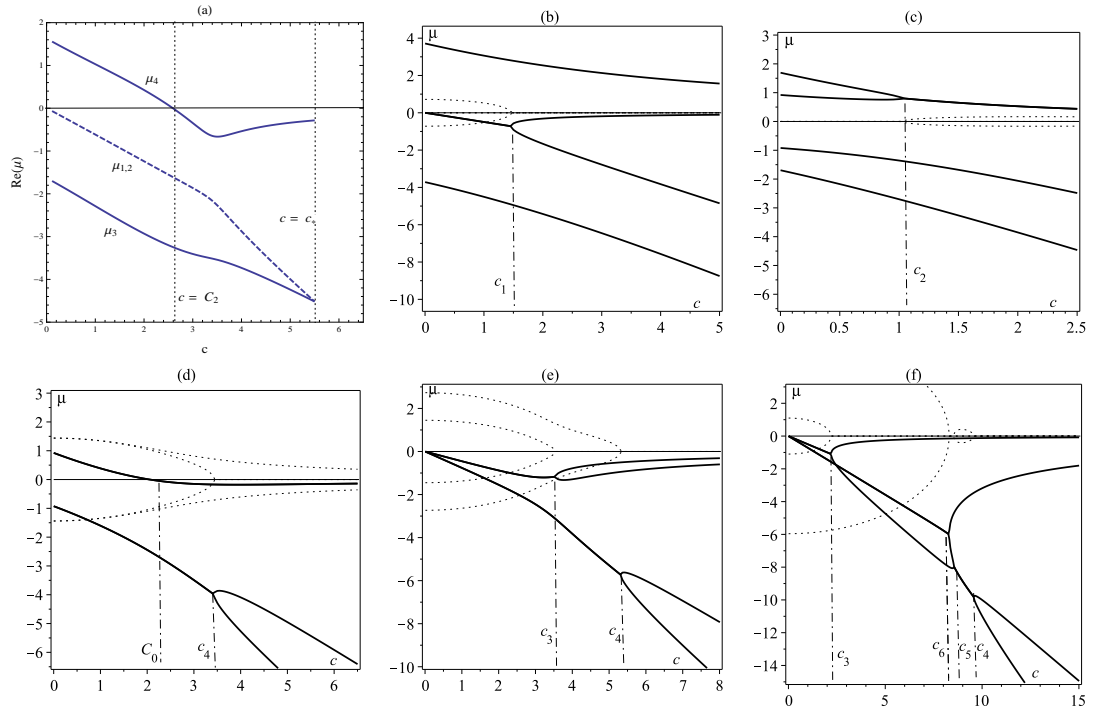
Figure 6.12: (a) The variation of the real part of the double root (dashed line, at $c = c_7$) and the other two roots (solid line) with speed c, $\lambda = 0.7$ and $\gamma = -5$. (b)-(f) The four eigenvalues versus speed c when $\lambda = 0.7$, $\gamma = -5$ and η is: (b) -10, (c) -3.5, (d) 1.0, (e) 5 and (f) 20, solid lines represent the real part and dotted line represent the imaginary part of eigenvalues.

6.2 Case S2

In this case $f_u < 0$, we refer to (4.17) with the negative sign to find that the characteristic equation is

$$\lambda\mu^4 + c(1+\lambda)\mu^3 + (c^2 - \lambda + \eta - i\nu(\lambda+1))\mu^2 + c(\eta - 1 - 2i\nu)\mu - \eta - \gamma - \nu^2 - i(\eta-1)\nu = 0,$$

$$(6.19)$$

126

and the double root equation is then

$$4\lambda\mu^3 + 3c(1+\lambda)\mu^2 + 2(c^2 - \lambda + \eta - i\nu(\lambda+1))\mu + c(\eta - 1 - 2i\nu) = 0, \quad (6.20)$$

where ν and c are real and μ can be complex.

6.2.1 Double root speed

One can repeat same procedure as in the previous case. We eliminant μ using the above two equations using the Sylvester's elimination method. The eliminant of (6.19) is complex and gives two real equations. These two equations are displayed in (A.22) - (A.23), and reduce to (A.24) when $\nu = 0$ (see appendix A). We solve these resultant equations for travelling wave parameters, speed c and modulating frequency ν. Then we insert these values of c and ν into the quartic equation (6.19) to determine the character of a double root and the corresponding two roots.

6.2.2 Triple root condition

A triple root satisfies the following equations (condition at which a transition from $\nu = 0$ to $\nu \neq 0$ occurs)

$$\lambda\mu^4 + c(1+\lambda)\mu^3 + (-\lambda + \eta + c^2)\mu^2 + c(\eta - 1)\mu - \eta - \gamma = 0, \quad (6.21)$$

$$4\lambda\mu^3 + 3c(1+\lambda)\mu^2 + 2(-\lambda + \eta + c^2)\mu + c(\eta - 1) = 0, \quad (6.22)$$

$$6\lambda\mu^2 + 3c(1+\lambda)\mu + (-\lambda + \eta + c^2) = 0, \quad (6.23)$$

and when we eliminate μ and c we obtain the triple root condition which is displayed in (A.25). This condition is shown in figure 6.13 in the γ, η space at different values of λ.

127
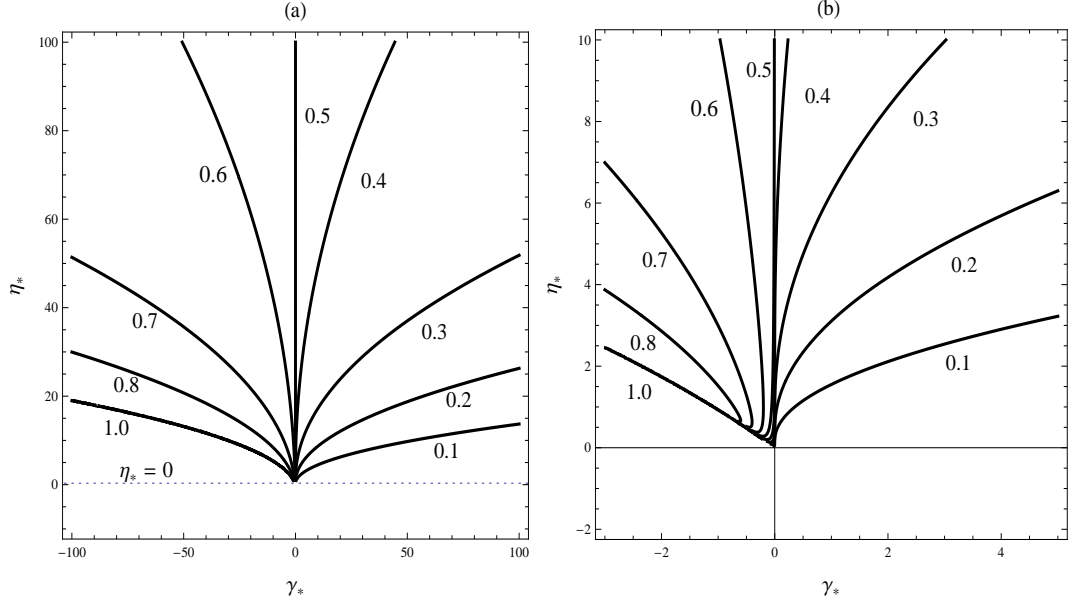
Figure 6.13: (a) Triple root locus for (6.10) in η, γ space, equation (A.25), for $\lambda = 0.1$ to 1. When $\gamma > -1$ a triple root exists when $0 < \lambda < 1/2$, and when $\gamma < 0$, it exists for $1/2 < \lambda \leq 1$. A triple root cannot exist for $\eta < 0$. (b) A close-up picture for the locus near the origin.

6.2.3 Purely imaginary root

As in the previous case, we need to compute the speed at which a real part switches from positive to negative. One can obtain this speed at which the characteristic equation has a purely imaginary root. There are two speeds, the first is

$$C_1 = \sqrt{\frac{2\lambda v^2}{\eta - \lambda + ((\eta - \lambda)^2 + 4\lambda(\eta + \gamma))^{1/2}}}, \tag{6.24}$$

provided that

$$(\eta - \lambda)^2 + 4\lambda(\eta + \gamma) \geq 0, \tag{6.25}$$

In addition, if $\eta - \lambda < 0$, then $\eta + \gamma > 0$. The second purely imaginary root speed $c = C_2$ is

$$C_2 = \sqrt{\frac{1+\lambda}{\eta - 1}} \left(v + \sqrt{-\frac{\gamma(1+\lambda)^2 + (\eta + \lambda)^2}{(1+\lambda)^2}} \right), \tag{6.26}$$

128

provided that

$$\eta > 1, \quad \gamma(1+\lambda)^2 + (\eta + \lambda)^2 \leq 0. \tag{6.27}$$

and from (6.26), the speed at which a purely imaginary root exists when $v = 0$ is given by

$$C_0 = \sqrt{-\frac{\gamma(1+\lambda)^2 + (\eta + \lambda)^2}{(1+\lambda)(\eta - 1)}}, \tag{6.28}$$

provided that conditions (6.27) are satisfied.

6.2.4   Summary of roots classification

Now by following same way in discussing the character of the eigenvalues in the previous case, we can easily obtain the results for this case. A summary of the results are shown in tables 6.3 and 6.4. Variation of double root speed and the eigenvalues with system parameters λ, γ, and η are plotted. These plots help in uncovering the classification of eigenvalues shown in summary tables.
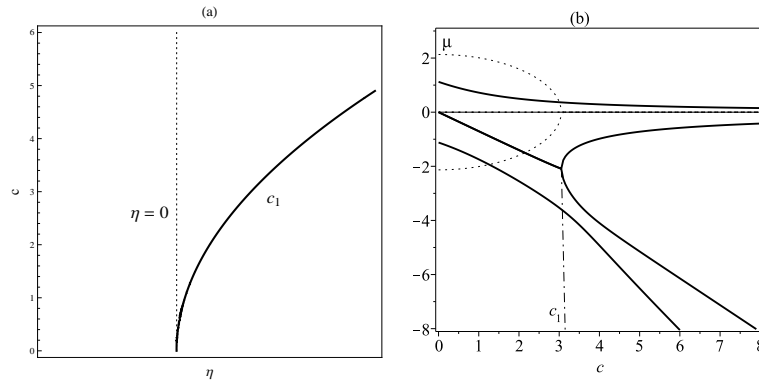
Figure 6.14: (a) Double root locus for (6.19) when $\gamma = 0$, $c_1 = 2\sqrt{\eta\lambda}$. (b) The four eigenvalues versus speed c, $\lambda = 0.4$ $\gamma = 0$ and $\eta = 3$.

Table 6.3: Types of eigenvalues for (6.19) when $0 < \lambda < 1/2$. Bold letters represent the double root, capital for real parts of a complex root, and small for purely real roots. The roots are in ascending order, $q_1 = (\eta + 1)^2 + 4\gamma$, $q_2 = (\eta + \lambda)^2 + 4\gamma\lambda$, and $q_3 = (\eta + \lambda)^2 + \gamma(1 + \lambda)^2$, and a real triple root exists at $\eta = \eta_*$.

	Conditions	(Speed)c	Roots Types	Figures
$\gamma = 0$	$\eta \leq 0$	$-$	$-$	6.14
	$\eta > 0$	c_1	nnp	
$\gamma > 0$	$\eta \leq -\gamma$	$-$	$-$	
	$-\gamma < \eta \leq -\lambda$	c_1	$n\mathbf{n}p$	6.15
	$-\lambda < \eta \leq \eta_*$	c_1	$n\mathbf{n}p$	
		c_4	$\mathbf{N}PP, \mathbf{N}NP$	
	$\eta > \eta_*$	c_1, c_2, c_3	$n\mathbf{n}p, n\mathbf{n}p, \mathbf{n}np,$	
$-1 \leq \gamma < 0$	$q_1 \geq 0$	$-$	$-$	
	$q_1 < 0, q_2 \geq 0$	c_1	$nn\mathbf{p}$	
	$q_2 < 0, q_1 \geq 0$	c_2	$\mathbf{n}PP$	
	$q_1 > 0, q_2 \leq 0$	c_2/c_3	$\mathbf{n}PP, \mathbf{n}pp/NN\mathbf{p}, nn\mathbf{p}$	6.16 , 6.17
	$q_2 > 0, \eta \leq -\gamma$	c_2, c_4	$\mathbf{n}pp, \mathbf{n}pp$	
	$-\gamma < \eta \leq \eta_*$	c_2, c_4, c_5	$\mathbf{n}np, \mathbf{n}np, nn\mathbf{p}$	
	$\eta > \eta_*$	c_2	$\mathbf{n}np$	
		c_6	$NN\mathbf{P}$	
$\gamma < -1$	$q_1 \geq 0$	$-$	$-$	
	$q_1 < 0, q_2 \geq 0$	c_1	$nn\mathbf{p}$	
	$q_2 < 0, \eta \leq 1$	c_2	nPP	
	$\eta > 1, q_3 \leq 0,$	c_2	$\mathbf{n}PP, \mathbf{n}NN$	
		c_4	$NN\mathbf{P}$	6.18 , 6.19
	$q_3 > 0, q_1 \leq 0$	c_2	$\mathbf{n}NN$	
		c_4	$NN\mathbf{P}$	
	$q_1 > 0, \eta \leq -\gamma$	c_2, c_3	$\mathbf{n}NN, \mathbf{n}nn/NN\mathbf{n}, nn\mathbf{n}$	
		c_4	$NN\mathbf{P}$	
	$\eta > -\gamma$	c_2	$\mathbf{n}np$	
		c_4	$NN\mathbf{P}$	
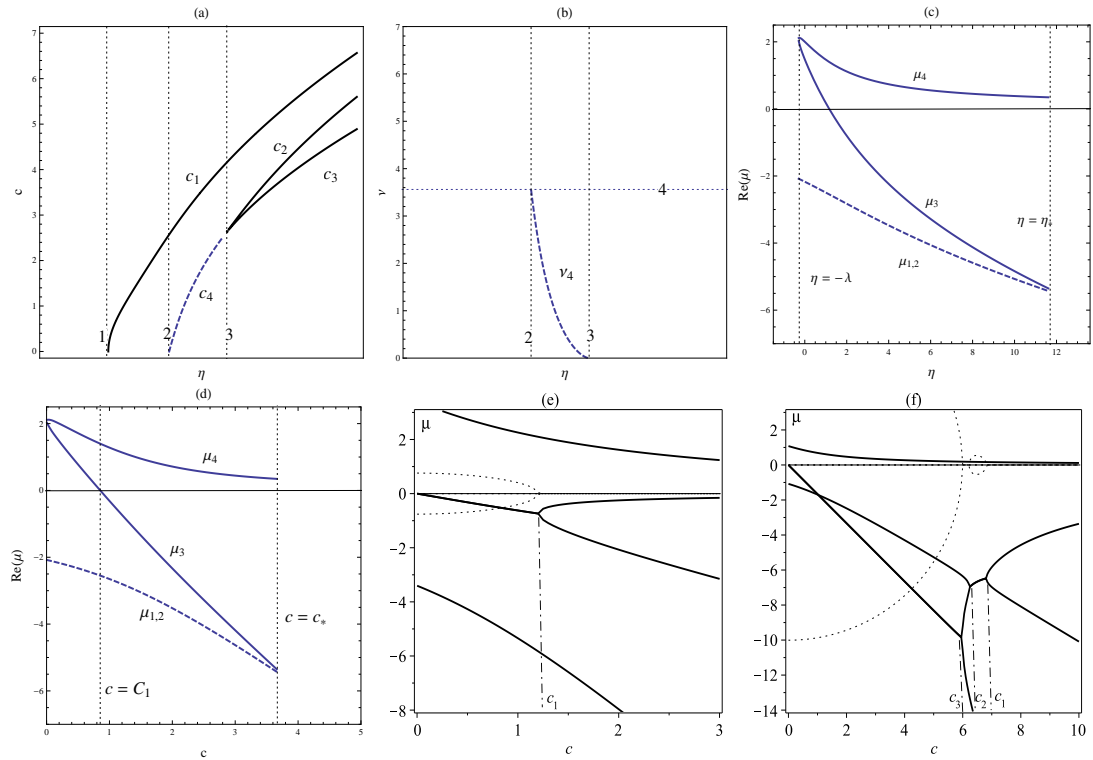
Figure 6.15: Double root locus for for (6.19) when $0 < \lambda < 1/2$, $\gamma > 0$, dotted lines are (1) $\eta = -\gamma$, (2) $\eta = -\gamma$, (3) $\eta = \eta_*$ and (4) $\nu = 2\sqrt{\gamma\lambda}/(1-\lambda)$. (c) and (d) The variation of the double root (dashed line) and the other two roots (solid line) with η and c_4, respectively, when $\lambda = 0.3$ and $\gamma = 5$. (e) and (f) The four eigenvalues versus speed c when, $\lambda = 0.3$ and $\gamma = 5$ and (e) $\eta = -3$, (f) $\eta = 20$, solid lines represent the real part and dotted line represent the imaginary part of eigenvalues.
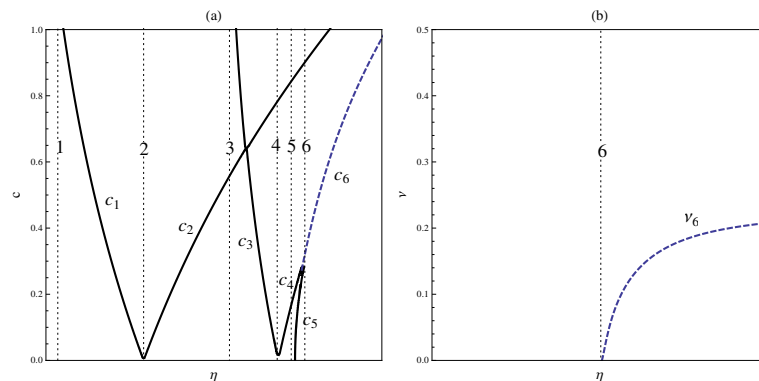
Figure 6.16: Double root locus for (6.19) when $0 < \lambda < 1/2$, $-1 < \gamma < 0$. (1) and (3) $(\eta+1)^2 + 4\gamma = 0$, (2) and (4) $(\eta+\lambda)^2 + 4\gamma\lambda = 0$, (5) $\eta = -\gamma$, (6) $\eta = \eta_*$

131
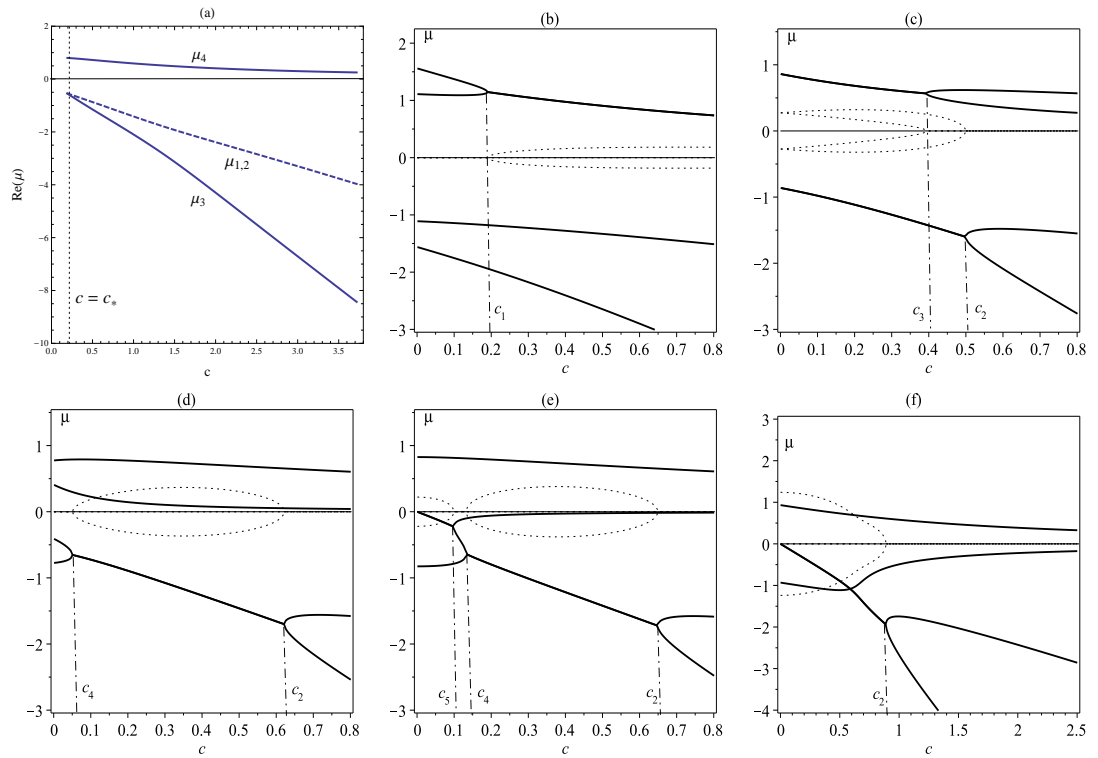
Figure 6.17: (a) The variation of the double root (dashed line) and the other two roots (solid line) with c_6 (see figure 6.16), $\lambda = 0.3$ and $\gamma = -0.1$. (b)-(f) The four eigenvalues versus speed c when $\lambda = 0.3$ and $\gamma = -0.1$ and (b) $\eta = -0.5$, (c) $\eta = -0.1$, (d) $\eta = 0.07$, (e) $\eta = 0.11$ and (f) $\eta = 0.5$, solid lines represent the real part and dotted line represent the imaginary part of eigenvalues.
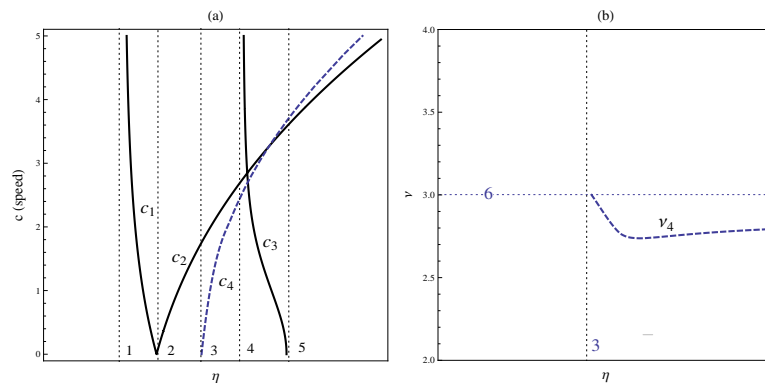
Figure 6.18: Double root locus for (6.19) when $0 < \lambda < 1/2$, $\gamma < -1$. (1) and (4) $(\eta+1)^2 + 4\gamma = 0$, (2) $(\eta + \lambda)^2 + 4\gamma\lambda = 0$, (3) $\eta = 1$, (5) $\eta = -\gamma$ and (6) $\nu = \sqrt{-1 - \gamma}$.

132
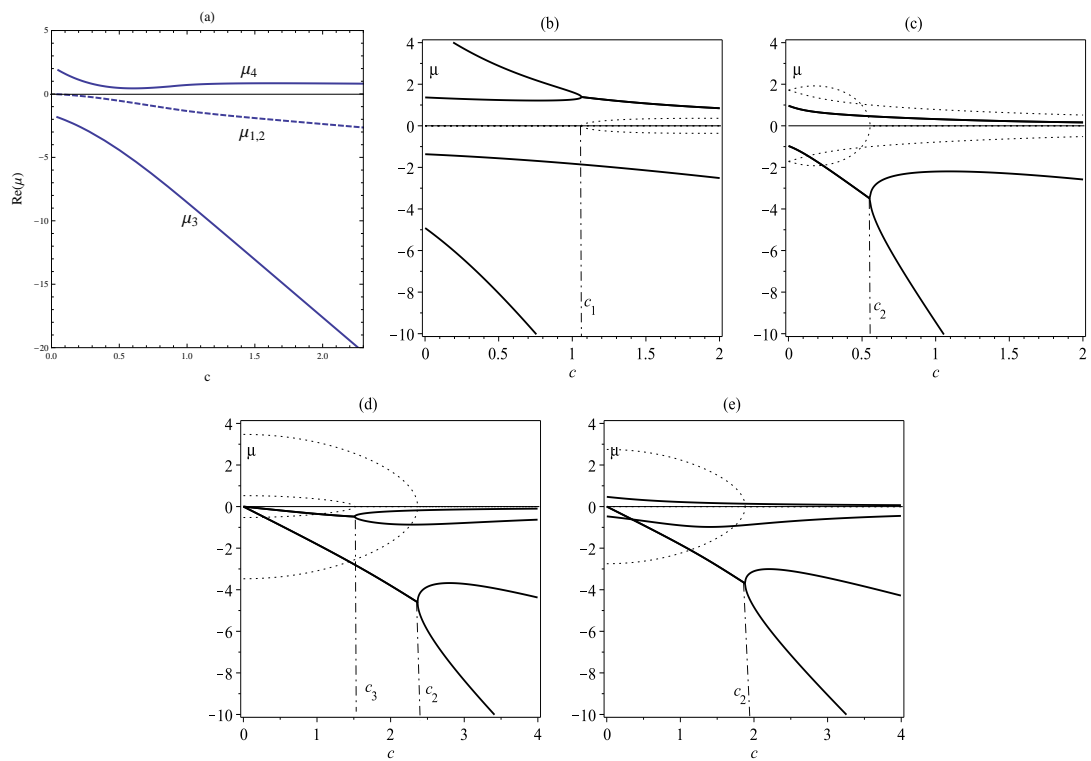
Figure 6.19: (a) The variation of the double root (dashed line) and the other two roots (solid line) with c_4 (see figure 6.18), $\lambda = 0.1$ and $\gamma = -2$. (b)-(e) The four eigenvalues versus speed c when $\lambda = 0.1$ and $\gamma = -2.0$ and (b) $\eta = -2.5$, (c) $\eta = 0.5$, (d) $\eta = 1.2$, (e) $\eta = 2.5$, solid lines represent the real part and dotted line represent the imaginary part of eigenvalues.

Table 6.4: Types of eigenvalues for (6.19) when $1/2 \leq \lambda < 1$. Bold letters represent the double root, capital for real parts of a complex root, and small for purely real roots. The roots are in ascending order, $q_1 = (\eta + 1)^2 + 4\gamma$, $q_2 = (\eta + \lambda)^2 + 4\gamma\lambda$, and $q_3 = (\eta + \lambda)^2 + \gamma(1 + \lambda)^2$, a real triple root exists at $\eta = \eta_*$.

	Conditions	(Speed)c	Roots Types	Figures
$\gamma = 0$		Same classification as in table 6.3.		
$\gamma > 0$	$\eta \leq -\gamma$	—	—	6.20
	$-\gamma < \eta \leq -\lambda$	c_1	$n\mathbf{n}p$	
	$\eta > -\lambda$	c_1	$n\mathbf{n}p$	
		c_2	$\mathbf{N}PP, \mathbf{N}NP$	
$-1 \leq \gamma < 0$	$q_1 \geq 0$	—	—	6.21 , 6.22
	$q_1 < 0, q_2 \geq 0$	c_1	$nn\mathbf{p}$	
	$q_2 < 0, q_1 \geq 0$	c_2	$\mathbf{n}PP$	
	$q_1 < 0, \eta \leq -\gamma$	c_2, c_3	$\mathbf{n}PP, \mathbf{n}pp/nn\mathbf{p}, NN\mathbf{p}$	
	$-\gamma < \eta < \eta_*$	c_2	$n\mathbf{n}p$	
		c_6	NNP	
	$\eta \geq \eta_*$	c_2, c_4, c_5	$n\mathbf{n}p, n\mathbf{n}p, n\mathbf{n}p$	
$\gamma < -1$	$q_1 \geq 0$	—	—	6.23 , 6.24
	$q_1 < 0, q_2 \geq 0$	c_1	$nn\mathbf{p}$	
	$q_2 < 0, \eta \leq 1$	c_2	$\mathbf{n}PP$	
	$\eta > 1, q_3 \leq 0,$	c_2	$\mathbf{n}PP, \mathbf{n}NN$	
		c_6	NNP	
	$q_3 > 0, q_1 \leq 0$	c_2	$\mathbf{n}NN$	
		c_6	NNP	
	$q_1 > 0, \eta \leq -\gamma$	c_2, c_3	$\mathbf{n}NN, \mathbf{n}nn/NN\mathbf{n}, nn\mathbf{n}$	
		c_6	NNP/NNN	
	$-\gamma < \eta < \eta_*$	c_2	$n\mathbf{n}p$	
		c_6	NNP	
	$\eta \geq \eta_*$	c_2, c_4, c_5	$n\mathbf{n}p, n\mathbf{n}p, n\mathbf{n}p$	

Figure 6.20: (a), (b) Double root locus for (6.19) when $1/2 \leq \lambda < 1$, $\gamma > 0$, dotted lines are (1) $\eta = -\gamma$, (2) $\eta = -\gamma$ and (3) $v = 2\sqrt{\gamma\lambda}/(1-\lambda)$. (c) The variation of the double root (dashed line) and the other two roots (solid line) with c_2. (d) The four eigenvalues versus speed c, when $\lambda = 0.7$ and $\gamma = 5$ and $\eta = 3$, solid lines represent the real part and dotted line represent the imaginary part of eigenvalues.
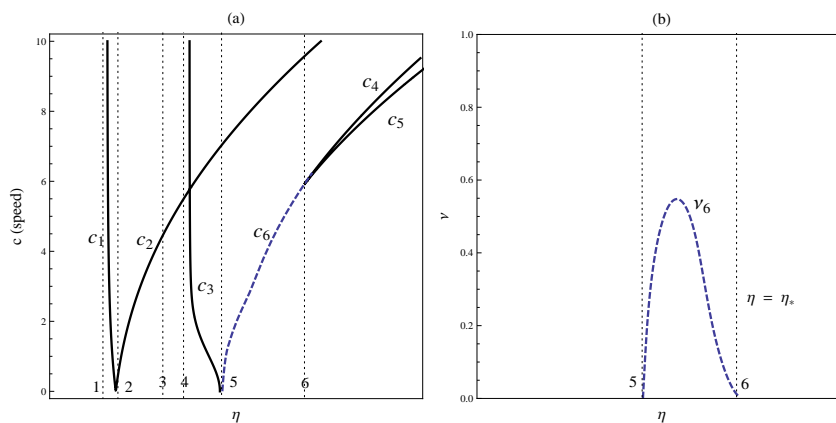
Figure 6.21: Double root locus for (6.19) when $1/2 \leq \lambda < 1$, $-1 < \gamma < 0$. (1) and (4) $(\eta+1)^2 + 4\gamma = 0$, (2) $(\eta+\lambda)^2 + 4\gamma\lambda = 0$, (3) $(\eta+\lambda)^2 + \gamma(1+\lambda)^2 = 0$, (5) $\eta = -\gamma$, (6) $\eta = \eta_*$.
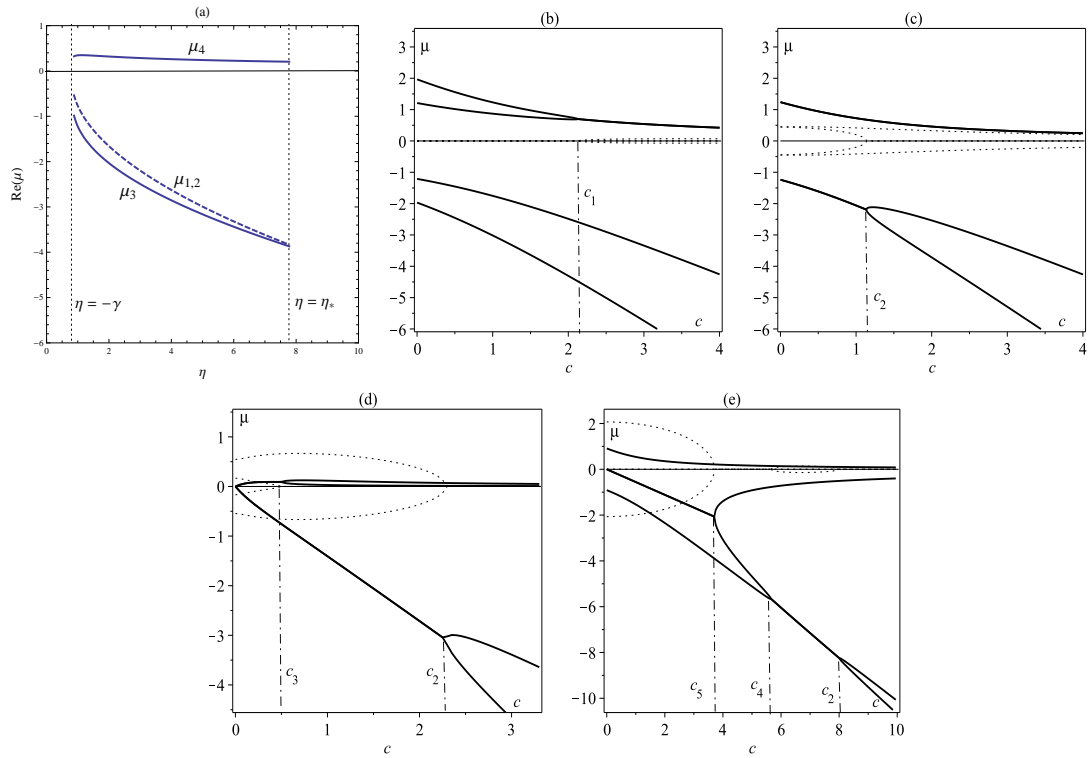
Figure 6.22: (a) The variation of the double root (dashed line) and the other two roots (solid line) with η at $c = c_6$ (see figure 6.21), $\lambda = 0.6$ and $\gamma = -0.8$. (b)-(d) The four eigenvalues versus speed c, when $\lambda = 0.6$ and $\gamma = -0.8$ and different values of η: (b) -2.6, (c) -1, (d) -0.7 and (e) 10, solid lines represent the real part and dotted line represent the imaginary part of eigenvalues.
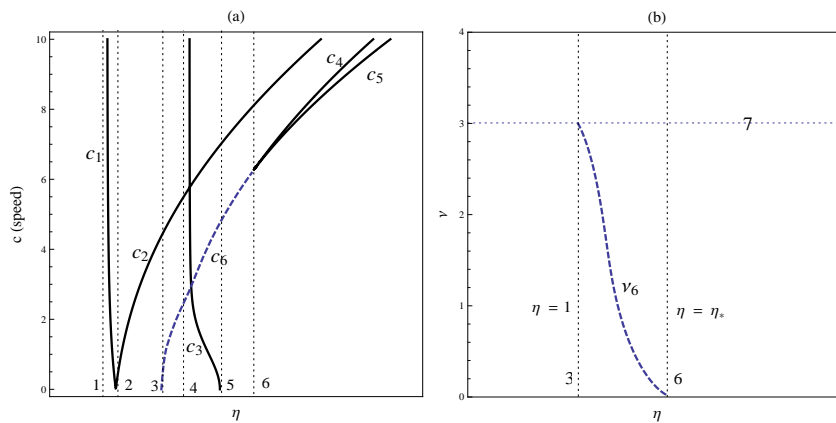
Figure 6.23: Double root locus for (6.19) when $1/2 \leq \lambda < 1$, $\gamma < -1$. (1) and (4) $(\eta+1)^2 + 4\gamma = 0$, (2) $(\eta + \lambda)^2 + 4\gamma\lambda = 0$, (3) $\eta = 1$, (5) $\eta = -\gamma$, (6) $\eta = \eta_*$ and (7) $v = \sqrt{-1-\gamma}$.

136
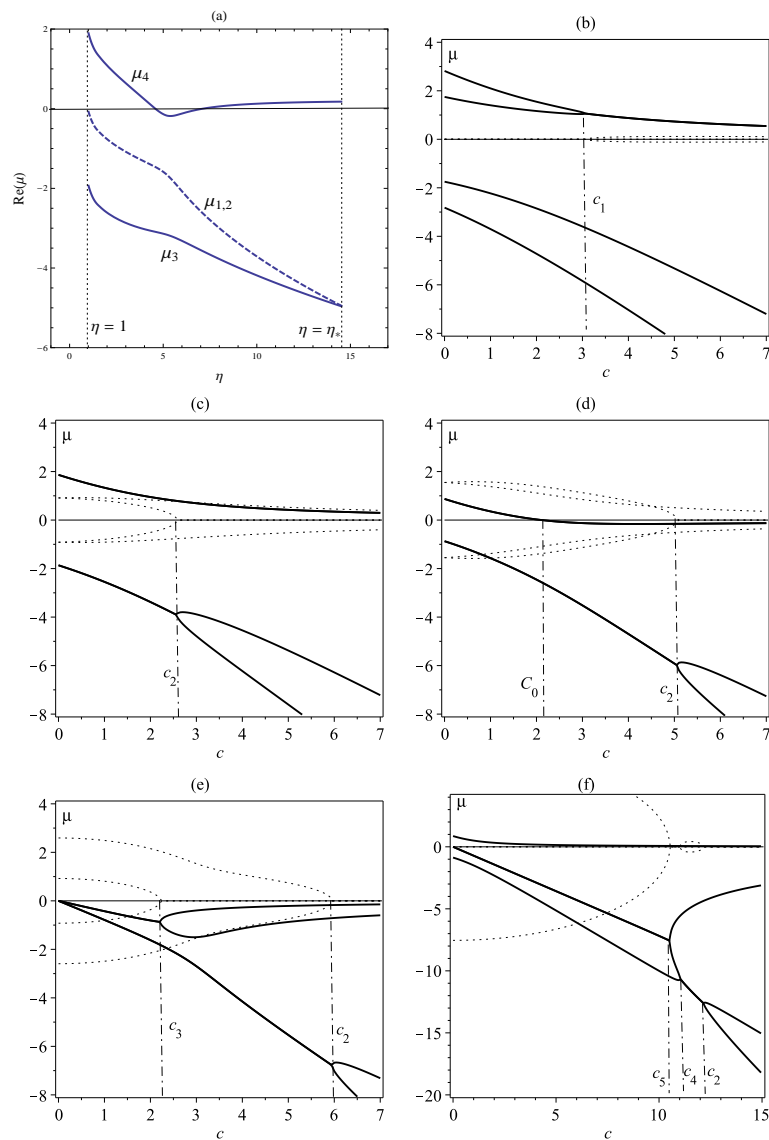
Figure 6.24: (a) The variation of the double root (dashed line, (see figure 6.23)) and the other two roots (solid line) with η at $c = c_6$ and $\lambda = 0.7$, $\gamma = -10$. (b)-(f) The four eigenvalues versus speed c when $\lambda = 0.7$ and $\gamma = -10$ and different values of η: (b) -7, (c) -3, (d) 3, (e) 6 and (f) 25, solid lines represent the real part and dotted line represent the imaginary part of eigenvalues.

6.3 Case S3

In this case $f_u = 0$ and $g_v > 0$, the characteristic equation ((4.21) with the positive sign in the second bracket) is

$$\lambda\mu^4 + c(\lambda+1)\mu^3 + \left(c^2+1-iv(\lambda+1)\right)\mu^2 + c(1-i2v)\mu - \rho - v^2 - iv = 0, \quad (6.29)$$

where v and c are real and μ can be complex. A summary of the roots type is shown in table 6.5. In the following we determine the wave speed at which equation (6.29) has a purely imaginary root, which can help in eigenvalues classification. Equation (6.29) has $\mu = \pm i\omega$ at $c = C$, and there two speeds. The first is such that

$$C = C_1 = \frac{v}{\omega_1}, \quad \omega_1^2 = \frac{1}{2\lambda}[1 + (1+4\lambda\rho)^{1/2}], \quad (6.30)$$

provided that $1 + 4\lambda\rho \geq 0$, and the second is given by

$$C = C_2 = \sqrt{1+\lambda}\left(v + \sqrt{-\frac{1+\rho(1+\lambda)^2}{(1+\lambda)^2}}\right), \quad \omega_2^2 = 1/(1+\lambda), \quad (6.31)$$

provided that $1 + \rho(1+\lambda)^2 \leq 0$. From this result, if $v = 0$ there is only one possible non-zero value, $C_2 = C_0$, and can be written as

$$C_0 = \sqrt{-\frac{1+\rho(1+\lambda)^2}{(1+\lambda)}}, \quad v = 0, \quad (6.32)$$

on the condition $1 + \rho(1+\lambda)^2 < 0$.

A double root speed and frequency can be obtained by solving the two equations (A.28) and (A.29) (Appendix A), the two equation represent the resultant of the characteristic equation (6.29) . They are solved for c and v at specific values of the system parameter λ and ρ and then we plot the obtained solutions.

A triple root conditions are

$$\lambda\mu^4 + c(\lambda+1)\mu^3 + \left(c^2+1\right)\mu^2 + c\mu - \rho \;=\; 0, \tag{6.33}$$

$$4\lambda\mu^3 + 3c(\lambda+1)\mu^2 + 2\left(c^2+1\right)\mu + c \;=\; 0, \tag{6.34}$$

$$6\lambda\mu^2 + 3c(\lambda+1)\mu^2 + \left(c^2+1\right) \;=\; 0, \tag{6.35}$$

and for a fixed λ ($0 < \lambda < 1$), the above conditions are solved for c, ρ and μ. Figure 6.25 shows the variation of c, ρ and μ with λ. We notice that a triple root exists when $\rho \geq -1/4$; when $0 < \lambda \leq 1/2$ it exists for $\rho \geq 0$, and when $1/2 < \lambda \leq 1$ it exists for $-1/4 < \rho < 0$. Thus in the summary table we present the eigenvalue classification considering these parameter regimes.
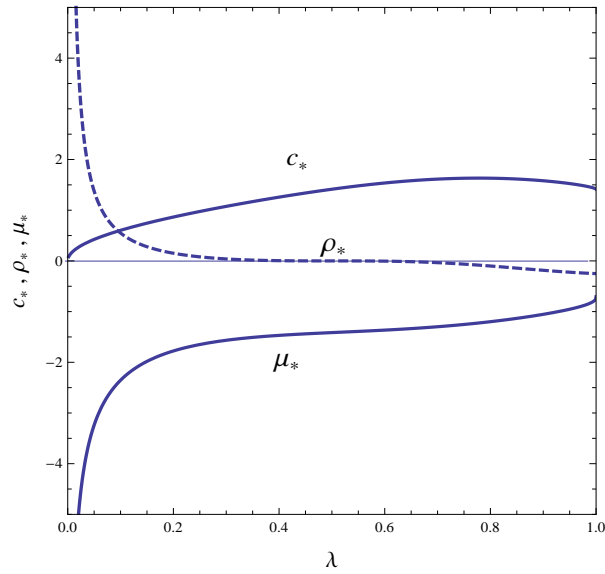
Figure 6.25: The variation of c, ρ and μ with λ when equation (6.29) (with $v = 0$) has a triple root, the solution of equations (6.33)-(6.35). The triple root $\mu = \mu_*$ is always negative and exists for $\rho \geq -1/4$; When $\rho \geq 0$, $0 < \lambda \leq 1/2$, and if $-1/4 \leq \rho < 0$, then $1/2 < \lambda \leq 1$.

When $v = 0$ the sequence of the characteristic polynomial coefficients is $\lambda, c(1+$

λ), $c^2 + 1, c, -\rho$. The the RH sequence B.3 (see Appendix B.2) will be

$$\lambda, \quad (1+\lambda)c, \quad \frac{(1+\lambda)c^2 + 1}{1+\lambda}, \quad \frac{(1+\lambda)c^2 + 1 + \rho(1+\lambda)^2}{(1+\lambda)c}, \quad -\rho. \qquad (6.36)$$

From this sequence we can discuss the character of the roots as follows. If $\rho > 0$, there will be only one sign change and this results in there is only one real and positive root, and consequently the other roots can either be negative or complex conjugate with negative real parts. When $-1/(1+\lambda)^2 < \rho < 0$, there is no sign changes and all the roots have a negative real part. However when $\rho < -1/(1+\lambda)^2$, two sign change is possible and in this case there will be two complex conjugate roots with positive real part and the other two roots are either negative or complex with negative real part.

Now let us demonstrate the character of the roots at double root speeds when $0 < \lambda \leq 1/2$. A double root exists at different wave speeds when $v = 0$, these speeds $c = c_i$, $i = 1, 2, 3, 4$ are represented by the solid lines shown in figure 6.26. Two other speeds c_5 and c_6 exist when $v \neq 0$, represented by the dashed lines. At these double root speeds, we determine the character of the double root and the other two roots as follows.
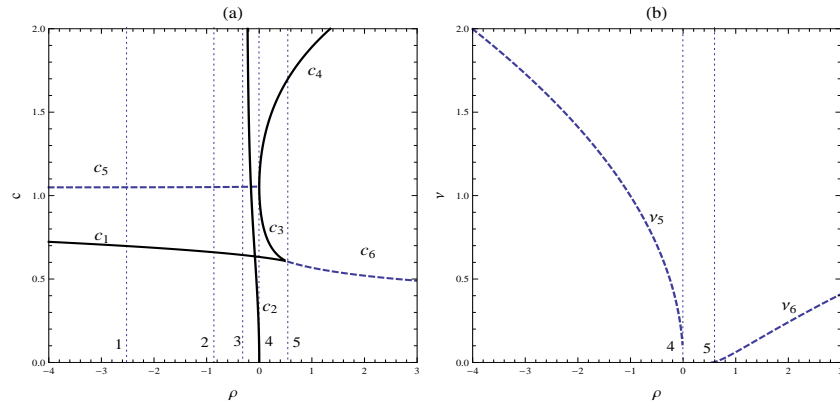
Figure 6.26: Double root locus for (6.29) when $0 < \lambda \leq 1/2$, possible solutions of (A.28) and (A.29). Vertical dotted lines are: (1) $\rho = -1/4\lambda$, (2) $\rho = -1/(1+\lambda)^2$, (3) $\rho = -1/4$, (4) $\rho = 0$ and (5) $\rho = \rho_*$. The character of the eigenvalues are shown in figure 6.27.
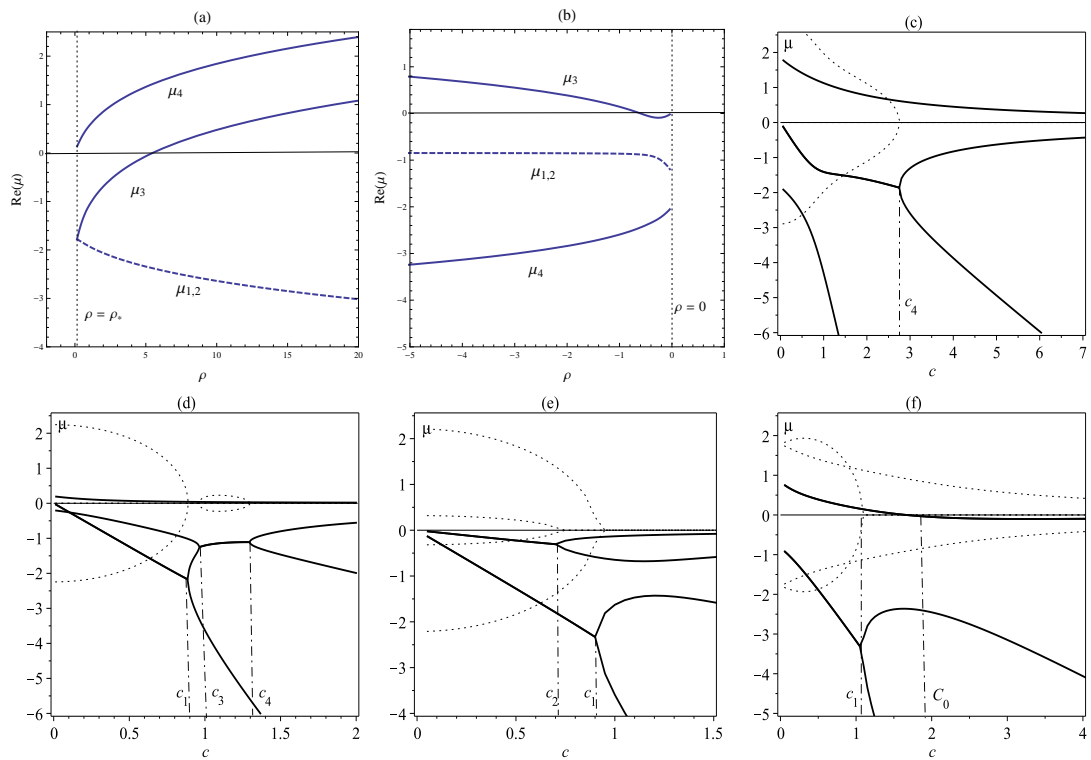
Figure 6.27: (a), (b) The variation of the double root (dashed line) and the other two roots (solid line) with ρ at $c = c_6$ and $c = c_5$ (see figure 6.26) when $\lambda = 0.2$. (c)-(f) The four eigenvalues versus speed c when $\lambda = 0.2$ and at different values of ρ: (c) $\rho = 6$, (d) $\rho = 0.05$, (e) $\rho = -0.1$, (f) $\rho = -1$, solid lines represent the real part and dotted line represent the imaginary part of eigenvalues.

When $0 < \lambda \le 1/2$ and $\rho > \rho_* > 0$, a double root exists at $c = c_4$ and $c = c_6$ (see figure 6.26). When $c = c_4$ a negative and real double root exits and the other two roots are one negative and one positive, the four roots of (6.29) versus speed c are shown in figure 6.27(c). Then the type of the roots at $c = c_4$ is $n\mathbf{n}p$. At $c = c_6$ and $v = v_6$, the real part of the double root and the other two root is plotted versus ρ, shown in figure 6.27(a), and the type of the roots can either be $\mathbf{N}NP$ or $\mathbf{N}PP$. The double root is complex with negative real part, and the other two roots are complex, one with positive real part and the real part of the second can be either positive or negative (a purely imaginary root exists at a speed $c = C_2$ displayed in (6.31)).

When $0 < \rho < \rho_*$ (see figure 6.26), three double root speeds exist, c_1, c_3 and c_4. We proved earlier that in this region, there is one real and positive root, and the other roots can either be negative or complex conjugate with negative real parts. Hence the double root at these speeds is negative and real and the other two roots are one positive and real and one is negative and real. Figure 6.27(d) indicates the character of the roots at the speeds c_1, c_3 and c_4 which are $\mathbf{n}np, n\mathbf{n}p$ and $n\mathbf{n}p$, respectively.

When $\rho < 0$, a complex double root with negative real part exists at $c = c_5$ and $v = v_5$, and the other two roots are complex, one with positive real part and the real part of the second can be either positive or negative (a purely imaginary root exists at a speed $c = C_1$ displayed in (6.30)). The real part of the double root and the other two root is plotted versus ρ, shown in figure 6.27(b), and the type of the roots can either be $N\mathbf{N}N$ or $N\mathbf{N}P$.

Also, when $\rho < 0$ two double roots which are real and negative, occur at the speeds $c = c_1$ and $c = c_2$. The speed c_2 exists only when $-1/4 < \rho < 0$, and the character of the root a this speed is $NN\mathbf{n}$ or $nn\mathbf{n}$, while at $c = c_1$ the roots type can be $\mathbf{n}NN$ or $\mathbf{n}nn$. The four eigenvalues versus the wave speed are shown in figure 6.27(e), which is clearly indicates the types of the roots at c_1 and c_2. When $\rho < -1/4$, a negative real double root exists at $c = c_1$, see figure 6.26(a), and the other two roots are complex conjugate with

either positive or negative real part. For these two roots, the switching occurs at $c = C_0$ which displayed in (6.32), and provided that $1 + \rho(1 + \lambda)^2 < 0$. Hence, we can say that for $-1/(1 + \lambda)^2 < \rho < -1/4$, the double root is negative and real and the other two roots are complex conjugate with a negative real part (the roots type is **n**NN). However when $\rho < -1/(1 + \lambda)^2$ (the speed C_0 exists), see figure 6.27(f). Thus we can say that the double root is real and negative and and the other two roots are complex conjugate with either positive or negative real part (the roots type is **n**PP or **n**NN). We finished the case $0 < \lambda \leq 1/2$, and for the case $1/2 < \lambda \leq 1$, one can follow same steps in discussing the roots types. The character of roots can easily be known from figures 6.28 and 6.29. In the end a summary of the root classification is indicated in table 6.5.
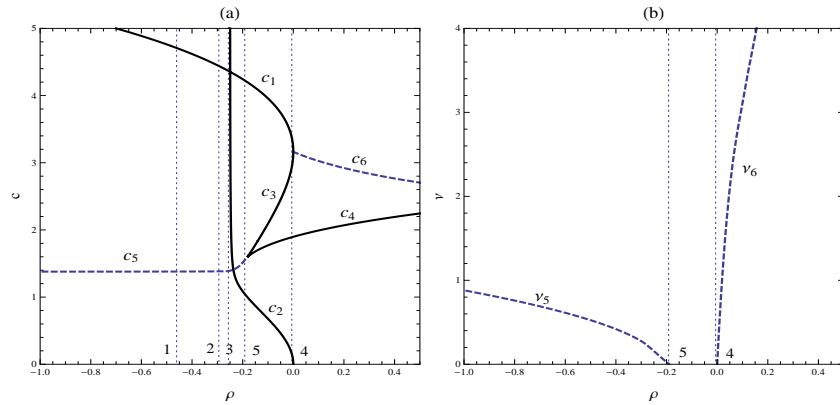
Figure 6.28: Double root locus for (6.29) when $1/2 < \lambda < 1$, possible solutions of (A.28) and (A.29). Vertical dotted lines are: (1) $\rho = -1/4\lambda$, (2) $\rho = -1/(1 + \lambda)^2$, (3) $\rho = -1/4$, (4) $\rho = 0$ and (5) $\rho = \rho_* (-1/4 < \rho_* < 0)$. The character of the eigenvalues are shown in figure 6.29.
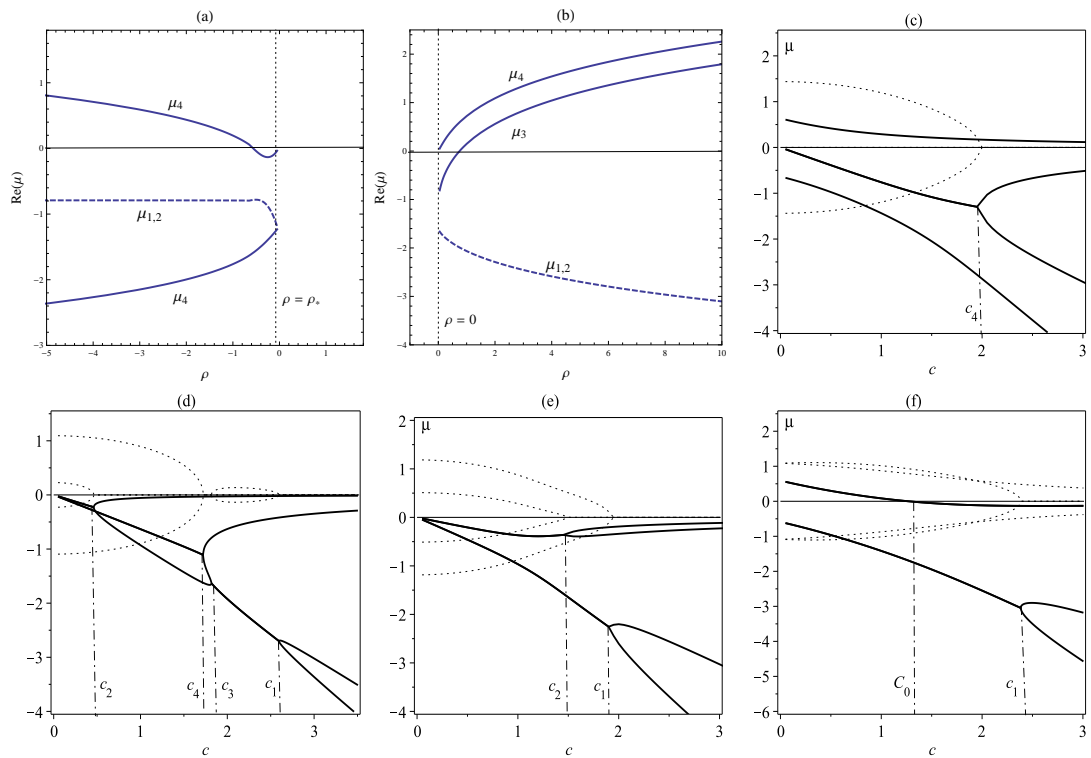
Figure 6.29: (a), (b) The variation of the double root (dashed line) and the other two roots (solid line) with ρ at $c = c_5$ and $c = c_6$ (see figure 6.28) when $\lambda = 0.6$. (c)-(f) The four eigenvalues versus speed c when $\lambda = 0.6$ and at different values of ρ: (c) $\rho = 0.5$, (d) $\rho = -0.05$, (e) $\rho = -0.22$ and (f) $\rho = -1.4$, solid lines represent the real part and dotted line represent the imaginary part of eigenvalues.

Table 6.5: Types of eigenvalues for (6.5). Bold letters represent the double root, capital for real parts of a complex root, and small for purely real roots. The roots are in ascending order, $\rho_1 = -1/4\lambda$ and $\rho_2 = -1/(1+\lambda)^2$, a negative triple root exists at $\rho = \rho_*$.

Conditions		(Speed)c	Roots Types	Figures
$0 < \lambda \leq 1/2$	$\rho \geq \rho_*$	c_4	$n\mathbf{n}p$	6.26 , 6.27
		c_6	$\mathbf{N}NP, \mathbf{N}PP$	
	$0 \leq \rho < \rho_*$	c_1, c_3, c_4	$\mathbf{n}np, n\mathbf{n}p, n\mathbf{n}p$	
	$-1/4 \leq \rho < 0$	c_1/c_2	$\mathbf{n}NN, \mathbf{n}nn/NN\mathbf{n}, nn\mathbf{n}$	
		c_5	$\mathbf{N}NN$	
	$\rho_2 \leq \rho < -1/4$	c_1	$\mathbf{n}NN$	
		c_5	$NNN, \mathbf{N}NP$	
	$\rho < \rho_2$	c_1	$\mathbf{n}NN, \mathbf{n}PP$	
		c_5	NNP	
$1/2 < \lambda \leq 1$	$\rho > 0$	c_4	$n\mathbf{n}p$	6.28 , 6.29
		c_6	$\mathbf{N}NP, \mathbf{N}PP$	
	$\rho_* \leq \rho < 0$	c_1, c_2, c_3, c_4	$\mathbf{n}nn, NN\mathbf{n}, \mathbf{n}nn, nn\mathbf{n}$	
	$-1/4 \leq \rho < \rho_*$	c_1, c_2	$\mathbf{n}nn, NN\mathbf{n}$	
		c_5	NNN	
	$\rho_2 \leq \rho < -1/4$	c_1	$\mathbf{n}NN$	
		c_5	NNN	
	$\rho_1 \leq \rho < \rho_2$	c_1	$\mathbf{n}NN, \mathbf{n}PP$	
		c_5	NNN	
	$\rho < \rho_1$	c_1	$\mathbf{n}NN, \mathbf{n}PP$	
		c_5	$NNN, \mathbf{N}NP$	

6.4 Case S4

In this case $f_u = 0$ and $g_v < 0$, and the characteristic equation is (refer to (4.21) with the negative sign in the first bracket)

$$\lambda\mu^4 + c(\lambda + 1)\mu^3 + \left(c^2 - 1 - iv(\lambda + 1)\right)\mu^2 - c(1 + i2v)\mu - \rho - v^2 + iv = 0, \quad (6.37)$$

where v and c are real and μ can be complex. The resultant is complex, which gives us two real equations (A.31) and (A.32) (the double root conditions, Appendix A). When $v = 0$, these two equations reduce to equation (A.33), which is solved to obtain the double root speed c when $v = 0$. The obtained solutions are shown in figure 6.30; the solid lines represent these speeds. From (A.33) a double root speed is zero when $\rho = 0$ or $\rho = -1/4\lambda$, and takes very large values as $\rho \to -1/4$. In this case, a triple root does not exists, hence a transition from $v = 0$ and $v \neq 0$ can not occur.

Let us discuss the roots character when $v = 0$. The sequence of the characteristic polynomial coefficients is $\lambda, c(1 + \lambda), c^2 - 1, -c, -\rho$. When $\rho > 0$, there is only one change of sign in this sequence, hence a positive real root always exists. Thus we can say that when $v = 0$ and $\rho > 0$, if a double root exists, it will be real and negative. At this result, when $\rho > 0$ the four roots are one real and positive, one real and negative, and the other two are either real and negative or complex conjugate with negative real part. When $\rho < 0$ there are always two sign change in the sequence. Thus there will be two real and positive roots or two complex conjugate roots with positive real part. Therefore the other two roots are negative or complex conjugate with negative real part.

Now from figure 6.30, speed c_2 exists when $-1/4\lambda \leq \rho < -1/4$, which is zero at $\rho = 0$ and goes to infinity as $\rho \to -1/4$. At $c = c_2$ a positive double root exists and the other two roots are negative. Thus the roots type is $nn\mathbf{p}$, see the eigenvalues versus speed in figure 6.31(c). For the other two speeds $c = c_1$ and $c = c_3$, a real and negative double
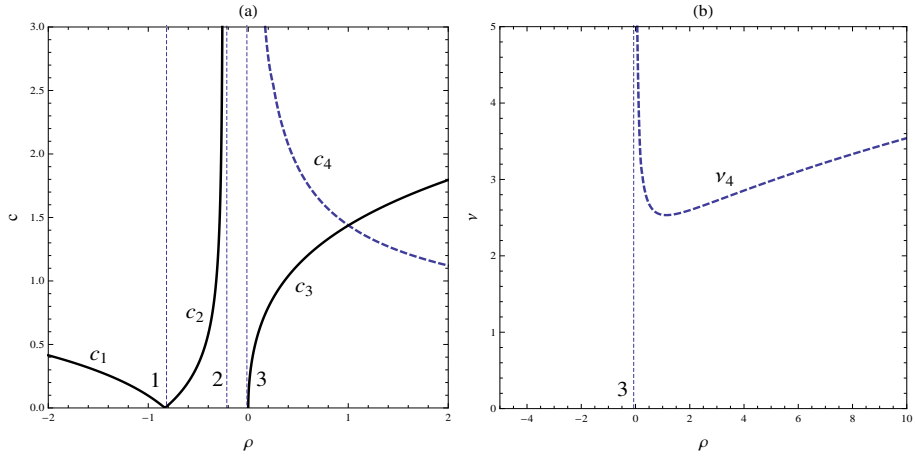
Figure 6.30: Double root locus for (6.29), possible solutions of (A.31) and (A.32). Vertical dotted lines are: (1) $\rho = -1/4\lambda$, (2) $\rho = -1/4$, (3) $\rho = 0$. At $c = c_4$, there a complex double root with positive real part, a real and negative double exists when $c = c_1$ and $c = c_3$, while at $c = c_2$ the double root is real and positive.The character of the eigenvalues are shown in figure 6.29.

eigenvalue exists, and the other two roots are: one positive and one negative when $c = c_3$ (see 6.31(b)), and complex conjugates with positive real part at $c = c_1$ (see 6.31(d)). Thus the root type at c_1 is **n**PP, while at c_3 is n**n**p.

Table 6.6: Types of eigenvalues for (6.37) when $0 < \lambda < 1$, see figure 6.30. Bold letters represent the double root, capital for real parts of a complex root, and small for purely real roots. The roots are in ascending order

Conditions	Speedc	Roots Type	Figures
$\rho > 0$	c_3	$n\mathbf{n}p$	
	c_4	$NN\mathbf{P}$	
$-1/4 \le \rho \le 0$	–	–	6.30 , 6.31
$-1/4\lambda \le \rho < -1/4$	c_2	$nn\mathbf{p}$	
$\rho < -1/4\lambda$	c_1	$\mathbf{n}PP$	

In case of v is nonzero, a complex double root with positive real part exists at $c = c_4$ and $v = v_4$, provided that $\rho > 0$. The speed $c = c_4$ and the frequency $v = v_4$ versus ρ shown in figure 6.30 (dashed line), which represent the solution of (A.31) and (A.32) when $\lambda = 0.2$. The double root is complex with positive real part and when we check the other two roots, they are complex with negative real parts. The variation of the real part

147
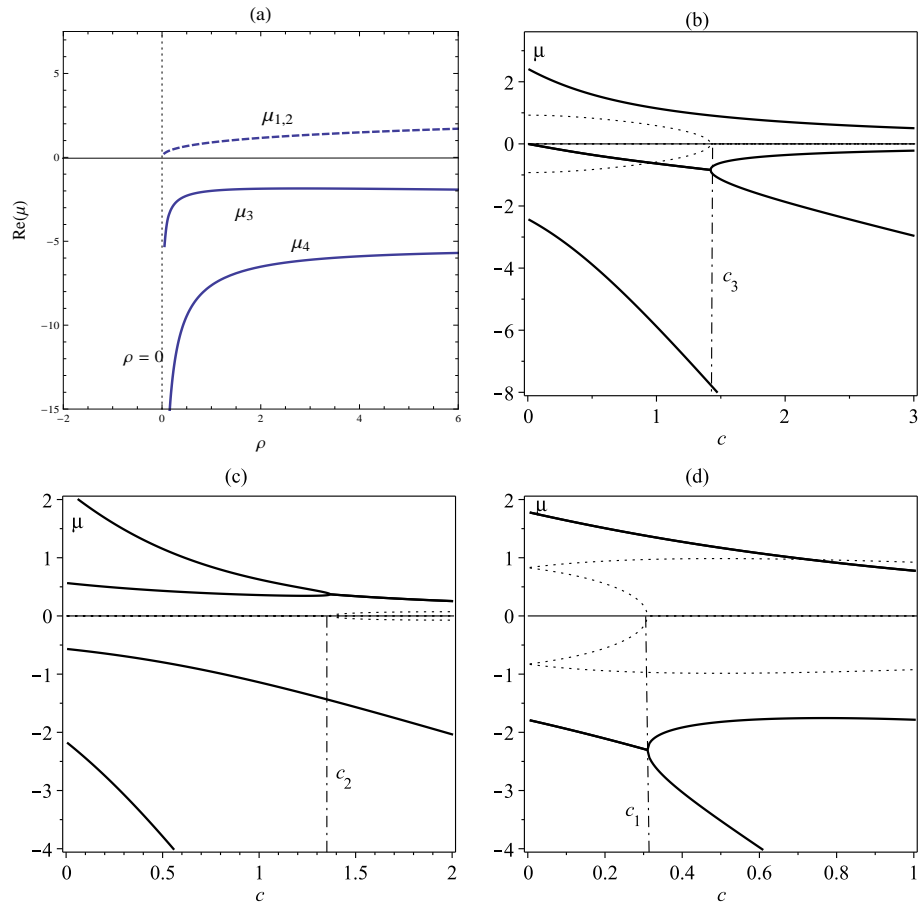
Figure 6.31: (a) The variation of the double root (dashed line) and the other two roots (solid line) with ρ at $c = c_4$ and $\lambda = 0.2$. (b)-(d) The four eigenvalues versus speed c when $\lambda = 0.2$ and at different values of ρ: (c) $\rho = 1.0$, (c) $\rho = -0.3$ and (d) $\rho = -3.0$, solid lines represent the real part and dotted line represent the imaginary part of eigenvalues.

148

of the double root and the real parts of the other two root is shown in figure see 6.31(a), hence the type of the roots is then *NN***P**. Hence c_4 can not be the selected speed. The character of the double root and the other two roots are shown in table 6.6

6.5   Summary

In this chapter a travelling wave analysis has been performed for a linearised two-component reaction-diffusion system in which the diffusion coefficients of the two components are different. We have discussed four cases, which gives a comprehensive study of the system. In each case, the characteristic equation is quartic and a double root mechanism (linear selection) is used to give some insights on a linear front speed. In our analysis we focused on indicating the character of the double root and other roots.

From the classification of the roots, we gave an idea about the imposed boundary conditions, which in turns make the double root the slowest decay (dominant exponential). We have given a recipe of borderlines between different regimes. For example, we have described where the double root speed switches between zero and non-zero frequency ($v = 0$ and $v \neq 0$), the triple root condition represents the borderline in this case. Also, we have pointed out the regimes where the speed at which the sign of a real part of an eigenvalue switches from positive to negative exists, which helps in uncovering the character of the roots.

At some parameter regimes, there are two different wave speeds associated with the same root character, and it is not immediately clear in the basis of the current analysis we need to know which speed is selected as a linear front speed. This is an open question and need further analysis, and we hope to answer it in the future.

Chapter 7

Conclusion and Future Work

This thesis has been concerned with studying scalar reaction-diffusion equations and a two-component reaction-diffusion systems with constant diffusion coefficients. We looked at the instabilities and bifurcation problems, along with travelling wave analysis has been performed, investigating the existence of front solutions. We have introduced a linear selection mechanism governing the development and propagation of nonlinear patterns.

A detailed analysis of the instabilities that arise in the system is performed, using linear stability analysis. There are two kinds of instabilities: the first type is *uniform* instability, as the most unstable wave number is $k = k_* = 0$, and the second type is a spatially *a spatially periodic* instability with $k = k_* \neq 0$. Depending on whether the eigenvalue σ is real or complex, each of these two types has two subtypes: *stationary* when the eigenvalue is a purely real and *oscillatory* in case of a complex eigenvalue. Thus there are four kinds of instabilities: (1) stationary uniform, (2) oscillatory uniform, (3) stationary periodic and (4) oscillatory periodic.

Pattern formation is typically associated with the second two types. There is a vast and rich body of literature dealing with the patterning properties of two-component reaction-

diffusion system, considering specific models (such as Gierer-Meinhardt model, Brusse-lator model and Gray-Scott model) can be found in the books by Briton [13], Fife [27] , Grindrod [33] and Murray [55]. Many kinds of patterns (spatial and/or temporal) are in-vestigated in biology [41, 49, 53], chemistry [50, 57, 77, 80], physics [2, 17, 36], ecology [4, 56, 59] and in epidemiology [51].

In the literature, the majority of researchers focus on a specific reaction-diffusion sys-tem, considering one or two types of instabilities, and that encourages us to give a com-prehensive study of the possible instabilities that arise in reaction-diffusion system of two components with constant diffusion coefficients. From our linear instability analysis, the first three types of instabilities can all arise in a two-component reaction-diffusion system, i. e. stationary uniform, oscillatory uniform and stationary periodic. Precise parameter regimes are identified for each type. For the stationary periodic type, it is a necessary condition that the diffusion coefficients be different (see Murray [55]). The most unstable wave number in this case and the associated temporal growth rate are obtained explicitly. The fourth instability does not arise and in the following we give the reason.

For a system of two variables, the quadratic characteristic equation is $\sigma^2 + p(k^2)\sigma + q(k^2) = 0$, where σ is the eigenvalue and k is the wave number. The coefficient $p(k^2)$ is always monotonic in the wave number ($p = a - bk^2$, where a and b are real and depend on the system parameters). Thus we can say that $Re(\sigma)$ is always monotonic in k; hence $Re(\sigma)$ never has a maximum at a wave number $k > 0$ which is a necessary condition for the *oscillatory periodic* type. Thus in our study, we concluded that in a two-component reaction diffusion system the oscillatory periodic instability never arises. However, this type of instability can arise for system of at least three variables, as in this type $Im(\sigma) \neq 0$ and $Re(\sigma)$ must a non-monotonic function of the wave number k (see Vanag [75]).

A three-component model (extended Brusselator model, system (7.1) with $f = a - (1+b)u + u^2v - cu + dw$, $g = bu - u^2v$ and $h = cu - dw$, a, b, c and d are real) has been

151

studied by Dolnik et al [79] and by Vanag [75], and complex patterns appeared as a result of instability of *oscillatory periodic* type. Therefore, in the future we aim to give a detailed analysis for the instabilities, similar to our study of two-component, that can arise in a three-component systems (with general kinetics), i.e.

$$
\begin{aligned}
\frac{\partial u}{\partial t} &= D_u \nabla^2 u + f(u, v, w), \\
\frac{\partial v}{\partial t} &= D_v \nabla^2 v + g(u, v, w), \\
\frac{\partial w}{\partial t} &= D_w \nabla^2 w + h(u, v, w),
\end{aligned}
\tag{7.1}
$$

where D_u, D_v and D_w are the diffusion coefficients which are positive and real.

Travelling wave analysis is performed for reaction-diffusion equations. We focused on a linear selection mechanism, the double root mechanism, that gives some insights on the lower bound of the selected speed of invasion of unstable state by a stable one, considering a fixed form of travelling wave and a modulated travelling wave. The characteristic equation we have studied is obtained by introducing the travelling wave coordinates $(z,t) = (x - ct, t)$ into differential equations, then we linearise the obtained travelling wave equations around the unstable rest state. From these linearised equations we obtain the characteristic equation. Through our discussion, we determine speeds at which a repeated root exists, and then classify the eigenvalues at these speeds (the double root and the other two roots). This gives some insights on the minimum wave speed and helps us to understand the speed selection problem for the class of reaction-diffusion equations we study.

A minimal front speed is the speed at which the double root is the slowest decaying eigenvalue (dominant root), assuming that the state at infinity is an unstable one and the front moves to the right. In chapter 2, we studied two scalar reaction diffusion equations, the extended Fisher's equation and the Swift-Hohenberg equation, applying the double

root mechanism. The obtained results (minimum front speeds) in chapter 2 were consistent with the results obtained by the marginal stability mechanism (see, [7, 64, 73]). From our results of a fourth order reaction diffusion equations, we wanted to apply the mechanism on systems. Thus we continued our analysis with a two-component reaction-diffusion system with constant diffusion coefficients, in chapters 4, 5 and 6. A detailed and comprehensive analysis of the linear mechanism investigating the development and propagation of nonlinear patterns is performed. We have given a recipe for investigating the dependence of the linear front speed on the system parameters.

In the future, we aim to include the three-component system (7.1) in the analysis. We want to give some highlights onto the wave instability that arises in these systems. Also, we hope to discuss the nonlinear fronts whose asymptotic speed is larger than the asymptotic linear front (which have been investigated). That is to consider analysis to linear (pulled) versus the nonlinear (pushed) fronts. However this needs different approaches to the analysis, requesting a nonlinear treatment. Some specific reaction-diffusion systems were discussed, considering the travelling wave existence problem and the speed of propagation (see for example King et al [35, 40] , Billingham [8–10], Leach[46], Qi[63], Landman et al [43], Kim[39], Sherratt [66, 67]). Thus in the future we aim to discuss two-component reaction-diffusion systems with more general nonlinearity in their kinetics.

Appendix A

Sylvester's Method of Elimination and Double Root Conditions

A.1   Sylvester's Method of Elimination

If p and q are two polynomials which can be factored into linear factors

$$p(x) \;=\; a_0(x-r_1)(x-r_2)\cdots(x-r_m) \tag{A.1}$$

$$q(x) \;=\; b_0(x-s_1)(x-s_2)\cdots(x-s_n), \tag{A.2}$$

then the *resultant $R(f,g)$* of f and g is defined as

$$R_x(p,q) = a_0^n b_0^m \prod_{i=1}^{m}\prod_{j=1}^{n}(r_i - s_j). \tag{A.3}$$

From the definition, it is clear that the resultant will equal zero if and only if p and q have at least one common root. An explicit formula for the resultant as a determinant was

given by Sylvester [1]. Suppose that

$$p(x) = a_0x^m + a_1x^{m-1} + \cdots + a_{m-1}x + a_m \tag{A.4}$$

$$q(x) = b_0x^n + b_1x^{n-1} + \cdots + b_{n-1}x + b_n, \tag{A.5}$$

Then $R_x(p,q)$ can be expressd as an $(m+n) \times (m+n)$ determinant:

$$\begin{vmatrix} a_0 & a_1 & a_2 & \ldots & a_m & 0 & \ldots & 0 \\ 0 & a_0 & a_1 & \ldots & a_{m-1} & a_m & \ldots & 0 \\ & & \ddots & & & & & \\ 0 & 0 & & & & & & a_m \\ b_0 & b_1 & b_2 & \ldots & b_n & 0 & \ldots & 0 \\ 0 & b_0 & b_1 & \ldots & b_{n-1} & b_n & \ldots & 0 \\ & & \ddots & & & & & \\ 0 & 0 & & & & & & b_n \end{vmatrix} = R_x(p,q) \tag{A.6}$$

To construct this determinant, one first lists the coefficients of p, padded with zeros at the end, then constructs subsequent rows by shifting one column to the right each time until one runs out of zeros at the end, then one repeats the same procedure with q. Resultants are very useful for solving simultaneous systems of polynomial equations. Suppose that one has a system of two equations $f(x,y) = 0, g(x,y) = 0$. Then f and g can be regarded as polynomials in x whose coefficients are functions of y. One can then form the resultant by computing the determinant of a matrix as above. Since the coefficients were polynomials in y, the resultant will be a polynomial in y. In order for the two equations to have a solution, the resultant must equal zero; hence setting the resultant to zero gives an equation for the y values of solutions of the system. Once one solves for these y values, one can substitute them back in to the original equations and solve for the corresponding

x values. In other words, the resultant allows one to eliminate a variable from a system of equations. For this reason, resultants are also known as eliminant. By using resultants to eliminate variables repeatedly one variable at a time, one solve systems of equations in more than two unknowns.

A.2 Double Root Conditions

Consider the case in which $q(x)$ is the derivative of $p(x)$ with respect to x. In this case, there must be at least one common root; a double root of $p(x)$ exists. Hence we can say that resultant $R_x(p,q)$ must be zero, i.e.,

$$R_x(p, \frac{dp}{dx}) = 0. \tag{A.7}$$

Consider a cubic polynomial equation

$$p(x) = A_3\mu^3 + A_2\mu^2 + A_1\mu + A_0 = 0, \tag{A.8}$$

then we construct the resultant using (A.6) and apply (A.7) to obtain

$$\begin{vmatrix} A_3 & A_2 & A_1 & A_0 & 0 \\ 0 & A_3 & A_2 & A_1 & A_0 \\ 3A_3 & 2A_2 & A_1 & 0 & 0 \\ 0 & 3A_3 & 2A_2 & A_1 & 0 \\ 0 & 0 & 3A_3 & 2A_2 & A_1 \end{vmatrix} = 0, \tag{A.9}$$

which can be simplified to

$$4A_3A_1^3 - A_2^2A_1^2 - 18A_0A_1A_2A_3 + 4A_0A_2^3 + 27A_0^2A_3^2 = 0, \tag{A.10}$$

which is a condition for $p(x)$ to have a double root. Also, a condition for a double root of the quartic polynomial equation

$$A_4\mu^4 + A_3\mu^3 + A_2\mu^2 + A_1\mu + A_0 = 0 \tag{A.11}$$

can be obtained. This condition is

$$\begin{vmatrix} A_4 & A_3 & A_2 & A_1 & A_0 & 0 & 0 \\ 0 & A_4 & A_3 & A_2 & A_1 & A_0 & 0 \\ 0 & 0 & A_4 & A_3 & A_2 & A_1 & A_0 \\ 4A_4 & 3A_3 & 2A_2 & A_1 & 0 & 0 & 0 \\ 0 & 4A_4 & 3A_3 & 2A_2 & A_1 & 0 & 0 \\ 0 & 0 & 4A_4 & 3A_3 & 2A_2 & A_1 & 0 \\ 0 & 0 & 0 & 4A_4 & 3A_3 & 2A_2 & A_1 \end{vmatrix} = 0, \tag{A.12}$$

and can appear as

$$\begin{aligned} &-27A_4^3A_1^4 + 18A_2A_3A_4^2A_1^3 - 4A_3^3A_4A_1^3 + 144A_0A_2A_4^3A_1^2 \\ &- 4A_2^3A_4^2A_1^2 - 6A_0A_3^2A_4^2A_1^2 + A_2^2A_3^2A_4A_1^2 - 192A_0^2A_3A_4^3A_1 \\ &- 80A_0A_2^2A_3A_4^2A_1 + 18A_0A_2A_3^3A_4A_1 + 256A_0^3A_4^4 - 128A_0^2A_2^2A_4^3 \\ &+ 16A_0A_2^4A_4^2 + 144A_0^2A_2A_3^2A_4^2 - 27A_0^2A_3^4A_4 - 4A_0A_2^3A_3^2A_4 = 0. \end{aligned} \tag{A.13}$$

A.2.1 Case S1

Here consider

$$A_4 = \lambda, \quad A_3 = c(1+\lambda), \quad A_2 = c^2 + \lambda + \eta - iv(1+\lambda) \quad,$$

$$A_1 = c(\eta + 1 - i2v), \quad A_0 = \eta - \gamma - v^2 - iv(1+\eta),$$

then equation (A.13) results in the two real equations

$$\lambda\left[(\eta-1)^2+4\gamma\right](\lambda-1)^2 c^8 - 2\lambda(\lambda-1)\left[\gamma(\lambda(3\lambda+10)+\eta(\lambda(9\lambda-10)-3)-9)\right.$$
$$+(\eta-1)\left((2(\lambda-1)\lambda-1)\eta^2-2((\lambda-3)\lambda+1)\eta+(\lambda-2)\lambda v^2+v^2-\lambda(\lambda+2)+2)\right]c^6$$
$$+\lambda\left[(1-8(\lambda-1)\lambda)\eta^4+4(\lambda(2\lambda(4\lambda-5)-1)+2)\eta^3\right.$$
$$+2\left(-4\lambda^4-20\lambda^3+51\lambda^2-20\lambda+(\lambda-1)^2(2\lambda-11)(2\lambda+1)v^2-4\right)\eta^2$$
$$+4\left((\lambda-1)^2(\lambda(2\lambda+23)+2)v^2+(\lambda-2)\lambda(\lambda(2\lambda+3)-4)\right)\eta+(\lambda-1)^4 v^4$$
$$-2(\lambda-1)^2(\lambda+2)(11\lambda-2)v^2+\lambda^2(\lambda(\lambda+8)-8)+\gamma^2(\lambda(\lambda(9(4-3\lambda)\lambda-2)+36)-27)$$
$$+2\gamma\left(-(\lambda(2\lambda+5)(3\lambda-4)+3)\eta^2+2(\lambda(\lambda(\lambda(9\lambda+13)-48)+13)+9)\eta\right.$$
$$-5(\lambda-1)^2(\lambda(3\lambda+14)+3)v^2-\lambda(\lambda(\lambda(3\lambda-20)+7)+6))\right]c^4$$
$$-4\lambda\left[(\lambda-1)^3(\lambda(4\lambda+13)+\eta((\lambda-13)\lambda-4)-1)v^4-2(\lambda-1)\left((\lambda(11\lambda-17)-2)\eta^3\right.\right.$$
$$+(9\lambda(1-2(\lambda-2)\lambda)-3)\eta^2+3\lambda(\lambda((\lambda-3)\lambda-12)+6)\eta+\lambda^2(\lambda(2\lambda+17)-11))\,v^2$$
$$+(\eta-\lambda)^2\left(\lambda\eta^3+(2(4-5\lambda)\lambda+1)\eta^2+\lambda(\lambda(\lambda+8)-10)\eta+\lambda^2\right)$$
$$+4\gamma^2\lambda(\lambda((10-9\lambda)\lambda+3)+\eta(\lambda(3\lambda+10)-9))$$
$$+\gamma\left((3\lambda(5\lambda-2)-1)\eta^3+\lambda(49-\lambda(31\lambda+26))\eta^2\right.$$
$$+(\lambda(\lambda((88-49\lambda)\lambda+38)-80)+3)v^2\eta+\lambda^2(\lambda(49\lambda-26)-31)\eta$$
$$+(\lambda-1)\lambda(\lambda(\lambda(3\lambda-77)-39)+49)v^2-\lambda^3(\lambda(\lambda+6)-15))\right]c^2+16\lambda^2\left[-(\lambda-1)^4 v^6\right.$$
$$-(\lambda-1)^2\left(-10\eta^2-5\eta+(\gamma-5(\eta+2))\lambda^2+\gamma+2(-5\gamma+\eta(2\eta+11)+2)\lambda\right)v^4$$
$$+\left(8\lambda((\lambda-4)\lambda+1)\gamma^2\right.$$
$$+2\left(3\lambda^4-18(\eta+1)\lambda^3+11(\eta(\eta+4)+1)\lambda^2-18\eta(\eta+1)\lambda+3\eta^2\right)\gamma$$
$$+(\eta-\lambda)^2\left(-5(2\eta+1)\lambda^2+2(\eta(2\eta+11)+2)\lambda-5\eta(\eta+2)\right)\right)v^2$$
$$+(\eta-\gamma)\left((\eta-\lambda)^2+4\gamma\lambda)^2\right)\right]=0,$$

$$(A.14)$$

158

$$\nu\lambda(\lambda-1)^2[6\gamma(\lambda+1)+(\eta-1)(\eta(\lambda+2)-2\lambda-1)]c^6$$
$$+\nu\lambda(\lambda-1)\big[\gamma(\eta(\lambda(39-\lambda(9\lambda+16))+6)$$
$$+\lambda(16-3\lambda(2\lambda+13))+9)$$
$$+\eta^3(2(5-4\lambda)\lambda+3)+\eta^2\left(4\lambda^3-21\lambda+2\right)$$
$$+\eta\left(-2\lambda^3+21\lambda^2-(\lambda-1)^2(2\lambda+3)\nu^2-4\right)$$
$$+(\lambda-1)^2(3\lambda+2)\nu^2-\lambda(\lambda+4)(3\lambda-2)\big]c^4$$
$$+\nu\lambda\big[-4\gamma^2\lambda(\lambda+1)(\lambda(9\lambda-22)+9)$$
$$+\gamma\big(\eta^2(\lambda((19-31\lambda)\lambda+31)-3)$$
$$+2\eta\lambda(\lambda+1)(\lambda(49\lambda-106)+49)$$
$$+\lambda^2(\lambda((31-3\lambda)\lambda+19)-31)$$
$$+(\lambda-1)^2(\lambda+1)((\lambda-42)\lambda+1)\nu^2\big)$$
$$+\eta^4((13-12\lambda)\lambda+1)+\eta^3(4\lambda(\lambda(11\lambda-16)+2)+4)$$
$$+2\eta^2\left((\lambda-3)(\lambda-1)^2(6\lambda+1)\nu^2\right.$$
$$-3\lambda(\lambda+1)(2\lambda-3)(3\lambda-2))$$
$$+4\eta\lambda^2(\lambda(\lambda(\lambda+2)-16)+11)$$
$$-4\eta(\lambda-1)^2(\lambda+1)((\lambda-9)\lambda+1)\nu^2$$
$$+\lambda^3(\lambda(\lambda+13)-12)+(\lambda-1)^4(\lambda+1)\nu^4$$
$$-2(\lambda-1)^2\lambda(\lambda+6)(3\lambda-1)\nu^2\big]c^2+8(\lambda$$
$$-1)\lambda^2\nu^3\big[2\gamma(\eta(\lambda(3\lambda-8)+1)-\lambda((\lambda-8)\lambda+3))+(\eta$$
$$-\lambda)\left(-5(\eta+1)\lambda^2+(\eta(3\eta+14)+3)\lambda-5\eta(\eta+1)\right)\big]$$
$$-4\nu\lambda^2\big[4\gamma\lambda+(\eta-\lambda)^2\big]\big[(\eta-\lambda)(\eta(\eta-5\lambda+5)-\lambda)$$
$$-4\gamma\left(-2(\eta+1)\lambda+\eta+\lambda^2\right)\big]$$
$$-4(\lambda-1)^3\lambda^2\nu^5(\eta(\lambda-5)+5\lambda-1)=0.$$

(A.15)

When $\nu = 0$, these two equations reduce to the following equation

$$\lambda \left[(\lambda-1)^2 \left[4\gamma+(\eta-1)^2\right] c^8 - 2(\lambda-1) \left[\gamma(\eta(\lambda(9\lambda-10)-3)+\lambda(3\lambda+10)-9) \right.\right. \quad \text{(A.16)}$$
$$+ (\eta-1)\left(\eta^2(2(\lambda-1)\lambda-1) - 2\eta((\lambda-3)\lambda+1) - \lambda(\lambda+2)+2\right)\right] c^6$$
$$+ \left[4\lambda^3\left(9\gamma^2 - \gamma(\eta-5)(3\eta+2) + \eta(2\eta(4\eta-5)-1)+2\right)\right.$$
$$- 2\lambda^2\left(\gamma^2 + \gamma(\eta(7\eta+96)+7) + \eta(\eta(4\eta(\eta+5)-51)+20)+4\right)$$
$$+ 4\lambda\left(9\gamma^2 + \gamma(2\eta+3)(5\eta-1) + (\eta-2)\eta(\eta(2\eta+3)-4)\right) - 27\gamma^2$$
$$+ \lambda^4\left(36\gamma\eta - 3\gamma(9\gamma+2) - 8\eta^2+8\eta+1\right) - 6\gamma\eta^2 + 36\gamma\eta + \eta^4 + 8\eta^3 - 8\eta^2\right] c^4$$
$$+ 4\left[-4\gamma^2\lambda(\eta(\lambda(3\lambda+10)-9) + \lambda((10-9\lambda)\lambda+3))\right.$$
$$+ \gamma\left(\eta^3(3(2-5\lambda)\lambda+1)+\eta^2\lambda(\lambda(31\lambda+26)-49)+\eta\lambda^2((26-49\lambda)\lambda+31)+\lambda^3(\lambda(\lambda+6)-15)\right)$$
$$- (\eta-\lambda)^2\left(\eta^3\lambda + \eta^2(2(4-5\lambda)\lambda+1) + \eta\lambda(\lambda(\lambda+8)-10)+\lambda^2\right)\right] c^2$$
$$- 16\lambda(\gamma-\eta)\left(4\gamma\lambda + (\eta-\lambda)^2\right)^2\right] = 0.$$

Also we can deduce that equation (A.11) has a triple root (for $\nu = 0$) when

$$324\gamma^3\lambda^5 - 1008\gamma^3\lambda^4 + 1432\gamma^3\lambda^3 - 1008\gamma^3\lambda^2 + 324\gamma^3\lambda$$
$$+ 108\gamma^2\eta^2\lambda^5 - 387\gamma^2\eta^2\lambda^4 + 780\gamma^2\eta^2\lambda^3 - 714\gamma^2\eta^2\lambda^2$$
$$+ 288\gamma^2\eta^2\lambda - 27\gamma^2\eta^2 - 522\gamma^2\eta\lambda^5 + 1896\gamma^2\eta\lambda^4$$
$$- 2844\gamma^2\eta\lambda^3 + 1896\gamma^2\eta\lambda^2 - 522\gamma^2\eta\lambda - 27\gamma^2\lambda^6$$
$$+ 288\gamma^2\lambda^5 - 714\gamma^2\lambda^4 + 780\gamma^2\lambda^3 - 387\gamma^2\lambda^2 + 108\gamma^2\lambda$$
$$- 9\gamma\eta^4\lambda^4 + 102\gamma\eta^4\lambda^3 - 138\gamma\eta^4\lambda^2 + 66\gamma\eta^4\lambda - 9\gamma\eta^4$$
$$- 126\gamma\eta^3\lambda^5 + 600\gamma\eta^3\lambda^4 - 1200\gamma\eta^3\lambda^3 + 996\gamma\eta^3\lambda^2$$
$$- 354\gamma\eta^3\lambda + 36\gamma\eta^3 - 9\gamma\eta^2\lambda^6 + 318\gamma\eta^2\lambda^5 - 1227\gamma\eta^2\lambda^4$$
$$+ 1908\gamma\eta^2\lambda^3 - 1227\gamma\eta^2\lambda^2 + 318\gamma\eta^2\lambda - 9\gamma\eta^2 + 36\gamma\eta\lambda^6 \quad \text{(A.17)}$$
$$- 354\gamma\eta\lambda^5 + 996\gamma\eta\lambda^4 - 1200\gamma\eta\lambda^3 + 600\gamma\eta\lambda^2$$
$$- 126\gamma\eta\lambda - 9\gamma\lambda^6 + 66\gamma\lambda^5 - 138\gamma\lambda^4 + 102\gamma\lambda^3 - 9\gamma\lambda^2$$
$$+ 8\eta^6\lambda^3 - 12\eta^6\lambda^2 + 6\eta^6\lambda - \eta^6 + 24\eta^5\lambda^4 - 96\eta^5\lambda^3$$
$$+ 102\eta^5\lambda^2 - 42\eta^5\lambda + 6\eta^5 + 24\eta^4\lambda^5 - 168\eta^4\lambda^4$$
$$+ 372\eta^4\lambda^3 - 303\eta^4\lambda^2 + 102\eta^4\lambda - 12\eta^4 + 8\eta^3\lambda^6$$
$$- 96\eta^3\lambda^5 + 372\eta^3\lambda^4 - 588\eta^3\lambda^3 + 372\eta^3\lambda^2 - 96\eta^3\lambda$$
$$+ 8\eta^3 - 12\eta^2\lambda^6 + 102\eta^2\lambda^5 - 303\eta^2\lambda^4 + 372\eta^2\lambda^3$$
$$- 168\eta^2\lambda^2 + 24\eta^2\lambda + 6\eta\lambda^6 - 42\eta\lambda^5 + 102\eta\lambda^4$$
$$- 96\eta\lambda^3 + 24\eta\lambda^2 - \lambda^6 + 6\lambda^5 - 12\lambda^4 + 8\lambda^3 = 0,$$

If we substitute $\mu = Re(\mu) + iIm(\mu) = x + iy$, where x and y are real, into the quartic equation (A.11) we obtain the two real equations

$$
\begin{aligned}
& c^2 x^2 - c^2 y^2 + c\lambda x^3 + cx^3 + c\eta x - 3c\lambda xy^2 - 3cxy^2 + cx + 2c\nu y - \gamma + \eta - \nu^2 \\
& + \lambda x^4 + \eta x^2 + \lambda x^2 - 6\lambda x^2 y^2 + 2\lambda \nu xy + 2\nu xy + \lambda y^4 - \eta y^2 - \lambda y^2 = 0,
\end{aligned} \tag{A.18}
$$

$$
\begin{aligned}
& 2c^2 xy + 3c\lambda x^2 y + 3cx^2 y - 2c\nu x - c\lambda y^3 - cy^3 + c\eta y + cy - \eta \nu - \nu \\
& + 4\lambda x^3 y - \lambda \nu x^2 - \nu x^2 - 4\lambda xy^3 + 2\eta xy + 2\lambda xy + \lambda \nu y^2 + \nu y^2 = 0,
\end{aligned} \tag{A.19}
$$

where x, y are the real and imaginary parts of the eigenvalue, c, ν, λ, γ and η are all real parameters. Now eliminating the parameter ν from these two equations gives

$$
\begin{aligned}
& 4c^4 x^4 + 8c^3 x^3 \left(\eta + (\lambda + 1)x^2 - (\lambda + 1)y^2 + 1 \right) \\
& + c^2 x^2 \left(-4\gamma + \eta(5\eta + 14) + (\lambda(5\lambda + 14) + 5)x^4 \right. \\
& + 2x^2 \left(5\eta\lambda + 7\eta + 7\lambda - 3(\lambda(\lambda + 6) + 1)y^2 + 5 \right) \\
& + (\lambda(5\lambda + 14) + 5)y^4 - 2y^2(5\eta\lambda + 7\eta + 7\lambda + 5) + 5 \big) \\
& + cx \left(\eta + (\lambda + 1)x^2 - (\lambda + 1)y^2 + 1 \right) \left(-4\gamma + \eta(\eta + 6) \right. \\
& + (\lambda(\lambda + 6) + 1)x^4 + 2x^2 \left((\eta + 3)\lambda + 3\eta + ((\lambda - 10)\lambda + 1)y^2 + 1 \right) \\
& + (\lambda(\lambda + 6) + 1)y^4 - 2y^2((\eta + 3)\lambda + 3\eta + 1) + 1 \big) \\
& - \gamma \left(\eta + (\lambda + 1)x^2 - (\lambda + 1)y^2 + 1 \right)^2 \\
& + (x^2 - y^2 + 1) \left(\eta + \lambda(x - y)(x + y) \right) \left((\lambda + 1)^2 x^4 \right. \\
& + 2x^2 \left(\eta\lambda + \eta + \lambda + ((\lambda - 6)\lambda + 1)y^2 + 1 \right) \\
& + \left(\eta - (\lambda + 1)y^2 + 1 \right)^2 \right) = 0,
\end{aligned} \tag{A.20}
$$

and for fixed values of λ, γ and η, this equation represents the constant speed contours in the x, y space (the $Re(\mu)$, $Im(\mu)$ space). If there is a double root exists the contours corresponding to double root speed meet to form a saddle point.

Also, we can deduce a formula similar to (A.20), but to represent contours for the parameter ν. We refer to (A.18) and (A.19) and eliminate c to obtain the following required

equation (constant v contours in the $Re(\mu)$, $Im(\mu)$ space)

$$(\lambda - 1)^2 \lambda x^{10} y^2 - (\lambda - 1)^2 (\lambda + 1) v x^9 y$$
$$+ x^8 \left((\lambda - 1)^2 v^2 + \lambda (\lambda (5\lambda - 6) + 5) y^4 + (\lambda^2 - 1) y^2 (\eta - \lambda) \right)$$
$$- v x^7 y \left((\lambda - 1)(\eta (\lambda + 3) - 3\lambda - 1) + 4(\lambda + 1) (\lambda^2 + 1) y^2 \right)$$
$$+ x^6 \left(2(\eta - 1)(\lambda - 1) v^2 + 2\lambda (\lambda (5\lambda - 2) + 5) y^6 - 4(\lambda + 1) y^4 (\eta + \lambda^2) \right.$$
$$\left. + y^2 \left(-\lambda (2\gamma + \eta^2 + 1) + \lambda^2 (3\gamma - \eta + 2) + 3\gamma + 2\eta^2 - \eta + (\lambda (7\lambda + 10) + 7) v^2 \right) \right)$$
$$+ v x^5 y \left(-4\gamma (\lambda + 1) + (\eta - 1)((\eta + 3)\lambda - 3\eta - 1) - 8(\lambda + 1) v^2 \right.$$
$$\left. - 6(\lambda + 1)^3 y^4 + y^2 \left((\eta + 13)\lambda^2 + 10(\eta + 1)\lambda + 13\eta + 1 \right) \right)$$
$$+ x^4 \left(v^2 \left(4\gamma + (\eta - 1)^2 + 4v^2 \right) + 2\lambda (\lambda (5\lambda + 2) + 5) y^8 - 6(\lambda + 1)^2 y^6 (\eta + \lambda) \right.$$
$$+ y^4 \left(\gamma (\lambda (5\lambda - 6) + 5) + \lambda (\eta^2 + \eta (\lambda + 8) + (11\lambda + 26) v^2 + 6\lambda) + 6\eta^2 + \eta + \lambda + 11v^2 \right)$$
$$\left. + y^2 \left((-\eta - 1)(2\gamma (\lambda + 1) + (\eta - 1)(\eta - \lambda)) - 8v^2 (\eta (\lambda + 2) + 2\lambda + 1) \right) \right)$$
$$- v x^3 y \left(-(\eta + 1) \left(4\gamma + (\eta - 1)^2 + 8v^2 \right) + 4(\lambda + 1)(\lambda (\lambda + 4) + 1) y^6 \right.$$
$$- y^4 \left((5\eta + 17)\lambda^2 + 26(\eta + 1)\lambda + 17\eta + 5 \right)$$
$$\left. + 2y^2 \left((\eta + 1)(\eta (\lambda + 5) + 5\lambda + 1) + 4(\lambda + 1) v^2 \right) \right)$$
$$+ x^2 y^2 \left(-4\gamma^2 + \eta \left((5\eta + 14) v^2 + (\eta - 2)\eta \right) + \eta + 5v^2 + \lambda (\lambda (5\lambda + 6) + 5) y^8 \right.$$
$$- 4(\lambda + 1) y^6 (2\eta \lambda + \eta + \lambda (\lambda + 2)) + \gamma \left(-(\eta - 6)\eta - 4v^2 + ((\lambda - 6)\lambda + 1) y^4 - 1 \right)$$
$$+ y^4 \left(\eta^2 (5\lambda + 6) + \eta (\lambda (5\lambda + 16) + 5) + (\lambda (5\lambda + 14) + 5) v^2 + \lambda (6\lambda + 5) \right)$$
$$\left. + 2y^2 \left((\eta + 1)^2 (-(\eta + \lambda)) - v^2 (\eta (5\lambda + 7) + 7\lambda + 5) \right) \right) - v x y^3 \left(-\eta + (\lambda + 1) y^2 \right.$$
$$\left. - 1 \right) \left(-4\gamma + \eta (\eta + 6) + (\lambda (\lambda + 6) + 1) y^4 - 2y^2 (\eta (\lambda + 3) + 3\lambda + 1) + 1 \right)$$
$$+ y^4 \left(\eta - (\lambda + 1) y^2 + 1 \right)^2 \left((y^2 - 1) (\lambda y^2 - \eta) - \gamma \right) = 0.$$

(A.21)

A.2.2 Case S2

Consider

$$A_4 = \lambda, \quad A_3 = c(1 + \lambda), \quad A_2 = c^2 - \lambda + \eta - iv(1 + \lambda) \quad ,$$

$$A_1 = c(\eta - 1 - i2v), \quad A_0 = -\eta - \gamma - v^2 - iv(\eta - 1),$$

then equation (A.13) results in the two real equations

$$\left(\lambda(\eta+1)^2+4\gamma\right)(\lambda-1)^2c^8-2\lambda(\lambda-1)\left(\gamma\left(3(3\eta-1)\lambda^2-10(\eta+1)\lambda-3\eta+9\right)\right.$$
$$+(\eta+1)\left((2(\lambda-1)\lambda-1)\eta^2+2((\lambda-3)\lambda+1)\eta+(\lambda-2)\lambda v^2+v^2-\lambda(\lambda+2)+2\right)\right)c^6$$
$$-\lambda\left[(8(\lambda-1)\lambda-1)\eta^4+4(\lambda(2\lambda(4\lambda-5)-1)+2)\eta^3\right.$$
$$+2\left(4\lambda^4+20\lambda^3-51\lambda^2+20\lambda-(\lambda-1)^2(2\lambda-11)(2\lambda+1)v^2+4\right)\eta^2$$
$$+4\left((\lambda-1)^2(\lambda(2\lambda+23)+2)v^2+(\lambda-2)\lambda(\lambda(2\lambda+3)-4)\right)\eta-(\lambda-1)^4v^4$$
$$+2(\lambda-1)^2(\lambda+2)(11\lambda-2)v^2-\lambda^2(\lambda(\lambda+8)-8)+\gamma^2(\lambda(\lambda(9\lambda(3\lambda-4)+2)-36)+27)$$
$$+2\gamma\left((\lambda(2\lambda+5)(3\lambda-4)+3)\eta^2+2(\lambda(\lambda(\lambda(9\lambda+13)-48)+13)+9)\eta\right.$$
$$\left.+5(\lambda-1)^2(\lambda(3\lambda+14)+3)v^2+\lambda(\lambda(\lambda(3\lambda-20)+7)+6)\right)\Big]c^4$$
$$-4\lambda\left[(\lambda-1)^3\left((\eta-4)\lambda^2-13(\eta+1)\lambda-4\eta+1\right)v^4-2(\lambda-1)\left((\lambda(11\lambda-17)-2)\eta^3\right.\right.$$
$$+3(3\lambda(2(\lambda-2)\lambda-1)+1)\eta^2+3\lambda(\lambda((\lambda-3)\lambda-12)+6)\eta+\lambda^2(11-\lambda(2\lambda+17))\Big)v^2$$
$$+(\eta+\lambda)^2\left(\lambda\eta^3+(2\lambda(5\lambda-4)-1)\eta^2+\lambda(\lambda(\lambda+8)-10)\eta-\lambda^2\right)$$
$$+4\gamma^2\lambda(\eta(\lambda(3\lambda+10)-9)+\lambda(\lambda(9\lambda-10)-3))$$
$$+\gamma\left((3\lambda(5\lambda-2)-1)\eta^3+\lambda(\lambda(31\lambda+26)-49)\eta^2\right.$$
$$+(\lambda(\lambda((88-49\lambda)\lambda+38)-80)+3)v^2\eta+\lambda^2(\lambda(49\lambda-26)-31)\eta$$
$$\left.\left.-(\lambda-1)\lambda(\lambda(\lambda(3\lambda-77)-39)+49)v^2+\lambda^3(\lambda(\lambda+6)-15))\right]c^2+16\lambda^2\left(-(\lambda-1)^4v^6\right.\right.$$
$$-(\lambda-1)^2\left(-10\eta^2+5\eta+(\gamma+5(\eta-2))\lambda^2+\gamma+2(-5\gamma+\eta(2\eta-11)+2)\lambda\right)v^4$$
$$+\left(8\lambda((\lambda-4)\lambda+1)\gamma^2\right.$$
$$+2\left(3\lambda^4+18(\eta-1)\lambda^3+11((\eta-4)\eta+1)\lambda^2-18(\eta-1)\eta\lambda+3\eta^2\right)\gamma$$
$$+(\eta+\lambda)^2\left((4\lambda-5)\eta^2+2(\lambda(5\lambda-11)+5)\eta+(4-5\lambda)\lambda\right)\right)v^2$$
$$+(-\gamma-\eta)\left((\eta+\lambda)^2+4\gamma\lambda\right)^2\right)=0,$$

(A.22)

$$\nu\lambda(\lambda-1)^2[6\gamma(\lambda+1)+(\eta+1)(\eta(\lambda+2)+2\lambda+1)]c^6$$
$$-\nu\lambda(\lambda-1)\left[\gamma(\eta(\lambda(\lambda(9\lambda+16)-39)-6)+\lambda(16-3\lambda(2\lambda+13))+9)\right.$$
$$+\eta^3(2\lambda-3)(4\lambda+1)+\eta^2\left(4\lambda^3-21\lambda+2\right)+\eta\left(2\lambda^3-21\lambda^2+(\lambda-1)^2(2\lambda+3)\nu^2+4\right)$$
$$+(\lambda-1)^2(3\lambda+2)\nu^2-\lambda(\lambda+4)(3\lambda-2)\Big]c^4+\nu\lambda\left[-4\gamma^2\lambda(\lambda+1)(\lambda(9\lambda-22)+9)\right.$$
$$+\gamma\big(\eta^2(\lambda((19-31\lambda)\lambda+31)-3)-2\eta\lambda(\lambda+1)(\lambda(49\lambda-106)+49)$$
$$+\lambda^2(\lambda((31-3\lambda)\lambda+19)-31)+(\lambda-1)^2(\lambda+1)((\lambda-42)\lambda+1)\nu^2\big)$$
$$+\eta^4((13-12\lambda)\lambda+1)-4\eta^3(\lambda(\lambda(11\lambda-16)+2)+1)$$
$$+2\eta^2\left((\lambda-3)(\lambda-1)^2(6\lambda+1)\nu^2-3\lambda(\lambda+1)(2\lambda-3)(3\lambda-2)\right)$$
$$-4\eta\lambda^2(\lambda(\lambda(\lambda+2)-16)+11)+4\eta(\lambda-1)^2(\lambda+1)((\lambda-9)\lambda+1)\nu^2$$
$$+\lambda^3(\lambda(\lambda+13)-12)+(\lambda-1)^4(\lambda+1)\nu^4-2(\lambda-1)^2\lambda(\lambda+6)(3\lambda-1)\nu^2\Big]c^2$$
$$+4\nu\lambda^2\left[-16\gamma^2\lambda(\eta(2\lambda-1)+(\lambda-2)\lambda)+4\gamma\big(\eta^3(1-3\lambda)+\eta^2(9-11\lambda)\lambda\right.$$
$$+\eta(11-9\lambda)\lambda^2+\eta(\lambda-1)(\lambda(3\lambda-8)+1)\nu^2-(\lambda-3)\lambda^3+(\lambda-1)\lambda((\lambda-8)\lambda+3)\nu^2\big)$$
$$+2(\lambda-1)\nu^2(\eta+\lambda)\left(5(\eta-1)\lambda^2+(\eta(3\eta-14)+3)\lambda-5(\eta-1)\eta\right)$$
$$+(\lambda-1)^3\nu^4(-(\eta(\lambda-5)-5\lambda+1))-(\eta+\lambda)^3(\eta(\eta+5\lambda-5)-\lambda)\Big]=0.$$

$$(\text{A.23})$$

When $\nu=0$, these two equations reduce to one equation

$$\lambda\left((\lambda-1)^2\left[4\gamma+(\eta+1)^2\right]c^8-2(\lambda-1)\left[\gamma\left(3(3\eta-1)\lambda^2-10(\eta+1)\lambda-3\eta+9\right)\right.\right.\quad(\text{A.24})$$
$$+(\eta+1)\left(\eta^2(2(\lambda-1)\lambda-1)+2\eta((\lambda-3)\lambda+1)-\lambda(\lambda+2)+2\right)\Big]c^6$$
$$-\left[-4\lambda^3\left(9\gamma^2-\gamma(\eta+5)(3\eta-2)-2\eta^2(4\eta+5)+\eta+2\right)\right.$$
$$+\lambda^4\left(27\gamma^2+6\gamma(6\eta+1)+8\eta(\eta+1)-1\right)$$
$$+2\lambda^2\left(\gamma^2+\gamma(\eta(7\eta-96)+7)+\eta(2\eta+1)(\eta(2\eta-11)-20)+4\right)$$
$$-4\lambda\left(9\gamma^2+\gamma(2\eta-3)(5\eta+1)+\eta(\eta+2)(\eta(2\eta-3)-4)\right)+27\gamma^2+6\gamma\eta^2$$
$$+36\gamma\eta-\eta^4+8\eta^3+8\eta^2\Big]c^4-4\left[4\gamma^2\lambda(\eta(\lambda(3\lambda+10)-9)+\lambda(\lambda(9\lambda-10)-3))\right.$$
$$+\gamma\left(\eta^3(3\lambda(5\lambda-2)-1)+\eta^2\lambda(\lambda(31\lambda+26)-49)+\eta\lambda^2(\lambda(49\lambda-26)-31)+\lambda^3(\lambda(\lambda+6)-15)\right)$$
$$+(\eta+\lambda)^2\left(\eta^3\lambda+\eta^2(2\lambda(5\lambda-4)-1)+\eta\lambda(\lambda(\lambda+8)-10)-\lambda^2\right)\Big]c^2$$
$$-16\lambda(\gamma+\eta)\left[4\gamma\lambda+(\eta+\lambda)^2\right]^2\right)=0.$$

Also in this case, the triple root condition is

$$
\begin{aligned}
&324\gamma^3\lambda^5 - 1008\gamma^3\lambda^4 + 1432\gamma^3\lambda^3 - 1008\gamma^3\lambda^2 + 324\gamma^3\lambda \\
&+ 108\gamma^2\eta^2\lambda^5 - 387\gamma^2\eta^2\lambda^4 + 780\gamma^2\eta^2\lambda^3 - 714\gamma^2\eta^2\lambda^2 \\
&+ 288\gamma^2\eta^2\lambda - 27\gamma^2\eta^2 + 522\gamma^2\eta\lambda^5 - 1896\gamma^2\eta\lambda^4 \\
&+ 2844\gamma^2\eta\lambda^3 - 1896\gamma^2\eta\lambda^2 + 522\gamma^2\eta\lambda - 27\gamma^2\lambda^6 \\
&+ 288\gamma^2\lambda^5 - 714\gamma^2\lambda^4 + 780\gamma^2\lambda^3 - 387\gamma^2\lambda^2 + 108\gamma^2\lambda \\
&- 9\gamma\eta^4\lambda^4 + 102\gamma\eta^4\lambda^3 - 138\gamma\eta^4\lambda^2 + 66\gamma\eta^4\lambda - 9\gamma\eta^4 \\
&+ 126\gamma\eta^3\lambda^5 - 600\gamma\eta^3\lambda^4 + 1200\gamma\eta^3\lambda^3 - 996\gamma\eta^3\lambda^2 \\
&+ 354\gamma\eta^3\lambda - 36\gamma\eta^3 - 9\gamma\eta^2\lambda^6 + 318\gamma\eta^2\lambda^5 - 1227\gamma\eta^2\lambda^4 \\
&+ 1908\gamma\eta^2\lambda^3 - 1227\gamma\eta^2\lambda^2 + 318\gamma\eta^2\lambda - 9\gamma\eta^2 - 36\gamma\eta\lambda^6 \\
&+ 354\gamma\eta\lambda^5 - 996\gamma\eta\lambda^4 + 1200\gamma\eta\lambda^3 - 600\gamma\eta\lambda^2 \\
&+ 126\gamma\eta\lambda - 9\gamma\lambda^6 + 66\gamma\lambda^5 - 138\gamma\lambda^4 + 102\gamma\lambda^3 - 9\gamma\lambda^2 \\
&+ 8\eta^6\lambda^3 - 12\eta^6\lambda^2 + 6\eta^6\lambda - \eta^6 - 24\eta^5\lambda^4 + 96\eta^5\lambda^3 \\
&- 102\eta^5\lambda^2 + 42\eta^5\lambda - 6\eta^5 + 24\eta^4\lambda^5 - 168\eta^4\lambda^4 \\
&+ 372\eta^4\lambda^3 - 303\eta^4\lambda^2 + 102\eta^4\lambda - 12\eta^4 - 8\eta^3\lambda^6 \\
&+ 96\eta^3\lambda^5 - 372\eta^3\lambda^4 + 588\eta^3\lambda^3 - 372\eta^3\lambda^2 + 96\eta^3\lambda \\
&- 8\eta^3 - 12\eta^2\lambda^6 + 102\eta^2\lambda^5 - 303\eta^2\lambda^4 + 372\eta^2\lambda^3 \\
&- 168\eta^2\lambda^2 + 24\eta^2\lambda - 6\eta\lambda^6 + 42\eta\lambda^5 - 102\eta\lambda^4 \\
&+ 96\eta\lambda^3 - 24\eta\lambda^2 - \lambda^6 + 6\lambda^5 - 12\lambda^4 + 8\lambda^3 = 0,
\end{aligned}
\tag{A.25}
$$

The constant speed contour is given by

$$
\begin{aligned}
&4c^4x^4 + 8c^3x^3\left(\eta + (\lambda + 1)x^2 - (\lambda + 1)y^2 - 1\right) \\
&+ c^2x^2\left(-4\gamma + \eta(5\eta - 14) + (\lambda(5\lambda + 14) + 5)x^4\right. \\
&- 2x^2\left(-5\eta\lambda - 7\eta + 7\lambda + 3(\lambda(\lambda + 6) + 1)y^2 + 5\right) \\
&+ (\lambda(5\lambda + 14) + 5)y^4 - 2y^2(5\eta\lambda + 7\eta - 7\lambda - 5) + 5) \\
&+ cx\left(\eta + (\lambda + 1)x^2 - (\lambda + 1)y^2 - 1\right)\left(-4\gamma + (\eta - 6)\eta\right. \\
&+ (\lambda(\lambda + 6) + 1)x^4 + 2x^2\left((\eta - 3)\lambda + 3\eta + ((\lambda - 10)\lambda + 1)y^2 - 1\right) \\
&+ (\lambda(\lambda + 6) + 1)y^4 + y^2(-2\eta(\lambda + 3) + 6\lambda + 2) + 1) \\
&- \gamma\left(\eta + (\lambda + 1)x^2 - (\lambda + 1)y^2 - 1\right)^2 \\
&+ (x^2 - y^2 - 1)(\eta + \lambda(x - y)(x + y))\left((\lambda + 1)^2x^4\right. \\
&+ 2x^2\left((\eta - 1)(\lambda + 1) + ((\lambda - 6)\lambda + 1)y^2\right) \\
&+ \left(-\eta + (\lambda + 1)y^2 + 1\right)^2\right) = 0
\end{aligned}
\tag{A.26}
$$

The constant frequency contour is

$$
\begin{aligned}
&(\lambda-1)^2\lambda x^{10}y^2 - (\lambda-1)^2(\lambda+1)vx^9y \\
&+ x^8\left((\lambda-1)^2v^2 + \lambda(\lambda(5\lambda-6)+5)y^4 + \left(\lambda^2-1\right)y^2(\eta+\lambda)\right) \\
&- vx^7y\left((\lambda-1)(\eta(\lambda+3)+3\lambda+1) + 4(\lambda+1)\left(\lambda^2+1\right)y^2\right) \\
&+ x^6\left(2(\eta+1)(\lambda-1)v^2 + 2\lambda(\lambda(5\lambda-2)+5)y^6 + 4(\lambda+1)y^4\left(\lambda^2-\eta\right)\right. \\
&\left.+ y^2\left(\gamma(\lambda(3\lambda-2)+3)+\eta^2(-(\lambda-2))+\eta\left(\lambda^2+1\right)+(\lambda(7\lambda+10)+7)v^2+\lambda(2\lambda-1)\right)\right) \\
&- vx^5y\left(4\gamma(\lambda+1) - (\eta+1)((\eta-3)\lambda-3\eta+1) + 8(\lambda+1)v^2\right. \\
&\left.+ 6(\lambda+1)^3y^4 + y^2(-\eta(\lambda(\lambda+10)+13)+\lambda(13\lambda+10)+1)\right) \\
&+ x^4\left(v^2\left(4\gamma+(\eta+1)^2+4v^2\right) + 2\lambda(\lambda(5\lambda+2)+5)y^8 - 6(\lambda+1)^2y^6(\eta-\lambda)\right. \\
&+ y^4\left(\gamma(\lambda(5\lambda-6)+5)+\eta^2(\lambda+6)-\eta(\lambda(\lambda+8)+1)+(\lambda(11\lambda+26)+11)v^2\right. \\
&\left.\left.+ \lambda(6\lambda+1)\right) + y^2\left((1-\eta)(2\gamma(\lambda+1)+(\eta+1)(\eta+\lambda))-8v^2(\eta(\lambda+2)-2\lambda-1)\right)\right) \\
&- vx^3y\left(-(\eta-1)\left(4\gamma+(\eta+1)^2+8v^2\right) + 4(\lambda+1)(\lambda(\lambda+4)+1)y^6\right. \\
&+ y^4(-\eta(\lambda(5\lambda+26)+17)+\lambda(17\lambda+26)+5) \\
&\left.+ 2y^2\left((\eta-1)(\eta(\lambda+5)-5\lambda-1)+4(\lambda+1)v^2\right)\right) \\
&+ x^2y^2\left(-4\gamma^2 + \eta\left((5\eta-14)v^2-\eta(\eta+2)\right) - \eta + 5v^2 + \lambda(\lambda(5\lambda+6)+5)y^8\right. \\
&+ 4(\lambda+1)y^6(\lambda(\lambda+2)-\eta(2\lambda+1)) + \gamma\left(-\eta(\eta+6)-4v^2+((\lambda-6)\lambda+1)y^4-1\right) \\
&+ y^4\left(\eta^2(5\lambda+6)-\eta(\lambda(5\lambda+16)+5)+(\lambda(5\lambda+14)+5)v^2+\lambda(6\lambda+5)\right) \\
&\left.+ 2y^2\left(v^2(-\eta(5\lambda+7)+7\lambda+5)-(\eta-1)^2(\eta-\lambda)\right)\right) - vxy^3\left(-\eta+(\lambda+1)y^2\right. \\
&\left.+ 1\right)\left(-4\gamma+(\eta-6)\eta+(\lambda(\lambda+6)+1)y^4+y^2(-2\eta(\lambda+3)+6\lambda+2)+1\right) \\
&- y^4\left(-\eta+(\lambda+1)y^2+1\right)^2\left(\gamma+\left(y^2+1\right)\left(\eta-\lambda y^2\right)\right) = 0.
\end{aligned}
$$

A.2.3 Case S3

Consider

$$
\begin{aligned}
A_4 &= \lambda, \\
A_3 &= c(1+\lambda), \\
A_2 &= c^2 + 1 - iv(1+\lambda), \\
A_1 &= c(1 - i2v), \\
A_0 &= -\rho - v^2 + iv,
\end{aligned}
$$

equation (A.13) results in the two real equations

$$
\begin{aligned}
\lambda \Big(&(\lambda - 1)^2 (4\rho + 1)c^8 \\
&- 2(\lambda - 1)\left[\lambda^2 \left(v^2 + 9\rho + 2\right) - 2\lambda \left(v^2 + 5\rho + 1\right) + v^2 - 3\rho - 1\right]c^6 \\
&+ \left[\lambda^4 \left(v^4 + v^2(8 - 30\rho) - 27\rho^2\right)\right. \\
&- 4\lambda^3 \left(v^4 + 2v^2(10\rho + 7) + 3(1 - 3\rho)\rho\right) \\
&+ 2\lambda^2 \left(3v^4 + 11v^2(10\rho + 3) - \rho(\rho + 7) - 4\right) \\
&+ 4\lambda \left(-v^4 + v^2(1 - 20\rho) + \rho(9\rho + 10) + 2\right) + v^4 \\
&\left. - 2v^2(15\rho + 11) - 3\rho(9\rho + 2) + 1\right]c^4 - 4\left[\lambda^5 v^4\right. \\
&- \lambda^4 \left(16v^4 + 49v^2\rho\right) + 2\lambda^3 \left(19v^4 + 11v^2(4\rho - 1) + 6\rho^2\right) \\
&+ \lambda^2 \left(-28v^4 + v^2(38\rho + 56) + 5\rho(8\rho + 3)\right) \\
&+ \lambda \left(v^4 - 10v^2(8\rho + 3) - 6\rho(6\rho + 1) + 1\right) \\
&\left. + 4v^4 + v^2(3\rho - 4) - \rho\right]c^2 \\
&- 16\lambda \left[(\lambda - 1)^4 v^6 + (\lambda - 1)^2 v^4(\lambda((\lambda - 10)\rho + 4) + \rho - 10)\right. \\
&- v^2(2\lambda(\rho(4((\lambda - 4)\lambda + 1)\rho + 11\lambda - 18) + 2) + 6\rho - 5) \\
&\left.\left. + \rho(4\lambda\rho + 1)^2\right]\right) = 0,
\end{aligned}
$$

(A.28)

$$\lambda v \Big((\lambda - 1)^2 (6(\lambda + 1)\rho + \lambda + 2)c^6$$
$$- (\lambda - 1) \big[\lambda \left(\lambda \left((2\lambda - 1)v^2 + (9\lambda + 16)\rho + 8 \right) - 4v^2 - 39\rho - 10 \right)$$
$$+ 3 \left(v^2 - 2\rho - 1 \right) \big] c^4$$
$$+ \Big[\lambda^5 v^2 \left(v^2 + \rho \right) - \lambda^4 \left(3v^4 + v^2(43\rho - 12) + 36\rho^2 \right)$$
$$+ \lambda^3 \left(2v^4 + v^2(42\rho - 58) + \rho(52\rho - 31) \right)$$
$$+ \lambda^2 \left(2v^4 + v^2(42\rho + 74) + \rho(52\rho + 19) - 12 \right)$$
$$- \lambda \left(3v^4 + v^2(43\rho + 22) + \rho(36\rho - 31) - 13 \right)$$
$$+ v^4 + v^2(\rho - 6) - 3\rho + 1 \Big] c^2$$
$$- 4\lambda \big[(\lambda - 5)(\lambda - 1)^3 v^4 - 2(\lambda - 1)v^2 (2(\lambda(3\lambda - 8) + 1)\rho + 3\lambda - 5)$$
$$+ (4\lambda\rho + 1)((8\lambda - 4)\rho + 1) \big] \Big) = 0. \tag{A.29}$$

When $v = 0$, these two equations reduce to one equation

$$\lambda \Big[(\lambda - 1)^2 (4\rho + 1)c^8 - 2(\lambda - 1)[\lambda(9\lambda\rho + 2\lambda - 10\rho - 2) - 3\rho - 1)c^6$$
$$+ \big[-8\lambda^2 + (\lambda(\lambda(9(4 - 3\lambda)\lambda - 2) + 36) - 27)\rho^2$$
$$- 2(\lambda(2\lambda + 5)(3\lambda - 4) + 3)\rho + 8\lambda + 1 \big] c^4$$
$$- 4 \big[4\lambda(\lambda(3\lambda + 10) - 9)\rho^2 + (3\lambda(5\lambda - 2) - 1)\rho + \lambda \big] c^2$$
$$- 16\lambda\rho(4\lambda\rho + 1)^2 \Big] = 0. \tag{A.30}$$

A.2.4   Case S4

In this case consider

$$A_4 = \lambda,$$
$$A_3 = c(1 + \lambda),$$
$$A_2 = c^2 - 1 - iv(1 + \lambda),$$
$$A_1 = -c(1 + i2v),$$
$$A_0 = -\rho - v^2 + iv,$$

then equation (A.13) results in the two real equations

$$
\begin{aligned}
\lambda\Big(& (\lambda-1)^2(4\rho+1)c^8 \\
& +2(\lambda-1)\left[\lambda^2\left(v^2+9\rho+2\right)-2\lambda\left(v^2+5\rho+1\right)+v^2-3\rho-1\right]c^6 \\
& +\left[\lambda^4\left(v^4+v^2(8-30\rho)-27\rho^2\right)\right. \\
& -4\lambda^3\left(v^4+2v^2(10\rho+7)+3(1-3\rho)\rho\right) \\
& +2\lambda^2\left(3v^4+11v^2(10\rho+3)-\rho(\rho+7)-4\right) \\
& +4\lambda\left(-v^4+v^2(1-20\rho)+\rho(9\rho+10)+2\right)+v^4 \\
& \left.-2v^2(15\rho+11)-3\rho(9\rho+2)+1\right]c^4+4\Big[\lambda^5v^4 \\
& -\lambda^4\left(16v^4+49v^2\rho\right)+2\lambda^3\left(19v^4+11v^2(4\rho-1)+6\rho^2\right) \\
& +\lambda^2\left(-28v^4+v^2(38\rho+56)+5\rho(8\rho+3)\right) \\
& +\lambda\left(v^4-10v^2(8\rho+3)-6\rho(6\rho+1)+1\right) \\
& +4v^4+v^2(3\rho-4)-\rho\Big]c^2 \\
& -16\lambda\Big[(\lambda-1)^4v^6+(\lambda-1)^2v^4(\lambda((\lambda-10)\rho+4)+\rho-10) \\
& -v^2(2\lambda(\rho(4((\lambda-4)\lambda+1)\rho+11\lambda-18)+2)+6\rho-5) \\
& +\rho(4\lambda\rho+1)^2\Big]\Big)=0,
\end{aligned}
$$

(A.31)

$$
\begin{aligned}
\lambda v\Big(& (\lambda-1)^2(6(\lambda+1)\rho+\lambda+2)c^6 \\
& +(\lambda-1)\left[\lambda\left(\lambda\left((2\lambda-1)v^2+(9\lambda+16)\rho+8\right)-4v^2-39\rho-10\right)\right. \\
& \left.+3\left(v^2-2\rho-1\right)\right]c^4 \\
& +\left[\lambda^5v^2\left(v^2+\rho\right)-\lambda^4\left(3v^4+v^2(43\rho-12)+36\rho^2\right)\right. \\
& +\lambda^3\left(2v^4+v^2(42\rho-58)+\rho(52\rho-31)\right) \\
& +\lambda^2\left(2v^4+v^2(42\rho+74)+\rho(52\rho+19)-12\right) \\
& -\lambda\left(3v^4+v^2(43\rho+22)+\rho(36\rho-31)-13\right) \\
& +v^4+v^2(\rho-6)-3\rho+1\Big]c^2 \\
& +4\lambda\left[(\lambda-5)(\lambda-1)^3v^4-2(\lambda-1)v^2(2(\lambda(3\lambda-8)+1)\rho+3\lambda-5)\right. \\
& +(4\lambda\rho+1)((8\lambda-4)\rho+1)]\Big)=0.
\end{aligned}
$$

(A.32)

When $v = 0$, the these two equations reduce to one equation

$$
\begin{aligned}
\lambda \Big(&(\lambda - 1)^2 (4\rho + 1)c^8 + 2(\lambda - 1)\left[\lambda(9\lambda\rho + 2\lambda - 10\rho - 2) - 3\rho - 1\right]c^6 \\
&- \left[(\lambda(\lambda(9\lambda(3\lambda - 4) + 2) - 36) + 27)\rho^2\right. \\
&\left. + 2\lambda(2\lambda + 5)(3\lambda - 4)\rho + 8(\lambda - 1)\lambda + 6\rho - 1\right]c^4 \\
&+ 4\left[4\lambda(\lambda(3\lambda + 10) - 9)\rho^2 + (3\lambda(5\lambda - 2) - 1)\rho + \lambda\right]c^2 \\
&- 16\lambda\rho(4\lambda\rho + 1)^2\Big) = 0.
\end{aligned}
\tag{A.33}
$$

Appendix B

Descartes' Rule of Signs and Routh-Hurwitz Conditions

B.1   Descartes' Rule of Signs

Consider the polynomial equation

$$Q(\mu) = a_0\mu^n + a_1\mu^{n-1} + ... + a_{n-1}\mu + a_n = 0, \tag{B.1}$$

where the coefficients a_i, $i = 0, 1, ..., n$ are all real. Let N be the number of sign changes in the sequence of coefficients a_0, a_1, ... , a_n, ignoring any which are zero. Deacartes'Rule of Signs says that there are at most N roots of (B.1), which are real and positive, and further, that there are N, $N-2$ or $N-4$,... real positive roots. For instance, if there are two sign changes in the sequence of coefficients of a polynomial ($N = 2$), then there are either 2 or 0 positive real roots (see Murray [54]).

B.2   Routh-Hurwitz Conditions

Consider the polynomial equation (B.1) with all the coefficients are real, and assume that $a_n \neq 0$, since otherwise $\mu = 0$ would be a solution and the order of the polynomial would then be of order $n - 1$. We require conditions on the a_i such that the roots of $Q(\mu)$ have $Re\mu < 0$. The necessary and sufficient conditions for this to hold are the *Routh-Hurwitz conditions*. They read

$$
\begin{aligned}
D_0 &= a_0 > 0 \\[2mm]
D_1 &= a_1 > 0 \\[2mm]
D_2 &= \begin{vmatrix} a_1 & a_3 \\ a_0 & a_2 \end{vmatrix} > 0 \\[2mm]
D_3 &= \begin{vmatrix} a_1 & a_3 & a_5 \\ a_0 & a_2 & a_4 \\ 0 & a_1 & a_3 \end{vmatrix} > 0 \\[2mm]
&\vdots \\[2mm]
D_k &= \begin{vmatrix} a_1 & a_3 & . & . & . & . \\ a_0 & a_2 & a_4 & . & . & . \\ 0 & a_1 & a_3 & . & . & . \\ 0 & a_0 & a_2 & . & . & . \\ . & . & . & . & . & . \\ 0 & 0 & . & . & . & a_k \end{vmatrix} > 0, \qquad k = 1, 2, ..., n.
\end{aligned}
\tag{B.2}
$$

The *Routh-Hurwitz criterion* requires that there is no sign change in the Routh-Hurwitz sequence (RH sequence)

$$
D_0, D_1, \frac{D_2}{D_1}, \frac{D_3}{D_2}, ..., \frac{D_n}{D_{n-1}}.
\tag{B.3}
$$

for the polynomial $Q(\mu)$ to have all of the roots be with negative real part. If there are sign changes, the number of these changes equals to the number of roots with positive real part (see [11], [54]). If all the roots of the polynomial $Q(\mu)$ are negative or complex with negative real part, then coefficients $a_i > 0$, $i = 0, 1, ..., n$ (necessary not sufficient condition).

Now for the cubic equation

$$a_0\mu^3 + a_1\mu^2 + a_2\mu + a_3 = 0 \tag{B.4}$$

the conditions for $Re\mu < 0$ can be written as

$$a_i \;\; > \;\; 0, \qquad i = 0, 1, 3 \tag{B.5}$$

$$a_1 a_2 - a_0 a_3 \;\; > \;\; 0, \tag{B.6}$$

and if these conditions are not satisfied then there must be roots with positive real part and the number of these roots equals to the number of sign change in the RH sequence (from (B.3))

$$a_0, a_1, \frac{a_1 a_2 - a_0 a_3}{a_1}, a_3. \tag{B.7}$$

Also, for the quartic equation

$$a_0\mu^4 + a_1\mu^3 + a_2\mu^2 + a_3\mu + a_4 = 0 \tag{B.8}$$

the Routh-Hurwitz conditions are

$$a_i \;\; > \;\; 0, \qquad i = 0, 1, 3, 4 \tag{B.9}$$

$$a_1 a_2 a_3 - a_0 a_3^2 - a_1^2 a_4 \;\; > \;\; 0. \tag{B.10}$$

If the RH conditions are not fulfilled, then there will be roots with positive real part and the number of these roots equals to the sign change in the RH sequence

$$a_0, a_1, \frac{a_1 a_2 - a_0 a_3}{a_1}, \frac{a_1 a_2 a_3 - a_0 a_3^2 - a_1^2 a_4}{a_1 a_2 - a_0 a_3}, a_4. \tag{B.11}$$

References

[1] D. Afolabi. Sylvester's eliminant and stability criteria for gyroscopic systems. *Journal of sound and vibration*, 182(2):229–244, 1995.

[2] F.T. Arecchi, S. Boccaletti, and P. Ramazza. Pattern formation and competition in nonlinear optics. *Physics Reports*, 318(1):1–83, 1999.

[3] D. Aronson and H. Weinberger. Nonlinear diffusion in population genetics, combustion, and nerve pulse propagation. *Partial differential equations and related topics. Lecture Notes in Mathematics*, 446:5–49, 1975.

[4] M. Baurmann, T. Gross, and U. Feudel. Instabilities in spatially extended predator–prey systems: spatio-temporal patterns in the neighborhood of Turing–Hopf bifurcations. *Journal of theoretical biology*, 245(2):220–229, 2007.

[5] E. Ben-Jacob, H. Brand, G. Dee, L. Kramer, and J.S. Langer. Pattern propagation in nonlinear dissipative systems. *Physica D: Nonlinear Phenomena*, 14(3):348–364, 1985.

[6] R.D. Benguria and M.C. Depassier. Speed of Fronts of the Reaction-Difusion Equation. *Physical Review Letters*, (6):1171–1173, 1996.

[7] R.D. Benguria and M.C. Depassier. On the transition from pulled to pushed mono-

175

tonic fronts of the extended Fisher–Kolmogorov equation. *Physica A: Statistical Mechanics and its Applications*, 356(1):61–65, 2005.

[8] J. Billingham and D.J. Needham. The development of travelling waves in quadratic and cubic autocatalysis with unequal diffusion rates. I. Permanent form travelling waves. *Philosophical Transactions of the Royal Society of London, Series A*, 334:1–24, 1991.

[9] J. Billingham and D.J. Needham. The development of travelling waves in quadratic and cubic autocatalysis with unequal diffusion rates. II. An initial-value problem with an immobilized or nearly immobilized autocatalyst. *Philosophical Transactions of the Royal Society of London Series A*, 336:497–539, 1991.

[10] J. Billingham and D.J. Needham. The development of travelling waves in quadratic and cubic autocatalysis with unequal diffusion rates. III Large time development in quadratic autocatalysis. *Quarterly of Applied Mathematics*, 50(2):343–372, 1992.

[11] R.H. Bishop and R.C. Dorf. *Modern Control Systems*. Prentice Hall College Division, 2004.

[12] P. Borckmans, A. De Wit, and G. Dewel. Competition in ramped Turing structures. *Physica A*, 188(1-3):137–157, 1992.

[13] N.F. Britton. *Reaction-Difusion Equations and Their Applications to Biology*. London: Academic Press, 1986.

[14] V. Castets, E. Dulos, J. Boissonade, and P. De Kepper. Experimental evidence of a sustained standing Turing-type nonequilibrium chemical pattern. *Physical review letters*, 64(24):2953–2956, 1990.

[15] G.A. Cordonier, F. Schüth, and L.D. Schmidt. Oscillations in methylamine decomposition on Pt, Rh, and Ir: Experiments and models. *The Journal of Chemical Physics*, 91:5374–5386, 1989.

[16] M.C. Cross. Traveling and standing waves in binary-fluid convection in finite geometries. *Phys. Rev. Lett.*, 57(23):2935–2938, 1986.

[17] M.C. Cross and P.C. Hohenberg. Pattern formation outside of equilibrium. *Reviews of Modern Physics*, 65(3):851–1112, 1993.

[18] G. Dee and J.S. Langer. Propagating pattern selection. *Physical Review Letters*, 50(6):383–386, 1983.

[19] M. Dolnik, A.M. Zhabotinsky, A.B. Rovinsky, and I.R. Epstein. Spatio-temporal patterns in a reaction–diffusion system with wave instability. *Chemical Engineering Science*, 55(2):223–231, 2000.

[20] V. Dufiet and J. Boissonade. Conventional and unconventional Turing patterns. *The Journal of Chemical Physics*, 96:664–673, 1992.

[21] V. Dufiet and J. Boissonade. Numerical studies of Turing patterns selection in a two-dimensional system. *Physica A*, 188:158–171, 1992.

[22] U. Ebert, W. Spruijt, and W. van Saarloos. Pattern forming pulled fronts: bounds and universal convergence. *Physica D: Nonlinear Phenomena*, 199(1-2):13–32, 2004.

[23] U. Ebert and W. van Saarloos. Front propagation into unstable states: universal algebraic convergence towards uniformly translating pulled fronts. *Physica D: Nonlinear Phenomena*, 146(1-4):1–99, 2000.

[24] I.R. Epstein and J.A. Pojman. *An introduction to nonlinear chemical dynamics: oscillations, waves, patterns, and chaos*. Oxford University Press, USA, 1998.

[25] Z. Fei, B.J. Green, and J.L. Hudson. Spatiotemporal patterns on a ring array of electrodes. *J. Phys. Chem. B*, 103(12):2178–2187, 1999.

[26] P.C. Fife. Asymptotic states for equations of reaction and diffusion. *American Mathematical Society*, 84(5), 1978.

[27] P.C. Fife. Mathematical Aspects of Reacting and Diffusing Systems, Lecture Notes in Biomathematics. 28, 1979.

[28] R.A. Fisher. The advance of advantageous genes. *Annals of Human Genetics*, 7(4):355–369, 1937.

[29] A. Gierer and H. Meinhardt. A theory of biological pattern formation. *Biological Cybernetics*, 12(1):30–39, 1972.

[30] J.I. Gmitro and L.E. Scriven. A physicochemical basis for pattern and rhythm. *Intracellular Transport*, pages 221–255, 1966.

[31] P. Gray and S.K. Scott. Autocatalytic reactions in the isothermal, continuous stirred tank reactor: isolas and other forms of multistability. *Chemical Engineering Science*, 38(1):29–43, 1983.

[32] P. Gray and S.K. Scott. Autocatalytic reactions in the isothermal continuous stirred tank reactor. oscillations and instabilities in the system $a + 2b \rightarrow 3b$; $b \rightarrow c$. *Chemical Engineering Science*, 39(6):1087–1097, 1984.

[33] P. Grindrod. *The theory and applications of reaction-diffusion equations: patterns and waves.* Clarendon Press Oxford, 1996.

[34] M. Hildebrand, A.S. Mikhailov, and G. Ertl. Traveling nanoscale structures in reactive adsorbates with attractive lateral interactions. *Phys. Rev. Lett.*, 81(12):2602–2605, 1998.

[35] D. Hilhorst, J.R. King, and M. Röger. Travelling-wave analysis of a model describing tissue degradation by bacteria. *European Journal of Applied Mathematics*, 18(05):583–605, 2007.

[36] W. Just, M. Bose, S. Bose, H. Engel, and E. Schöll. Spatiotemporal dynamics near a supercritical Turing-Hopf bifurcation in a two-dimensional reaction-diffusion system. *Phys. Rev. E*, 64(2):26219, 2001.

[37] R. Kapral and K. Showalter. *Chemical waves and patterns*. Kluwer Academic Pub, 1995.

[38] A.L. Kay, J.A. Sherratt, and J.B. McLeod. Comparison theorems and variable speed waves for a scalar reaction–diffusion equation. *Proceedings of the Royal Society of Edinburgh: Section A Mathematics*, 131(05):1133–1161, 2001.

[39] B. Kim. Computing traveling wave front solutions in a diffusive predator prey model. *REU Program, University of Michigan*, 2004.

[40] J.R. King, A.J. Koerber, J.M. Croft, J.P. Ward, P. Williams, and R.E. Sockett. Modelling host tissue degradation by extracellular bacterial pathogens. *Mathematical Medicine and Biology*, 20(3):227–260, 2003.

[41] C.A. Klausmeier. Regular and irregular patterns in semiarid vegetation. *Science*, 284(5421):1826–1828, 1999.

[42] A. N. Kolmogorov, I. G. Petrovskii, and N. S. Piskunov. A study of the equation of diffusion with increase in the quantity of matter, and its application to a biological problem. *Bjol. Moskovskovo Gos. Univ*, 17:1–72, 1937.

[43] K.A. Landman, A.Q. Cai, and B.D. Hughes. Travelling waves of attached and de-

tached cells in a wound-healing cell migration assay. *Bulletin of mathematical biology*, 69(7):2119–2138, 2007.

[44] J.A. Leach and D.J. Needham. The evolution of travelling waves in generalized fisher equations via matched asymptotic expansions: algebraic corrections. *The Quarterly Journal of Mechanics and Applied Mathematics*, 54(1):157, 2001.

[45] J.A. Leach and D.J. Needham. The evolution of travelling waves in generalized fisher equations via matched asymptotic expansions: Exponential corrections. *Zeitschrift für Angewandte Mathematik und Physik (ZAMP)*, 55(5):756–768, 2004.

[46] J.A. Leach and D.J. Needham. *Matched asymptotic expansions in reaction-diffusion theory*. Springer Verlag, 2004.

[47] J.A. Leach, D.J. Needham, and A.L. Kay. The evolution of reaction-diffusion waves in a class of scalar reaction-diffusion equations: algebraic decay rates. *Physica D: Nonlinear Phenomena*, 167(3-4):153–182, 2002.

[48] R. Lefever and I. Prigogine. Symmetry-breaking instabilities in dissipative systems II. *J. chem. Phys*, 48:1695–1700, 1968.

[49] O. Lejeune, M. Tlidi, and P. Couteron. Localized vegetation patches: A self-organized response to resource scarcity. *Phys. Rev. E*, 66:010901–1:4, 2002.

[50] I. Lengyel and I.R. Epstein. Modeling of Turing structures in the chlorite-iodide-malonic acid-starch reaction system. *Science*, 251(4994):650–652, 1991.

[51] Q.X. Liu and Z. Jin. Formation of spatial patterns in an epidemic model with constant removal rate of the infectives. *Journal of Statistical Mechanics: Theory and Experiment*, 5:P05002, 2007.

[52] R.T. Liu, S.S. Liaw, and P.K. Maini. Oscillatory Turing Patterns in a Simple Reaction-Diffusion System. *Journal of the Korean Physical Society*, 50(1):234–238, 2007.

[53] P.K. Maini. Using mathematical models to help understand biological pattern formation. *Comptes rendus-Biologies*, 327(3):225–234, 2004.

[54] J.D. Murray. *Mathematical Biology I: An introduction*. Springer, 2003.

[55] J.D. Murray. *Mathematical Biology II: Spatial Models and Biomedical Applicaitons*. Springer, 2003.

[56] C. Neuhauser. Mathematical challenges in spatial ecology. *Notices Amer. Math. Soc.*, 48(11):1304–1314, 2001.

[57] K. Page, P.K. Maini, and N.A.M. Monk. Pattern formation in spatially heterogeneous Turing reaction–diffusion models. *Physica D*, 181(1-2):80–101, 2003.

[58] G.C. Paquette, L.Y. Chen, N. Goldenfeld, and Y. Oono. Structural stability and renormalization group for propagating fronts. *Physical review letters*, 72(1):76–79, 1994.

[59] M. Pascual, M. Roy, and A. Franc. Simple temporal models for ecological systems with complex spatial patterns. *Ecology Letters*, 5(3):412–419, 2002.

[60] L.A. Peletier and V. Rottschafer. Pattern selection of solutions of the swift-hohenberg equation. *Physica D: Nonlinear Phenomena*, 194(1-2):95–126, 2004.

[61] J.J. Perraud, A. De Wit, E. Dulos, P. De Kepper, G. Dewel, and P. Borckmans. One-dimensional spirals: novel asynchronous chemical wave sources. *Phys. Rev. Lett.*, 71(8):1272–1275, 1993.

[62] G. Philippou, F. Schultz, and D. Luss. Spatiotemporal temperature patterns on an electrically heated catalytic ribbon. *J. Phys. Chem.*, 95(8):3224–3229, 1991.

[63] Y. Qi. The development of travelling waves in cubic auto-catalysis with different rates of diffusion. *Physica D: Nonlinear Phenomena*, 226(2):129–135, 2007.

[64] V. Rottschafer and C.E. Wayne. Existence and stability of traveling fronts in the extended fisher-kolmogorov equation. *Journal of Differential Equations*, 176(2):532–560, 2001.

[65] L.A. Segel and J.L. Jackson. Dissipative structure: an explanation and an ecological example. *Journal of Theoretical Biology*, 37(3):545–559, 1972.

[66] J.A. Sherratt. On the evolution of periodic plane waves in reaction-diffusion systems of| lambda-| omega type. *SIAM Journal on Applied Mathematics*, pages 1374–1385, 1994.

[67] J.A. Sherratt. Periodic travelling wave selection by dirichlet boundary conditions in oscillatory reaction-diffusion systems. *SIAM Journal on Applied Mathematics*, pages 1520–1538, 2003.

[68] J.A. Sherratt and B.P. Marchant. Algebraic decay and variable speeds in wavefront solutions of a scalar reaction-diffusion equation. *IMA journal of applied mathematics*, 56(3):289, 1996.

[69] J.A. Sherratt and B.P. Marchant. Nonsharp travelling wave fronts in the fisher equation with degenerate nonlinear diffusion. *Applied Mathematics Letters*, 9(5):33–38, 1996.

[70] H.L. Swinney and V.I. Krinsky. *Waves and patterns in chemical and biological media*. MIT press, 1992.

[71] A.M. Turing. The chemical basis of morphogenesis. *Philosophical Transactions of the Royal Society of London Series B*, 237:37–72, 1952.

[72] W. van Saarloos. Front propagation into unstable states: marginal stability as a dynamical mechanism for velocity selection. *Physical Review A*, 37(1):211–229, 1988.

[73] W. Van Saarloos. Front propagation into unstable states. *Physics reports*, 386(2-6):29–222, 2003.

[74] W. van Saarloos and P.C. Hohenberg. Fronts, pulses, sources and sinks in generalized complex ginzburg-landau equations. *Physica D: Nonlinear Phenomena*, 56(4):303–367, 1992.

[75] V.K. Vanag. Waves and patterns in reaction-diffusion systems. Belousov-Zhabotinsky reaction in water-in-oil microemulsions. *Physics-Uspekhi*, 47(9):923–941, 2004.

[76] V.K. Vanag and I.R. Epstein. Front velocity in models with quadratic autocatalysis. *The Journal of Chemical Physics*, 117(18):8508–8514, 2002.

[77] V.K. Vanag and I.R. Epstein. Pattern formation mechanisms in reaction-diffusion systems. *The International journal of developmental biology*, 53(5-6):673–681, 2009.

[78] D. Walgraef. *Spatio-temporal pattern formation*. Springer, 1997.

[79] L. Yang, M. Dolnik, A.M. Zhabotinsky, and I.R. Epstein. Pattern formation arising from interactions between Turing and wave instabilities. *The Journal of Chemical Physics*, 117(15):7259–7265, 2002.

[80] L. Yang, M. Dolnik, A.M. Zhabotinsky, and I.R. Epstein. Turing patterns beyond hexagons and stripes. *Chaos*, 16:037114, 2006.

[81] L. Yang, A.M. Zhabotinsky, and I.R. Epstein. Stable squares and other oscillatory Turing patterns in a reaction-diffusion model. *Phys. Rev. Lett.*, 92(19):198303, 2004.

[82] A.M. Zhabotinsky, M. Dolnik, and I.R. Epstein. Pattern formation arising from wave instability in a simple reaction-diffusion system. *J. Chem. Phys.*, 103(23):10306–10314, 1995.